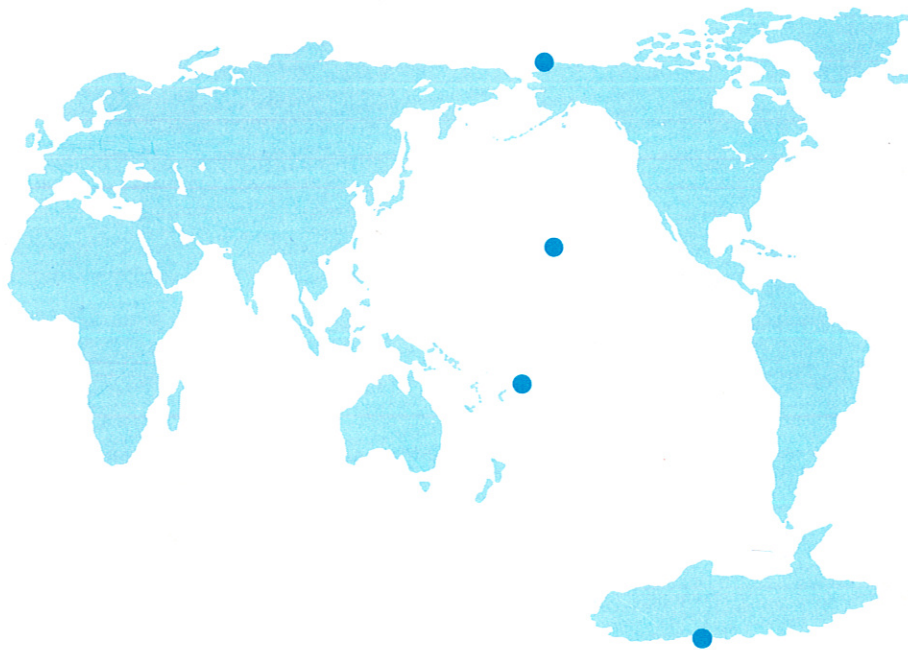


Geophysical Monitoring for Climatic Change

No. 9

Summary Report 1980



U.S. DEPARTMENT
OF COMMERCE

NATIONAL
OCEANIC AND
ATMOSPHERIC
ADMINISTRATION

ENVIRONMENTAL
RESEARCH
LABORATORIES





Geophysical Monitoring for Climatic Change No. 9

Summary Report 1980

John J. DeLuisi, Editor
Air Resources Laboratories
Boulder, Colorado

December 1981

U.S. DEPARTMENT OF COMMERCE
Malcolm Baldrige, Secretary

National Oceanic and Atmospheric Administration
John V. Byrne, Administrator

Environmental Research Laboratories
George H. Ludwig, Director

NOTICE

Mention of a commercial company or product does not constitute an endorsement by NOAA Environmental Research Laboratories. Use for publicity or advertising purposes of information from this publication concerning proprietary products or the tests of such products is not authorized.

CONTENTS

	Page
ACRONYMS AND ABBREVIATIONS	v
FOREWORD	vi
PREFACE.	viii
1. SUMMARY	1
2. OBSERVATORY REPORTS	4
2.1 Mauna Loa	4
2.2 Barrow	10
2.3 Samoa.	13
2.4 South Pole	15
3. CONTINUING GMCC PROGRAMS.	19
3.1 Carbon Dioxide	19
3.2 Total Ozone	23
3.3 Ozone Vertical Distribution	29
3.4 Surface Ozone	31
3.5 Stratospheric Water Vapor	33
3.6 Halocarbons and N ₂ O	34
3.7 Surface Aerosols	36
3.8 Solar Radiation	44
3.9 Station Climatology	46
3.10 Precipitation Chemistry	56
3.11 Data Management	58
4. SPECIAL PROJECTS.	62
4.1 Wind Climatology of American Samoa.	62
4.2 Pyrheliometer Observations as an Indicator of the Climatological Persistence of Clouds	64
4.3 Sampling Strategy to Obtain Data Used in Models of Global Annual CO ₂ Increase and Global Carbon Cycle	68
4.4 Decomposition of Annual Variations of CO ₂ Concentration at GMCC Flask Sampling Stations Into Three Patterns	71
4.5 Comparison of Airborne CO ₂ Flask Samples and Measurements From MLO During the HAMEC Project (June 1980)	74
4.6 CO ₂ Measurements at Barrow, Alaska.	80
4.7 Some Optical Properties of Arctic Haze at Barrow, Alaska.	83
4.8 Mauna Loa Atmospheric Transmission: An Update	86
4.9 A Relationship Between Pacific Ocean Temperatures and Atmospheric CO ₂ Concentrations at Barrow and Mauna Loa.	88
4.10 A Possible Drought-Induced Signal in the Global Atmospheric CO ₂ Record	89
4.11 Studies of Variability in CO ₂ Concentration at Barrow Related to Synoptic Meteorology	91
4.12 A Report on the Short Umkehr Method	92
4.13 Remote-Sensing Observations of the Mt. St. Helens Cloud	96

4.14	Interpretation of Precipitation Chemistry Event Sampling at Elevations From Sea Level to 3400 Meters on the Island of Hawaii.	99
4.15	Stratospheric Lidar Investigations of the Mt. St. Helens Volcanic Cloud over Boulder, Colorado	99
5.	COOPERATIVE PROGRAMS	103
5.1	Size-Elemental Profiles of Fine Particulate Matter at Mauna Loa and Hilo, Hawaii (Univ. of Calif., Davis)	103
5.2	Ultraviolet Erythema Global Measuring Network (Temple Univ.).	104
5.3	Radiation Balance Measurements at Barrow (Univ. of Alaska).	104
5.4	Characteristics of Aerosol Concentrations at the Threshold of Detectability (SUNYA)	105
5.5	Aerosol Characteristics at Mauna Loa Observatory, Hawaii, After East Asian Dust Storm Episodes (Fla. State Univ.)	107
5.6	Arctic Haze Studies at Barrow (URI)	113
5.7	The SEAREX Program--An Overview (URI)	116
5.8	Site Evaluation and Facility Construction for SEAREX Experiments in American Samoa (URI-CIT)	118
5.9	Carbon Particles in the Arctic Aerosol (LBL-NOAA)	122
5.10	Solar Spectral Irradiance and Transmissivity of the Atmosphere at Mauna Loa During 1980 (Univ. of Alaska).	127
5.11	Increases in Atmospheric Concentrations of Halocarbons and N ₂ O (OGC)	134
5.12	Precipitation Chemistry at Samoa and Mauna Loa (DOE/EML).	139
5.13	Atmospheric Particulate Chemistry at the South Pole and Mauna Loa (Univ. of Md.).	141
6.	INTERNATIONAL ACTIVITIES	148
7.	PUBLICATIONS AND PRESENTATIONS.	150
8.	REFERENCES	153
9.	GMCC STAFF	162

ACRONYMS AND ABBREVIATIONS

ARL	Air Resources Laboratories, Washington, D.C. (NOAA)
BRW	Barrow Observatory, Barrow, Alaska (GMCC)
CAF	Clean Air Facility, South Pole Observatory, Antarctica (GMCC)
CIT	California Institute of Technology, Pasadena, Calif.
CNC	Condensation nucleus counter
DOE	U.S. Department of Energy, Washington, D.C.
ECC	Electrochemical concentration cell
EML	Environmental Measurements Laboratory, U.S. Department of Energy, New York, N.Y.
EPA	Environmental Protection Agency
G.E.	General Electric
HAMEC	Hawaii Mesoscale Energy and Climate project
HVO	Hawaii Volcano Observatory
IAEA	International Atomic Energy Agency, Vienna, Austria
IAMAP	International Association of Meteorology and Atmospheric Physics
ICDAS	Instrumentation control and data acquisition system
ISWS	Illinois State Water Survey
LBL	Lawrence Berkeley Laboratory, Berkeley, Calif.
MLO	Mauna Loa Observatory, Mauna Loa, Hawaii (GMCC)
MPI	Max Planck Institute, Mainz, Germany
NADP	National Atmospheric Deposition Program
NARL	Naval Arctic Research Laboratory, Barrow, Alaska
NBS	National Bureau of Standards, Gaithersburg, Md.
NCAR	National Center for Atmospheric Research, Boulder, Colo.
NCC	National Climatic Center, Asheville, N.C.
NIP	Normal incidence pyrheliometer
NOAA	National Oceanic and Atmospheric Administration, U.S. Dept. of Commerce
NRL	Naval Research Laboratory
NSF	National Science Foundation, Washington, D.C.
NWS	National Weather Service, Washington, D.C. (NOAA)
OGC	Oregon Graduate Center, Beaverton, Ore.
PIXE	Particle (or proton) induced X-ray emission
SEAREX	Sea-Air Exchange program
SIO	Scripps Institution of Oceanography, La Jolla, Calif.
SMO	Samoa Observatory, American Samoa (GMCC)
SPO	South Pole Observatory, Antarctica (GMCC)
SRL	Smithsonian Institution Radiation Biology Laboratory
SUNYA	State University of New York at Albany
URI	University of Rhode Island, Kingston, R.I.
USGS	United States Geological Survey
WMO	World Meteorological Organization, Geneva, Switzerland
WDC-A	World Data Center-A, Asheville, N.C.

FOREWORD

However we may define climate, and I know of no satisfactory formal way, we do know that it changes. We know this from the 200 or 300 years of local instrumental records, from the 100 years of global instrumental coverage, and, more certainly and significantly, from what Wilmot Hess, in the foreword to the first of these Summary Reports, called "ingenious studies of glaciers, pollen, tree rings, sea sediments, and vintners' records." The changes appear on all the time and space scales we have been able to study, and, where it has been possible to quantify the changes statistically, the statistics are neither stationary nor homogeneous and, furthermore, do not lend themselves easily even to quantitative extrapolation in time.

What then can be the purpose of an organization devoted to "Geophysical Monitoring for Climatic Change"? Clearly not to establish the fact that climate changes, nor, in view of the very large quantity of standardized meteorological observations and of the growing potential of satellite systems, to document climate change on the global or any regional scale. The traditional role of monitoring is to provide a timely indication of situations which are about to become manifest, and the traditional monitor is a very sensitive detector of some parameter which is itself a very sensitive indicator that the situation is in being. (A simple analogy to this is a smoke detector alarm.) I do not believe that such an indicator of climate change has yet been unambiguously identified, but there are some very likely candidates, and GMCC is observing them, systematically and with the greatest precision possible, in locations where interference by strictly local activity is absent or can be contained. Such locations are remote, preferably barren, and usually uncomfortable, and operation there is expensive.

Economic conditions change as well as statistics of weather, and, as I write, I am only too well aware of a potentially significant reduction in the resources available for study of the atmosphere. Therefore, the general atmospheric research community is being faced with the problem of curtailing certain programs. Serious thought must be given to retaining the continuity of measurement programs that offer a reasonable chance for unraveling the factors and combinations thereof that cause climate change. Consider, for example, the record of CO₂ concentration in the atmosphere. If much of the thinking on this problem is not in error, the effects of CO₂ concentration increases on global climate should begin to show in the global statistics (perhaps of temperatures in the higher stratosphere) within the next 10 years. If effects do not show, we will have a scientific problem, and, in considering the problem, detail in the record of CO₂ concentration will be important. If the effects do show, we will have an economic problem with enormous implications, and detail in the record of CO₂ concentration will be important in studying its impact. At the present time GMCC carries a major responsibility for the continuity and precision of the CO₂ record. The same reasoning can be applied to the other trace gases and aerosols measured by GMCC. It is a responsibility to the world community.

For a 10-yr period some time ago, I was the Superintendent of Kew Observatory. This institution, for a total of 120 years, has maintained a commendably continuous record of certain weather elements measured in precisely defined conditions. This record has been used for assessments of past climate conditions. (For example, it clearly showed the cold spell of 1880-1890.) When the record was begun, I believe it was unique. After very careful consideration of the Kew record in relation to other records from nearby sources,

and for reasons of economy, the Observatory was recently closed and the record ended. It was ascertained that continuity would not be lost because of the overlapping measurements made by the other nearby observation facilities. The physical surroundings of Kew had unavoidably changed over the years, and the effects could be seen in the record. Therefore, although I have sentimental regrets, I cannot think of any possible adverse effect of the closure on atmospheric science.

I view GMCC as representing a new generation of observatories which are designed partially on the basis of experiences of the older observatories, but which are now internationally connected and judiciously located for detecting changes that are more likely to be global in nature. Modern equipment has greatly improved capabilities for measuring an extended variety of atmospheric variables, including aerosols and chemistry, and it is expected that the remotely located sites will ensure minimum influence from changes in surroundings for many years. A valuable and more complete record for climate research is now being accumulated by these newer observatories, and I believe it will be a considerable number of years before these observatories will have found their mission fulfilled.

G. D. Robinson
Past President and Honorary Member
Royal Meteorological Society

PREFACE

This document presents a summary of the research operations and accomplishments by the Geophysical Monitoring for Climatic Change (GMCC) program and by outside investigators working cooperatively with GMCC in 1980. It includes descriptions of management and operations at GMCC's four baseline sites, scientific data from the measurement projects, conclusions from analyses of data, and recent basic research achievements.

The GMCC program, established in 1971, is one of five research programs within the Air Resources Laboratories under the directorship of Lester Machta. Its four observatories are located at Barrow, Alaska (in service since 1973); Mauna Loa, Hawaii (in service since 1956); American Samoa (in service since 1973); and South Pole (in service since 1957). Background measurements of aerosols, gases, and solar radiation that are important to the climate of the Earth are made at the observatories. The primary groups within GMCC are Monitoring Trace Gases, Aerosols and Radiation Monitoring, Acquisition and Data Management, and Analysis and Interpretation. Specific names of individuals in GMCC are not given in the main text of the report; however, the membership of each GMCC group is given in sec. 9. Publications and presentations by GMCC staff are given in sec. 7.

GEOPHYSICAL MONITORING FOR CLIMATIC CHANGE

NO. 9

Summary Report 1980

1. SUMMARY

At Mauna Loa, an LSI-11 computer system was ordered for the Hilo office to be used for local research projects. An investigation of CO₂ vertical gradients started. Complete refurbishing of the lidar system laser greatly improved operations in 1980. The Meteorological Museum was in operation for its first full year. At Barrow, the Naval Arctic Research Laboratory went to caretaker status, thus terminating its science support activities. GMCC personnel moved to housing provided by NWS in the town of Barrow.

At Samoa, five temporary facility additions were made in preparation for hosting the SEAREX experiment. A comprehensive tracer study of the airflow around Matatula Point was performed by SEAREX and GMCC personnel to determine possible contamination effects from local vegetation and terrain. At South Pole, no additions to facilities were made and all programs operated normally.

The main ongoing GMCC measurement programs at the Observatories continued; these include carbon dioxide, surface and total column ozone, fluorocarbons-11 and -12, nitrous oxide, aerosol scattering coefficient, Aitkin nuclei, solar radiation components, chemistry of precipitation, and associated meteorology. In addition, balloon measurements of stratospheric water vapor and ozone profiles were made at Boulder along with frequent Umkehr ozone profiles. Lidar measurements continued at Mauna Loa. Total ozone was regularly measured at eight additional sites by Dobson spectrophotometers. The CO₂ flask sampling program was expanded by three, to 18 locations (including the Observatories). Many of these data are being archived at the World Data Center-A, Asheville, N.C., and at the World Ozone Data Center, Downsview, Ontario.

Upgrading of foreign Dobson spectrophotometers, under the auspices of the WMO Global Ozone Research and Monitoring Project, continued. To date, 40 instruments have been directly calibrated and 40 others indirectly calibrated relative to the World Primary Standard Dobson no. 83, maintained at GMCC in Boulder. Work continued on automation of a Dobson for routine Umkehr measurements using the short technique. This will allow an increased number of ozone profiles at reduced staff costs.

Climatology analyses for the four GMCC Observatories, using the stations' meteorology data, were performed and reported. Precipitation chemistry protocol at the baseline and regional stations was changed significantly in 1980; all GMCC sites adopted common protocol and procedures of the National Atmospheric Deposition Program.

New hardware was acquired to upgrade the Boulder data reduction facility. This included a NOVA 4/X minicomputer and a Winchester-type disk. Also, stand-alone microprocessor-based data loggers were being developed.

GMCC personnel conducted numerous research projects and data analyses from ongoing programs. Among the topics included were analyses of secular trends of North American total ozone, fluorocarbon-11 and -12, N₂O, Aitkin nuclei, and aerosol light scatter. In recent years, total ozone showed a slight decrease, whereas fluorocarbons continued their marked increase. Aitkin nucleus values at the South Pole (for example) have shown little year-to-year change.

A climatology of airflow arriving at Samoa indicates that during late summer Northern Hemisphere air occasionally, but infrequently, reaches the Observatory. CO₂ anomalies have been detected during such times.

Mauna Loa normal incidence pyrhelimeter data were used to develop a technique for obtaining thin-cloud climatology. A persistent trend in thin-cloud transmittance would indicate regional changes in cloud optical thickness.

GMCC CO₂ data were used for several studies. Intermittent flask samplings at selected sites around the globe are expected to contain fluctuations due to small-scale events not of interest for global-scale concerns. The effect of station distribution and frequency of sampling was studied to develop a strategy for providing a truly global annual CO₂ increase. In another study, an eigenvalue analysis of GMCC flask samples yielded large-scale characteristic patterns.

The GMCC CO₂ measurement record from Barrow, 1973-79, was analyzed in some detail. An annual cycle of about 15 ppm was identified. These other investigations of atmospheric CO₂ characteristics are summarized in this report: relationships between Pacific Ocean temperatures and concentrations of atmospheric CO₂ concentrations at Barrow and Mauna Loa; a possible drought-induced signal in the global atmospheric CO₂ record; the variability of CO₂ concentration at Barrow related to synoptic meteorology; and a comparison of midtropospheric airborne samples with measurements at MLO as part of the HAMEC project.

Further work was accomplished on the short Umkehr method. A computer program to invert short Umkehr measurements was completed and tested on 46 short Umkehr observations, and the results were compared with concurrent ozonesonde measurements. Generally good agreement was obtained.

Measurements of the atmospheric radiative effects of the Mt. St. Helens volcanic cloud that appeared over Boulder on May 19 and June 3 were made and subsequently analyzed for the optical properties of the cloud. About 5% of the solar attenuation occurred as absorption. Stratospheric lidar measurements were also made of the cloud at various times between May and August. Distinct aerosol layers were detected at altitudes between 10 and 20 km.

Solar radiation measurements made at Barrow were analyzed for optical properties of the Arctic haze during specific episodes when haze was evident. The technique used to analyze radiation measurements for aerosol properties indicates that a preponderance of small particles exist in the haze. The direct solar beam was depleted by as much as 29%.

In 1980, GMCC supported a substantial number of cooperative research projects. (At Mauna Loa alone, there were about 20 cooperative programs.)

Thirteen summary reports from the projects were contributed to this volume. Several aerosol chemistry investigations were conducted, leading to valuable quantitative interpretation of the characteristics of aerosols sampled at the Observatories. Measurements at Barrow further confirmed that Arctic haze is probably anthropogenic. Moreover, the radiative properties of the Barrow winter aerosol appear to be strongly absorbing in the solar visible band. The solar spectral irradiance and transmission by the atmosphere at Mauna Loa were critically investigated. Sampling of atmospheric gases, crucial to the photochemistry of ozone production, continued, further extending the record built from the previous sampling projects. Methane measurements at Barrow and Samoa were used to document a global secular increase. A major atmospheric chemistry field program, SEAREX, with multi-institution participation, began at Samoa.

2. OBSERVATORY REPORTS

2.1 Mauna Loa

2.1.1 Equipment and Facilities

No major changes to the basic facilities at Mauna Loa (MLO) were effected during the year. Perhaps the most important action was identifying a new computer system for quality control of MLO data and for computations related to special research projects of MLO staff members. The specified system is based on the LSI-11 microprocessor, with peripherals including a disk system, video terminal, and line printer. In addition, an automatic plotter was obtained as government excess equipment.

Aside from the computer system order, the following problems with, or modifications to, the MLO facilities occurred during 1980.

- (1) A severe storm accompanied by winds gusting to 85 mi h^{-1} buffeted Hawaii during the period January 8-12 and caused some damage to the buildings at the observatory. The most serious damage was sustained by the storage building, which lost part of its roof. Minor damage at other locations was caused by flooding from the 5-in rainfall accompanying the strong wind. Cleanup and repairs of the damage were completed by the end of January.
- (2) Operation of the instrumentation control and data acquisition system (ICDAS) was interrupted 25 times during the year, most frequently because of instantaneous dropouts of line power, but, closely second, because of static discharges in the vicinity of the computer. The reason for one 5-day outage was inadvertent shorting of a destructive voltage through a special circuit that had been installed for monitoring the magnetic tape unit. Problems in reading the operating system tape were experienced on occasion. In general, however, ICDAS operations were as satisfactory as can be expected for a complicated system in a remote location.
- (3) A damaged sun photometer was replaced by a new one in March.
- (4) A major improvement of the lidar system was completed, with an increase of laser power by about an order of magnitude. The previously used 3/8-in ruby rod was replaced by a 5/8-in rod, and previously damaged windows and mirrors were replaced by new ones. Fortunately, this was all accomplished before the eruption of the Mt. St. Helens volcano.
- (5) A detailed map of the MLO site, the first such map ever developed for MLO, was completed in June. Not only are the building locations defined precisely for the first time, but a very useful diagram of the electric power distribution system of the observatory was developed. As a result, two completely useless loops in the electric cables were discovered and eliminated.
- (6) A URAS-1 carbon dioxide analyzer was received from Boulder in July and was set up with a multilevel air intake system for investigating vertical gradients of CO_2 concentration under different meteorological conditions.
- (7) In a continuing effort to protect the observatory from possible lava flows resulting from eruptions of the volcano, a very detailed and precise topographic map of the upper regions of Mauna Loa was completed in December by

the U.S. Geological Survey (USGS), Flagstaff, Arizona, from special aerial photos. Arrangements for both the aerial survey and construction of the map were made by J. P. Lockwood of the Hawaii Volcano Observatory (HVO), who is also developing plans for the construction of lava barriers above the observatory for deflecting any lava flows that may originate on the higher slopes of the volcano.

(8) One of the automobiles (a Plymouth Fury) assigned to MLO was replaced by a newer model (a Ford Fairmont station wagon) in 1980. This vehicle is much more suitable for hauling the many boxes of flasks and instruments used at the observatory.

2.1.2 Programs at MLO during 1980.

The principal programs carried out at MLO during 1980 are listed in table 1. Brief comments on the programs follow.

Carbon Dioxide

The URAS-2 infrared analyzer continued to operate without major problems during the year, the output being recorded on both the ICDAS magnetic tape and a strip chart recorder. In addition, pairs of 500-ml glass flasks were exposed weekly at MLO and Cape Kumukahi and sent to Boulder for analysis. A number of special high density, flask sampling periods occurred throughout the year in connection with programs such as the HAMEC (Hawaii Mesoscale Energy and Climate) project and tests of new methods of flask sample analysis in Boulder.

A special project for investigating vertical gradients of CO₂ concentration was started near the end of the year. Samples are taken at five different levels up to a maximum height of 88 ft above the surface. No definite results were obtained before the end of the year.

Outgassing from the volcanic caldera at the summit of Mauna Loa continued to be recorded in the CO₂ continuous-monitoring measurements, mainly during a downslope windflow regime. Table 2 shows the monthly frequency of occurrence of the outgassing for 1980. The total frequency of outgassing from the caldera for 1980 corresponded well with frequencies in 1978 and 1979, as shown by table 3, but was lower than the years immediately following the July 1975 summit eruption of Mauna Loa. Seismic and other measurements of HVO indicate that the volcano will remain in a generally stable condition, with a slow expansion of the summit area.

Atmospheric Ozone

Total ozone in the atmospheric column was measured on each of approximately 250 days during 1980 by Dobson spectrophotometer no. 63. In addition, the standard reference spectrophotometer no. 83 was shipped from Boulder to make a special series of measurements over approximately 2 months.

Surface ozone concentration was monitored continuously throughout the year by Dasibi and ECC (electrochemical concentration cell) instruments.

Table 1.--Summary of monitoring programs at Mauna Loa in 1980

Monitoring Program	Instrument	Sampling frequency	Remarks
<u>Gases</u>			
Carbon dioxide	URAS-2 infrared gas analyzer	Continuous	
	Evacuated glass flasks	Weekly	Mountain and seacoast
Surface ozone	Electrochemical concentration cell	Continuous	
	Dasibi ozone meter	Continuous	
Total ozone	Dobson spectrophotometer (#63)	Discrete	3 meas., weekdays; 0, weekends
	Dobson spectrophotometer (#83)	Discrete	Special obs. during summer
Fluorocarbons	Pressurized flasks	Weekly	
<u>Aerosols</u>			
Stratospheric aerosols	Lidar	Weekly	694.3 nm, 1 J
Condensation nuclei	Pollak CN counter	Discrete	4 meas., weekdays; 0, weekends
	G.E. CN counter	Continuous	
Optical properties	Four-wavelength nephelometer	Continuous	Wavelengths 450, 550, 700, 850 nm
Skylight polarization	Polarizing radiometer	Discrete	8 wavelengths
<u>Solar radiation</u>			
Global irradiance	Four Eppley pyranometers	Continuous	Cutoff filters at 280, 390, 530, 695 nm
Ultraviolet irradiance	Eppley ultraviolet pyranometer	Continuous	Wavelength range 295 to 385 nm
Direct beam irradiance	Eppley pyrliometer	Continuous	Wavelength range 280 to 3,000 nm
	Eppley pyrliometer with filters	Discrete	Cutoff filters at 280, 530, 630, 695 nm
	Eppley 13-channel pyrliometer	Continuous	13 spectral regions
<u>Meteorology</u>			
Maximum temperature	Maximum thermometer	Daily	
Minimum temperature	Minimum thermometer	Daily	
Ambient temperature	Thermistor	Continuous	
	Hygrothermograph	Continuous	At MLO and Kulani Mauka
Dewpoint temperature	Dewpoint hygrometer	Continuous	
Relative humidity	Hygrothermograph	Continuous	At MLO and Kulani Mauka
Total precipitable water	Foskett infrared hygrometer	Continuous	
Pressure	Electronic pressure transducer	Continuous	
	Microbarograph	Continuous	
Precipitation	Rain gage, 8-in	Daily	At MLO
	Rain gage, 8-in	Twice weekly	At Kulani Mauka
	Rain gage, tipping bucket	Continuous	
Windspeed	Anemometer	Continuous	
Wind direction	Wind vane	Continuous	
<u>Precipitation chemistry</u>			
Acidity of rainwater	pH meter	Discrete	Rainwater collections at 6 sites
Conductivity of water	Conductivity bridge	Discrete	
Chemical components	Ion chromatograph	Discrete	
<u>Cooperative programs</u>			
Carbon dioxide (SIO)	Infrared analyzer (Applied Physics)	Continuous	
	Evacuated flasks	8 mo ⁻¹	Mountain and seacoast
Carbon monoxide (MPI)	Special system	Continuous	Chemical reaction with HgO
Surface SO ₂ (EPA)	Chemical bubbler system	Every 12 days	
Total surface particulates (DOE)	High-volume filter	Continuous	Dependent on wind direction
Total surface particulates (EPA)	High-volume filter	Every 12 days	
Atmospheric electricity (Univ. of Minnesota)	Field mill, air conductivity meter, surface antenna	Continuous	
Ultraviolet radiation (Temple Univ.)	Ultraviolet radiometer	Continuous	Radiation responsible for sun-burning of skin
Precipitation collection (DOE)	Wet-dry collector (Health and Safety Lab.)	Continuous	
Precipitation collection (EPA)	Misco model 93	Continuous	
Precipitation collection (Univ. of Paris)	Likens funnel collector	Twice weekly	
Precipitation collection (IAEA)	Likens funnel collector	Twice weekly	
Wet-dry deposition (Univ. of Illinois)	Exposed collection pails	Continuous	Natl. Atmos. Deposition Program
Atmospheric aerosols (Florida State Univ.)	Special filters	Continuous	
Atmospheric aerosols (Univ. of Maryland)	Nuclepore filters	Continuous	Day-night discrimination
Atmospheric aerosols (Univ. of California)	Nuclepore filters and impactors	Night only	
Atmospheric aerosols (Univ. of Arizona)	Quartz filters	Continuous	Day-night discrimination

Table 2.--Monthly occurrences of outgassing from the volcanic caldera on Mauna Loa

	Jan	Feb	Mar	Apr	May	Jun	Jul	Aug	Sep	Oct	Nov	Dec
No. of days	3	0	9	8	7	16	19	21	11	10	9	8
Percent of days	10	0	29	27	23	53	61	68	37	32	30	26

Atmospheric Aerosols

The aerosol-monitoring program, including the volume scattering coefficient and concentration of condensation nuclei (CN) in the air, continued without major interruptions during the year.

Lidar Observations

As mentioned above, complete refurbishing of the laser, a process which involved purchasing new optical components and repolishing some existing components, resulted in lidar operations in 1980 that were much improved over previous years. Although the optics were all in order by the end of March, electronic problems continued to prevent regular observations for another month. Beginning in May, however, lidar observations were made routinely throughout summer and fall. Twice-weekly observations were made for several weeks following the Mt. St. Helens eruption, but this schedule caused an undue burden on the available staff, so a weekly schedule was set up. The Mt. St. Helens volcanic cloud was first detected over Mauna Loa in early July, some 6 weeks after the May 18 eruption. Intense public interest in the cloud was evidenced by numerous telephone calls received in Hilo following a press release on the event issued by NOAA in Boulder. The lidar continued to operate well, and evidence of the volcanic cloud persisted, until failure of the laser on December 24 terminated lidar measurements for the year.

Solar Radiation

Solar radiation observations continued without serious problems during 1980. Perhaps the most significant difficulty was that improper alignment of

Table 3.--Annual frequency of occurrence of outgassing from the caldera on Mauna Loa during the period immediately before and since the last summit eruption, July 1975

	1975		1976	1977	1978	1979	1980
	Jan-Jul	Aug-Dec					
Percent of occurrences	28	49	42	43	32	32	33

the shading disk for diffuse solar radiation measurements degraded the measurements on occasion during the first 8 months of the year. A careful realignment on September 11 eliminated the difficulty, however, and completely reliable diffuse data were obtained during the remainder of the year. Lightning discharge near the observatory burned out the preamplifier for diffuse radiation measurements on May 12 and again on May 20. Installation of lightning protectors on May 25 apparently corrected the problem. The quartz window pyranometer and two normal incidence pyrhemometers were compared with the Boulder traveling standards, from January 29 to February 1.

Meteorological Parameters

Satisfactory monitoring of the basic meteorological parameters continued during 1980, with only the normal number of equipment problems. An intermittent problem was encountered in automatic recording of ambient temperature, an erroneous thermometer calibration constant in the data acquisition system was discovered and corrected in August, and a spare temperature card and sensor were installed in late September. The aerovane directional servomotor malfunctioned and caused erroneous wind direction data from July 17 to 23. The triple register for wind and precipitation was inoperable April through May, but was put back online on June 6 and operated satisfactorily for the remainder of the year.

Precipitation Chemistry

Measurements of the acidity, conductivity, and ion content of rainwater samples from six sites in Hawaii, as well as of samples from the other GMCC observatories, were continued on a regular basis, and rainwater samples were sent regularly to the International Atomic Energy Agency (IAEA) and the University of Paris. A special effort in collecting and analyzing numerous rainwater samples was made during the HAMEC project, the official period of which was June 11 to 24. Aid was also given to the Illinois State Water Survey (ISWS) in its sequential rain-sampling program.

Fluorocarbons (Halocarbons)

Dual flask samples were taken on a weekly basis and mailed to Boulder for analysis.

Skylight Polarization and Intensity

Measurements of the polarization and intensity of skylight, mainly during periods of morning twilight, were coordinated with lidar measurements of stratospheric aerosols.

Cooperative Programs

A significant component of MLO is the cooperative projects that are carried out by observatory personnel for various universities and government agencies. Most of the cooperative programs listed in table 1 were continued through 1980 without major difficulties. The following items are worthy of special note.

(1) A. Dittenhoefer, an associate in the National Research Council Associateship Program, spent the entire year at MLO conducting a study of

the sulfate content of atmospheric aerosols. The results are scheduled for publication during 1981.

(2) Special solar radiation measurements, which covered the period of January 22 to the end of the year, were conducted by G. Shaw of the University of Alaska. The measurements were made by a 10-filter solar tracking radiometer operated by G. Ferrel, a University of Alaska technician who was stationed at MLO throughout the period.

(3) New instrumentation for carbon monoxide measurements was installed during March by scientists from the Max Planck Institut (MPI), Mainz, Germany. This equipment is much more sensitive than the previous instrument, and, except for a short period during early May, it operated satisfactorily the remainder of the year.

(4) Special solar radiation measurements were made by R. Angione, R. Roosen, and F. Beale of San Diego State University for several days during late March. A malfunction of the microprocessor caused a premature termination of the measurements, however, and the equipment was returned to San Diego in time for investigating the radiative effects of the Mt. St. Helens volcanic cloud as it passed over San Diego.

(5) At the request of R. Fraser of the Goddard Space Flight Center, special measurements of solar radiation in eight different spectral bands were made during late June and early July to obtain an approximate calibration of Fraser's radiometer using Langley plots of the radiation data.

(6) During March, V. Neitzert of MPI took fifty 3-h samples for atmospheric formaldehyde analysis. Liquid nitrogen was used to freeze from the samples many of the atmospheric gases, formaldehyde among them, and the resulting material was fixed in a liquid reagent and taken back to Germany for analysis.

(7) Also during March, M. Darzi of Florida State University used Cascade impactors at several locations on the island for special aerosol collections that were later analyzed in Darzi's laboratory by the particle induced X-ray emission technique (PIXE).

(8) A major revision of the aerosol collection experiment of the University of Maryland was made during the latter part of April. The previous three pumps were replaced by much more powerful ones, thereby increasing the airflow rate by a factor of 4 to 5. Operation of the new pumps is controlled by a sophisticated system of circuitry triggered by four environmental parameters at the observatory: windspeed, wind direction, atmospheric scattering coefficient, and concentration of condensation nuclei. The system operated well during the remainder of the year.

(9) A new procedure for handling wet-dry atmospheric deposition samples was instituted on June 19, at the time of the HAMEC project. Following that date, weekly samples of wet fallout and bimonthly samples of dry fallout have been submitted to ISWS for chemical analysis. The samples are taken as a part of the National Atmospheric Deposition Program (NADP).

(10) Word was received during July that management of the atmospheric electricity program was being transferred from W. Boeck, Niagara University,

to D. Olson, University of Minnesota. One month later, a new and improved field mill and a new antenna for measuring air-Earth current were installed at the observatory. It had been anticipated that data from all the atmospheric electricity instruments would be recorded on magnetic tape by an electronic data acquisition system to be delivered with the new instruments. Unfortunately, the theft of the data logger from an automobile parked overnight in Hilo forced the use of two antiquated strip chart recorders on an interim basis until a new electronic system can be obtained. The strip chart recorders were still in use at the end of 1980.

(11) Two scientists, A. Ashbridge and J. Bellfleur of the Environmental Service of Canada, brought the Canadian Dobson spectrophotometer and a Brewer ozone meter to MLO in late July for comparison of their instruments with the standard Dobson no. 83. They returned to Canada on August 8, having experienced exceptionally good sky conditions at MLO during the comparison period.

(12) A. Hogan, State University of New York at Albany (SUNYA), made some special aerosol collections at MLO during the period June 10 to 18 to measure the size-frequency distribution of the particles.

(13) The laborious task of reading values from the meteorological data charts and transcribing them by hand into tabular format for use by the Scripps Institution of Oceanography (SIO) carbon dioxide program was terminated on July 1. After that date, the meteorological data were transcribed in Boulder from the MLO magnetic data tape. Hand reduction of the CO₂ data from recorder strip charts continues as it has since the start of the measurements in 1958.

2.1.3 Mauna Loa Meteorological Museum

1980 was the first full year of the existence of the Meteorological Museum at MLO. The collections were increased during the year by the following items:

- (1) A 4- by 8-ft airbrush painting of Mauna Loa and its environs.
- (2) Eight meteorological instruments of various types.
- (3) Several dozen books, charts, pamphlets, and other published material on meteorological and related topics.
- (4) Original hand-written letters and manuscripts, mainly by the late C. G. Abbot.
- (5) Magnetic tape cassettes of conversations with C. P. Butler, former observer at the Smithsonian Solar Observatory, Mt. Montezuma, Chile.

2.2 Barrow

2.2.1 Facilities

The only modification of Barrow (BRW) station facilities in 1980 was the installation of a thermostat-controlled ventilation system in May. Heating and cooling were previously regulated by adjusting individual heaters or cranking windows open, which had little effect during long summer days.

The Naval Arctic Research Laboratory (NARL) started closedown procedures in 1980, culminating in the termination of science support activities and the

departure of University of Alaska staff in October. Operations and maintenance personnel were also reduced as closedown operations progressed, although the final phase has not yet been implemented. GMCC staff moved to housing provided by the National Weather Service (NWS) in the town of Barrow in July and found alternate sources for all supplies and services formerly provided by NARL, with the exception of station electricity, which is still being supplied by NARL.

2.2.2 Programs

Programs carried out at BRW are listed in table 4. Comments on some of the programs follow.

Carbon Dioxide

The continuous analyzer was switched from CO₂-in-N₂ reference gases to CO₂-in-air gases in 1980, with three intercomparisons of CO₂/N₂ and CO₂/air standards being done onsite. Unfortunately, the CO₂/N₂ standards were drained while in transit to Scripps for final calibration, necessitating another series of runs to infer a final value for the lost tanks. Now our procedure for shipping valuable reference tanks is to send the tanks and valve handles separately.

The Cincinnati subzero freezer for freezing water vapor out of samples failed in April, causing suspension of the continuous CO₂ program until a new Cryo-Cool freezer arrived in May.

A second CO₂ sampling line was installed in May. This line, which alternately serves as a quality check on the sampling stack and a ground-level sampling line for periods of high CO₂ activity in the tundra, runs on a time-share basis with the stack.

A 5-ℓ glass flask sampling program began in 1980. Pairs of 5-ℓ flask samples are taken twice-monthly to augment the other CO₂ flask programs.

ICDAS

Severe difficulties with the Xerox multiplexor and Wang tape drive caused much downtime late in the year. New components and a visit to Barrow by some of the Boulder electronics staff solved most of the problems.

Lidar

The lidar hut was repositioned in July to get it out of the winter snow-drift pattern caused by neighboring buildings. System components began arriving in August, but the final parts did not arrive until December. Consequently, there were no lidar operations in 1980.

Total and Surface Ozone

Barrow's Dobson spectrophotometer no. 76 was in Boulder from January to May 1980 for calibration and refitting.

A modernized Dasibi ozone meter was installed in September.

Table 4.--Summary of sampling programs at Barrow in 1980

Monitoring program	Instrument	Sampling frequency
<u>Gases</u>		
Carbon dioxide	URAS-2T infrared analyzer	Continuous
	Glass flask pairs	1 pair wk ⁻¹
	5-ℓ glass flask pairs	2 pair mo ⁻¹
Surface ozone	Dasibi ozone meter	Continuous
Halocarbons	Flask samples	1 pair wk ⁻¹
Total ozone	Dobson spectrophotometer #76	3 day ⁻¹
<u>Aerosols</u>		
Condensation nuclei	G.E. CN counter	Continuous
	Pollack counter	Discrete
Optical properties	Four-wavelength nephelometer	Continuous
Vertical distribution	Lidar	Discrete
<u>Solar radiation</u>		
Global spectral irradiance	Four Eppley pyranometers with Q1, GG22, OG1 and RG8 filters	Continuous
Direct spectral irradiance	Eppley normal incidence pyrhemometer with filter wheel	Discrete
Turbidity	Eppley sun photometer	Discrete
<u>Meteorology</u>		
Air temperature	Thermistor	Continuous
	Hygrothermograph	Continuous
Relative humidity	Dewpoint hygrometer	Continuous
	Sling psychrometer	Discrete
Air pressure	Transducer	Continuous
	Microbarograph	Continuous
	Mercurial barometer	Discrete
Wind (speed and direction)	Bendix aerovane	Continuous
Ground temperature	Thermistor	Continuous
<u>Precipitation chemistry</u>		
pH and conductivity	Wide-mouth polyethylene collector (samples analyzed at MLO)	Discrete
	Collection of snow on tundra (samples analyzed at MLO)	2 mo ⁻¹
<u>Cooperative programs</u>		
Total surface particulates (DOE/EML)	High-volume sampler	Continuous
Arctic haze particulates (URI)	High-volume samplers	Continuous
	Radon monitors	Discrete
Global radiation (SRL)	Eppley pyranometers	Continuous
	Temple U. sunburning meter	Continuous
CO ₂ sampling (SIO)	Flask samples	2 sets mo ⁻¹
Precipitation gage (Soil Conservation Service)	Wyoming shielded precipitation gage	2 readings mo ⁻¹
Carbonaceous particles (LBL)	High-volume sampler	Continuous
	Surface snow samples	2 mo ⁻¹
Halocarbons (OGC)	Flask samples	3 flasks wk ⁻¹
Incident and reflected radiation (U. of Alaska)	Up-down pyranometers	Continuous

2.2.3 Cooperative Programs

A halocarbon flask sampling program began with the Oregon Graduate Center (OGC) in May. Three flask samples are taken per week.

The University of Rhode Island (URI) radon experiment was terminated in August.

OGC, Brookhaven National Laboratories, and the National Bureau of Standards ran filters on one of URI's samplers during winter, 1980-81.

A four-radiometer system, composed of two upward-looking and two downward-looking instruments, was installed by the University of Alaska Geophysical Institute in September.

The Barrow staff began making occasional trips to the neighboring village of Atkasuk, 60 mi SSW of Barrow, to read and record measurements by a Wyoming shielded precipitation gage located near there, for the U.S. Soil Conservation Service.

A temporary filter project, to sample for HNO_3 , NH_3 , and SO_2 , was run for the National Center for Atmospheric Research (NCAR) from April through June.

2.3 Samoa

2.3.1 Facilities

There were no permanent additions or modifications to the Samoa Observatory (SMO) facilities during 1980. However, temporary facility additions were made for SEAREX (Sea-Air Exchange program), a planned 1981 project sponsored by the National Science Foundation (NSF). The additions consisted of a number of small prefab buildings located on Matatula Point, where the SEAREX air-sampling experiments will be performed. Five buildings were added: four on the point and one on the ridge adjacent to the GMCC remote sampling tower. Three of the five buildings will be used for laboratory work and two for storage and personnel shelter. Disposition of the buildings after completion of the experiments will be decided later.

The primary SEAREX facility at Matatula Point consists of two walkup towers (Upright Scaffold brand) of 60- and 42-ft heights, used for air and precipitation samplings, respectively. All materials for the buildings and towers were furnished by SEAREX. In anticipation of the increased electrical load from air-sampling pumps, an additional power line was also installed to Matatula Point, with its own meter. The SEAREX project will thus be able to purchase its own electrical power and not overload the GMCC system and backup generator.

2.3.2 Programs

All 1980 programs at SMO are summarized in table 5. Additional comments follow.

Table 5.--Summary of sampling programs at Samoa in 1980

Monitoring program	Instrument	Sampling frequency
<u>Gases</u>		
Carbon dioxide	URAS-2T NDIR analyzer	Continuous
	Evacuated glass flasks	Discrete
Surface ozone	Electrochemical concentration cell	Continuous
	Dasibi ozone meter	Continuous
Total ozone	Dobson spectrophotometer #42	Discrete
Fluorocarbons	Flask sampling	1 wk ⁻¹
<u>Aerosols</u>		
Condensation nuclei	G.E. CN counter	Continuous
	Pollak CN counter	Discrete
Scattering properties (surface air)	Four-wavelength nephelometer	Offline all year
Atmospheric turbidity	Volz sun photometer	Discrete
<u>Solar Radiation</u>		
Global spectral irradiance	Four Eppley pyranometers with quartz, GG22, OG1, and RG8 filters	Continuous
Direct spectral irradiance	Eppley NIP with filter wheel (OG1, RG2, RG8)	Discrete
	Eppley NIP/equatorial mount combination	Continuous
<u>Meteorology</u>		
Temperature (air)	Thermistor	Continuous
	Thermograph	Continuous
	Psychrometer	Discrete
	Max.-min. thermometers	Discrete
Temperature (soil)	Thermistor	Continuous
Temperature (dew-point)	thermistor with LiCl dew cell	Continuous
Relative humidity	Hygrothermograph	Continuous
Wind (speed and direction)	Bendix aerovane	Continuous
Pressure	Transducer (capacitance type)	Continuous
	Microbarograph	Continuous
	Mercurial barometer	Discrete
<u>Precipitation chemistry</u>		
pH and conductivity	Orion pH meter	Discrete
	Beckman conductivity bridge	
	Samples sent to MLO for further analysis on ion chromatograph	
<u>Cooperative programs</u>		
ALE project--F-11, F-12, N ₂ O, CHCl ₃ , CCl ₄ (OGC)	HP 5840A gas chromatograph	1 h ⁻¹
CH ₄ , CO, CO ₂ (OGC)	Carle gas chromatograph	3 h ⁻¹
Flask program--CH ₃ I, CH ₃ Cl, CH ₄ , CO (OGC)	SS flasks, analyzed at OGC-- 3 flasks per set	1 wk ⁻¹
Wet-dry deposition-- since may 1980 (NADP)	HASL wet-dry collector	1 wk ⁻¹
Wet-dry deposition (DOE/EML)	HASL wet-dry collector	1 mo ⁻¹
Wet deposition	Misco collector	1 mo ⁻¹

The GMCC group of trace gas and aerosol sensors remained unchanged at the Samoa station during 1980. Absent, however, for the entire year, was the four-wavelength nephelometer. It had been returned to the United States for installation of a new PM tube detector that requires no cooling. It is hoped that this modification will eliminate the moisture problems experienced with the older model detector that required cooling.

A comprehensive CO₂ flask sampling program was also maintained throughout the year as a check for the GMCC/SMO continuous-analyzer air sample line and also as a means of examining possible effects of excessive water vapor, characteristic of Samoan ambient air, on flask samples sent to Boulder.

2.3.3 Cooperative Programs

In May 1980, Samoa GMCC became an NADP collection site, and a weekly rain sample plus a bimonthly dry-deposition sample has been sent regularly to the Central Analytical Laboratory of ISWS. The EPA Misco collector as well as the DOE/EML wet-dry collector will eventually be phased out.

The OGC gas chromatograph installation was operational all year and is the only other major cooperative program. In addition, an OGC weekly flask sampling program was begun to measure methyl iodide concentrations.

2.3.4 Special Projects

A comprehensive tracer study of Matatula Point was performed during April. F. Shais, professor of chemical engineering at California Institute of Technology (CIT), was the principal investigator. D. Reible (CIT), R. Cayer (URI/SEAREX), and Samoa GMCC personnel assisted in 18 experiments using SF₆, smoke flares, and balloons. The purpose of the investigation was to examine the possible contamination effects that local vegetation and terrain might have on planned SEAREX operations in 1981. Results of the tracer study confirmed Cape Matatula as a very good sampling platform. Discussions have begun that may possibly result in publication of the tracer experiment results as a NOAA Technical Memorandum.

2.4 South Pole

2.4.1 Facilities

A structural defect in the Clean Air Facility (CAF) at the South Pole Observatory (SPO) was discovered in late 1979. Cross-member I-beams were found to be deflected more than the design allowed. Reinforcements were made in the 1980-81 summer season.

Electrical power to the CAF was adequate. The room housing GMCC equipment, however, was not adequately wired for the load. Additional equipment placed on certain outlets caused circuit breakers to trip because the room was wired more as living quarters than as a scientific laboratory.

The CAF was adequately built and insulated so that the provided heaters maintained an average room temperature of 21°C. Since all the heaters were

manually set, outside fluctuations in windspeed and temperature caused room temperature fluctuations. There appeared to be a direct correlation between room temperature change and CO₂ analyzer drift. Thermostatically controlled heat would reduce these fluctuations.

The sampling stacks used by GMCC, the University of Maryland, and the Department of Energy (DOE), all required cleaning during the winter because of snow and frost accumulations. At one time, high winds blowing from grid 310° over the inlet of the GMCC gas-sampling stack caused sufficient vacuum force to draw room air up into the stack.

A humidifier was used throughout the year to suppress static discharge. At no time was static buildup noticed.

2.4.2 Programs

SPO programs for 1980 are listed in table 6 and briefly described below.

ICDAS

The NOVA 1220 and associated equipment ran well during the year with only minor outages. (The NOVA power supply failed in December 1979.) The Wang tape drive failed on October 19, 1980, with a burned-out fixed-reel file arm sense lamp.

Modifications to ICDAS included a new NOVA front panel, new Chronolog clock, and a revised edition of the basic operating software (BOSS 79001). The revised software was implemented in November 1979.

The Deltec uninterruptible power supply was shipped to American Samoa in December 1979.

Carbon Dioxide

Continuous measurements of carbon dioxide began on November 18, 1979. The program was restarted after being shut down in November 1978. The same reference gases used before this shutdown were used in the restart. During the first few months the program was characterized by a high zero drift rate and a need for frequent alignments. After station closing, the analyzer settled down and the program proceeded smoothly. A CO₂-in-air reference tank was installed on March 16, 1980, as a surveillance gas. Discrete sampling by flasks continued but at a rate of one pair per week. Samples were alternately taken on the CAF roof and through the analyzer system.

Solar Radiation

The heater blower system worked fairly well in preventing ice buildup on the pyranometer domes. Heavy insulation of the system prevented heat loss and allowed more warm air to the domes.

Calibrations were made once per month on the solar radiation preamplifiers.

Data were collected to study the effect of thermal gradients on the pyranometers' casings and filters caused by heating from the deicing blowers.

Table 6.--Summary of sampling programs at South Pole in 1980

Monitoring program	Instrument	Sampling frequency	Data record
<u>Gases</u>			
Carbon dioxide	0.5-l evacuated glass flasks, hand aspirated/through analyzer	1 pair wk ⁻¹	Nov 79-present
Surface ozone	Dasibi ozone meter	Continuous	Jan 76-present
Total ozone	Dobson spectrophotometer #80	Discrete	Dec 63-present
Fluorocarbons	300-ml stainless steel sampling cylinders	1 pair wk ⁻¹ 1 pair wk ⁻¹ austral summer 2 pair mo ⁻¹ austral winter	Jan 77-Dec 79 Jan 80-present Jan 80-present
<u>Aerosols</u>			
Condensation nuclei	G.E. CN counter Pollak CN counter Long-tubed Gardner CN counter	Continuous Discrete, 2-4 day ⁻¹ Discrete, 1 day ⁻¹	Jan 74-present Jan 74-present Jan 74-Aug 80
Optical properties	Four-wavelength nephelometer	Continuous	Jan 79-Jan 80
<u>Solar radiation</u>			
Global spectral irradiance	Four Eppley pyranometers with quartz, G622, OG1, and RG8 filters Ultraviolet radiometer	Continuous during austral summer	Feb 74-present
Direct spectral irradiance	NIP on equatorial tracker Filter wheel normal incidence pyrheliometer with quartz, OG1, RG2, and RG8 filters	Continuous during austral summer Discrete during austral summer	Oct 75-present Jan 77-present
<u>Meteorology</u>			
Air temperature	Thermistor (naturally venti- lated shield)	Continuous	Mar 77-present
Snow temperature	Thermistor	Continuous	Jul 77-present
Pressure	Transducer Microbarograph Mercury column	Continuous Continuous 3 day ⁻¹	Dec 75-present Feb 80-present Jan 80-present
Wind (speed and direction)	Bendix-Friez aerovane and recording system	Continuous	Dec 75-present
Atmosphere moisture content	Du Pont 303 moisture monitor	Continuous	Mar 77-present
<u>Miscellaneous</u>			
Room temperature	Thermistor	Continuous	Jul 78-present
<u>Cooperative programs</u>			
Carbon dioxide (SIO)	5-l evacuated glass flasks	2 mo ⁻¹ (3 flasks per sample)	1957-present
Total surface particulates (atmosphere trace metals) (DOE/ERDA/HASL)	Motor-driven rotary lobe blower (high-volume air sampling through filters)	Continuous (filters changed 4 times mo ⁻¹)	May 70-present
Turbidity (NOAA/ARL)	Dual-wavelength sun photometer	Discrete during austral summer	Jan 74-present
Carbon-14 sampling (NOAA/ARL)	Pressurized steel spheres	500 lb in ⁻² ambient air day ⁻¹ , for 6 days	Jan 74-present
Atmospheric chemistry (U. of Maryland and URI)	High-volume filters	Continuous	Jan 79-present
Fluorocarbons (OGC)	5-l evacuated stainless steel cylinders	3 times during austral summer (3 flasks per sample)	1980

Aerosols

The four-wavelength nephelometer was shipped to Boulder in January 1980 for upgrading. Observations with the long-tubed Gardner CN counter stopped in November 1980 because of poor performance. Continuous aerosol measurements with the G.E. CN counter were made all year and were checked daily with the Pollak CN counter.

Surface Ozone

Surface ozone was measured using a Dasibi ozone meter. Measurements with the ECC meter were discontinued the previous year. No major problems occurred. The MEC-1000 ozone generator failed on two occasions.

The Dasibi manual recommends inspection of the absorption tubes once every 2 months, and cleaning if necessary. Regular cleaning of the tubes, regardless of the inspection, reduced meter noise significantly.

Halocarbons

Sampling frequency was once per week during the austral summer as in previous years. Sampling in the winter was changed from once per month to twice per month. Flasks for use in the winter were pressurized with outside air and stored.

Meteorology

The GMCC wind sensor was realigned to a north-south line surveyed by USGS. The system was overhauled at the same time.

A microbarograph and a mercury column were received in early 1980. These provided a backup and check on the pressure transducer.

The Du Pont 303 moisture monitor malfunctioned between February 14 and November 9, 1980. At that time, the data were found to be several orders of magnitude low. The problem was corrected by replacing the sensor cell.

2.4.3 Special Project

A special project involving processing of GMCC data tapes was carried out at SPO. Fortran programs were written to enable SPO, for the first time, to examine the tapes written by ICDAS. These programs print and plot data in various ICDAS channels for data quality checks. Visual checks of the data by means of graphs help ensure that the instruments and ICDAS are performing properly. These programs are rudimentary, but can be expanded for more sophisticated use.

The computer system at SPO is composed of two 32K and one 16K Hewlett-Packard minicomputers. Peripherals include five tape drives, three terminals, two line printers, and one x-y plotter. The programming languages available on the system are Basic and Fortran IV.

During the winter-over period, six separate Fortran programs were written to read and print compositely either the six solar radiation channels, the six meteorological channels, the resultant windspeed and wind direction, or the separate channels of carbon dioxide, surface ozone, and aerosols. Plots of data in the various channels are made through a different program. For convenience, a program was written to pack hourly averages from the GMCC data tape onto a separate tape. One tape holds nearly 1 year of hourly averaged data. All programs that read directly from the GMCC data tape make use of a routine, written by W. Smythe of UCLA, which converts Data General floating point numbers to HP floating point numbers.

In the future, the SPO system could be used to provide many additional services: for example, to perform statistical calculations, to provide tape-copying facilities to ensure against data loss, and to maintain detailed records of instrument performance.

3. CONTINUING GMCC PROGRAMS

3.1 Carbon Dioxide

3.1.1 Analyzer CO₂ Measurements

CO₂ measurements made with continuously operating nondispersive infrared gas analyzers were continued during 1980 at the four GMCC stations. Data acquisition and processing procedures remained identical to those used in the past. The complete record (including 1980 data) of provisional mean monthly CO₂ mole fractions for BRW, MLO, SMO, and SPO is given in table 7. Plots of the data are shown in fig. 1.

The data are presented in the WMO 1974 CO₂-in-air mole fraction scale, i.e., with tentative pressure-broadening corrections applied. Final corrections to the data are yet to be made and will be based on reprocessing of the data, using improved working-reference-gas concentration values and applications of more precise pressure-broadening corrections. Additional corrections to the SMO data will be needed to account for air line sampling problems that were experienced at the station in the past, caused by the high moisture content of the Samoa atmosphere.

Table 7.--Provisional mean monthly CO₂ mole fractions in ppm for Barrow, Mauna Loa, Samoa, and South Pole

Year	Jan	Feb	Mar	Apr	May	Jun	Jul	Aug	Sep	Oct	Nov	Dec
<u>Barrow</u>												
1973	--	--	--	--	--	--	324.4	322.7	325.7	330.3	334.1	334.5
1974	339.1	336.8	337.6	338.9	337.4	336.4	331.0	325.5	326.4	330.1	333.3	336.7
1975	338.5	338.7	338.2	338.5	339.6	336.1	329.9	324.7	325.8	330.2	335.3	337.0
1976	337.6	337.8	338.8	338.9	338.2	337.1	331.3	323.8	325.1	330.1	334.2	336.5
1977	336.7	336.9	338.2	339.1	339.3	337.8	330.1	326.8	328.0	332.2	334.9	338.8
1978	339.4	340.2	341.7	341.1	340.8	339.6	332.0	328.3	328.6	332.2	338.1	338.6
1979	339.4	340.6	341.7	341.4	341.9	340.9	332.4	327.4	329.4	332.3	337.6	340.7
1980	341.1	341.9	342.9	343.5	343.1	342.7	336.5	331.7	331.3	338.1	340.4	342.9
<u>Mauna Loa</u>												
1974	--	--	--	--	332.9	331.8	330.5	328.5	326.9	326.8	328.0	329.3
1975	330.5	331.2	331.9	333.0	333.6	333.0	331.3	329.4	328.1	328.4	329.4	330.7
1976	331.6	332.5	333.3	334.6	334.8	334.2	332.5	330.3	328.8	328.6	329.9	330.4
1977	332.7	333.1	334.7	335.9	336.6	336.0	334.4	332.3	331.1	331.2	332.6	333.9
1978	335.1	335.3	336.4	337.8	337.9	337.9	336.3	334.2	332.0	332.4	333.7	334.8
1979	336.0	336.5	337.9	338.5	339.0	339.1	337.4	335.2	333.8	334.3	335.1	336.4
1980	337.6	337.9	339.6	340.4	341.1	340.8	338.7	336.8	335.1	335.2	336.4	337.5
<u>Samoa</u>												
1976	333.4	333.0	332.5	332.4	331.7	332.2	332.1	332.2	332.4	332.5	333.1	333.3
1977	333.0	332.5	333.3	333.3	333.6	334.6	334.2	334.1	333.8	335.0	335.2	--
1978	--	335.6	335.4	335.8	335.4	335.7	335.2	335.7	--	--	--	--
1979	--	--	335.7	336.6	336.0	336.4	336.7	336.7	336.6	336.9	337.0	337.3
1980	338.1	338.1	338.1	337.8	338.3	338.0	338.0	337.4	337.3	337.4	337.8	338.6
<u>South Pole</u>												
1975	329.1	329.2	329.3	328.9	328.6	329.1	329.8	330.5	331.0	331.3	330.5	329.4
1976	329.2	328.8	328.7	328.6	328.7	328.9	329.3	329.8	330.4	330.5	330.6	330.5
1977	330.0	330.9	330.7	330.8	330.9	331.1	331.3	331.7	332.1	332.4	332.4	332.1
1978	331.8	331.9	332.6	333.1	333.1	333.5	333.9	334.8	335.4	335.4	335.2	0.0
1979	--	--	--	--	--	--	--	--	--	--	--	--
1980	335.2	335.1	335.1	334.9	335.1	335.4	335.9	336.2	336.5	337.1	337.0	336.7

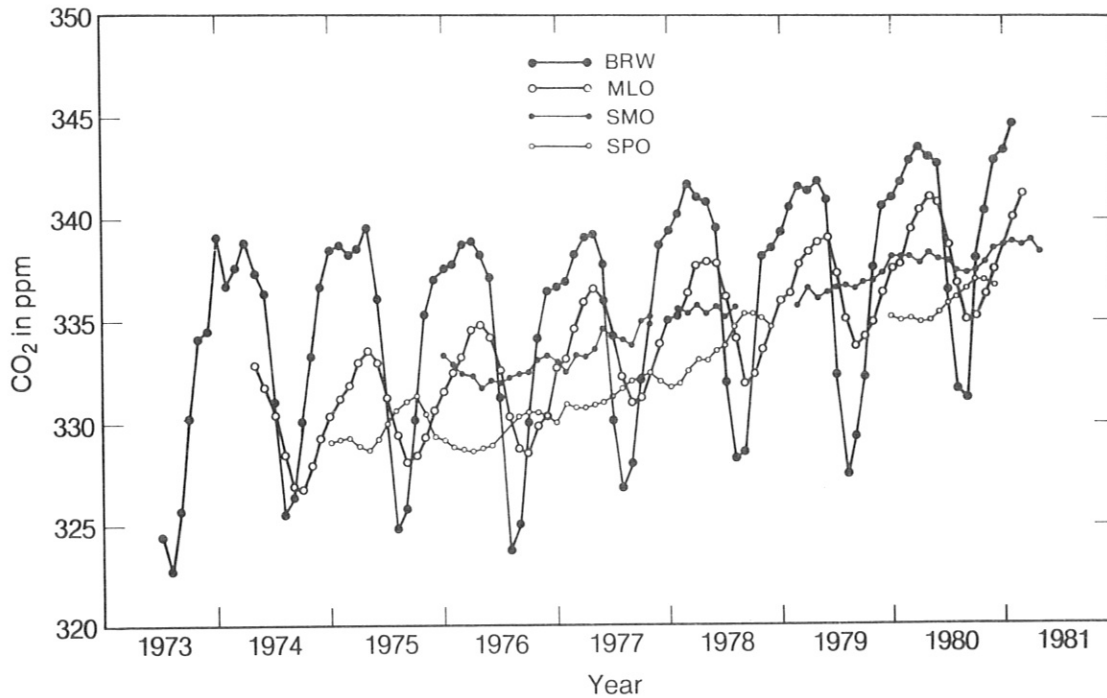


Figure 1.--Provisional mean monthly CO₂ mole fractions for GMCC observatories.

Relative errors in the data are estimated to be less than 1 ppm, except for the first 3 years of the Barrow data and sporadic intervals of the South Pole data where pressure-broadening corrections have been estimated only roughly. Systematic errors are believed to be generally less than ± 1 ppm when referred to an absolute CO₂ mole fraction calibration scale.

3.1.2 Flask Sample CO₂ Measurements

The GMCC CO₂ flask sampling program was expanded in 1980 to include three new stations, viz., Azores (Terceira Island, North Atlantic), Mould Bay (N.W.T.), and Seychelles (Mahé Island, Indian Ocean). A list of stations operating in 1980 is given below. Detailed information about these stations, e.g., location, siting, and cooperative agencies, is provided on page 19 of the GMCC No. 8 Summary Report for 1979 (Herbert, 1980).

1980 CO₂ flask sampling station network

American Samoa, S. Pac.	Mauna Loa, Hawaii
Amsterdam Is., Ind. Oc.	Mould Bay, N.W.T.
Ascension Is., S. Atl.	Niwot Ridge, Colo.
Azores (Terceira Is.), N. Atl.	Ocean Station M, N. Atl.
Cape Kumukahi, Hawaii	Palmer Station (Anvers Is.), Ant.
Cold Bay, Alaska	Pt. Barrow, Alaska
Cosmos, Peru	Pt. Six Mountain, Mont.
Guam (Marianas Is.), N. Pac.	Seychelles (Mahé Is.), Ind. Oc.
Key Biscayne, Fla.	South Pole, Ant.

Plots of 1979 and 1980 provisional CO₂ mole fractions, expressed in the 1974 WMO CO₂-in-air mole fraction scale, are shown in fig. 2. Here, pair sample CO₂ values agreeing to within 1 ppm have been averaged; for pair samples differing by more than 1 ppm, the lower value has been plotted. Some available data have been excluded from the plots following subjective analysis because of sampling problems experienced particularly in 1980.

These problems resulted primarily from contamination of the glass flasks with silicone grease residue following annealing of the flasks for cleaning. Additional problems were experienced when contamination occurred at times during flask evacuation and when CO₂-rich air leaked occasionally into evacuated flasks through improperly greased stopcocks. To avoid these sampling problems, the collection of ambient pressure samples in evacuated flasks is currently being phased out. Instead, a method of collecting pressurized air samples in reference-gas-filled flasks is being introduced. Flushing and filling of the flasks during sample collection is accomplished with a portable, mechanized pump apparatus. The flask stopcocks are, furthermore, now greased with Apiezon-N grease.

A prominent feature of the data plots of fig. 2 is the decrease in the amplitude of the CO₂ annual cycle in the Northern Hemisphere, with far-northern peak-to-peak values of approximately 15 ppm decreasing to essentially 0 ppm at the Equator. In the Southern Hemisphere, peak-to-peak annual cycle amplitudes of about 1 ppm are discernible.

Provisional 1979 annual mean, winter (January through March), and summer (July through September) CO₂ latitudinal gradients have been derived from the 1979 and 1980 flask sample data (see fig. 3). Note the large drawdown of CO₂ by growing plants in the Northern Hemisphere summer. The annual mean gradient plot of fig. 3 exhibits several interesting features. The pole-to-pole CO₂ difference is slightly greater than 3 ppm. Also, several maxima appear in the distribution. One occurs in the Northern Hemisphere north of approximately 40°N, which is where most fossil fuel CO₂ is released into the atmosphere. A second occurs at the Equator. A third maximum, possibly representing a Southern Hemisphere CO₂ source, is evident at about 65°S latitude. The existence of this maximum has been inferred from highly tenuous CO₂ observations made at Palmer Station, Antarctica. Additional analyses of the data as well as CO₂ measurements in middle-to-high latitudes of the Southern Hemisphere are needed to verify that this maximum is real.

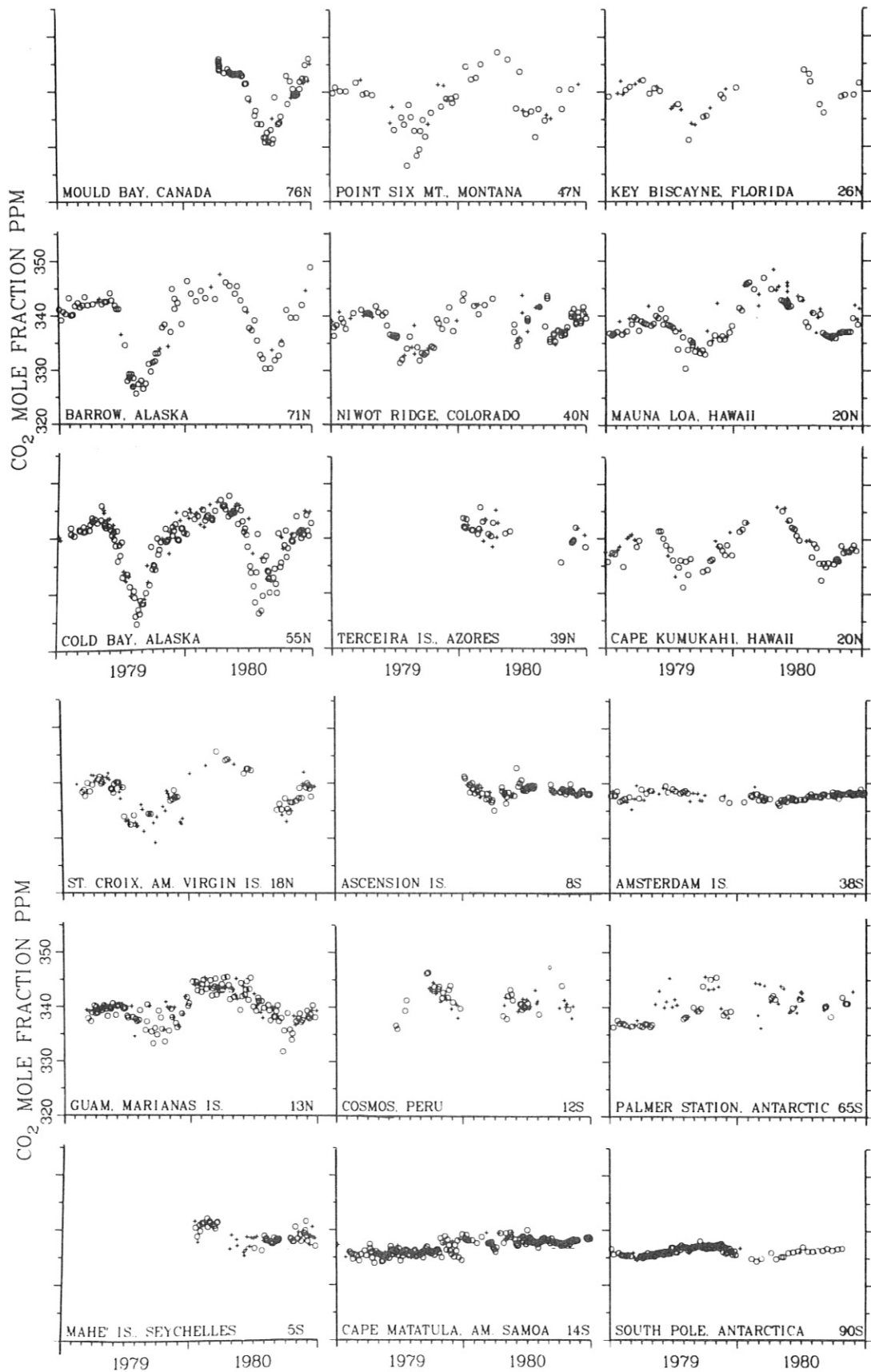


Figure 2.--Flask sample CO₂ mole fractions for stations in the GMCC CO₂ station network.

Plots of 1979 and 1980 provisional CO₂ mole fractions, expressed in the 1974 WMO CO₂-in-air mole fraction scale, are shown in fig. 2. Here, pair sample CO₂ values agreeing to within 1 ppm have been averaged; for pair samples differing by more than 1 ppm, the lower value has been plotted. Some available data have been excluded from the plots following subjective analysis because of sampling problems experienced particularly in 1980.

These problems resulted primarily from contamination of the glass flasks with silicone grease residue following annealing of the flasks for cleaning. Additional problems were experienced when contamination occurred at times during flask evacuation and when CO₂-rich air leaked occasionally into evacuated flasks through improperly greased stopcocks. To avoid these sampling problems, the collection of ambient pressure samples in evacuated flasks is currently being phased out. Instead, a method of collecting pressurized air samples in reference-gas-filled flasks is being introduced. Flushing and filling of the flasks during sample collection is accomplished with a portable, mechanized pump apparatus. The flask stopcocks are, furthermore, now greased with Apiezon-N grease.

A prominent feature of the data plots of fig. 2 is the decrease in the amplitude of the CO₂ annual cycle in the Northern Hemisphere, with far-northern peak-to-peak values of approximately 15 ppm decreasing to essentially 0 ppm at the Equator. In the Southern Hemisphere, peak-to-peak annual cycle amplitudes of about 1 ppm are discernible.

Provisional 1979 annual mean, winter (January through March), and summer (July through September) CO₂ latitudinal gradients have been derived from the 1979 and 1980 flask sample data (see fig. 3). Note the large drawdown of CO₂ by growing plants in the Northern Hemisphere summer. The annual mean gradient plot of fig. 3 exhibits several interesting features. The pole-to-pole CO₂ difference is slightly greater than 3 ppm. Also, several maxima appear in the distribution. One occurs in the Northern Hemisphere north of approximately 40°N, which is where most fossil fuel CO₂ is released into the atmosphere. A second occurs at the Equator. A third maximum, possibly representing a Southern Hemisphere CO₂ source, is evident at about 65°S latitude. The existence of this maximum has been inferred from highly tenuous CO₂ observations made at Palmer Station, Antarctica. Additional analyses of the data as well as CO₂ measurements in middle-to-high latitudes of the Southern Hemisphere are needed to verify that this maximum is real.

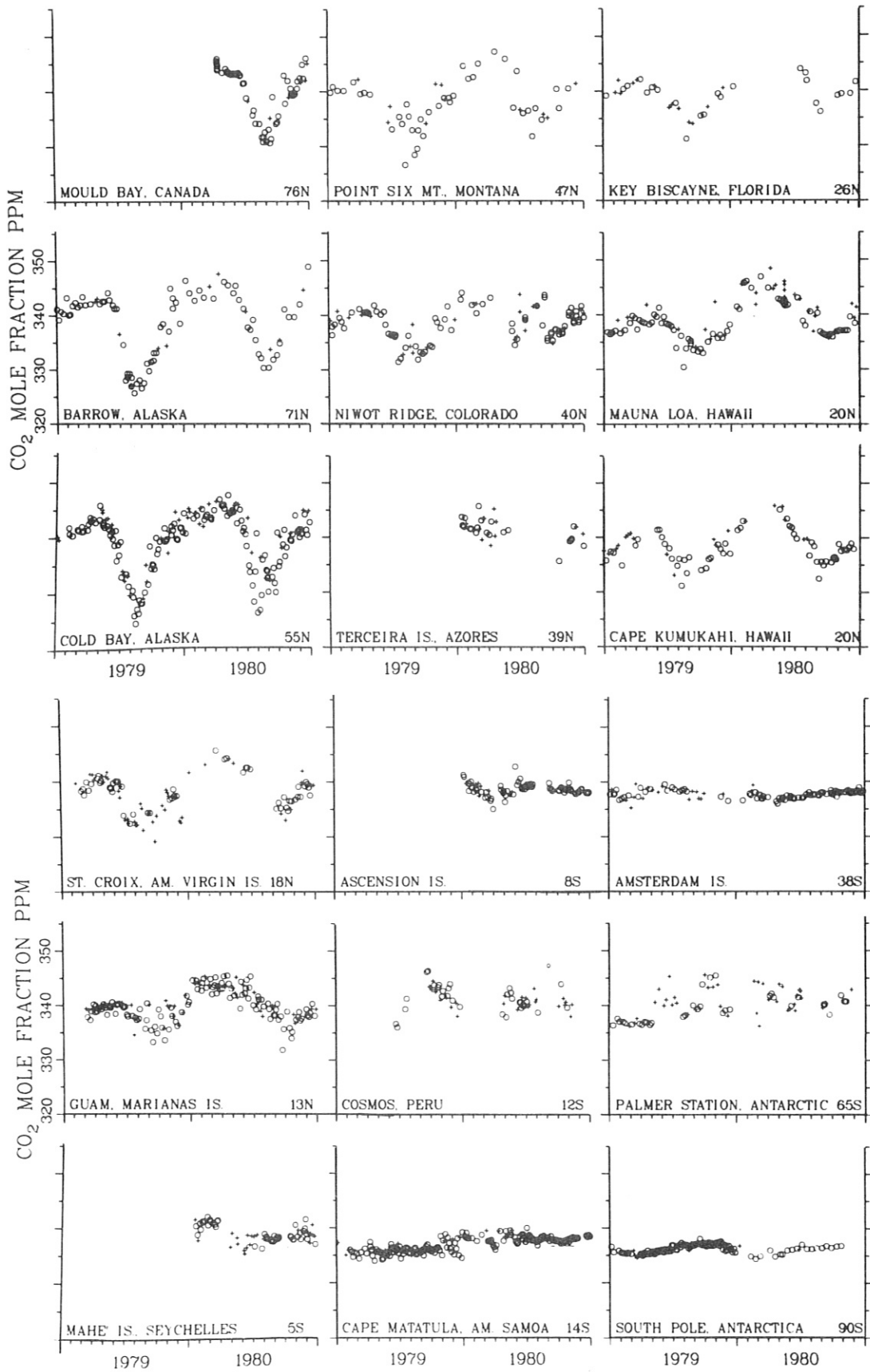


Figure 2.--Flask sample CO₂ mole fractions for stations in the GMCC CO₂ station network.

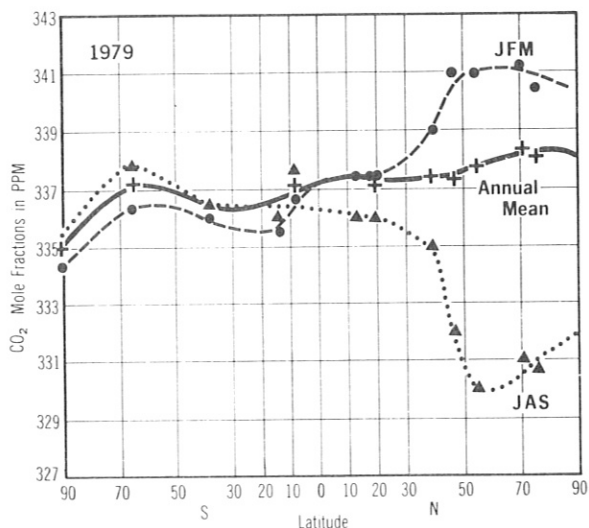


Figure 3.--Provisional 1979 annual mean, winter (January-March), and summer (July-September) CO₂ latitudinal gradients.

3.2 Total Ozone

3.2.1 Total Ozone Observations

Total ozone observations were continued during 1980 at 11 of 12 Dobson spectrophotometer stations that constitute the U.S. total ozone station network (see table 8). Observations at the 12th station, Tallahassee, Florida, are expected to be resumed in 1981.

3.2.2 Modernization and Calibration of Dobson Instruments

GMCC continued a program begun in 1977 within the global total ozone station network to upgrade foreign Dobson spectrophotometers under the auspices of the WMO Global Ozone Research and Monitoring Project. Instruments

Table 8.--1980 U.S. Dobson ozone spectrophotometer station network

Station	Period of record	Instrument number	Agency
Bismarck, N. Dak.	010163-present	33	NOAA/NWS
Caribou, Maine	010163-present	34	NOAA/NWS
Tutuila Is., Samoa	121975-present	42	NOAA/GMCC
Mauna Loa, Hawaii	010264-present	63	NOAA/GMCC
Wallops Is., Va.	070167-present	38	NOAA-NASA
Barrow, Alaska	080273-present	76	NOAA/GMCC
Nashville, Tenn.	010163-present	79	NOAA/NWS
Boulder, Colo.	090166-present	82	NOAA/GMCC Hdq.
White Sands, N. Mex.	010572-present	86	NOAA-Dept. of Army
Huancayo, Peru	021464-present	87	NOAA-Huancayo Obs.
Amundsen-Scott, Ant.	120563-present	80	NOAA/GMCC

Table 9.--1980 provisional mean monthly total ozone amounts (milli-atm-cm)

Station	Jan	Feb	Mar	Apr	May	Jun	Jul	Aug	Sep	Oct	Nov	Dec
Bismarck, N. Dak.	354	393	402	377	--	329	321	316	307	298	308	293
Caribou, Maine	378	454	418	416	408	383	360	326	328	309	320	372
Tutuila Is., Samoa	260	253	245	241	248	244	241	255	261	263	259	259
Mauna Loa, Hawaii	242	237	257	264	286	273	269	269	261	264	254	251
Barrow, Alaska	--	--	--	--	--	366	336	326	319	324	--	--
Wallops Is., Va.	315	374	352	370	363	358	330	322	303	305	287	322
Nashville, Tenn.	325	363	355	380	375	356	--	321	321	320	296	322
Boulder, Colo.	313	342	376	365	347	320	312	309	300	293	288	291
White Sands, N. Mex.	291	309	338	344	336	305	318	311	--	307	291	291
Huancayo, Peru	268	264	260	254	255	261	252	--	277	273	272	270
Amundsen-Scott, Ant.	324	303	--	--	--	--	--	--	--	--	318	361

modernized and calibrated in 1980 were nos. 97 and 99 in Buenos Aires, Argentina, and no. 114 in Cachoeira Paulista, Brazil.

To date, 40 instruments (see fig. 4) have been directly calibrated and 40 other instruments have been indirectly calibrated relative to World Primary Standard Dobson Instrument no. 83 that is maintained at GMCC in Boulder, Colorado. These 80 instruments represent a substantial fraction of approximately 110 existing Dobson spectrophotometers, 73 of which are currently in use for observations.

To standardize operating and calibrating procedures for Dobson spectrophotometers throughout the world, Operations Handbook--Ozone Observations with a Dobson Spectrophotometer was prepared (Komhyr, 1980) under the auspices of the World Meteorological Organization. Copies of the handbook are available from WMO in Geneva, Switzerland, or from the World Dobson Spectrophotometer Calibration Center, Air Resources Laboratories, R329, Boulder, CO 80303.

3.2.3 The Data

Daily 1980 total ozone amounts (applicable at local apparent noon at each station) for all stations in the U.S. network have been submitted for publication on behalf of WMO and are available in Ozone Data for the World, published by the World Ozone Data Center, Atmospheric Environment Service, 4905 Dufferin Street, Downsview, Ontario M3H5T4 Canada. Table 9 lists provisional mean monthly 1980 total ozone amounts for the NOAA observatories and cooperative stations.

3.2.4 Data Analysis and Related Research

Several research papers on ozone were presented by GMCC staff at the Quadrennial International Ozone Symposium held in Boulder, Colorado, 4-9 August 1980. Two papers were presented on the subject of ozone measurements and their accuracy. The first (Komhyr et al., 1981c) gave results of the SMO International Comparison of Dobson Ozone Spectrophotometers held in Boulder in

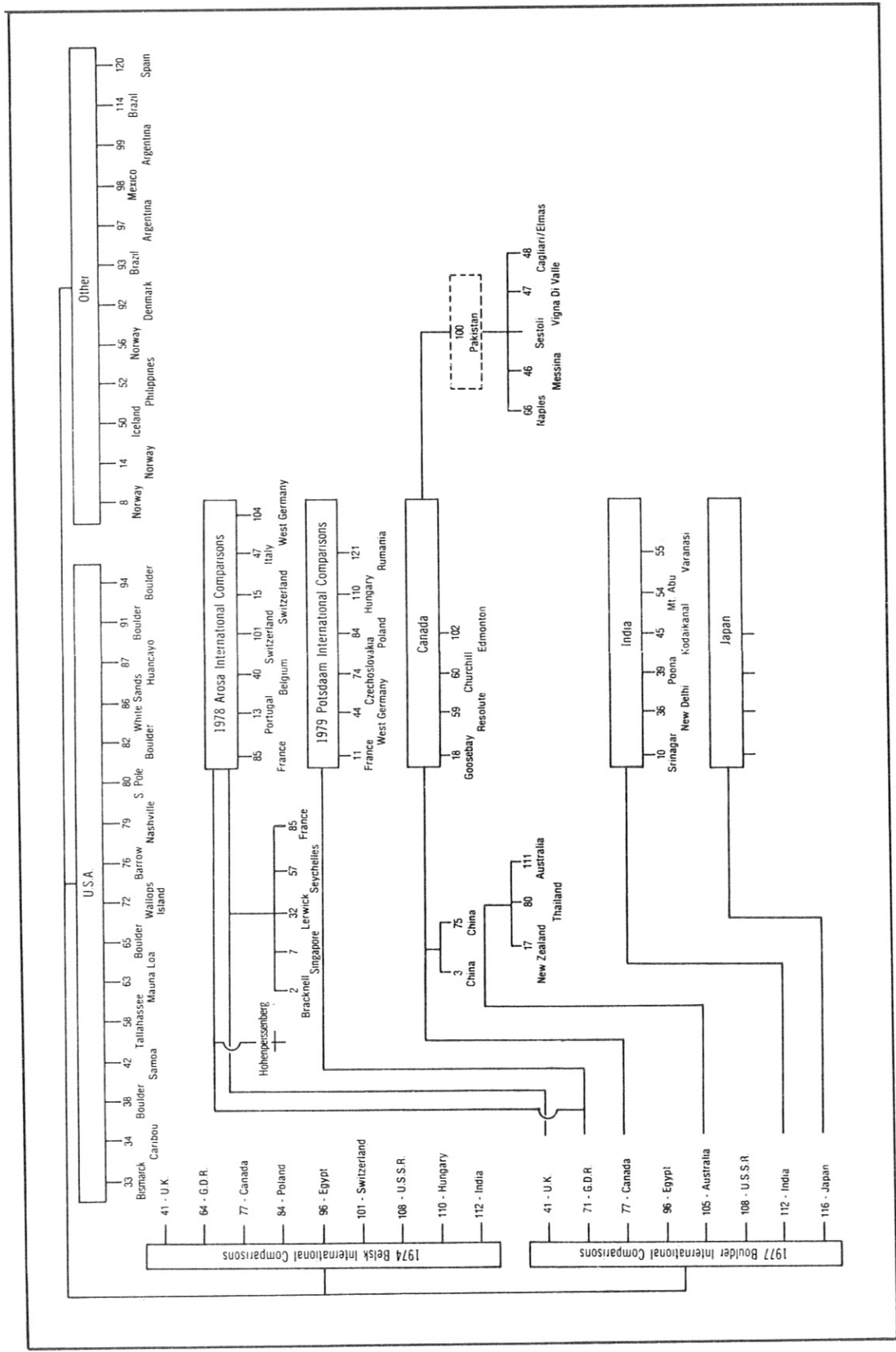


Figure 4.--Calibration of global network Dobson ozone spectrophotometers relative to World Primary Standard Instrument no. 83 (August 1980).

1977. Included were Umkehr observation comparisons and the results of a study made to determine the feasibility of calibrating Dobson spectrophotometers by standard lamps. The second (Komhyr et al., 1981b) dealt with the subject of a possible 5% systematic error in Dobson instrument total ozone measurements, as well as possible errors due to interfering absorbing species such as SO₂, NO₂, N₂O₅, H₂O₂, HNO₃, acetaldehyde, acetone, and acrotoin. Under the subject of data analysis, topics covered were a study of the quasi-biennial oscillation in ozone (Oltmans and London, 1981), and determination of the ozone trend at Bismarck, North Dakota, for the years 1963-79 (Komhyr et al., 1981a).

More recently, a least-squares-fit autoregressive trend model has been used to provide ozone trend data for North America for 1961-80. (An ozone trend is defined as the slope coefficient of the linear term in the autoregressive model applied to an ozone data record of about 10 years.) Results of the analysis confirm earlier findings that ozone increased over North America during the 1960's and indicated, further, that ozone decreased over North America during the 1970's.

Data used in the analysis were monthly mean total ozone values published by the World Ozone Data Centre in Canada. Included were Canadian and U.S. total ozone data for 1980 submitted to Canada for publication but not yet published. In the few instances where monthly mean total ozone amounts were not available, the data gaps were filled by interpolation.

The autoregressive trend model used was of the form

$$O(t) = b_0 + b_1 t + a_1 \cdot O(t - K_1) + a_2 \cdot O(t - K_2) + \dots + a_N \cdot O(t - K_N)$$

where

$O(t)$ = ozone concentration at time t ;

b_0 = linear trend intercept;

$b_1 t$ = time dependent linear trend; and

$a_N \cdot O(t - K_N)$ = autoregressive coefficients multiplied by the data at previous times (lags).

Model input data were ozone deviations from monthly normals (i.e., ozone data from which the annual cycle was removed.) The data were weighted according to the standard deviation of the long-term averages. An autocorrelation technique was used to identify significant lags (up to 30 months), and a sufficient number of the lag terms were included in the model, through a process of backward or forward elimination, to render the model residuals white noise. Results of the modeling, for various periods of record and 13 North America stations, are shown in tables 10 and 11 and fig. 5.

Note from table 10 that for the 1960's (~1961-70) the ozone trends computed for all stations are positive and significant in a number of cases. The combined* trend is significant at 3.4 ± 1.5 percent per decade, confirming

*Combined trend errors in this preliminary report have been computed without regard to the statistical homogeneity of the various data sets and may, therefore, require modification.

Table 10.--Autoregressive model ozone trend data for North America
Dobson spectrophotometer stations

Station	Period of record							~1961-1980
	~1961-1969	~1961-1970	1970-1980	1971-1980	1972-1980	1973-1980	1971-1979	
Bedford	5.4 ± 8.4	3.0 ± 6.1	--	--	--	--	--	--
Bismarck	-0.9 ± 6.9	4.4 ± 4.5	-3.8 ± 1.9	-3.3 ± 3.3	-2.5 ± 2.8	-3.5 ± 4.3	-2.8 ± 2.7	-1.7 ± 1.2
Boulder	-1.4 ± 7.7	2.9 ± 5.9	-0.5 ± 2.4	-2.6 ± 2.1	-2.0 ± 2.2	-0.4 ± 2.4	-3.7 ± 2.6	-0.7 ± 1.3
Caribou	1.9 ± 4.9	5.2 ± 5.0	-1.6 ± 2.7	-1.6 ± 3.1	-2.0 ± 4.0	0.4 ± 4.8	-6.0 ± 4.8	-1.9 ± 1.2
Churchill	0.4 ± 8.4	(10.8 ± 8.6)	-0.9 ± 2.6	-0.5 ± 3.9	-0.9 ± 4.1	0.9 ± 3.6	-3.1 ± 3.8	-0.8 ± 2.0
Edmonton	-0.9 ± 4.8	4.0 ± 3.1	-1.9 ± 3.2	-3.7 ± 4.2	-4.5 ± 4.6	-2.7 ± 5.6	-1.8 ± 3.5	-0.1 ± 1.1
Goose Bay	2.6 ± 5.0	5.7 ± 3.9	-2.1 ± 2.9	-5.0 ± 4.1	-3.7 ± 3.9	-4.3 ± 4.1	-6.4 ± 3.3	0.2 ± 1.2
Green Bay	2.1 ± 5.1	2.0 ± 3.4	--	--	--	--	--	0.6 ± 2.1
Nashville	(15.2 ± 5.8)	(9.7 ± 4.5)	-0.5 ± 2.0	0.5 ± 2.0	0.2 ± 3.3	0.7 ± 2.7	-0.5 ± 3.5	0.0 ± 1.1
Resolute	2.3 ± 4.7	1.5 ± 4.2	-0.4 ± 4.4	-1.7 ± 5.0	-3.8 ± 4.0	(8.6 ± 7.8)	-2.1 ± 3.7	-2.0 ± 1.8
Tallahassee	6.9 ± 8.8	--	--	--	--	--	-3.7 ± 6.1	--
Toronto	3.3 ± 3.9	2.3 ± 3.3	-0.9 ± 2.7	-1.0 ± 2.7	-1.5 ± 3.5	-2.8 ± 4.3	0.4 ± 3.7	0.7 ± 0.9
White Sands	--	--	--	-3.8 ± 4.3	-3.8 ± 4.3	-3.1 ± 4.3	-2.5 ± 4.3	--
Combined trends	2.0 ± 2.0	3.4 ± 1.5	-1.4 ± 1.0	-2.3 ± 1.2	-2.5 % 1.2	-1.6 % 1.4	-2.5 % 1.3	-0.6 % 0.5

Note: Trends are expressed in percent change in ozone per decade. Indicated trend uncertainties are 95% confidence interval standard errors. Combined trend values do not include anomalous data in parentheses.

Table 11.--Running 10-yr linear ozone trends derived from
North America Dobson spectrophotometer total ozone data

Station	Period of record													
	58-67	59-68	60-69	61-70	62-71	63-72	64-73	65-74	66-75	67-76	68-77	69-78	70-79	71-80
Bismarck						1.48 ±2.23	-0.37 ±2.48	-0.91 ±2.47	-2.45 ±2.65	-4.46 ±2.62	-2.81 ±2.13	-3.94 ±2.18	-3.7 ±2.12	-3.3 ±2.45
Boulder							-0.07 ±2.04	-1.85 ±2.31	-1.14 ±2.52	-6.48 ±2.99	-5.63 ±2.51	-9.12 ±3.30	-4.49 ±2.55	-1.76 ±2.08
Caribou						0.17 ±3.33	-0.51 ±2.25	-3.88 ±3.86	-3.17 ±3.34	-4.34 ±3.77	-1.34 ±2.98	-3.58 ±2.79	-2.78 ±3.08	-4.27 ±3.88
Churchill								-1.90 ±3.81	-2.84 ±3.37	-6.15 ±4.02	-10.77 ±4.24	-7.58 ±3.12	-2.36 ±2.73	-2.02 ±3.85
Edmonton	0.04 ±3.28	5.77 ±3.99	5.70 ±3.67	1.45 ±3.51	-0.34 ±3.35	-1.13 ±3.21	-3.02 ±2.93	-1.24 ±2.58	2.77 ±2.98	-0.61 ±3.07	-1.78 ±3.75	-4.02 ±4.02	-3.41 ±4.25	-3.88 ±3.82
Goose Bay					8.26 ±3.99	8.37 ±4.26	5.73 ±4.29	6.36 ±4.09	3.96 ±2.70	-1.93 ±3.11	-2.61 ±2.56	-1.41 ±1.90	-3.29 ±2.44	-4.29 ±3.05
Nashville						0.94 ±3.21	1.96 ±2.63	1.59 ±2.22	-0.17 ±2.11	-0.68 ±2.23	-1.21 ±3.61	-4.88 ±3.11	-0.61 ±2.79	1.17 ±2.77
Resolute	2.15 ±3.86	3.93 ±4.04	2.21 ±3.91	4.35 ±4.71	0.52 ±4.59	-0.67 ±5.33	-0.37 ±5.11	3.29 ±4.43	1.22 ±3.99	-4.07 ±5.64	-0.46 ±4.33	-2.13 ±5.18	0.88 ±5.32	-1.91 ±3.18
Toronto			4.01 ±3.18	0.11 ±2.93	-0.19 ±2.73	0.16 ±3.03	-2.48 ±2.72	1.24 ±2.76	1.18 ±2.93	0.63 ±2.72	4.00 ±3.81	-0.72 ±3.44	0.24 ±3.11	-0.14 ±2.99
Combined trends	1.1 ±2.5	4.8 ±2.8	4.0 ±2.1	2.0 ±2.2	2.1 ±1.9	1.3 ±1.4	0.1 ±2.8	0.3 ±1.1	-0.1 ±1.0	-3.1 ±1.2	-2.5 ±1.1	-4.2 ±1.1	-2.2 ±1.1	-2.3 ±1.1

Note: Trends are expressed in percent ozone change per decade. Indicated trend uncertainties are 95% confidence level standard errors. Above results have been derived from autoregressive model ozone trend analyses.

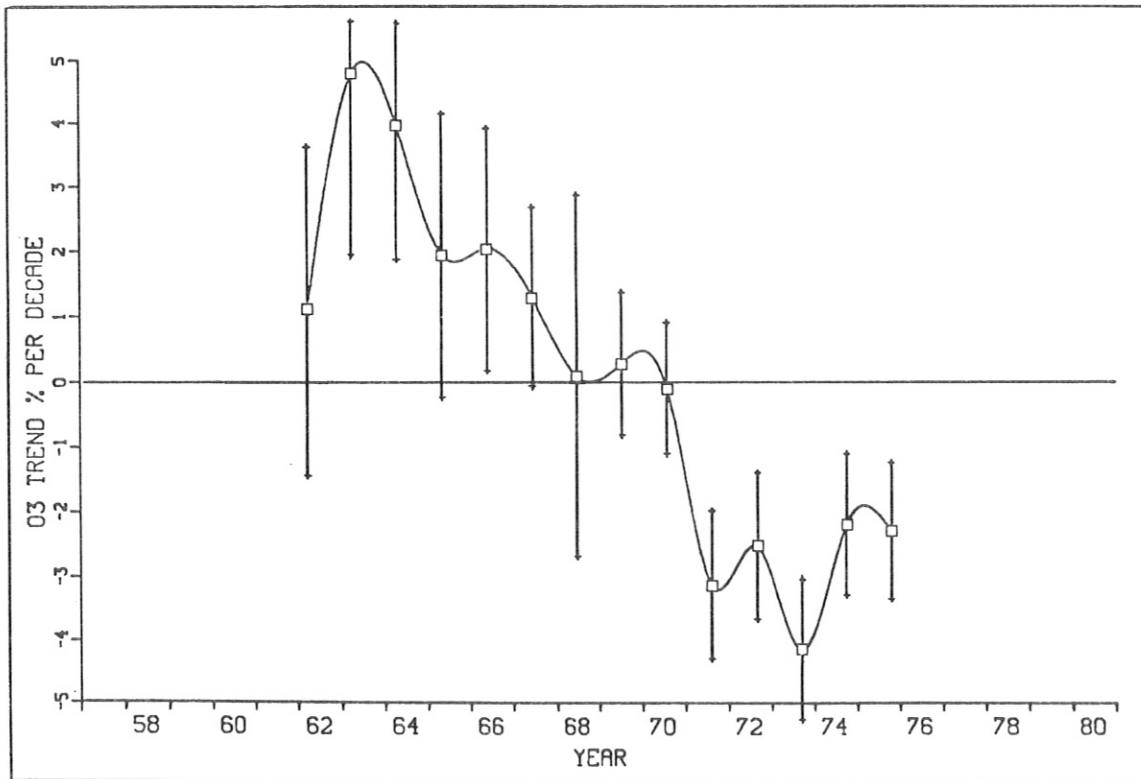


Figure 5.--Mean ozone trend data for North America. Values above the zero line indicate increasing ozone; negative values indicate decreasing ozone.

results obtained in the past. (The indicated error is the 95% confidence interval standard error.) If 1970 data are eliminated from the analysis (see table 10, ~1961-69 data) the computed combined trend is 2.0 ± 2.0 percent per decade which is just barely significant, suggesting that the ozone increase determined for the 1960's may or may not have been the result of an anomalously high ozone amount in 1970 over North America.

For time intervals in the 1970's (see table 10) the ozone trends for the various stations are predominantly negative but not significant individually in most cases. However, the combined trends for the various time periods ranging from 8 to 11 years are all negative and significant at the 95% confidence interval.

It is interesting to note from the last column in table 10 that ozone decreased, on the average, over North America during 1961-80 at a rate of about -0.6% per decade; i.e., there has been an ozone decrease of about 1% since the early 1960's.

Table 11 shows running 10-yr linear ozone trends for nine North American stations for intervals 1958-67 through 1971-80. The combined-trend data of table 11 are plotted in fig. 5. Here the ozone increase prior to 1970 and ozone decrease after 1970 are clearly portrayed.

3.3 Ozone Vertical Distribution

3.3.1 Operations

Regular measurements of the vertical distribution of ozone using the Umkehr technique were continued at Boulder with an average of between seven and eight observations completed each month. During the course of the year, a computer program was implemented that simplifies the selection of data at the designated sun angles and prepares data for submission to the World Ozone Data Centre in Toronto. This program also provides more efficient quality control of the data.

Work began on modification of a Dobson ozone spectrophotometer to allow for automatic acquisition of zenith skylight intensity information used in obtaining ozone vertical distribution by the Umkehr technique. Since this instrument will be able to make observations on the A-, C-, and D-wavelength pairs, it will gather data suitable for inversion to ozone profiles using the "short" Umkehr method. (See GMCC Summary Report No. 7 [Mendonca, 1979], sec. 4.1.) This microprocessor-controlled instrument will greatly increase the number of observations and reduce the manpower required to carry out such observations.

Ozonesonde observations with the ECC sensor were made throughout the year in support of three research projects: (1) comparison of Umkehr and ozonesonde ozone vertical profiles; (2) an intensive series of flights following the Mt. St. Helens volcanic eruption; and (3) tests to see if successful flights can be made to 40-km altitudes to measure ozone in this photochemically important region.

3.3.2 Data Analysis

Mean-monthly ozone partial pressures derived from Umkehr observations for nine levels in the atmosphere are shown in fig. 6 for the period of observations at Boulder. In the days following the eruption of Mt. St. Helens, the frequency of vertical ozone profile measurements was increased to see if that event had any discernible immediate effect upon the ozone distribution. The time history of these measurements for eight layers, beginning in mid-April and extending through June 1980 is shown in fig. 7. These values represent the average ozone partial pressure in layers approximately 5 km thick extending from 5 to 45 km. Also shown is the total ozone amount for this period.

In the days following the eruption, there are no readily discernible effects in the measured ozone amounts except perhaps in the two highest Umkehr layers (35-40, 40-45 km) where there seems to be an indication of lower ozone content. Such a dip in ozone is not inconsistent with measurement uncertainties and natural atmospheric variability, but might also be due to the effect of stratospheric aerosols upon the measurements. Such aerosols can produce errors in measured ozone amounts with lower than actual amounts indicated. (See GMCC Summary Report No. 8 [Herbert, 1980], sec. 4.1.) Note that the dip does not appear until 3 to 4 days after the eruption. Why the effect would not show up when the original plume passed over Boulder is not clear, although the dispersion of particles into a geometrically thicker layer in the stratosphere might have been a factor. Any effects by the eruption upon the ozone measurements appear to have been minor and transitory at most.

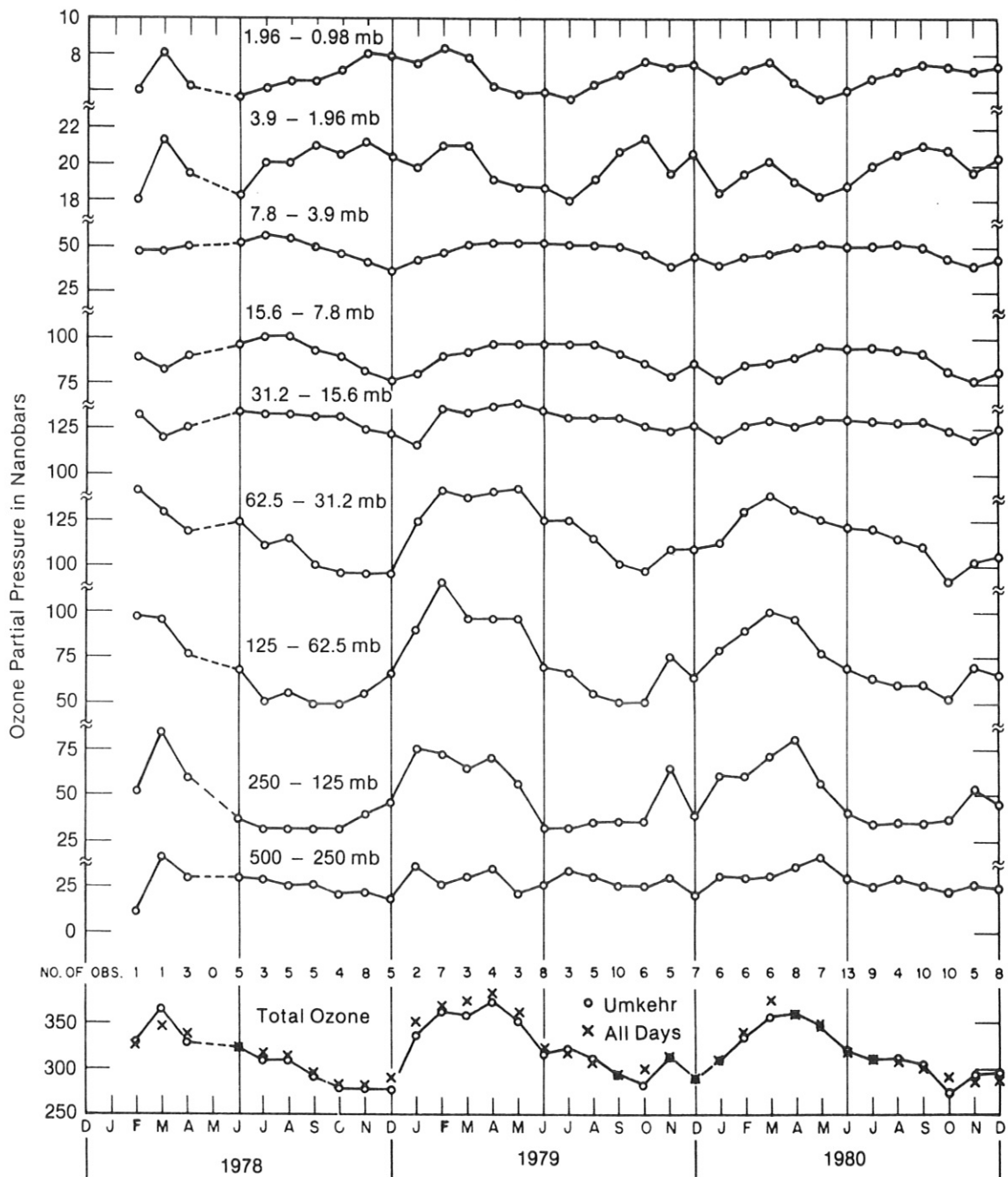


Figure 6.--Mean monthly ozone amounts at various levels from Umkehr observations at Boulder, Colorado.

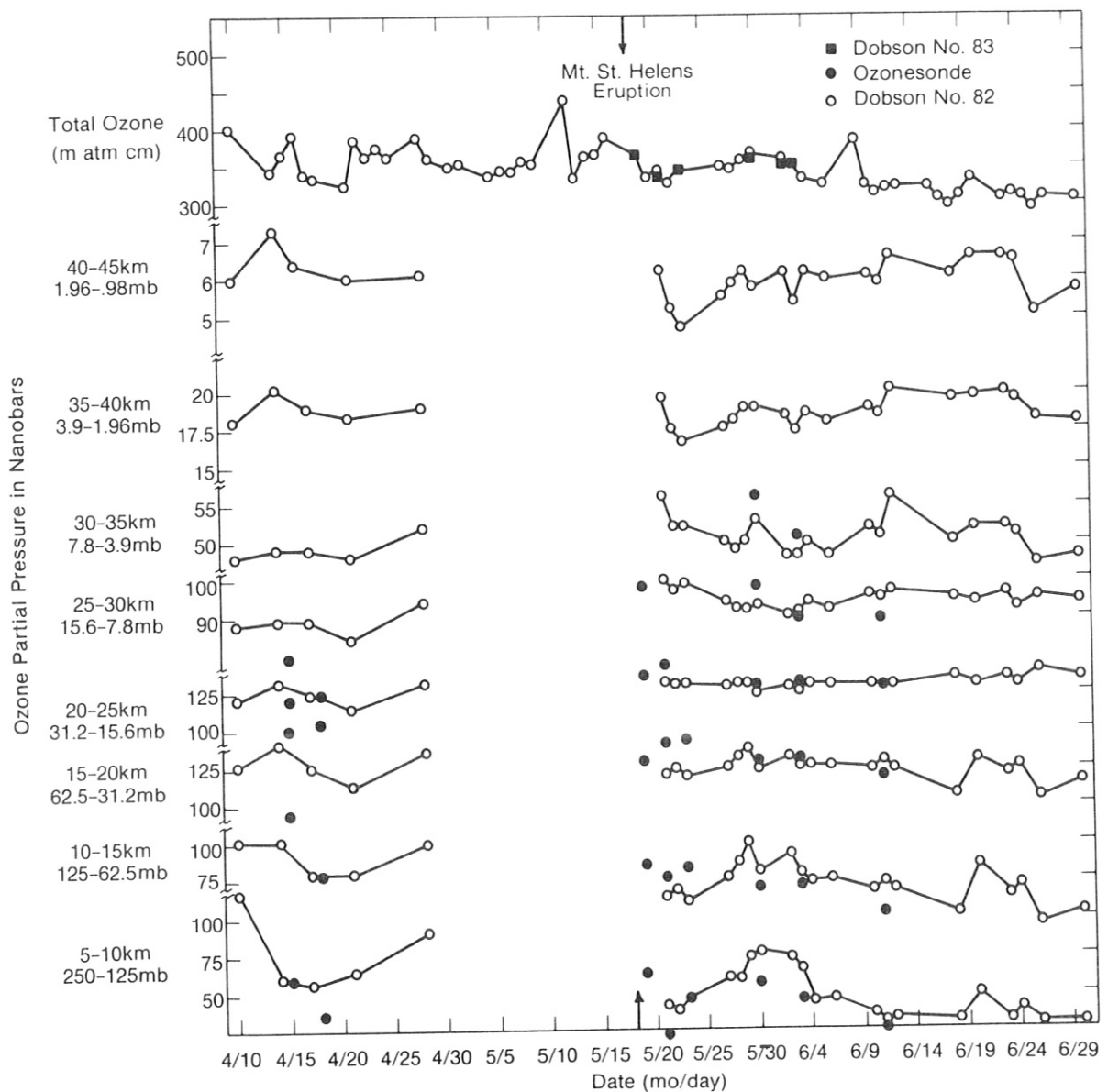


Figure 7.--Ozone amounts at various levels in the atmosphere at Boulder, Colorado, around the time of the Mt. St. Helens volcanic eruption, 1980. Filled circles are ozonesonde observations. Open circles are data derived from Umkehr observations on Dobson instrument no. 82, whereas filled squares are Umkehr observations on Dobson no. 83.

3.4 Surface Ozone

3.4.1 Operations

Surface ozone measurements were continued at the four GMCC observatories. All stations operated Dasibi ozone photometers that by the end of 1980 had been updated to include more reliable gas-handling systems and updated electronics. In addition, concurrent ECC ozone meter measurements were made at Mauna Loa and Samoa. Use of the ECC meter was discontinued at Mauna Loa at the end of the year.

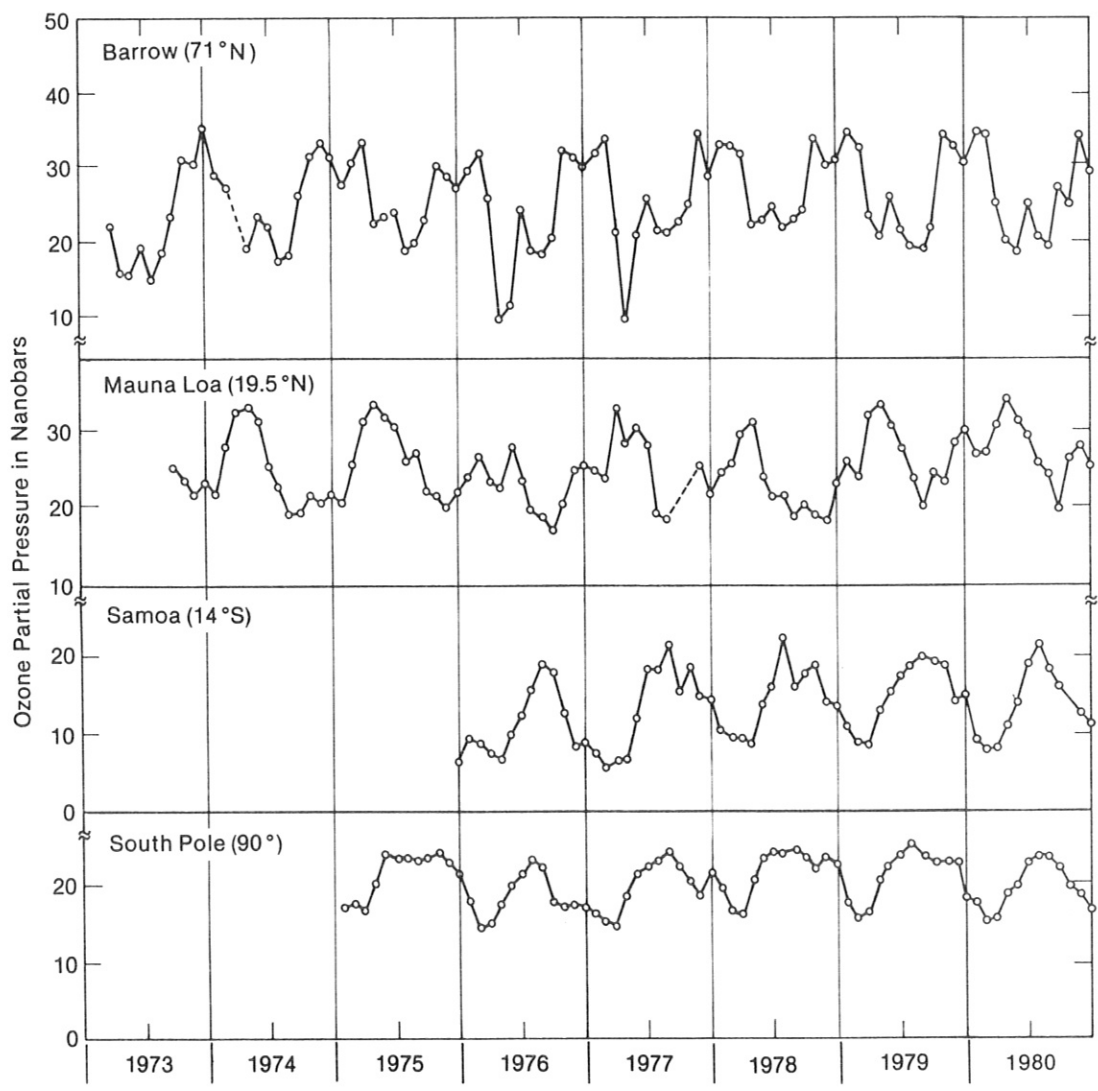


Figure 8.--Mean monthly surface ozone amounts.

3.4.2 Data Analysis

Local synthesis of ozone in clean tropospheric air has been suggested as a major contributor to the tropospheric ozone budget. (See, for example, Fishman and Crutzen, 1978; Liu et al., 1980.) A recent paper by Ramanathan (1981) indicates that tropospheric ozone may play an important role in the climatic effects of a change in the ozone column amount. Because the number of tropospheric ozone measuring locations representative of clean atmospheric conditions is very limited, renewed emphasis is being placed on extended-term surface ozone measurements at the GMCC locations. Monthly mean data since 1973 are shown in fig. 8. The annual cycle and other variations have been discussed in a recent paper (Oltmans, 1981).

3.5 Stratospheric Water Vapor

3.5.1 Operations

Work continued throughout the year on the development of a reliable balloon system. After extensive testing of a plastic balloon designed to release gas at about 15 mb and then descend in a controlled manner, it was found that the balloon was often subject to tearing if sufficient descent rates were achieved. Although there were several successful balloon tests, this system was set aside when it was determined that a smaller neoprene balloon would be adequate to carry the hygrometer to the desired altitude. After considerable testing, a 4,000-g balloon manufactured by Kaysam Corporation was found to perform reliably and to achieve the proper gas valving for the desired descent rate.

The manufacturer of the frost-point hygrometer experienced great difficulty in properly mounting the miniature thermistor in the instrument's mirror face (see GMCC Summary Report No. 7 [Mendonca, 1979], sec. 3.4, for details of construction) and in accurately calibrating the thermistor. This led to a delivery delay until late in 1980.

3.5.2 Data Analysis

One of the aims of the GMCC stratospheric water vapor measurement program was to establish comparability between the Boulder location and the Washington, D.C., location used for a number of years by J. Mastenbrook of the Naval Research Laboratory (NRL). To do this a series of flights was planned from both locations. Continuing problems with the balloon system limited comparisons to one flight each during April 1980. The water vapor mixing ratios for the two flights are shown in fig. 9. Both profiles show that the strong seasonal minimum between 140 and 100 mb is typical for this time of year. They

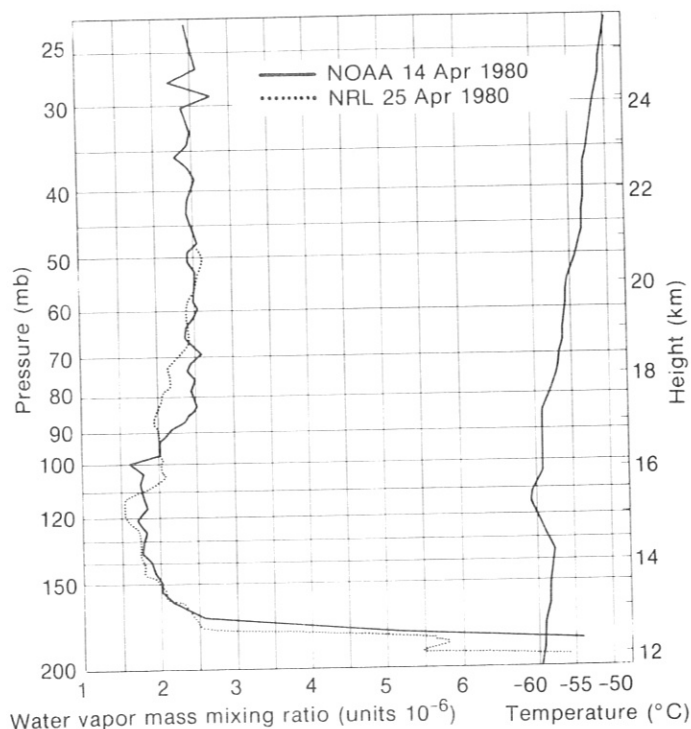


Figure 9.--Comparison of stratospheric water vapor measurements in Boulder, Colorado, (NOAA) and Washington, D.C., (NRL) in April 1980.

also show nearly constant mixing ratios above 60 mb at concentrations of approximately 2.5 parts per million by mass (ppmm). The differences below 70 mb are probably associated with shorter term (less than a month) variability within the atmosphere. The results obtained from this comparison suggest that Boulder is a suitable location to continue the stratospheric water vapor measurement series begun in Washington, D.C.

3.6 Halocarbons and N₂O

3.6.1 Operations

Collection of air samples for CCl₃F (freon-11), CCl₂F₂ (freon-12), and N₂O (nitrous oxide) analyses was continued during 1979 at the four GMCC stations and Niwot Ridge (NWR), Colorado. Sampling and chromatographic analysis procedures remained virtually identical to those established in mid-1977 (Komhyr et al., 1980), except that during late October and November a second chromatograph (Perkin Elmer model 3920) was used to analyze air samples collected mainly at South Pole.

Additional work was performed in 1980 to assess the validity of water vapor corrections derived theoretically and used in converting halocarbon and N₂O trace gas ambient (moist) air concentrations to concentrations in dry air. It was found, using a newly acquired General Eastern Corporation dewpoint hygrometer, that measured and theoretically derived amounts of water vapor differed by no more than about 5%. Such an error translates to a 0.15% error in trace gas concentrations expressed in terms of dry air, and is inconsequential.

The GMCC F-11, F-12, and N₂O calibration gases are periodically calibrated by R. A. Rasmussen of the Oregon Graduate Center, Beaverton, Oregon. A question has existed about the validity of the absolute calibration values originally assigned by Rasmussen to his N₂O standards since, for example, the N₂O calibration scale associated with gas standards prepared by R. F. Weiss of the Scripps Institution of Oceanography (personal communication, 1980) was approximately 10% lower than that of Rasmussen. To resolve the discrepancy, a new technique was developed in our laboratory (Komhyr et al., 1982) for preparing N₂O and other calibration gas standards. As applied to N₂O, the method involves preparation by gravimetric means of an N₂O/CO₂ gas mixture of highly accurately known mass ratio, and subsequent dilution of this mixture with N₂O- and CO₂-free air to approximately ambient air concentrations of these trace gases. From a determination of the absolute CO₂ concentration in this dilution gas mixture, using highly accurately calibrated CO₂ gas standards and an infrared measurement technique, the N₂O concentration in the dilution mixture is readily inferred.

Application of this calibration method to our N₂O calibration gas in tank 3072 yielded an N₂O mole fraction of $297.7 \pm 2\%$ ppbv compared with the originally assigned Rasmussen value of $331.4 \pm 5\%$ ppbv. (The 2% error for our value is an estimate based on possible systematic errors associated with the performance of this preliminary calibration.) This new result agrees with N₂O calibration values of R. F. Weiss, as well as of Connell et al. (1981) who employed a tunable diode laser to measure N₂O in air. More recently, Goldan et al. (1981) obtained similar results following recalibration of their N₂O primary standards prepared in 1975 by static and dynamic dilution techniques.

Table 12.--Summary of CCl₃F and CCl₂F₂ measurement results derived from linear regression analyses from 3 years of data centered around 7 September 1978

Station	No. obs.	Growth rate (pptv yr ⁻¹)	95% s.e. growth rate	Mixing ratio (pptv)	95% s.e. mixing ratio
<u>CCl₃F</u>					
BRW	133	12.10	±0.62	172.9	±0.51
NWR	130	10.78	±0.72	168.6	±0.65
MLO	128	12.84	±0.64	163.8	±0.52
SMO	136	12.35	±0.57	155.3	±0.49
SPO	42	11.17	±2.77	157.0	±2.54
<u>CCl₂F₂</u>					
BRW	112	15.10	±1.39	298.6	±1.09
NWR	58	18.24	±1.46	295.9	±1.26
MLO	112	18.97	±1.54	295.0	±1.16
SMO	118	17.48	±0.81	273.1	±0.68
SPO	32	17.93	±1.96	264.7	±1.72

3.6.2 Data and Data Analysis

F-11, F-12, and N₂O data obtained at the GMCC baseline stations and NWR are shown plotted in figs. 10, 11, and 12, respectively. Outliers have been removed from the data, using data selection criteria described elsewhere (Komhyr et al., 1981e).

Positive F-11 and F-12 growth rates are indicated in the plots of figs. 10 and 11. Actual growth rates at the five stations, derived from linear regression analyses for a 3-yr period of record centered at 7 September 1978, are shown in table 12. From the data, provisional minimum atmospheric lifetimes of 41 and 65 years have been computed for F-11 and F-12, respectively. In performing the lifetime calculations, random measurement errors were taken into account as well as assumed ±5% systematic errors in year-to-year F-11 and F-12 release rates and in reference gas calibrations.

N₂O growth rates shown in table 13, derived from linear regression analyses from 3 years of data centered around 1 July 1979, are also positive and

Table 13.--Summary of N₂O measurement results derived from linear regression analyses from 3 years of data centered around 1 July 1979

Station	No. obs.	Growth rate* (ppbv yr ⁻¹)	95% s.e. growth rate	Mixing ratio† (ppbv)	95% s.e. mixing ratio
BRW	143	0.43	±0.25	301.50	±0.21
NWR	121	0.90	±0.30	301.78	±0.25
MLO	136	0.88	±0.32	300.66	±0.28
SMO	144	1.44	±0.36	303.17	±0.29
SPO	63	0.44	±0.36	299.44	±0.33

*Mean growth rate: 0.82 ppbv yr⁻¹.

†Northern Hemisphere concentration minus Southern Hemisphere concentration (excluding SMO): 301.1 - 299.4 = 1.9 ppbv.

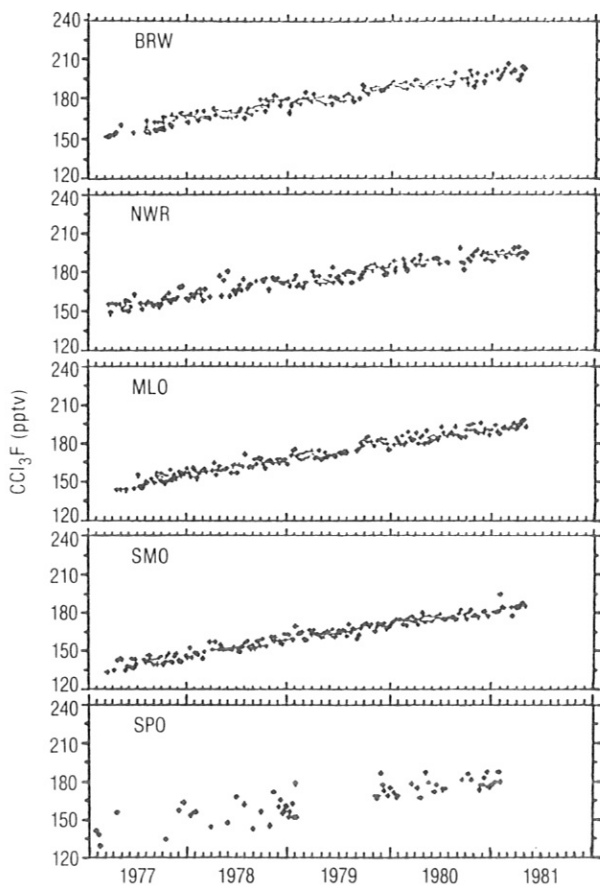


Figure 10.--NOAA Air Resources Laboratories' CCl_3F data record.

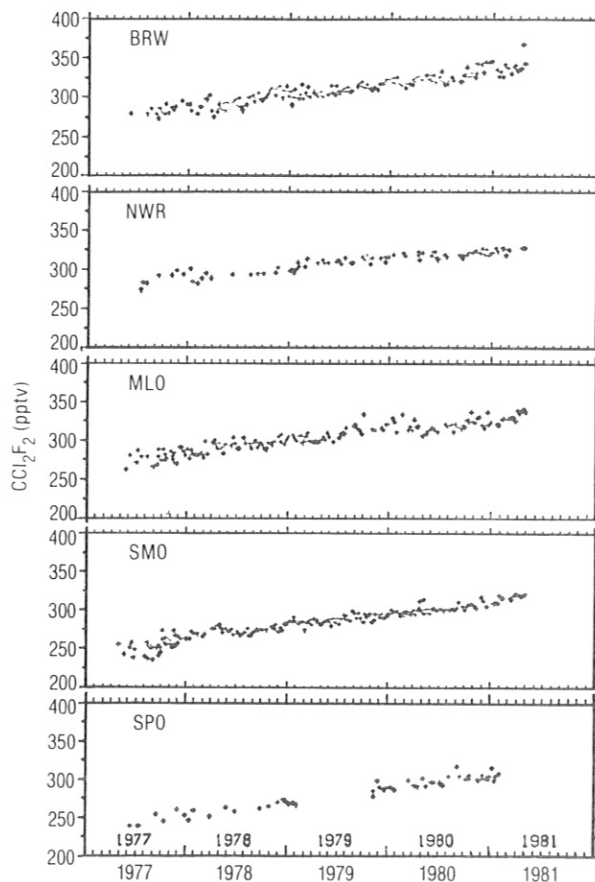


Figure 11.--NOAA Air Resources Laboratories' CCl_2F_2 data record.

significant. Note from fig. 12 that the N_2O mixing ratio appears to have peaked at Samoa in late 1979. The data indicate, furthermore, that an excess N_2O mixing ratio of 1.9 ppbv exists in the Northern Hemisphere.

3.7 Surface Aerosols

The GMCC surface aerosol monitoring program during 1980 included the measurement of condensation nuclei at BRW, MLO, SMO, and SPO, and light scattering at BRW and MLO. Condensation nuclei were measured continuously using the G.E. automatic condensation nucleus (CN) counter (catalog no. 112L428) with modifications to the electronics suggested by N. Ahlquist of the University of Washington. These modifications have been discussed in GMCC Summary Report No. 5 (Hanson, 1977) and have resulted in improved sensitivity and reliability of the instrument. A Pollak CN counter (model P, BGI, Inc., Waltham, Mass.) is located at each site to act as a secondary standard and provide routine calibration for the other nucleus counters onsite.

Light scattering was measured at the GMCC stations using specially constructed four-wavelength integrating nephelometers manufactured by MRI, Inc.,

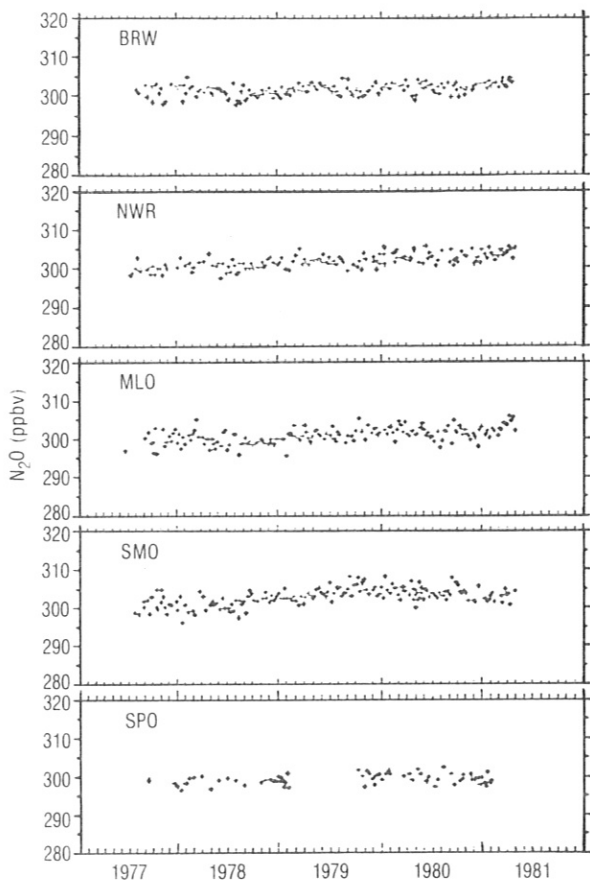


Figure 12.--NOAA Air Resources Laboratories' N₂O data record.

Altadena, Calif. The details of this instrument were discussed in GMCC Summary Report No. 5 (Hanson, 1977). These instruments were calibrated by filling them with CO₂ at 2-mo intervals and adjusting their outputs to agree with the known scattering coefficients of CO₂. In addition to the absolute calibrations performed at 2-mo intervals, weekly relative calibrations were made using the internal calibration objects built into the instruments.

3.7.1 Barrow

The BRW Pollak CN counter (SN 16) operated routinely throughout 1980 without problems. Daily observations provided routine checks for the G.E. automatic CN counter, and a more extensive calibration was performed if necessary on a weekly basis.

The G.E. counter produced acceptable data for 77% of the year. Although there were minor periods of downtime, the main period was from day-of-year (DOY) 152 to 179, accounting for most of the month of June.

The nephelometer produced acceptable data for 86% of the year. The majority of the downtime occurred during the months of May and June for unknown reasons. All data were recorded on magnetic tape and a backup chart recorder.

3.7.2 Mauna Loa

The MLO Pollak CN counter (SN 13) operated routinely throughout 1980. Daily observations provided calibration checks for the G.E. automatic counter, and a series of five Pollak observations performed at weekly intervals provided the weekly calibrations.

The G.E. counter produced acceptable data for 98% of the year. Routine maintenance accounted for most of the small amount of downtime.

The nephelometer produced acceptable data for 88% of the year. Downtime was caused primarily by an intermittent problem in the channel-2 amplifier circuit card. The problem was finally solved by replacing all of the integrated circuits and transistors on the card. All data were recorded on magnetic tape and a backup chart recorder.

A new Leeds and Northrup multipoint recorder was installed at Mauna Loa on DOY 57, 1980.

3.7.3 Samoa

The SMO Pollak CN counter (SN 20) operated properly throughout 1980, with daily and weekly observations providing calibration for the G.E. automatic CN counter. The G.E. counter produced acceptable data for 98% of the year. Routine maintenance and power outages accounted for most of the downtime.

The nephelometer was at the University of Washington for modifications and repair for the entire year, 1980. Therefore, no light-scattering data are available.

3.7.4 South Pole

The SPO Pollak CN counter (SN 15) operated twice daily during 1980. Meteorological variables were recorded along with each observation and are available along with the nucleus concentrations in the final form of the Pollak data file. Daily and weekly observations provided calibration data for the G.E. automatic nucleus counter. The G.E. counter produced acceptable data for 86% of the year. Downtime was caused by a frozen rotary valve, and data were lost for the period DOY 315-356, accounting for the last 3 weeks of November and the first 2½ weeks of December.

The nephelometer was sent to the University of Washington for repairs during the 1980 austral winter season. Therefore, no light-scattering data are available for SPO during 1980.

3.7.5 Data Analysis

Data analysis has proceeded as described in the previous GMCC annual reports. All observer notes and chart recorder data are examined upon receipt in Boulder to assure proper instrument performance. The monthly tapes available from the Data Acquisition and Management group are stripped of aerosol data, and files of hourly means and 10-min mean graphics are produced.

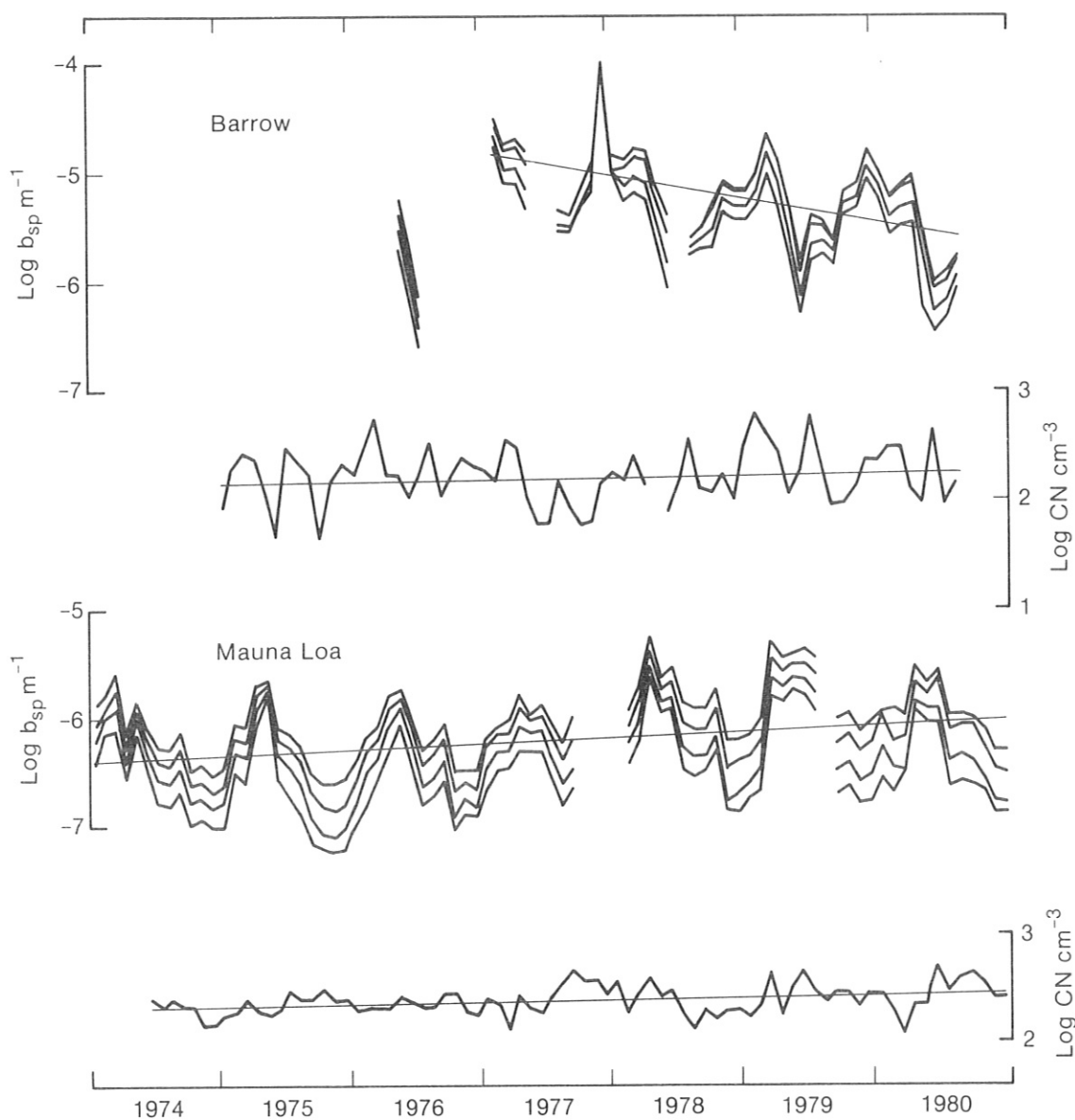


Figure 13.--Monthly geometric means of all light-scattering (b_{sp}) and condensation nucleus (CN) data acquired at Barrow and Mauna Loa^{SP}. Only 0000-0800 LST data for Mauna Loa were used to eliminate the possible influence of upslope winds. Linear least squares trend lines are shown for the four data sets. Details of the trend analyses are given in table 14.

Missing data are then filled in, and any necessary editing and calibration are performed, producing a file of acceptable hourly means for the year. All aerosol data are available from GMCC in computer printout, microfiche, magnetic tape, or graphic form.

3.7.6 Discussion of Selected Data

Light-scattering (b_{sp}) and condensation nucleus (CN) data for the four GMCC stations are presented in figs. 13 and 14. All available data were used

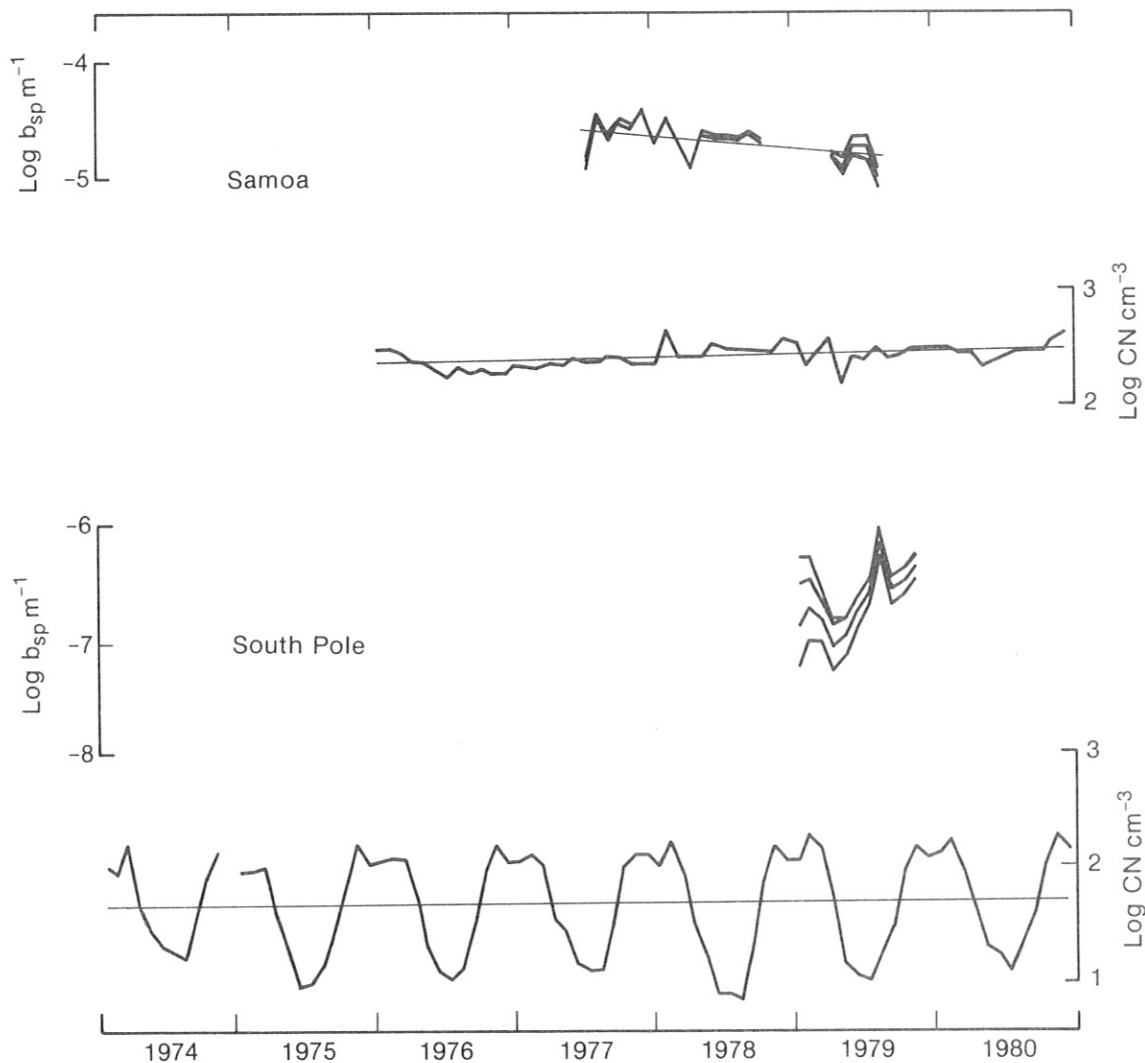


Figure 14.--Monthly geometric means of all light-scattering (b_{sp}) and condensation nucleus (CN) data acquired at Samoa and South Pole. Linear least squares trend lines are shown for all data sets except South Pole light scattering. Details of the trend analyses are given in table 14.

to calculate monthly geometric means, except for MLO for which only data from 0000-0800 LST were used, to avoid possible contamination from the upslope wind.

A linear least squares trend line was passed through each data set. All data were used except for BRW for which the 1976 light-scattering data were omitted. The mean of the data set, the trend in percent per year, and the total change over the time period were calculated for each case. A trend was considered significant if the total change of a trend line over the time period of the data set exceeded the standard deviation of the data points about the trend line. The results of this analysis are presented in table 14.

BRW and SMO light-scattering data both show significant downward trends over their respective time periods. However, because of the sparse data for

Table 14.--Linear least squares long-term trend analysis for light-scattering and condensation nucleus data at the four GMCC stations*

	BRW	MLO	SMO	SPO
\overline{b}_{sp}	$5.77 \times 10^{-6} \text{ m}^{-1}$	$6.64 \times 10^{-7} \text{ m}^{-1}$	$1.83 \times 10^{-5} \text{ m}^{-1}$	--
Trend	-55% yr ⁻¹	11% yr ⁻¹	-24% yr ⁻¹	--
Signif.?	Yes	No	Yes	--
\overline{CN}	167 cm^{-3}	235 cm^{-3}	262 cm^{-3}	48 cm^{-3}
Trend	4.0% yr ⁻¹	3.3% yr ⁻¹	4.5% yr ⁻¹	0.6% yr ⁻¹
Signif.?	No	No	No	No

*A trend was considered significant if the total change over the length of the trend line exceeded the standard deviation of the data points about the trend line.

SMO, its trend must be considered questionable. On the other hand, the BRW light-scattering data appear to exhibit a clear downward trend over the 4-yr period. This has not been confirmed by simultaneous aerosol mass measurements; however, only 1 or 2 more years of data should establish the trend.

A summary of monthly geometric mean light scattering and condensation nucleus concentration for BRW and MLO for 1980 is given in table 15. Monthly geometric means of condensation nucleus concentration for Samoa and South Pole for 1980 are given in table 16.

BRW light-scattering data for 1980 follow the same seasonal cycle as in previous years with winter values approximately an order of magnitude higher than summer values and with a double maximum in winter and spring. The BRW condensation nucleus concentration follows the same general trend but exhibits the (now familiar) anomalous July-August peak, probably caused by a local source of biogenic aerosol but not yet identified conclusively.

MLO light-scattering data for 1980 follow the same seasonal cycle as in previous years with a maximum in April and a minimum in November-December, and a change by a factor of about 5. The Mauna Loa condensation nucleus concentration again shows no apparent annual cycle and no obvious relationship to the light-scattering data.

MLO light-scattering data are especially interesting because they are strongly correlated with the solar radiation data. Bodhaine et al. (1981) analyzed 5 years of aerosol, atmospheric transmission (calculated from normal-incidence solar radiation data), ozone, and precipitable water data for MLO in order to explain the seasonal cycle of atmospheric transmission in terms of the seasonal cycles of optical depth due to aerosols, ozone, and water vapor. Figure 15 presents monthly means of aerosol light scattering (solid line) and atmospheric transmission (dashed line). A 3-mo binomial weighted running mean was applied to both data sets, and the smooth curve associated with each is a least squares cubic spline with a knot each year to

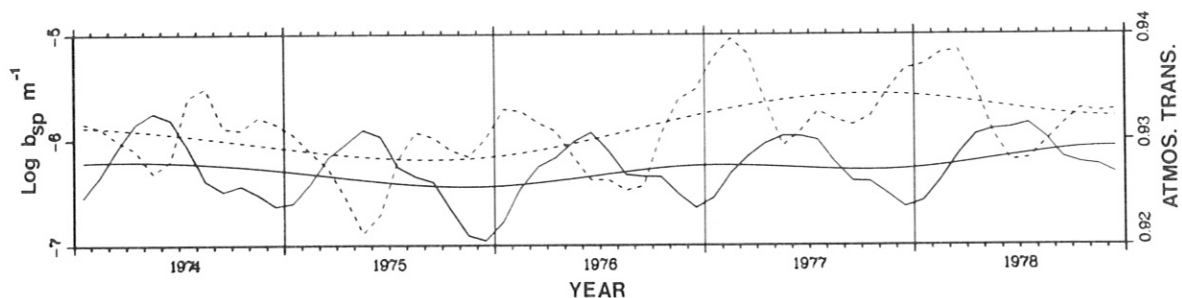


Figure 15.--Monthly geometric means of aerosol light scattering (solid line) and atmospheric transmission (dashed line) measured at Mauna Loa. A 3-mo binomial weighted running mean was applied, and a cubic spline (smooth curves) was fit to each data set to approximate long-term trends.

Table 15.--Monthly geometric means of light-scattering and condensation nucleus data for 1980 at Barrow and Mauna Loa

Month	$b_{sp} \text{ m}^{-1}$				CN cm^{-3}
	450 μm	550 μm	700 μm ($\times 10^{-6}$)	850 μm	
<u>Barrow</u>					
1	10.5	10.4	7.83	5.98	232
2	5.46	5.12	3.57	2.57	307
3	7.33	6.86	4.48	3.06	300
4	8.99	7.60	4.96	3.36	124
5	3.10	2.65	1.71	1.10	91
6	1.26	1.05	0.628	0.430	--
7	1.18	0.996	0.645	0.456	99
8	2.58	2.38	1.75	1.37	164
9	3.36	2.91	2.05	1.54	55
10	2.36	2.09	1.36	1.01	54
11	6.06	5.31	3.48	2.49	46
12	13.2	12.6	8.78	6.53	309
<u>Mauna Loa</u>					
1	0.742	0.672	0.353	0.196	258
2	1.26	0.853	0.519	0.303	231
3	2.15	1.51	0.925	0.692	154
4	3.09	2.30	1.63	1.21	232
5	2.55	2.03	1.52	1.20	237
6	2.88	2.10	1.39	0.963	372
7	1.29	0.981	0.553	0.339	278
8	1.37	1.06	0.616	0.383	329
9	1.30	1.02	0.550	0.345	357
10	0.954	0.649	0.384	0.276	329
11	0.615	0.423	0.256	0.198	268
12	0.639	0.423	0.253	0.205	282

Table 16.--Monthly geometric means of condensation nucleus data for 1980 at Samoa and South Pole

Month	1	2	3	4	5	6	7	8	9	10	11	12
SMO	309	303	271	282	211	233	261	291	275	279	357	411
SPO	131	207	96	46	21	17	11	22	38	103	179	133

approximate any long-term trend. It is apparent that transmission is low when aerosol scatter is high, and vice versa.

To study the seasonal variations more closely, the cubic splines were removed from the data sets and monthly means were calculated from the residuals. A similar procedure was applied to ozone, precipitable water, and Angstrom exponent; the results for the five data sets are presented in fig. 16. It is apparent that the annual cycles of transmission, light scattering, Angstrom exponent, and ozone are strongly correlated, and that water vapor is out of phase with the other variables.

Calculations show that the contributions of aerosols, ozone, and water vapor to the seasonal variation of optical depth above MLO are 0.006, 0.0014, and -0.0006, respectively, for a total seasonal variation in optical depth of 0.0068. This compares favorably with the measured seasonal variation in optical depth of 0.007 above MLO. Further details of the calculations and analysis may be found in Bodhaine et al. (1981). The origin of the aerosols

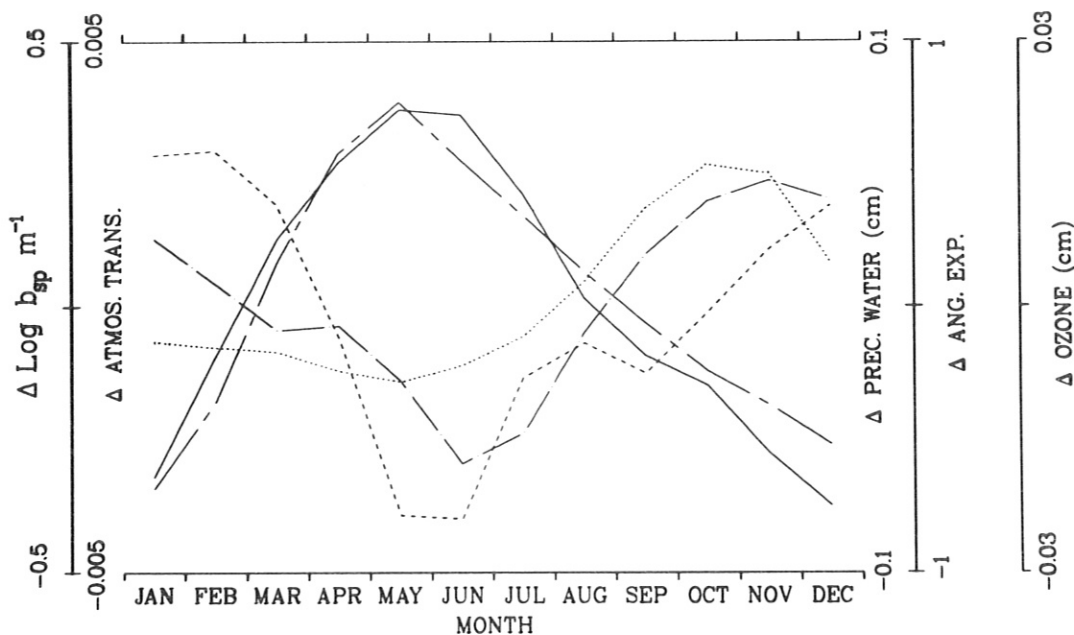


Figure 16.--Monthly departures from the long-term trend of five data sets taken at Mauna Loa during 1974-78. The data shown are Y_1 = atmospheric transmission (dashed line), Y_2 = aerosol light scattering (solid line), Y_3 = Angstrom exponent (chain-dotted line), Y_4 = precipitable water (dotted line), Y_5 = total ozone (chain-dashed line). The 5-yr means of the data are $\bar{Y}_1 = 0.9311$, $\bar{Y}_2 = 5.35 \times 10^{-7} \text{ m}^{-1}$, $\bar{Y}_3 = 1.627$, $\bar{Y}_4 = 0.4347 \text{ cm}$, $\bar{Y}_5 = 0.271 \text{ cm}$.

responsible for the springtime peak at MLO is probably the Asian continent with long-range transport by upper tropospheric westerly flow.

SMO CN concentration data for 1980 continue at about the same level, typical of a clean marine aerosol, with no obvious seasonal or long-term trends. An analysis given in the GMCC No. 7 Summary Report for 1978 (Mendonca, 1979) found no annual or diurnal cycle in the Samoa data.

The SPO CN record continues as in previous years with a strong annual cycle but no long-term trend.

3.8 Solar Radiation

It is well known that changes in the composition of the Earth's atmosphere will alter the nature of the solar radiation reaching the ground. Considering the numerous hypotheses about potential atmospheric composition changes, natural or anthropogenic, the purpose of the GMCC solar radiation measurement effort is to monitor solar radiation as received at the Earth's surface at remote sites in an attempt to detect atmospheric induced variations. The measurements include nonspectral global and direct shortwave (0.28-3.0 μm) using Eppley quartz pyranometers and pyrhemometers, respectively. In addition, broadband spectral resolution is achieved using various filters. Although these measurements are in themselves not sufficient to monitor changes in the complete global radiation budget, high-quality data from these instruments could be sufficient to be indicative of substantial changes in the radiation properties of the atmosphere.

For a list of specific measurements being made at GMCC sites, see GMCC annual reports for 1976 through 1979 (Hanson, 1977; Peterson, 1978; Mendonca, 1979; Herbert, 1980). The complement of monitoring instrumentation for these measurements has remained virtually unchanged, except for instrument replacement after a malfunction, through 1980. In an effort to improve data quality control, instruments of minimal importance and/or quality will be discontinued in 1981. The instruments to be taken offline at all stations are the UV (0.295-0.395 μm), GG22 (0.395-3.0 μm), and OG1 (0.530-3.0 μm) global radiometers.

New emphasis is being placed on measurements of direct solar radiation using active nonspectral cavity radiometers and measurements of total vertical water vapor utilizing a solar infrared hygrometer. These new field instruments are being initially tested at Mauna Loa.

Whereas maintaining routine observational programs of the highest possible quality at the GMCC observatories is a primary objective, increasing importance is being placed on research into problem areas of radiation: properties of and processes in the atmosphere, in particular those associated with climate mechanisms. These specific problem areas are to be addressed:

- (1) Comparison of observations with complex atmospheric transmission models.
- (2) Water vapor absorption characteristics in narrow spectral regions.
- (3) Spectral extinction of aerosols, in particular, definition of the background stratospheric aerosol.
- (4) Optical properties of the Arctic aerosol.
- (5) Radiation balance in the Antarctic, in particular, the effect of clouds.

3.8.1 Data Archiving

A standard procedure has been adopted for archiving the routine pyranometer data from the four baseline stations. Hourly integrals in Research-Cooperator format are routinely archived at the National Climatic Center (NCC) in Asheville, North Carolina. The Research Cooperator format conforms to NCC's recommended format for this type of data. Data through 1980 have been archived.

3.8.2 Data Quality Control

Paramount to our data quality control efforts for our online instruments is an annual intercomparison between the station instruments, pyranometers and pyrhemimeters, and designated standard instruments. The results of these comparisons through 1980 are given in last year's annual report (Herbert, 1980). These comparisons will continue. The only instrument showing a significant ($>1\% \text{ yr}^{-1}$) calibration drift is the quartz pyranometer located at Samoa. Preliminary analysis of the 1981 intercomparison shows that the drift is continuing at a rate of $1.1\% \text{ yr}^{-1}$. This instrument will be replaced, and the back data must be adjusted.

Additional quality control is achieved during the archiving process by a visual inspection of plotted minute values for the entire year. Currently only the pyranometer data are routinely checked and archived.

All of our standard instruments are currently being calibrated by the NOAA calibration facility to check long-term stability and relate the absolute calibration to an independent calibration facility.

The quality control of the data-recording process at the stations is maintained by the GMCC Acquisition and Data Management Group, which provides the Solar Radiation Group with monthly data tapes for each station.

Examples of typical data from the monitoring program at each station are given in previous GMCC annual reports (Mendonca, 1979; Herbert, 1980).

3.8.3 Plans

Pursuant to the research goals listed earlier, the following special measurements are planned:

- (1) Total water vapor (precipitable H_2O) at MLO and SPO.
- (2) Surface spectral albedo at SPO.
- (3) Spectral extinction at MLO and BRW.
- (4) Spectral diffuse-direct insolation at BRW.

3.9 Station Climatology

3.9.1 Instrumentation and Data Processing

Some years ago, when plans were being formulated for new monitoring stations in Barrow and American Samoa, consideration was given to the meteorological variables measured at MLO as a basic set. This set includes wind, station pressure, air and dewpoint temperature, and a soil or lava temperature. Pressure and temperature measurements allow the correction of gas and radiation measurements for nonstandard atmospheric conditions. The dewpoint temperature or relative humidity is required whenever infrared absorption techniques are used to determine the concentration of other gases. The moisture content of the air is useful for interpreting aerosol measurements. The windspeed and wind direction are used to identify regions of local pollution or contamination.

National Weather Service (NWS) instrumentation and practices were being used at MLO, and for the most part the exposures were according to NWS and World Meteorological Organization (WMO) standards. The anemometer was mounted at a height of 10 m, the thermometer at 2 m, above ground. Hourly average values were being computed.

To facilitate recording by automatic data processing equipment, GMCC procured and installed standard instrumentation for the four baseline stations. A propeller-type anemometer (no. 141, Aerovane, Bendix, Environmental Science Division, Baltimore, Md.) was selected and mounted on a mast in the vicinity of the gas-sampling inlet. A capacitance-type static pressure transducer (no. 1201C, Rosemount, Inc., Minneapolis, Minn.), calibrated for use at sea level or 3-km altitude, depending on the station, was used. Air temperatures were measured with linearized thermistors encased in steel shells (no. YSI 15133 (44212), Yellow Springs Instrument Co., Yellow Springs, Ohio) mounted in aspirated sun shields (no. 43404, R. M. Young Co., Traverse City, Mich.). Linearized thermistors are reasonably linear over a range of $+50^{\circ}$ to -50°C . Thus at the South Pole a resistance-type thermometer with a lower limit of -85°C was used. Because of the extreme cold at the Arctic stations and high contamination at the Samoa station it has been difficult to settle on a single humidity instrument for all stations; thus three types are in use. At Barrow, Mauna Loa, and Samoa dewpoint hygrometers are in use (no. 911, EG & G, Inc., Newton, Mass.--BRW and SMO; no. 1200 ASP, General Eastern Instrument Co., Watertown, Mass.--MLO). At the South Pole an absorption-type hygrometer is used (no. 303 moisture monitor, Du Pont Instruments, Wilmington, Del.).

The signals from each sensor are transformed into fluctuating DC voltages in the range of -10 to +10 V. A central data system samples the voltages at 1-s increments and forms 1-min averages. The 1-min average voltages are averaged for 1 hour, scaled in scientific units, and recorded on magnetic tape along with the 1-min average voltages. In addition to the arithmetic average, the 1-s readings of wind direction and speed are combined trigonometrically to form north-south and east-west wind components. These are individually averaged at 1-min and 1-h intervals. The hourly averaged components are subsequently transformed back to a resultant wind direction and speed. All components and resultant winds are recorded along with the averages. The hourly averaged values constitute the basic GMCC data set; as such, the following quality assurance is performed. Each value is checked against climatological limits determined from past data. Discontinuities are tested by measuring

the difference between each value and a 5-h mean centered on that hour. In cases where physical limits apply, tests are made; if any value falls outside test limits a flag is set. Flagged values are checked against chart records when available and new values are inserted. In most cases when a single value is flagged a new value is obtained by simple interpolation. The final test is in the form of comparing month-to-month and year-to-year changes in the distribution, and then comparing statistics derived from this analysis.

3.9.2 Barrow Climatology

The Barrow GMCC Observatory is located about 9 km southwest of Point Barrow on a small rise in the tundra between two saltwater lagoons. With the Arctic Ocean to the north, east, and west, and relatively level tundra stretching more than 200 km to the south, there are no local wind barriers to redirect the wind field. A uniform snow and ice cover hides the Alaskan shoreline for 8 months of the year. Thus between stormy periods, and the associated westerly winds, the surface winds are generally northeasterly in response to the general circulation around the two dominant continental high-pressure regions in the Arctic. A low-level inversion (0.1 to 1 km) separates the more easterly surface winds from more northerly winds aloft. In a recent study of the wind climatology along the Alaskan north slope, Kozo (1980) found evidence of a turning of the wind in the surface layer as result of a baroclinic effect caused by the Brooks Range to the south. The effect is such that to the east of Barrow, where the mountain barrier is close to the coast, the winds are turned to the south, whereas surface winds at Barrow are northeasterly. Wind direction shifts of as much as 140° both in the vertical and along the coast were observed.

Maykut and Church (1973) describe the radiation climatology at Barrow in terms of four albedo seasons: (1) a winter stationary period, (2) a spring transitional period, (3) a summer stationary period, and (4) an autumn transitional period. Because of the prevalence of summer clouds, the incident radiation reaches a peak in early June. For the most part the boundary layer is stable throughout summer as well as winter. Kozo (1979) has studied summer wind regimes and has found evidence of a local sea breeze effect along the Beaufort Sea. The barriers to mixing in the surface layer throughout the year make the mountain barrier effect in the winter and the sea breeze effect in summer important factors in evaluating the wind direction histograms. It is also possible, especially in the winter months, for air that has originated over land to the east of Barrow (e.g., Prudhoe Bay) to be transported to the north and recirculated over Barrow in the northeasterlies.

The histograms of the hourly averaged resultant windspeed as a function of direction (fig. 17) for 1977-79 and for 1980 show excellent agreement. Except for the predominance of the five most easterly directions, the distribution is surprisingly symmetrical. For the period 1977-79, easterly sector winds (NE, ENE, E, ESE, and SE) occurred 55% of the time, whereas for winds 10 m s^{-1} or greater the occurrence from this quadrant is 75% (see Harris and Herbert, 1980). As in previous years, the prevailing wind is easterly-northeasterly, and sometimes northerly and westerly in December. Table 17 gives a monthly breakdown of average and extreme values of wind, air temperature, and station pressure. A maximum windspeed of 17 m s^{-1} was reported in April.

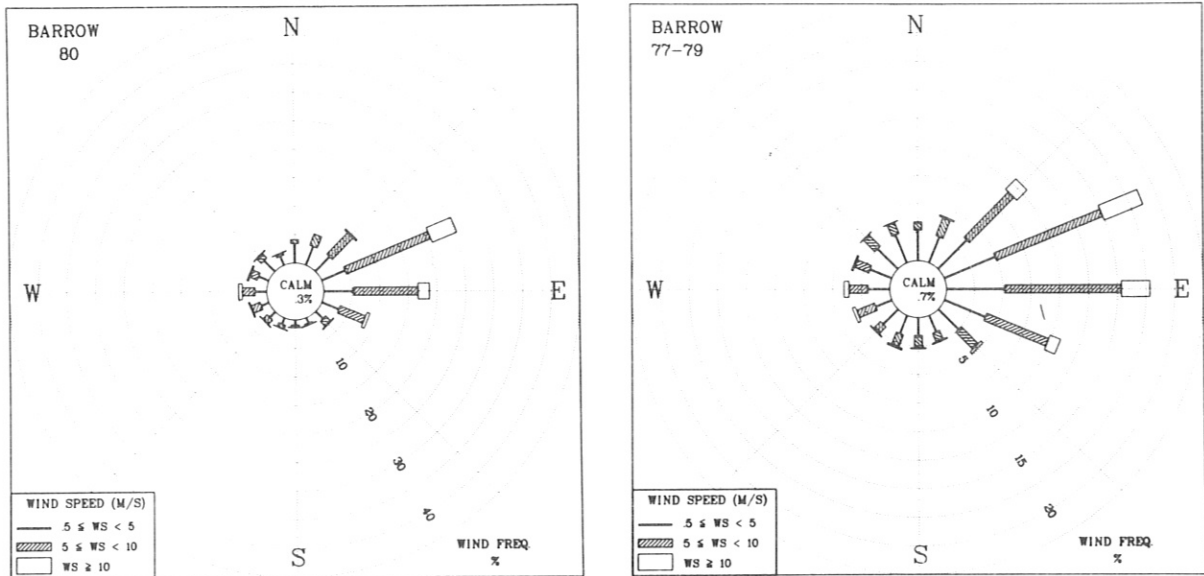


Figure 17.--Windrose of surface winds for the GMCC Barrow Observatory, 1980, left, and 1977-79, right. The distribution of the resultant wind direction and windspeed are in units of percent occurrence for the year and 3-yr period, respectively. Windspeed is shown as a function of direction in three speed classes: $<5 \text{ m s}^{-1}$, $5\text{-}10 \text{ m s}^{-1}$, and $\geq 10 \text{ m s}^{-1}$.

The month-to-month changes in temperature and wind (table 17) indicate the full extent of the winter in Barrow. Winds are stronger during winter, and the temperature follows an orderly progression for 6 months with mean temperatures below the annual average of -13.4°C . In 1980 the minimum hourly average temperature was -47°C ; the maximum, $+18^{\circ}\text{C}$. The average pressure was 1015.0 mb.

3.9.3 Mauna Loa Climatology

Throughout much of the year the midtropospheric winds in the south-central Pacific are determined by the position of the Pacific anticyclone. This is especially the case in the summer months when the anticyclone is in its northernmost position, and the winds are light and easterly. During the winter months the Pacific anticyclone moves farther south and diminishes in size, allowing the southern extent of the midlatitude cyclones to pass the islands. This period is characterized by a much higher occurrence of westerly winds at all levels. In the transition periods between these two dominant patterns, stronger easterly winds are commonly observed. A recent study of the beginning point of 10-day back trajectories from MLO shows this seasonal breakdown (Miller, 1981). The study is based on a wind layer bounded at 3 and 5 km, and it included data for the 5-yr period beginning February 1975. The largest percentage of the trajectories originate to the east of MLO during the summer

Table 17.--1980 Barrow Observatory monthly climate summary*

	Jan	Feb	Mar	Apr	May	Jun	Jul	Aug	Sep	Oct	Nov	Dec
Prevailing wind direction	E	N	ENE	ENE	ENE	E	ENE	NNE	NE	E	ENE	W
Average wind-speed (m s ⁻¹)	6	6	6	8	7	4	5	4	6	7	9	6
Maximum wind-speed† (m s ⁻¹)	16	15	13	17	12	13	11	11	13	14	16	14
Direction of max. wind† (deg.)	270	80	280	70	80	230	60	340	260	120	70	260
Average station pressure (mb)	1021.7	1014.5	1016.7	1017.8	1017.6	1011.7	1011.6	1010.8	1015.9	1005.9	1011.5	1024.4
Maximum pressure‡ (mb)	1046	1038	1038	1035	1037	1024	1025	1022	1028	1026	1027	1050
Minimum pressure‡ (mb)	992	990	996	1005	1004	986	996	1000	997	982	999	1003
Average air temperature (°C)	-26.8	-24.8	-24.9	-20.3	-8.7	1.6	1.6	1.5	-3.8	-9.4	-19.9	-26.3
Maximum temperature‡ (°C)	-8	-2	-14	-10	0	7	12	18	6	-2	-8	-3
Minimum temperature‡ (°C)	-47	-41	-36	-31	-24	-5	-2	-4	-12	-23	-32	-39

*Instrument heights are as follows: wind, 16 m; pressure, 9.5 m (MSL), air and dewpoint temperature, 3 m.

Wind and temperature instruments are on a tower located 25 m east of the main building.

Pressure instruments are located in the building.

†Maximum and minimum values are hourly averages.

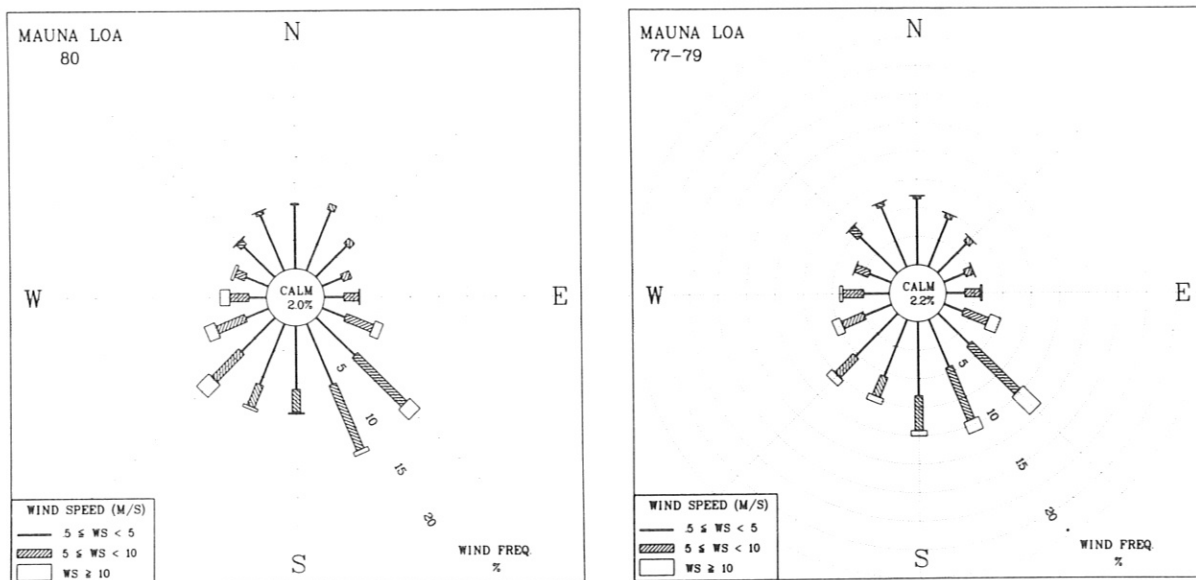


Figure 18.--Windrose for the Mauna Loa Observatory for 1980, left, and 1977-79, right. See legend for fig. 17.

months and to the northwest during winter months. The highest percentage of long trajectories (greatest number beginning beyond 2,000 km from MLO) also occurs in the winter. Significant year-to-year variations are also observed.

The surface wind (10-m height) measured at the observatory represents a more complex flow regime. For much of the time the synoptic-scale pressure gradient influence is overpowered by the local influence of surface heating and cooling causing a diurnal upslope-downslope flow (Mendonca, 1969; Miller, 1978). In even more well-defined flow situations, the twin peaks of Mauna Kea and Mauna Loa redirect the flow. This is illustrated in part by systematic differences between the climatology of trajectory source points and the wind distribution at the observatory, as in fig. 18. The combined wind distribution for 1977, 1978, and 1979 shows a much higher occurrence of winds with a southerly component than does the trajectory analysis. While the synoptic-scale flow pattern is more easterly or westerly, the effect of Mauna Loa is to redirect stronger winds from aloft down the slope with a more southerly component. The dip in the symmetry in the distribution of the southerly winds is to the south-southwest, the exact direction of the summit of Mauna Loa. Higher windspeeds ($\geq 10 \text{ m s}^{-1}$) occur most commonly (80% of the time) with stormy periods and are almost exclusively confined to the southerly directions. The upslope-downslope winds are generally represented by speeds of 5 m s^{-1} or less. Such conditions occur approximately 62% of the time. Calm conditions (windspeed $< 0.5 \text{ m s}^{-1}$) occur 2.2% of the time on the basis of the 3-yr average. With only small deviations, the annual windrose for 1980 was 24.7 m s^{-1} , associated with an early January storm. Monthly mean and extreme values for wind, pressure, and temperature are given in table 18. Temperature measurements are made at MLO using similar instrumentation to that at the Barrow station.

Table 18.--1980 Mauna Loa Observatory monthly climate summary*

	Jan	Feb	Mar	Apr	May	Jun	Jul	Aug	Sep	Oct	Nov	Dec
Prevailing wind direction	W	SW	SE	SE	SE	SE	SSE	SSE	SSE	SSE	SSE	SW
Average wind-speed (m s ⁻¹)	6.9	7.7	5.5	4.9	4.2	3.8	4.0	3.3	3.6	4.9	5.2	5.1
Maximum wind-speed† (m s ⁻¹)	25	18	15	14	9	16	18	8	12	11	11	12
Direction of max. wind† (deg.)	260	230	120	130	120	140	170	170	160	140	160	230
Average station pressure (mb)	678.4	679.4	679.8	681.3	681.4	681.8	682.1	681.3	681.8	682.1	681.9	680.1
Maximum pressure† (mb)	685	685	684	685	684	685	686	684	685	685	686	683
Minimum pressure† (mb)	672	671	677	678	679	679	679	679	677	679	679	674
Average air temperature (°C)	4.8	6.9	4.1	6.6	7.0	8.7	8.8	8.4	8.2	7.9	4.1	7.8
Maximum temperature† (°C)	14	15	11	16	16	18	18	18	18	18	18	16
Minimum temperature† (°C)	-3	-1	-6	1	0	1	2	-1	0	1	0	1

*Instrument heights are as follows: wind, 10 m; pressure, 3399 m (MSL); air and dewpoint temperature, 2 m. Wind and temperature sensors are located approximately 15 m southwest of the main building on a tower. Pressure sensors are in the observatory building.
 †Maximum and minimum values are hourly averages.

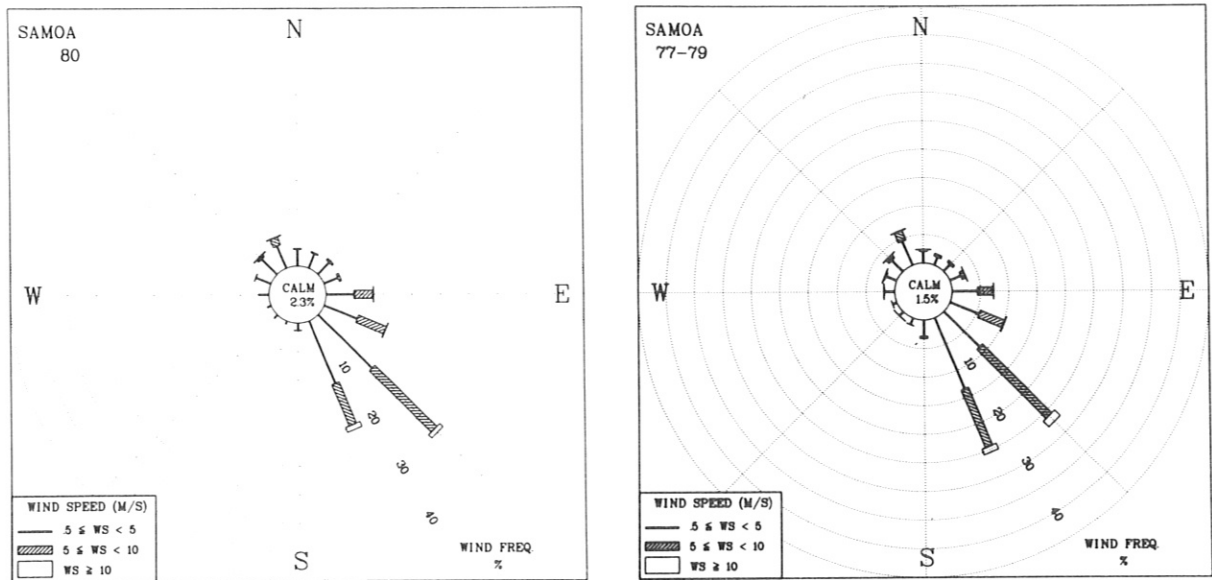


Figure 19.--Windrose for the Samoa Observatory for 1980, left, and 1977-79, right. See legend for fig. 17.

3.9.4 Samoa Climatology

The anemometer and thermometer at the Samoa station were located on the sampling tower atop Lauagae Ridge throughout 1980. Since February 1977 both instruments have been at this location: the anemometer at a height of 14 m, the air and dewpoint thermometers at 4 m. For the period 1977-79 and 1980, fig. 19 shows the distribution of the resultant windspeed, in 3 classes, as a function of the resultant wind direction, in 16 classes. During 1980, the trade winds at Cape Matatula occurred 71% of the time, considering winds from the southeastern quadrant to be representative. This compares with 74% for the same quadrant (including directions E, ESE, SE, SSE, S) for the period 1977-79. During the year, winds from the northwesterly quadrant (W, WNW, NW, NNW, N) occurred 18% of the time, compared with 16% for the preceding 3 years. The previous summary report (Herbert, 1980) shows that 74% of the winds greater than 5 m s^{-1} from the northwestern quadrant occurred during the summer months.

Seasonal variations of all other meteorological variables are small (table 19). There are only small indications of higher winds and cooler temperatures in the winter than in summer. The annual average pressure and temperature for 1980 were 999.1 mb and 28.1°C , respectively. The average resultant windspeed was 4.4 m s^{-1} . These values compare with 1010.1 mb, 27.1°C , and 4.8 m s^{-1} , respectively, measured at the airport NWS station in Tafuna. The height difference between the GMCC station and the airport is about 78 m, accounting for 8.9 mb of the 11-mb difference.

Table 19.--1980 Samoa Observatory monthly climate summary*

	Jan	Feb	Mar	Apr	May	Jun	Jul	Aug	Sep	Oct	Nov	Dec
Prevailing wind direction	SE	SE	SE	SE	SSE	SE	SSE	SE	SE	SE	SE	SSE
Average wind-speed (m s ⁻¹)	2.7	2.8	4.0	4.3	3.9	6.2	5.4	6.7	5.5	4.7	3.6	2.7
Maximum wind-speed† (m s ⁻¹)	11	11	14	12	14	11	12	13	12	10	9	7
Direction of max. wind† (deg.)	330	320	320	150	150	150	150	150	150	140	150	150
Average station pressure (mb)	987.9	998.8	997.4	998.8	1000.1	1001.3	1001.7	1002.5	1001.8	1001.1	999.6	998.6
Maximum pressure† (mb)	1004	1005	1002	1003	1005	1006	1007	1006	1006	1006	1005	1007
Minimum pressure† (mb)	991	992	991	993	996	998	998	997	998	997	995	993
Average air temperature (°C)	28.5	29.1	29.2	29.1	27.5	27.8	27.4	26.8	27.5	27.5	28.3	28.5
Maximum temperature† (°C)	32	33	33	33	33	33	31	30	30	31	32	32
Minimum temperature† (°C)	24	25	25	25	24	25	24	24	24	24	25	24

*Instrument heights are as follows: wind, 14 m; pressure, 30 m (MSL); air and dewpoint temperature, 7 m. Wind and temperature sensors are located atop Lauague Ridge, a distance 110 m northeast of the main station building. Pressure sensors are in the building.

†Maximum and minimum values are hourly averages.

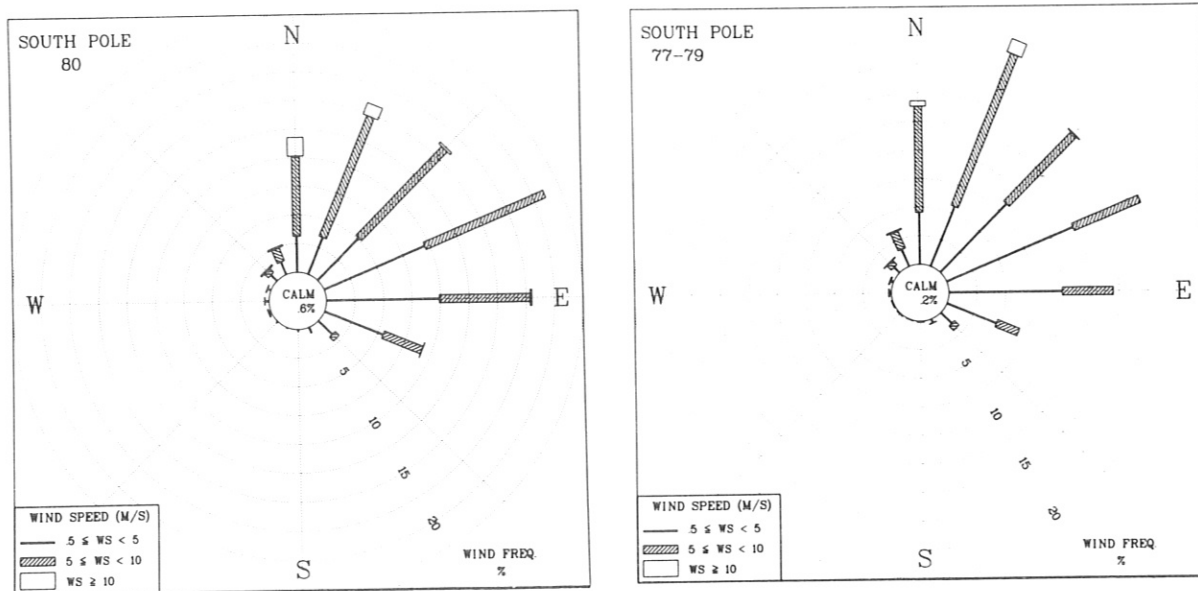


Figure 20.--Windrose for the South Pole Observatory for 1980, left, and 1977-79, right. See legend for fig. 17.

3.9.5 South Pole Climatology

The very persistent surface wind from a grid northeasterly direction is the overriding climatological feature at SPO. This wind is an inversion wind from 50° , which is from the right side of the Antarctic ice dome. The speed is steady, about 6 m s^{-1} . SPO is located on the Amundsen-Scott plateau (elev. 2.85 km), which has little topographic relief within a 100-km radius of the station. The plateau is near the western edge of the main ridge of eastern Antarctica. The highest point (elev. 4 km) on the plateau is about 900 km east-northeast of the geographic South Pole.

Figure 20 displays in polar coordinates the distribution of the wind as a function of speed and direction. As in previous years the most prevalent wind direction in 1980 was east-northeasterly. Considering the wind sectors bounded and including north and east, wind from these directions occurs 83% of the time. In the previous 3-yr period winds from this sector were observed 85.4% of the time. As indicated by the wind distribution, the stronger winds ($\geq 10 \text{ m s}^{-1}$) associated with stormy periods are from northerly directions. During the previous 3 years, windspeeds greater than 10 m s^{-1} have occurred only 2% of the time. Easterly winds greater than 10 m s^{-1} were observed for the first time in 3 years. Calm conditions were reported for 0.6% of the time in 1980, whereas in the previous 3 years the average was only 0.2%.

The full extent of the austral winter on the Antarctic plateau is shown in the monthly average air temperature in table 20. The average monthly air temperature is below the annual average (-49.3°C) for 8 months of the year. The annual average was 0.4°C colder than in 1979. The maximum hourly average temperature of -19.5°C (day-of-year, 364) is compared with the minimum reading of -74.9°C (day-of-year, 226). The air temperature is measured with a platinum resistance temperature sensor (no. 954 PL-C, Stow Laboratory, Hudson, Mass.) in a naturally ventilated radiation shield (no. 43103A, R. M. Young, Traverse City, Mich.) at a height of 2 m.

Table 20.--1980 South Pole Observatory monthly climate summary*

	Jan	Feb	Mar	Apr	May	Jun	Jul	Aug	Sep	Oct	Nov	Dec
Prevailing wind direction	ENE	ESE	NNE	ENE	E	NNE	E	ENE	E	N	N	N
Average wind-speed (m s ⁻¹)	3.8	2.4	5.7	5.3	3.7	6.0	4.9	4.6	3.7	4.1	5.3	4.3
Maximum wind-speed† (m s ⁻¹)	9	9	11	15	12	13	11	12	12	13	12	10
Direction of max. wind† (deg.)	30	110	20	30	90	350	90	40	320	350	30	10
Average station pressure (mb)	686.9	684.8	680.3	681.5	679.0	673.4	678.2	677.8	676.8	672.2	685.4	684.8
Maximum pressure‡ (mb)	693	689	690	695	702	686	691	689	689	699	692	694
Minimum pressure‡ (mb)	680	672	667	672	669	658	656	663	660	657	678	678
Average air temperature (°C)	-26.3	-39.6	-55.0	-57.8	-56.9	-58.7	-60.9	-63.6	-60.7	-51.6	-34.0	-25.5
Maximum temperature‡ (°C)	-20	-24	-45	-41	-37	-43	-51	-48	-40	-37	-23	-20
Minimum temperature‡ (°C)	-32	-54	-64	-69	-71	-71	-71	-75	-74	-69	-45	-31

*Instrument heights are as follows: wind, 10 m; pressure, 2800 m (MSL); air temperature, 2 m. The anemometer and thermometer are located on a mast 30 m grid north of the Clean Air Facility. Pressure measurements are made inside the facility.

†Maximum and minimum values are hourly averages.

Table 21.--The average ion concentration in precipitation collected at MLO and SMO during the latter half of 1980

Ion	Average ion concentration	
	MLO* (mg ℓ^{-1})	SMO† (mg ℓ^{-1})
SO ₄	1.00	1.87
NO ₃	0.15	0.11
Cl	0.30	10.60
PO ₄	<0.003	<0.003
NH ₄	<0.02	<0.02
Na	0.29	5.84
K	0.03	0.24
Mg	0.02	0.72
Ca	0.10	0.31

*Average pH = 5.45.

†Average pH = 5.30.

3.10 Precipitation Chemistry

The GMCC precipitation chemistry protocol at the baseline and regional stations was changed significantly in 1980. The 12 sites became a part of the National Atmospheric Deposition Program (NADP). This program, which is a cooperative network involving several government and private organizations, is the major precipitation chemistry monitoring effort in the United States. In joining this program, all GMCC sites adopted NADP collection procedures. These procedures include weekly sampling, use of a common precipitation chemistry collector, analysis at the Illinois State Water Survey laboratory, and quarterly publication of the data (Miller, 1979).

3.10.1 Baseline Measurements

The changeover dates to NADP protocols at MLO and SMO were June 10 and May 20, 1980, respectively. Monthly sampling procedures described in earlier reports were continued through the end of the year. The monthly collections were sent to EPA at Research Triangle Park, N.C. The average values for samples taken under the NADP weekly sampling program during 1980 are shown in table 21.

The short-period measurements (<3 days) at MLO, SMO, BRW, and SPO continued throughout the year. An example of the results from Hawaii is shown in fig. 21. Details of the sampling sites and collection techniques were given in past Summary Reports.

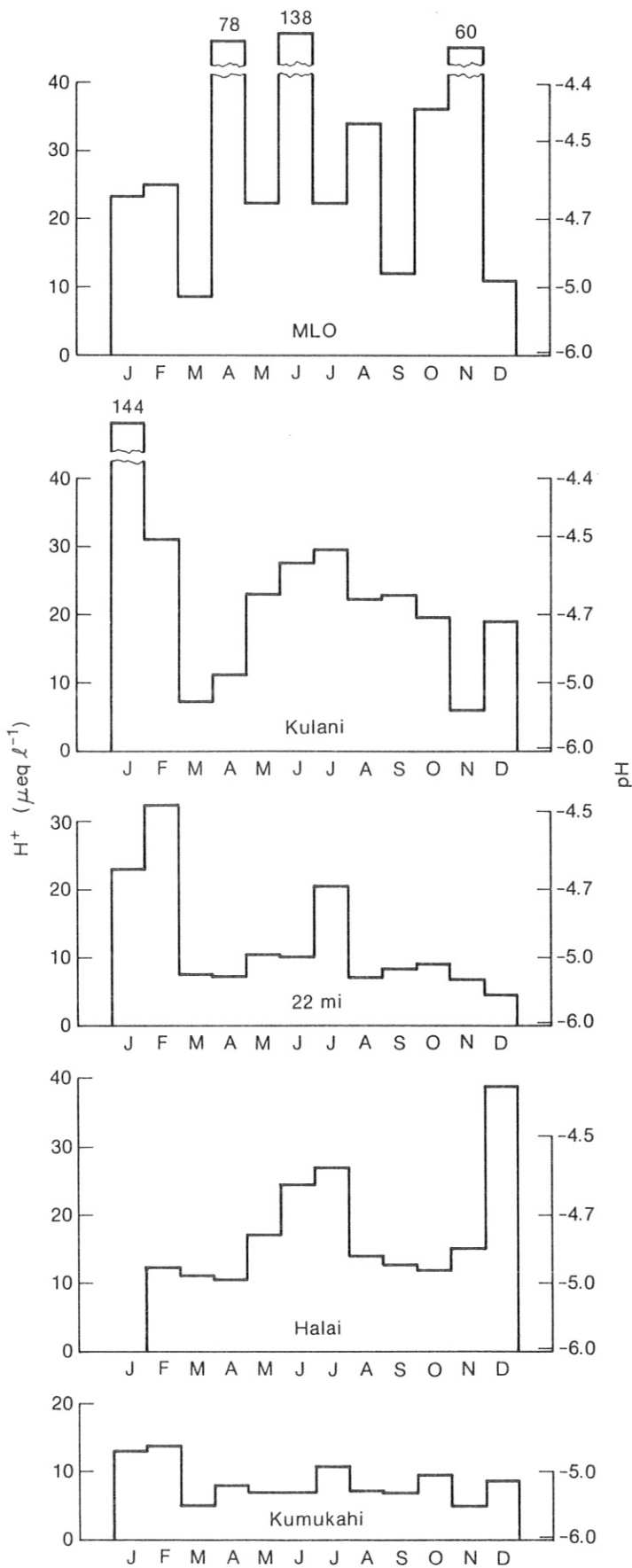


Figure 21.--The monthly precipitation and weighted hydrogen ion concentrations for five sites on the island of Hawaii.

Table 22.--Average ion concentration and pH values at the WMO regional sites for the latter half of 1980

WMO regional site	pH	Average ion concentration (mg ℓ^{-1})		
		SO ₄	NO ₃	Cl
Alamosa, Colorado	5.80	0.35	0.30	0.21
Bishop, California	5.96	0.34	0.20	0.30
Caribou, Maine	4.27	1.61	1.25	0.20
Huron, South Dakota	6.33	2.50	2.00	0.53
Meridian, Mississippi	4.32	1.25	1.11	0.46
Pendleton, Oregon	5.92	1.10	0.80	0.52
Princeton, New Jersey	4.30	2.22	2.21	0.55
Raleigh, North Carolina	4.30	2.51	1.36	0.47
Salem, Illinois	4.20	3.21	2.05	0.57
Victoria, Texas	5.10	2.00	0.51	1.50

3.10.2 Regional Measurements

A summary of the regional measurements made at the 10 WMO regional sites is given in table 22 for May to December 1980. These values represent measurements made under NADP procedures.

3.10.3 Washington, D.C., Network

The data for the Washington network are shown in fig. 22. A NOAA Technical Memorandum is planned in 1981 to summarize the data from the D.C. network.

3.11 Data Management

3.11.1 Hardware

The Acquisition and Data Management Group oversees the Instrumentation Control and Data Acquisition System (ICDAS), which collects atmospheric data

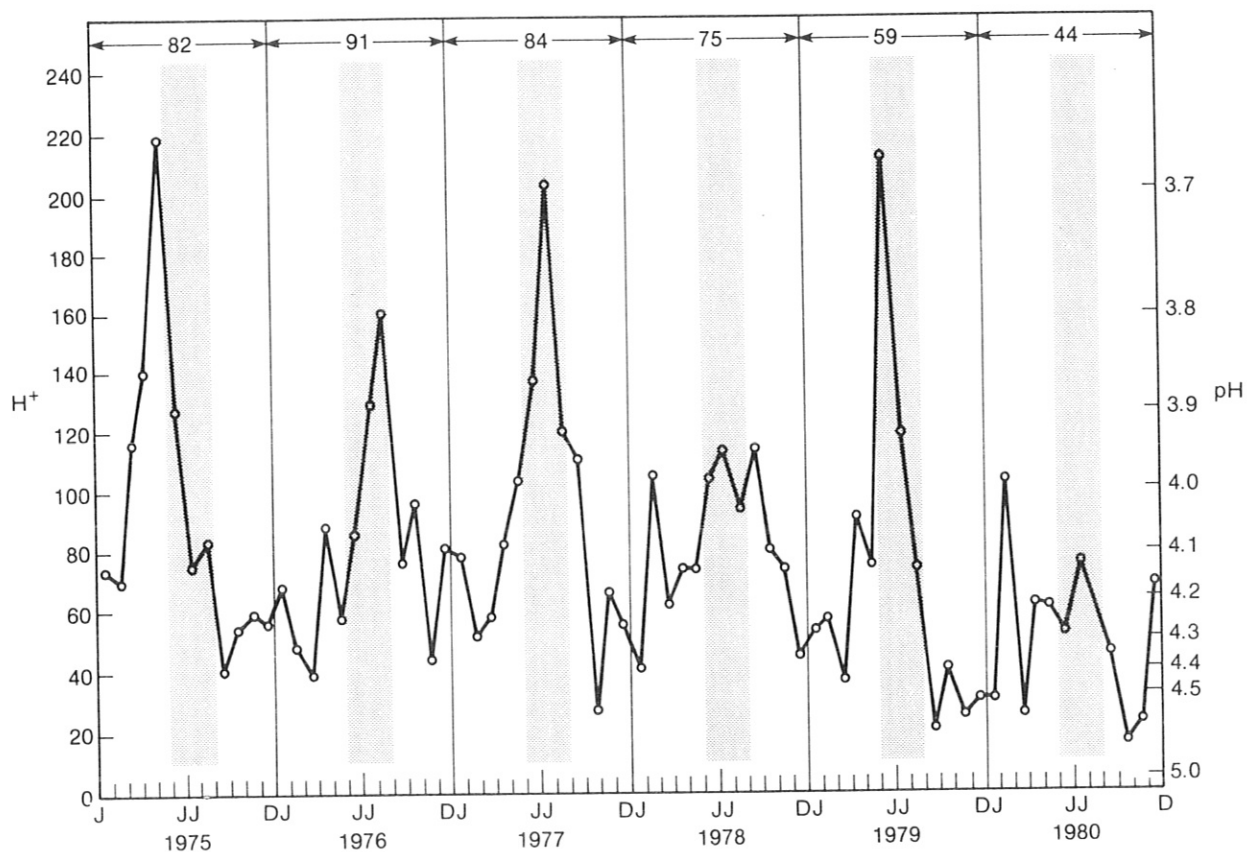


Figure 22.--Weighted monthly average pH and H⁺ concentrations (μmol l⁻¹) × 10⁶ for the ARL, Washington, D. C., area network from January 1975 through 1980. The weighted annual average H⁺ concentration is also given by the numbers at the top of the figure. Shaded areas indicate the summer months (June-August).

on magnetic tape at GMCC's four observatories. During 1980 the overall performance of ICDAS was down only slightly from the previous year. The system was nonoperational only 7% of the year (see fig. 23).

The South Pole station continued its extraordinary record with less than 1% downtime in 1980, matching its ICDAS performance in 1979. At MLO we saw an improvement in operation time to 94%. The downtime at MLO was mainly due to tape drive problems early in the year and an occasional power failure. The two remaining stations, BRW and SMO, had protracted difficulties with the Xerox multiplexor-digitizer. Because of the old age of this piece of hardware, failures have become more frequent and spare parts and replacements are hard to find. BRW's operational performance dropped to 82%, and SMO's dropped to 94%. In an effort to avoid further ICDAS downtime we have contracted an outside engineering firm (ERBTEC Engineering) to develop a repair facility for the multiplexor-digitizers.

During the year, the procedure for aligning the Wang magnetic tape drives was documented in a training manual. The drives in Boulder, BRW, SPO, and MLO have been realigned using this new procedure.

The new, "quiet" power supply was installed in the spare NOVA that was returned from the South Pole, thus completing this modification, which began

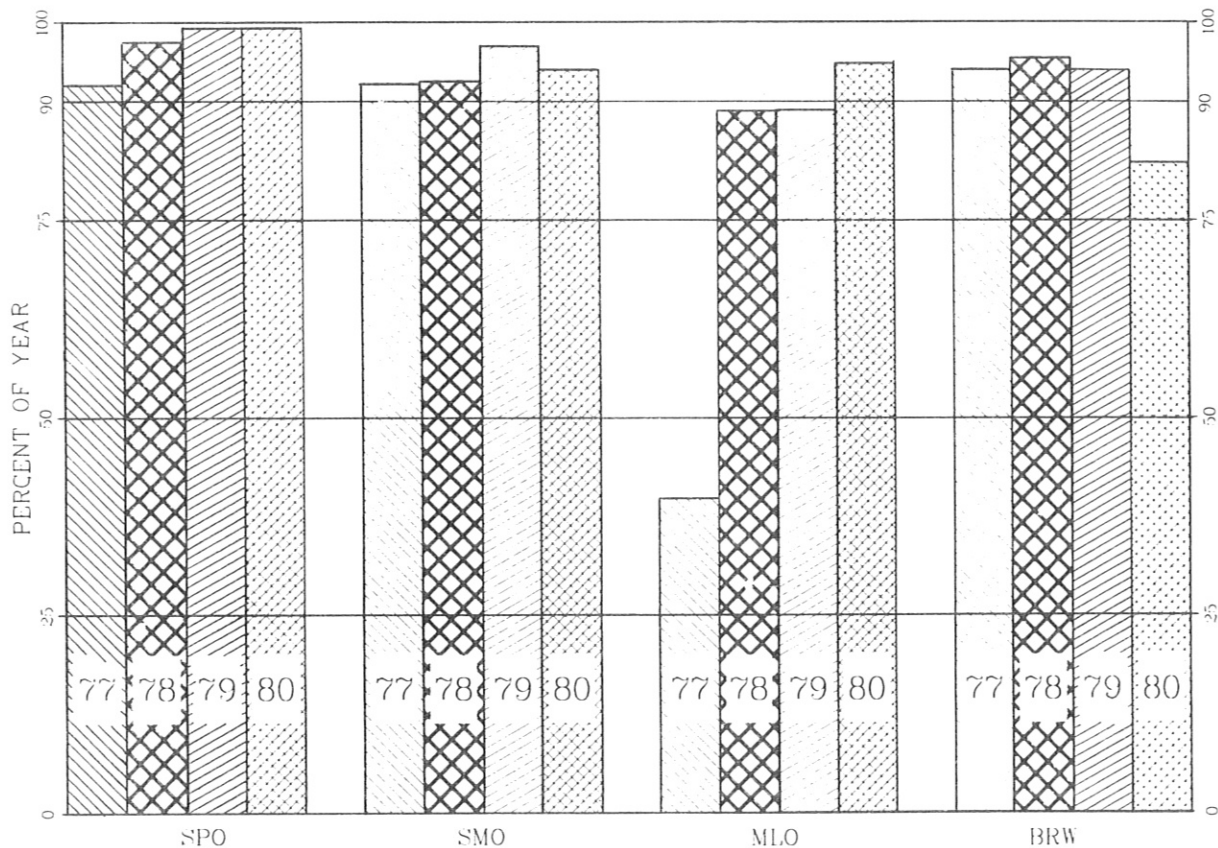


Figure 23.--ICDAS operations for 1977 through 1980. The percentage of operation time is shown for each year.

last year, for all NOVA computers in the network. The old switching power supplies were replaced with linear supplies in an effort to reduce system noise.

In 1980 new hardware, which included a NOVA 4/X minicomputer and a Winchester-type disk, was ordered to upgrade the reduction facility. This new configuration will allow us to use Data General's Real-time Disk Operating System (RDOS). This system will be faster than the old operating system and will allow two users at the same time.

A calibration procedure for the aerovanes was developed at the NCAR wind tunnels. We have begun now to refurbish and calibrate the aerovanes for each observatory.

The development of stand-alone microprocessor-based data loggers for the observatories continued. The necessary input-output programs were written and tested. These assembly language links to peripherals will enable us to write the main program in Fortran for each field controller. The Deck Tape II cartridge system was tested for reliability and found to be viable for field use.

3.11.2 Archiving

Table 23 lists the GMCC data archived at the World Data Center-A (WDC-A) in Asheville, North Carolina. Each file on the archive tapes is preceded by

Table 23.--Inventory of GMCC data tapes at World Data Center-A

No.	Tape name	Date of issue	Parameter	Station	Period of data
1	MLONFI	12/9/77	Volumetric light scattering	MLO	1974-1976
2	GPOLO1	1/16/78	Condensation nucleus concentration	BRW MLO SPO	1975-1976 1975-1976 1975-1976
3	A78076	3/17/78	Solar irradiance	MLO	1977
4	A78083	3/24/78	Solar irradiance	SMO	1977
5	A78100	4/20/78	Solar irradiance	BRW	1977
6	A78104	4/14/78	Solar irradiance	MLO	1976
7	A78132	5/12/78	NIP radiation	BRW, MLO, SMO, SPO	1977
8	A78139	5/19/78	Wind, pressure, temperature, humidity	BRW, MLO, SMO, SPO	1977
9	A78146	5/26/78	Solar irradiance	SMO	1976
10	A78160	6/9/78	Solar irradiance	SPO	1976-1977
11	A78230	8/18/78	Solar irradiance	BRW	1976
12	A78272	9/29/78	Solar irradiance	BRW, MLO	First half 1978
13	A78279	10/6/78	Solar irradiance	SMO	First half 1978
14	A79127	5/7/79	Solar irradiance (Research-Cooperator format)	SMO	1976
15	A79128	5/7/79	Solar irradiance (Research-Cooperator format)	SMO	1977
16	A79208	7/27/79	Solar irradiance	MLO	Second half 1978
17	A79222	8/10/79	Solar irradiance	SMO	Second half 1978
18	A80010	1/25/80	Carbon dioxide	MLO	1974-1978
19	A80011	1/25/80	Carbon dioxide	SPO	1976
20	A80012	1/25/80	Carbon dioxide	BRW	1973-1978
21	A80036	2/5/80	Solar irradiance	BRW	Second half 1978
22	A80075	3/16/80	Solar irradiance	SPO	1978

a description of the data in alphanumeric form, except for the tapes written in Research-Cooperator format. Copies of these tapes can be obtained from User Services Branch, Digital Products Section, National Climatic Center, Asheville, NC 28801 (FTS 672-0203 or (704) 258-2850, ext. 303). GMCC archive tapes are located in tape deck no. 9708.

In addition to these data tapes, GMCC has archived all available carbon dioxide flask data from stations in the CO₂ flask network, through 1978, in a yearly WDC-A publication, "Global Monitoring of the Environment for Selected Atmospheric Constituents."

4. SPECIAL PROJECTS

4.1 Wind Climatology of American Samoa

Three major sources for Samoan air were identified from an investigation of the tropical Pacific winds. The full report (Bortniak, 1981), which describes these in detail, should be useful to investigators who use the Samoa GMCC data. An annotated appendix gives sources of data for Samoan and, in general, equatorial Pacific winds.

Figures 24 and 25 are schematic views of the equatorial Pacific surface winds for the austral winter and summer seasons. The dotted lines represent possible trajectories of the surface air that might reach American Samoa. These three major sources are, in the order in which they most often occur, easterly trade winds that originate off the west coast of South America, southerly winds that originate from south of 40° S, and direct Northern Hemisphere air that passes Samoa en route to the monsoon low. These three winds are separated by two major boundaries: the Intertropical Convergence Zone (ITCZ), which separates the Northern and Southern Hemisphere trade winds; and the monsoon trough, a unique South Pacific feature that separates the South Pacific trade winds from the southerly flow.

The monsoon trough regularly moves northeast and southwest of Samoa, alternately, to give first southern winds, then trade winds to Samoa. An event that occurs infrequently, however, is an eastward retreat of the west edge of the ITCZ allowing direct Northern Hemisphere air to reach Samoa.

Table 24 gives an estimation of the approximate percentage of occurrence of each of these wind sources. It can be seen that the Northern Hemisphere source occurs only in the austral summer around March.

Table 24.--Estimation of the air source percentages for Pago Pago made from observations of 1974-77 satellite photographs

Month	Easterly trade winds (%)	Southerly from 30° to 40° south (%)	From Northern Hemisphere (%)
Jan	60	39	1
Feb	70	27	3
Mar	70	27	3
Apr	60	37	3
May	60	40	--
Jun	70	30	--
Jul	70	30	--
Aug	60	40	--
Sep	80	20	--
Oct	80	20	--
Nov	70	30	--
Dec	50	49	1

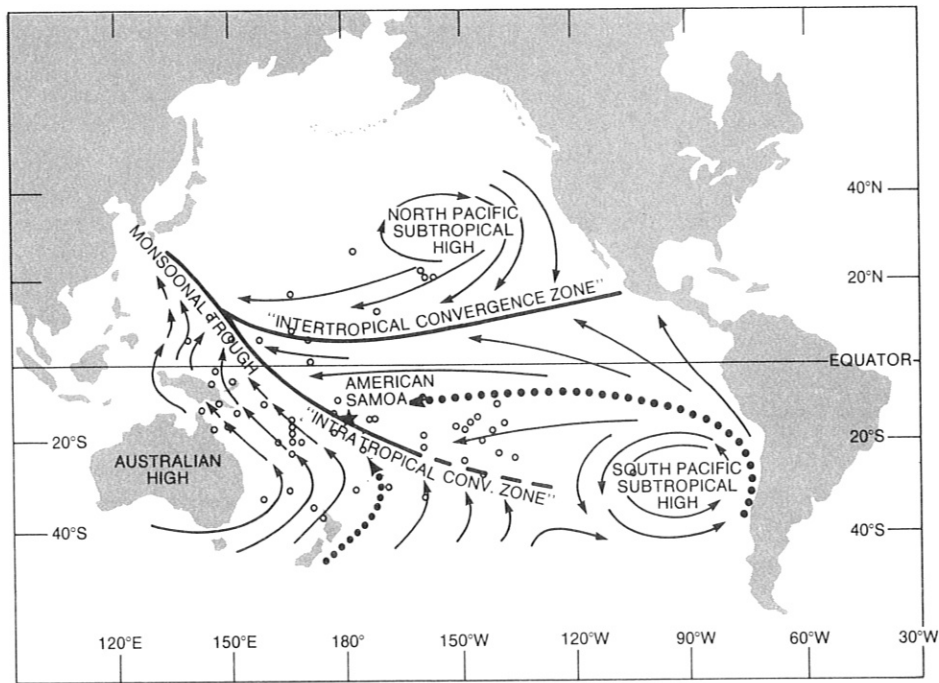


Figure 24.--Schematic of an average austral winter surface wind pattern. The star indicates the location of the GMCC Samoa station. Dotted lines indicate possible wind source trajectories to Samoa.

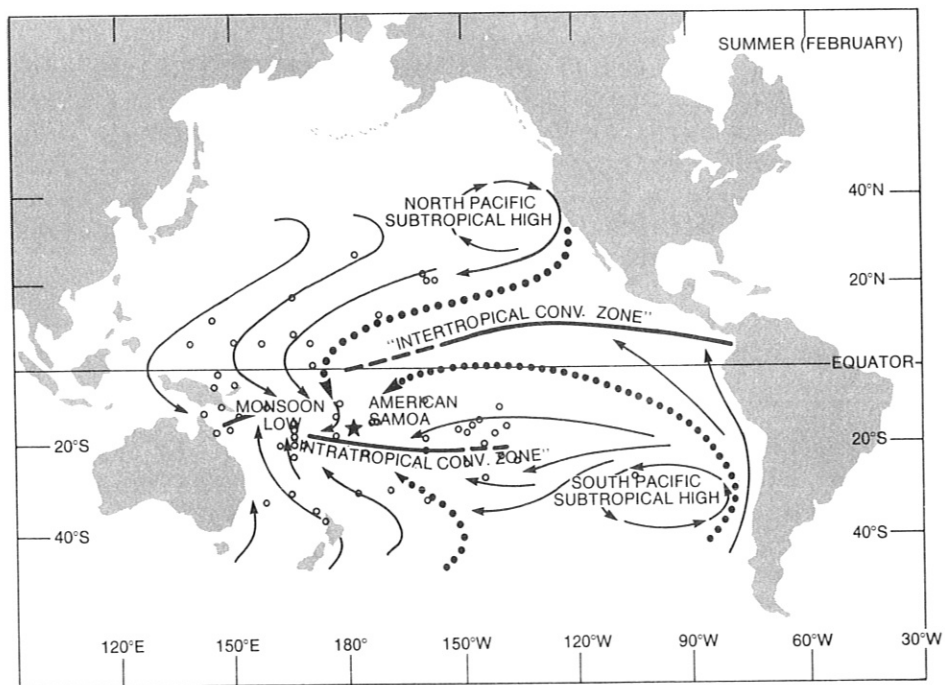


Figure 25.--An average austral summer surface wind pattern (see fig. 24). Note that the proximity of the monsoon low to Samoa introduces a third possible wind source trajectory (from the Northern Hemisphere).

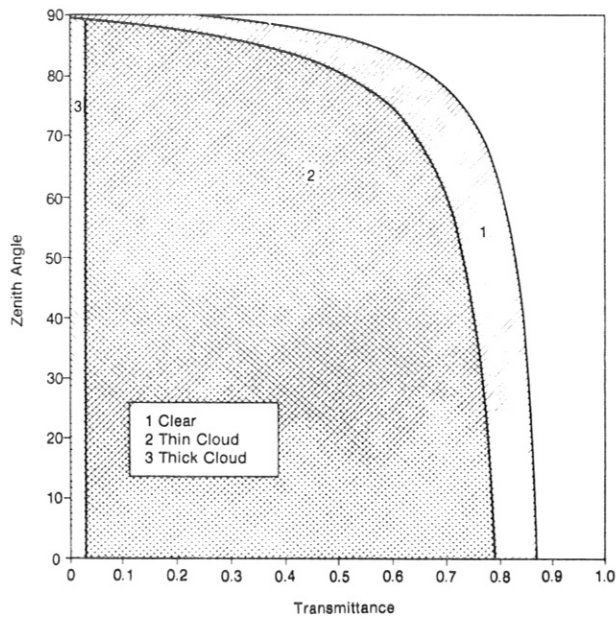


Figure 26.--Direct-beam transmittance divided into three subgroups for MLO.

4.2 Pyrheliometer Observations as an Indicator of the Climatological Persistence of Clouds

Because clouds modulate solar energy reaching the surface, significant changes in cloud occurrence and thickness would modify the climate of a region. The normal incidence pyrheliometer (NIP), though historically used to measure only clear-sky transmittance, was used at MLO to indicate whether significant high-level cloud changes were occurring in the subtropics.

When clouds come into the field of view of the NIP instrument, the direct solar beam is measurably attenuated. This sensitivity of the observation makes the instrument a cloud-sampling device. Because 1-min average data samples were collected, rapidly changing transmittances of the direct solar beam were monitored and a direct-beam climatology developed. Data reduction involved converting instrument voltages to transmittance values and associating a solar zenith angle with each minute value.

Data used in this study cover the period from 1976 to 1980 with 86% of the minute average NIP data being acquired for 50 months within this 5-yr period.

NIP data were divided into three general regimes. In the first, the field of view was cloud free and a relatively high transmittance was obtained. The opposite extreme is the third regime, in which the solar disk was behind clouds and the transmittance was zero or near zero. The second, intermediate regime is the interval between the two extremes where thin clouds and edges of thick clouds moderately reduced the transmittance. Each transmittance-zenith angle pair was categorized into one of these three regimes; these categories are illustrated in fig. 26. The boundaries between the regions were ascertained by radiative-transfer models.

The average direct-beam transmittances for the total data set and also for the clear- and thin-cloud subgroups are .488, .720, and .384, respectively,

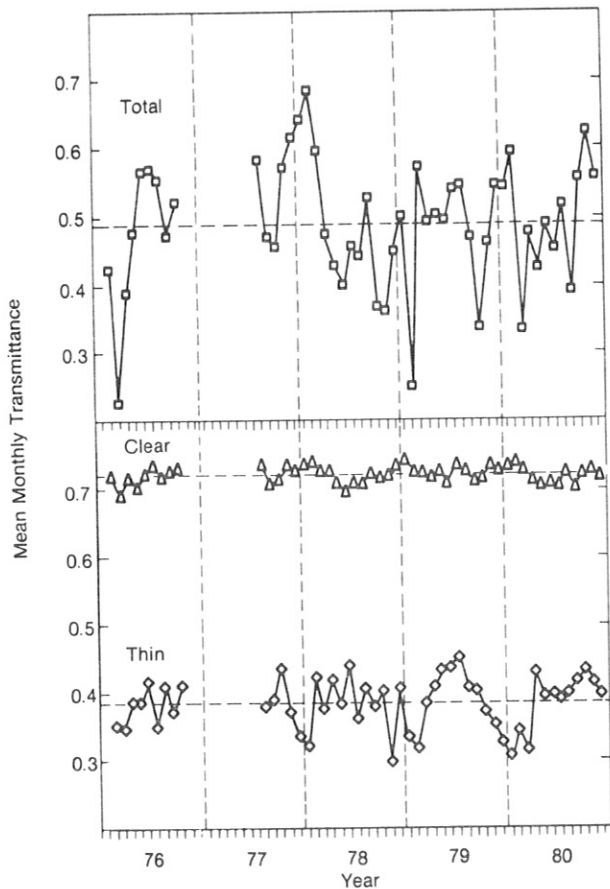


Figure 27.--Time series of monthly mean total and subgroup transmittance at MLO.

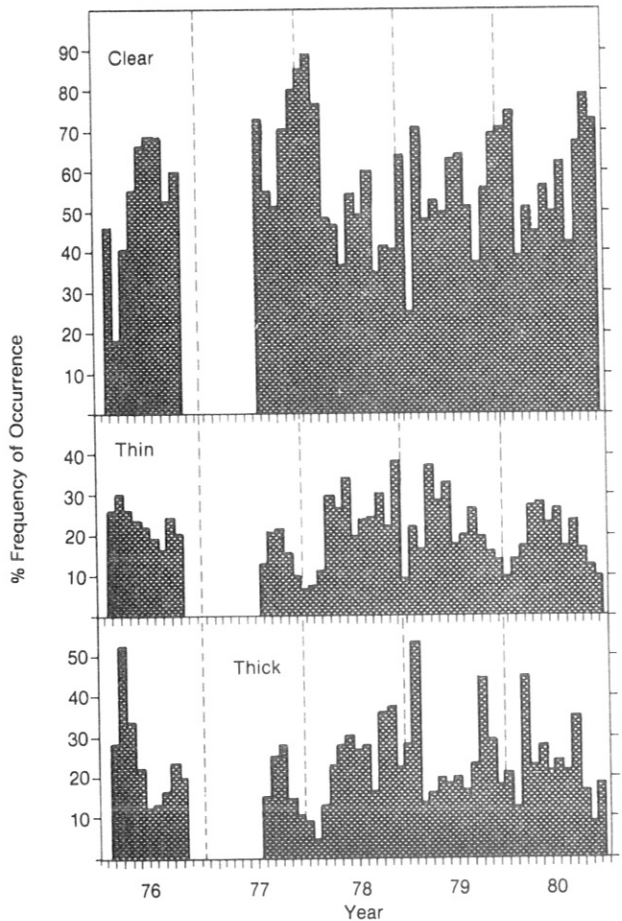


Figure 28.--Time series of monthly frequency of occurrence for clear and cloud conditions.

with associated standard deviations of .095, .012, and .038. On the average, only one-half of the solar direct beam reaches down to an altitude of 3.4 km.

A time series of monthly mean transmittance is shown in fig. 27. The horizontal dashed lines are the means for each data set. Thick-cloud monthly mean transmittance is not included because it is influenced largely by instrument noise. A straight-line least squares fit to each group of data resulted in no statistically significant slopes at the 95% confidence level.

Total transmittance is highly variable because a large proportion of clear-sky values increases the monthly mean transmittance, whereas a large proportion of thick-cloud occurrences decreases the transmittance.

The mean frequency of occurrence over the period for clear, thin, and thick clouds, respectively, is .563, .206, and .231, with a standard deviation of .153, .077, and .106. Clouds influence the direct-beam transmittance 44% of the time. Figure 28 shows the monthly frequency of occurrence in histogram form for the three subgroups. Statistically, the second quarter (April, May, and June) consistently had a higher mean occurrence of thin clouds at the 95% confidence level. No other comparisons proved significant.

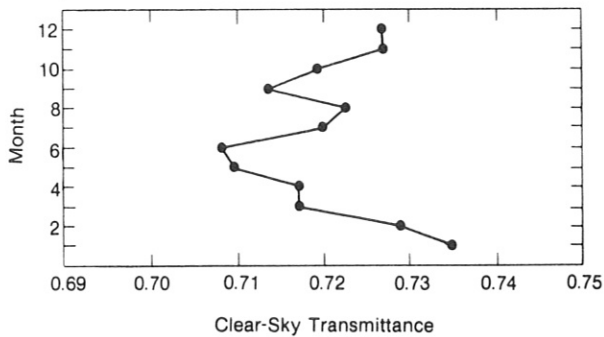


Figure 29.--Annual march of clear-sky transmittance.

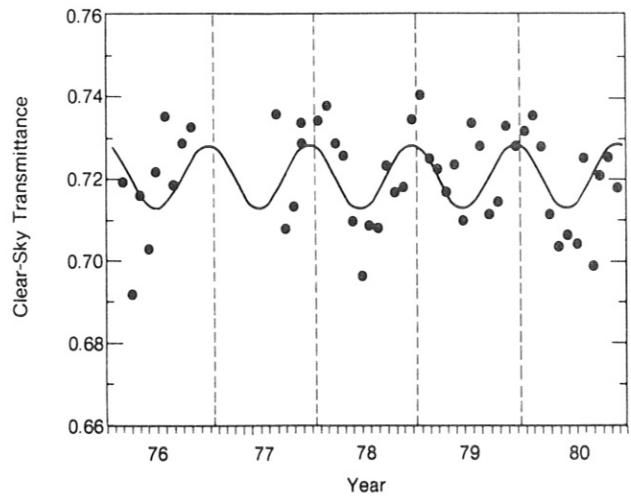


Figure 30.--Annual cycle of clear transmittance obtained by using a sine-cosine regression model. Circles represent the monthly mean data.

4.2.1 Clear Skies

An annual march of clear-sky transmittance for Mauna Loa is created (fig. 29) by taking the monthly data from each year and combining all the Januaries, Februaries, and so on into means. The figure shows that the winter months are clearer than those of summer. Because the data are zenith angle dependent, it is expected that the summer period would be clearer than the winter, all else remaining fixed. However, atmospheric extinction, which is enhanced in the summer, dominates.

An annual cycle in the clear-sky NIP record at MLO has been shown by other investigators. Applying a simple sine-cosine regression model to these clear-sky data yields a significant reduction in the variance at the 99.9% level. Figure 30 shows the monthly data and the modeled annual cycle. Again, the winter period is clearer than the summer.

4.2.2 Thin Clouds

The monthly mean thin-cloud transmittance can serve as a tool for monitoring possible climate change. A persistent trend in thin-cloud transmittance would indicate regional changes in cloud optical thickness. Significant changes in cloud occurrence could be monitored using the monthly frequency of occurrence.

One important question of any monitoring effort is how long observations must be made to establish a significant trend. From data obtained in this study, estimates of monitoring time can be made. A t-statistic can be calculated as each month of new data is added by using the thin-cloud standard deviation of monthly means as a measure of the variability of the data about a regression line. This is continued until a 95% confidence level is reached for a given slope. As the slope gets smaller, the time required to determine

Table 25.--Percent mean occurrence of vertical transmittance and variability over 3 years

Interval number	Transmittance interval	Mean frequency of occurrence (%)	Standard deviation
1	.00-.12	24.2	11.8
2	.12-.24	3.30	1.30
3	.24-.36	2.59	.98
4	.36-.48	2.56	1.18
5	.48-.60	2.93	1.47
6	.60-.72	4.13	2.03
7	.72-.84	51.6	12.1
8	.84-.96	8.69	10.1

the slope from the data gets appreciably longer, following an inverse power law,

$$\text{monitoring time} = 46 / (\text{percent slope})^{.6636}$$

For a 1% slope the monitoring time is 46 months. For a 0.1% slope, 212 months are required.

Because it is difficult to make valid comparisons from month to month or from place to place when the data are zenith angle dependent, it is worthwhile to remove this dependence by transforming the transmittance into the vertical. However, this is not a straightforward task since clouds are inhomogeneous. For the sake of comparison, a consistent transformation would be useful as a climate-monitoring technique.

It is possible to predict closely the vertical transmittance for clear skies by using the empirical maximum transmittance function, obtained as an upper bound for the clear-sky region in fig. 26, as the transformation equation. When this is applied to the thin-cloud region the assumption made is that the cloud is a homogeneous layer with optical properties that resemble clear skies. One important point that should be noted is that transmittance values near zero in the thick-cloud region cannot be transformed, but they can be counted if the zenith angle range is properly restricted.

The Mauna Loa transmittance data for 1978 through 1980, restricted to zenith angles less than 66.75° , were transformed to zero zenith angle and then categorized into eight transmittance intervals beginning at .00, in steps of .12, up to .96 for each month.

The mean vertical transmittance frequency of occurrence and variability for the 3 years are outlined in table 25. In intervals 2 through 5, the percent occurrence is remarkably uniform, and generally the values in the intervals change upward and downward together. Intervals 7 and 8, which contain the clear-sky data, as well as interval 1, which includes the thick-cloud data, are highly variable.

4.2.3 Final Remarks

This investigation shows how direct-beam irradiance observations may be used to infer a climatology of optically thin cloudiness. The complete results and details of the method will be published as a NOAA Technical Memorandum (Thompson, 1981).

It is well known that when clouds attenuate the direct solar beam, the diffuse radiation increases. Future work with the diffuse component of radiation at Mauna Loa is anticipated. Together, the diffuse and direct subtropical climatologies can be used to understand better the solar energy budget and its variation from high-level clouds.

4.3 Sampling Strategy to Obtain Data Used in Models of Global Annual CO₂ Increase and Global Carbon Cycle

4.3.1 Introduction

To work toward the goal of providing a truly global annual CO₂ increase and to determine details of the carbon cycle, smooth fluctuations of CO₂ concentration representing global scales are needed rather than highly detailed short-term fluctuations that would require microscale measurements for explanation. However, since data obtained can be expected to contain fluctuations due to small-scale events not of interest for the global-scale concerns, this variation will produce uncertainty in the estimates of interest. The effect of sampling strategy (i.e., number of globally distributed stations and frequency of sampling) on the variance or uncertainty of estimates is considered here. (For a more complete analysis, see Gillette and Hanson, 1981.)

At the time of this analysis, CO₂ concentration data for 3 years from seven globally distributed locations were available. The data were not continuous, but rather were representative of air samples obtained in pairs of 500-ml flasks at roughly equally spaced intervals over the year. All of the samples were analyzed at the same GMCC laboratory in Boulder, Colorado. The data contained some sampling gaps from uncontrollable factors and were not taken at exactly the same time at all stations. A model of CO₂ concentration was constructed to evaluate the data, despite these deficiencies, for variance of global annual CO₂ increase and ratio of standard deviation of monthly means to annual amplitude of CO₂ fluctuation.

A Model of CO₂ Concentration for a Given Location

CO₂ concentration at a given location, as determined from flask samples taken within a few minutes of each other and obtained regularly over the year at no less than 2-day intervals, may be expressed as

$$[\text{CO}_2]_{kij} = \mu_k + A_{ki} + f_{kij} + \varepsilon_{kij}$$

where

$[\text{CO}_2]_{kij}$ is the concentration of CO₂ during year k at station i for time j within the year,

μ_k is the global mean CO₂ concentration for year k,

A_{ki} is the deviation from μ_k of the CO₂ concentration yearly mean at location i during year k ,

f_{kij} is a function of day of year (j), which is a polynomial of degree 5 or less, and

ε_{kij} is a normally distributed random variable.

The variables f_{kij} , A_{ki} , and ε_{kij} all have means of zero. Values of ε_{kmj} were assumed to be independent of ε_{kij} ($i \neq m$) since they represent random noise at individual stations i and m located thousands of kilometers apart.

4.3.2 Estimates for Climate and Carbon Cycle Models

Two estimates of interest to climate and carbon cycle modelers are the global annual increase of CO₂ concentrations and the variation of CO₂ concentration throughout the year, which reflects the actions of sources and sinks of atmospheric CO₂. These estimates were analyzed in light of the model and flask data for 3 years at seven locations.

Global Annual Increase of Atmospheric CO₂

The quantity $\bar{\Delta} = \mu_k - \mu_{k-1}$ is estimated by forming the annual CO₂ concentration means for years k and $k-1$ of all locations, pooling the means into global means for years k and $k-1$, and finding the difference. The variance of the estimate is calculated by subtracting the individual values for years 2 and 1 from their global annual means, squaring, summing, and then dividing the mean by the number of observations.

$$\text{Var} (\bar{\Delta}) = \frac{\sigma_A^2}{M} + \frac{\sigma_F^2 + \sigma_1^2 + \sigma_2^2}{NM} \quad (1)$$

where

N is the number of flask pairs per year at each station,

M is the number of locations,

σ_A^2 is the variance of the $A_{2i} - A_{1i}$ terms,

σ_F^2 is a function of the differences between two smooth F functions for years 1 and 2, and

σ_1^2 and σ_2^2 are the global means of residual ε_{kij} variances for years 1 and 2.

Values for the terms in (1) were used to plot the standard deviation of the estimate of $\bar{\Delta}$ vs. number of samples per year N and number of sampling locations M (fig. 31). As N and M become large, assumptions concerning lack of serial correlation and spatial correlation are violated, and the calculation underestimates the standard deviation of the global annual increase. As is seen, the most advantageous region of the plot for optimizing results is in the bending region where increases of both M and N lead to decreases in standard deviation of $\bar{\Delta}$. Since it can be argued that it is cheaper to sample at a

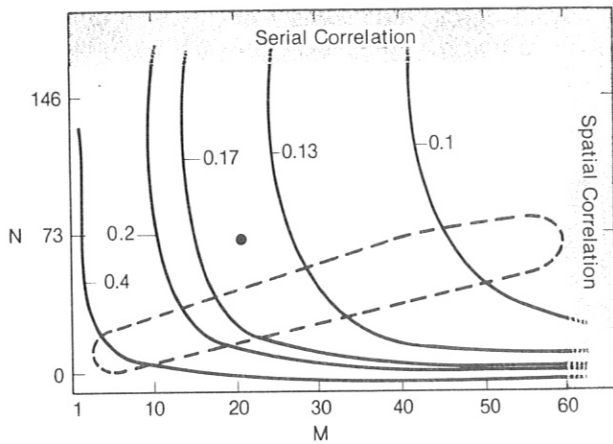


Figure 31.--Standard deviation of global annual CO₂ increase Δ , as a function of number of equally spaced flask samples obtained per year, N, and number of globally distributed flask sampling locations, M.

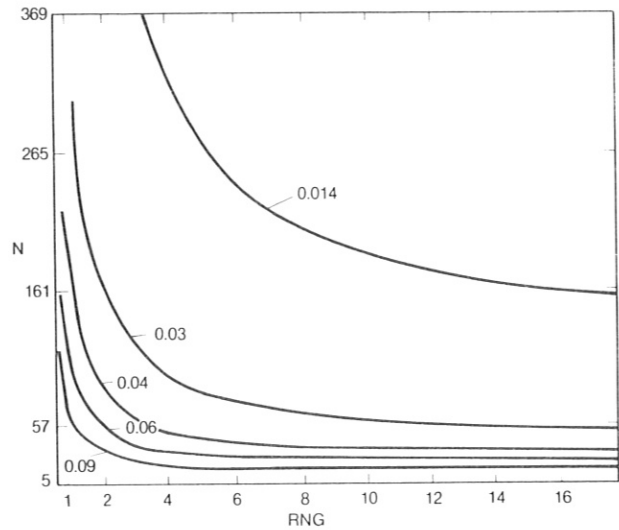


Figure 32.--Fraction ϵ as a function of number of equally spaced flask air samples obtained per year, N, and range of the annual cycle, RNG.

slightly higher rate than to establish new sampling locations, the optimal sampling region may be slightly above the bend (circled in fig. 31). The values of N and M for the GMCC flask sampling network fall slightly above this circled area of the plot.

Variation of Mean CO₂ Concentrations Throughout the Year

To investigate the pattern of mean concentration throughout the year, the standard deviation of the mean concentration should be small in comparison with the difference between the minimum and the maximum CO₂ concentration during the year. By calling the difference between the maximum and minimum values of the fitted function f_{kij} the annual range RNG and specifying a monthly mean, a condition may be written

$$\sigma_{km} (N)^{-\frac{1}{2}} = \epsilon \text{ RNG}_{km} \quad (2)$$

where ϵ is a fraction smaller than one.

Examination of the data revealed an apparent correlation between RNG_{km} and σ_{km} . A first-order linear regression model was fitted to the data:

$$\sigma_{km} = C1 + C2 \text{ RNG}_{km} \quad (3)$$

Mean values for the regression constants C1 and C2 were used in (3) to solve (2) for N, the number of evenly spaced samples taken during the year for arbitrary values of ϵ . The results are shown in fig. 32 where a weekly sampling rate is plotted vs. RNG. The figure shows that $\epsilon \leq 0.1$ is obtainable for $\text{RNG} > 3$ for sampling rates of about twice per week.

4.3.3 Discussion

The principal objectives of CO₂ flask sampling are to obtain reliable detail on fluctuation of mean concentrations through the year as well as to obtain annual CO₂ increases with small confidence intervals. It would seem, however, from the above analysis that the two objectives do not allow exactly the same sampling strategy. The optimization of the annual CO₂ increase would require more sampling locations and a lower sampling rate for the same effort spent than would a strategy that minimizes the variance about monthly or sub-monthly means for individual locations. A compromise strategy is required that provides for acceptably small variances about monthly means while providing sufficient sampling locations for a small variance of the global annual increase estimate. For the GMCC group the compromise has been to strive for a sampling rate of twice per week at about 20 globally distributed sampling locations.

4.4 Decomposition of Annual Variations of CO₂ Concentration at GMCC Flask Sampling Stations Into Three Patterns

4.4.1 Introduction

Typical patterns of CO₂ variation during the year were sought such that linear combinations of the patterns would duplicate most of the observed CO₂ variation at the GMCC flask sampling stations. Such statistically independent (orthogonal) patterns were obtained by calculating eigenvectors (Stidd, 1966; Wylie, 1966).

4.4.2 Input Data

CO₂ concentration data from 1979 for 14 globally distributed locations were taken from the paper by Komhyr et al. (1981d). Air was collected in pairs of 0.5-ℓ glass flasks at 19 stations (fig. 33). The data were selected to remove CO₂ concentrations that are probably in error by the algorithm described by Gillette and Steele (1981).

The selected data were used to form monthly means for the 14 locations. Annual means of the 12 monthly means were formed for each station. These annual means were subtracted from each of the monthly means for each station to give the values b_{ij} . The values a_{ij} were calculated by dividing b_{ij} by the standard deviation σ_j of monthly means about the annual mean for station j :

$$a_{ij} = b_{ij}/\sigma_j.$$

One of the sampling locations reported by Komhyr et al. (1981d), Palmer Station, on Anvers Island, Antarctica, was not used because of a discontinuity in CO₂ concentration during the year. The cause of this discontinuity had not been determined at the time of this writing.

4.4.3 Results

The first three eigenvalues, when normalized to the total, represent 90% of the variance. The annual CO₂ patterns (eigenvectors) corresponding to

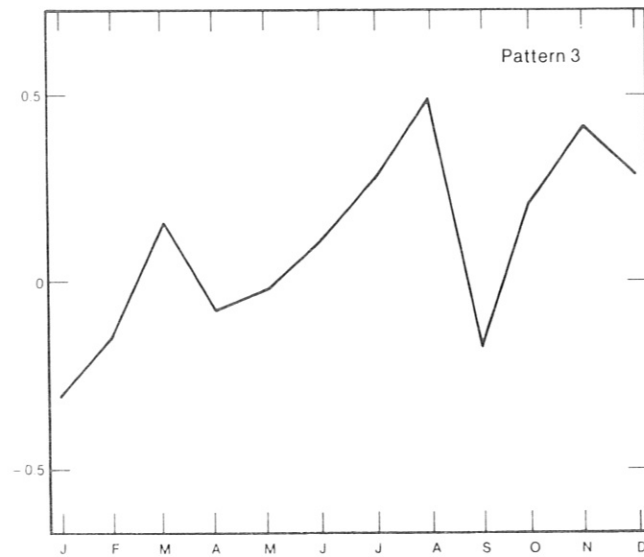
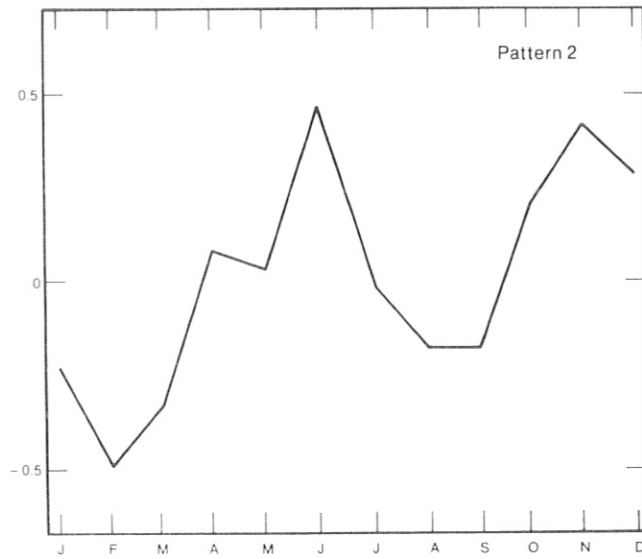
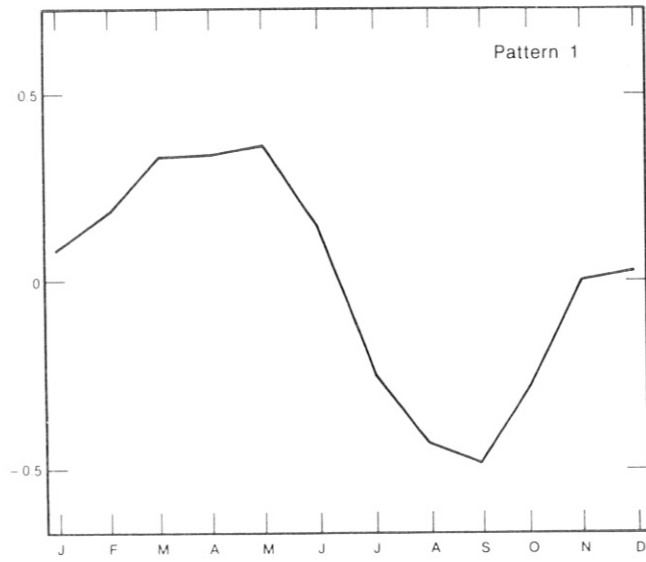


Figure 33.--CO₂ annual fluctuation, patterns 1, 2, and 3.

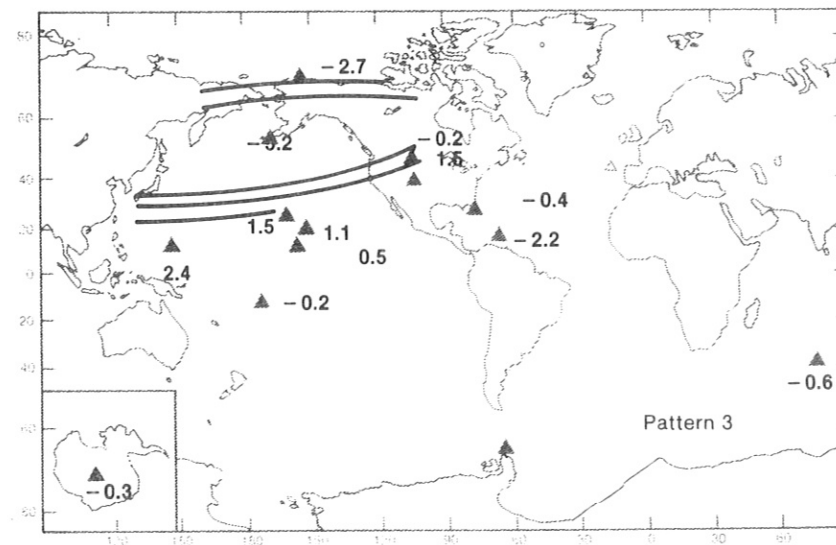
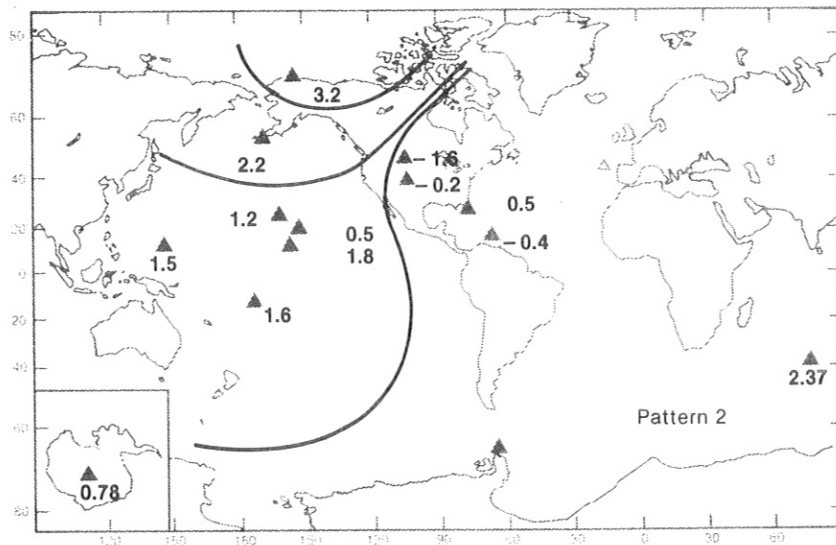
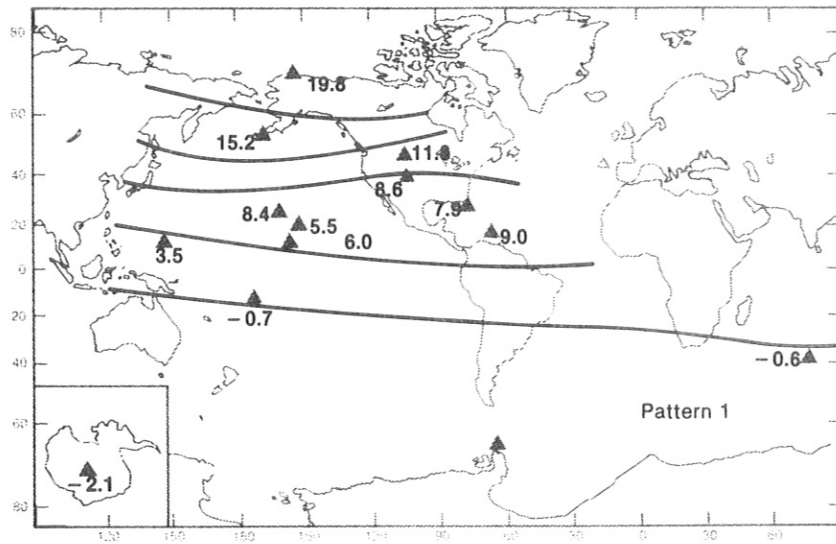


Figure 34--Loading factors for patterns 1, 2, and 3.

these three eigenvalues, when multiplied by loading factors and added together, should duplicate the b_{ij} of the original data fairly well. Loading factors ld_{lj} were found for each station for each eigenvector from the matrix equation:

$$LD = E \cdot B$$

where LD is composed of ld_{lj} , E is composed of eigenvector e_{li} , and B is composed of b_{ij} .

The first three characteristic patterns are plotted in fig. 33. The loading factors ld_{lj} are plotted on maps in fig. 34.

4.4.4 Interpretation and Discussion

The following interpretations were arrived at after examination of the patterns and loading factors in figs. 33 and 34:

(1) Pattern 1. This pattern is a rather idealized or averaged annual cycle, which resembles the individual patterns to a lesser or greater extent. It represents 69% of the variance of the CO₂ patterns. The loading factors ld_{lj} for this pattern are similar to the annual amplitudes of the patterns for individual locations. In fig. 34, ld shows a strong north-south gradient. In the Southern Hemisphere, loading factors are negative, reflecting half-year phase difference with the Northern Hemisphere.

(2) Pattern 2. This pattern, when added to pattern 1, gives a steeper increase in the early months of 1979, a later maximum, and a steeper increase from September to November. It has large loading factors mainly in the Pacific and may reflect an oceanic adjustment. It represents 13% of the variance.

(3) Pattern 3. This pattern, when added negatively to pattern 1, causes a lower CO₂ minimum in September and lower values in November and December. The negative loading factors are largest at Cold Bay and Pt. Barrow, Alaska, and may reflect an intense removal of CO₂ by the biosphere or by the cold waters of the northern oceans. It represents 7.5% of the variance.

In summary, the first pattern is simply a rather idealized annual cycle, which has much in common with the annual fluctuation of CO₂ at all locations. The loading factors of this pattern express the magnitude of fluctuation of CO₂ when regional effects are removed. Pattern 2 suggests a phase change due to oceanic temperature fluctuations and appears to be strongest near the poles. Pattern 3 suggests a biospheric effect, deepening the annual cycle minimum at northern locations. (See Gillette, 1981, for an extended discussion.)

4.5 Comparison of Airborne CO₂ Flask Samples and Measurements From MLO During the HAMEC Project (June 1980)

4.5.1 Introduction

At all GMCC stations the interpretation of the measurements in terms of global-scale changes requires the measurement of other constituents such as

aerosols, wind, and air trajectories, and detailed analysis to isolate possible local contamination (Keeling et al., 1976, Miller and Chin, 1978; Bodhaine et al., 1980). Thus, when the opportunity became available to measure a climatically significant variable such as CO₂ in the free atmosphere away from local sources and sinks, it was exercised. The Hawaii Mesoscale Energy and Climate Project (HAMEC) provided such an opportunity (Nolt et al., 1980).

4.5.2 Background

The HAMEC flask sampling experiment was not the first attempt to obtain representative tropospheric samples outside the mesoscale effects of Mauna Loa. Two flights were made in a small aircraft (Cessna 206) in 1971. The first, on November 24, began in Kona, climbed to 3.3 km off Upolu Point, and continued around the island at this altitude to a point over Volcano National Park where the plane descended to 1.8 km. From South Point to Kona the flight altitude was 1.8 km. The flight began at 0530 HST and lasted 2 hours; during this time 41 flasks were exposed. The second flight, on December 3, began at Hilo at 1500 HST. The flight proceeded to a point off Ninale where a sounding was made by climbing to 3.4 km. Via a route north of Mauna Kea, the flight proceeded to Kona at an altitude of 3.0 km. Off the Kona coast the aircraft spiraled down to a level of 0.6 km and returned to Hilo around Upolu Point. As on the first flight, flask samples were taken at 1,000-ft increments during each climb and descent, and at regular intervals during level flight. Thirty flasks were exposed on the second flight.

The accompanying diagram (fig. 35) shows the distribution of the measured concentration of the flask samples as a function of altitude, according to the coding shown. It is important to notice that the main group of points between concentrations of 320 and 325 ppm contains values measured at all altitudes. Also many of the larger values, especially during the first flight, were obtained during flight, at the altitude of the observatory. Both flights were conducted on days of moderate instability, according to the notes of the observer. The Hilo rawinsonde confirms the absence of a distinct trade inversion and shows northerly winds at about 5 m s^{-1} in the lowest 4 km. Clearly the majority of the concentrations fell between 321 and 324 ppm. The average for each day was computed, considering this population to be representative of midtropospheric CO₂ concentrations in these mixed and variable conditions. On 24 November the average was 322.4 ppm; on 3 December, 322.1 ppm.

Sixteen flasks were exposed along the road at vertical intervals of 1,000 ft as MLO staff proceeded to the observatory. Sampling started at 0700 HST on November 24. Whereas some of the flasks were contaminated, especially those taken in the lowest 3,000 ft, eight fell between the limits defined above. The average concentration from this set of flasks was 321.7 ppm. Considering the large variations in this sampling period, a difference of only 0.7 ppm speaks well for the representativeness of the MLO observations. (Comparable samples were not taken during the December 3 flight.)

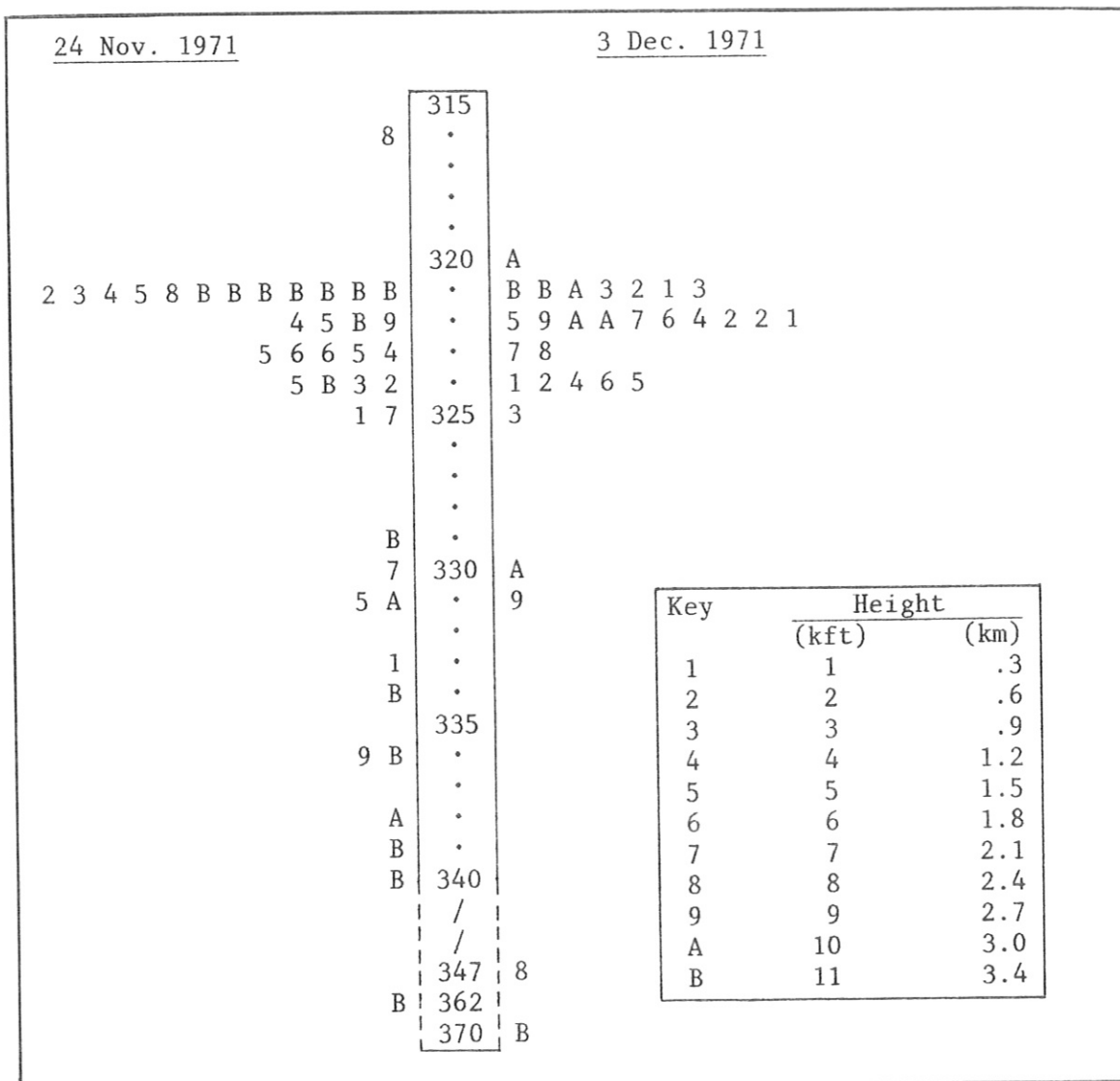


Figure 35.--Distribution of the CO₂ concentrations measured from flask samples taken from aircraft. CO₂ concentrations (ppm) are in the 1974 manometric mole fraction scale.

4.5.3 HAMEC Operations

The primary objective of HAMEC was to obtain measurements for initialization and validation of the dependent variables explicitly predicted by the mesoscale warm-rain model of Nickerson and Magaziner (1976). In particular, the NOAA P3 aircraft was equipped with instrumentation to measure the microphysical properties of tropical clouds, to determine interface temperatures radiometrically, and to measure the distribution of wind, temperature, and humidity. At times when soundings were made to measure the vertical profile of meteorological variables, flask samples were exposed for subsequent analysis for CO₂. Plans called for samples to be taken at 0.5-km levels, 3 km above and below the level of MLO. Unfortunately, tests conducted at the beginning of the program showed that the sampling manifold leaked when the

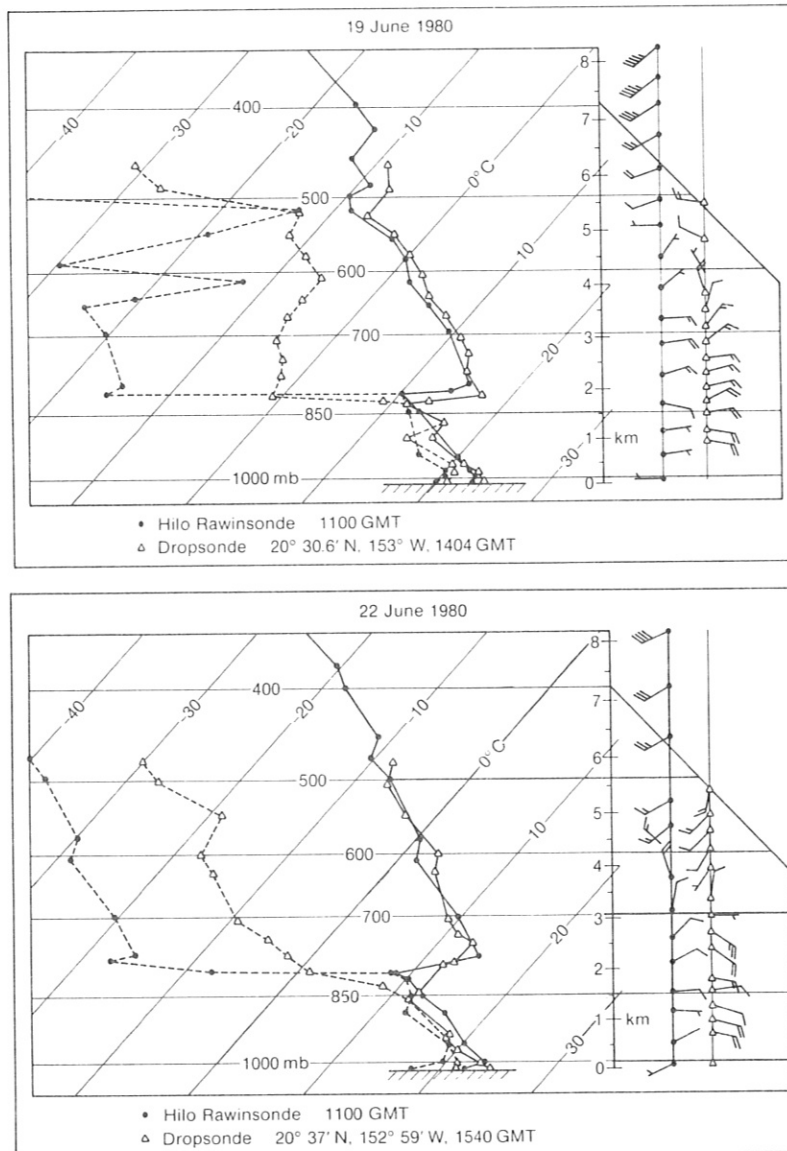


Figure 36.--Wind, temperature, and dewpoint temperature soundings plotted as a function of pressure.

cabin was pressurized. Although the leak was subsequently repaired, samples were obtained only when the cabin was unpressurized (below 3.5-km altitude). Both soundings were made to the northeast of the island of Hawaii, in the early morning.

4.5.4 Meteorological Conditions

On both days, and for the 6-h period before the CO₂ samples were taken, the Hilo temperature sounding (fig. 36) showed considerable uniformity in the lowest 6 km. Dropsondes were released in the vicinity of the airborne CO₂ samples, about 250 km northeast of Hilo, 5 to 6 hours after the Hilo sounding (Dias et al., 1981). A temperature inversion at a height of 2 km clearly

Table 26.--Hourly average wind and Aitken nucleus measurements at the Mauna Loa Observatory

Time (GMT)	19 June 1980			22 June 1980		
	Resultant direction (deg.)	Wind- speed (m s ⁻¹)	Aitken nuclei (cm ⁻³)	Resultant direction (deg.)	Wind- speed (m s ⁻¹)	Aitken nuclei (cm ⁻³)
1200	160	6.1	370	170	1.5	290
1300	150	6.8	280	170	1.7	280
1400	150	6.2	260	150	1.3	280
1500	160	3.2	265	160	1.8	300
1600	150	4.1	270	200	0.5	335
1700	130	5.7	270	320	0.3	315
1800	120	6.0	275	330	1.7	300
1900	080	5.7	280	330	2.4	275
2000	120	6.2	290	330	2.7	270

separates a midtropospheric transition layer from the moist marine boundary layer. For the most part, a second stable (though weak) layer, at a height of 5.5 km on 19 June and 4.3 km on 22 June, marks the top of the transition layer from easterly winds to westerly winds. The uniformity in the soundings over the distances and times involved indicates that midtropospheric conditions were reasonably steady during the period of comparison. Streamline analysis of the 700-mb level (3.2-km height) shows the island of Hawaii located at the northern edge of the equatorial easterlies on June 19. Three days later the easterlies were replaced by two small regions of anticyclonic flow, one near the Hawaiian Islands and the other to the east. Although it may not be as certain for the June 22 sounding as for the one on the 19th, the aircraft soundings conducted about 280 km northeast of Hilo were generally in an area that was free from island influence.

The wind direction, windspeed, and concentration of Aitken nuclei at MLO proved very useful in the past for determining the presence of contamination or for identifying peculiarities in the local wind field (Keeling et al., 1976; Bodhaine et al., 1980). The hourly mean resultant winds and Aitken nucleus counts for the 9-h period beginning at 1200 GMT (0200 LST) are listed in table 26. On June 19 a steady 6 m s⁻¹ southeasterly wind prevailed throughout the observation period. Downslope winds in excess of a few meters per second probably reflect the combination of a gradient wind and redirection of the midtropospheric easterlies by the island of Hawaii. The Aitken nucleus concentration ranged between 260 and 370 nuclei cm⁻³ with little hour-to-hour variability. The wind conditions on June 22 were somewhat different with very light (1.5 m s⁻¹), but steady, southeasterly winds through the first 4 hours of the period, shifting at sunrise to a steady, but weak (about 2 m s⁻¹), northwesterly wind for the remainder of the period. The venting of gases from the main caldera of the Mauna Loa Volcano or rift zones on its eastern slope have contaminated the southerly winds in the past (Pales and Keeling,

Table 27.--Measured values of CO₂ concentration from flask samples taken on the aircraft and hourly averaged continuous measurements from MLO

Time (GMT)	Source*	Altitude (km)	CO ₂ mole-fraction (ppm)	
			Flask pair and differences†	Hourly average
<u>19 June 1980</u>				
1430	P3 aircraft	3.4	344.2 (Δ0.1)	
1452	P3 aircraft	2.7	344.2 (Δ0.8)	
1300	MLO (continuous)	3.4		345.5
1400	MLO (continuous)	3.4		345.5
1500	MLO (continuous)	3.4		345.3
1600	MLO (continuous)	3.4		345.5
1700	MLO (continuous)	3.4		345.0
<u>22 June 1980</u>				
1610	P3 aircraft	3.4	345.4 (Δ0.9)	
1620	P3 aircraft	2.7	346.3 (Δ4.0)	
1630	P3 aircraft	2.1	347.8 (Δ7.0)	
1500	MLO (continuous)	3.4		345.0
1600	MLO (continuous)	3.4		345.0
1700	MLO (continuous)	3.4		345.1
1800	MLO (continuous)	3.4		345.2
1900	MLO (continuous)	3.4		345.2

*On 19 June, the aircraft sampling was performed at 19°30'N and 155°31'W; on 22 June, at 20°24'N and 153°0'W. MLO is at 19°32'N and 155°35'W.

†The Δ value in parentheses indicates the difference between the flasks.

1965; Miller and Chin, 1978; Bodhaine et al., 1980). In such situations the continuous records of CO₂ and Aitken nuclei showed short-period increases of a highly intermittent nature. CO₂ traces recorded during the period of intercomparison were examined and found to be free of the variations that typically accompany volcanic venting. On the basis of the steadiness of the wind and Aitken nucleus and CO₂ concentrations at MLO, it seems reasonable to conclude that the conditions on both mornings are typical of background situations.

4.5.5 Results

Samples of atmospheric CO₂ taken aboard the aircraft were analyzed in Boulder using the system of Komhyr et al. (1980). CO₂ concentrations listed in table 27 are obtained by averaging the values of the two flasks exposed in

succession at the levels indicated. The difference for each pair is denoted by the delta value. The second part of table 27 contains a listing of the hourly average CO₂ concentrations measured continuously at MLO for the 5-h period centered on the time of the aircraft samples. The values have been corrected for altitude. Hour-to-hour variations are small, indicating a consistency with other data presented earlier.

One-half-liter sampling flasks were attached to the first impactor port on the isokinetic aerosol sampling system (Parungo et al., 1981). The flow rate was approximately 20 l min⁻¹. The flasks were opened for approximately 3 minutes allowing 60 l to flow through.

The agreement between the flask samples at 3.4 and 2.7 km on June 19 was excellent. The height of the marine inversion was 2 km so both samples were clearly in the dry, easterly midtropospheric flow. The agreement indicates the absence of a significant gradient in the lower levels. The larger difference between the two flasks at 2.7 km (0.8 compared with 0.1 at 3.4 km) may be caused by larger variability in the ambient CO₂ concentration at lower altitude. On June 22 the average value and the disagreement between the flasks were larger, and both increased markedly at the height of the trade inversion. The top of the inversion was 0.2 to 0.4 km higher on June 22 than on the 19th (fig. 36). Thus we attribute the larger values measured at 2.1 and 2.7 km to be in or partly in the marine layer. With the arrival of air from below the trade inversion in the morning at MLO, the continuously measured CO₂ concentrations have been observed to increase (Keeling et al., 1976). When the average of the early morning continuous CO₂ measurement from MLO was compared with the flask sample at the same level the difference was -1.3 ppm on June 19 (the flask values being less than the continuous). On June 22 the difference was +0.3. The relatively large difference on June 19 may indicate that the CO₂ concentrations observed at MLO during strong down-slope situations represent a level 1 to 2 km above the observatory. In this particular situation, that would correspond to the level of the stable layer observed at 5.2 km. Unfortunately it was not possible to sample above 3.5 km, as was planned, for such data would have proved very useful in the interpretation of these results.

In conclusion, on two mornings during the HAMEC project all the meteorological criteria were satisfied for making comparative CO₂ measurements at MLO and by aircraft upwind of the islands. The most important condition was a steady flow regime in the midtroposphere with a well-developed trade inversion. Considering that the average difference between the flasks was 0.5 ppm and that flask values were being compared with continuous measurements with a difference of about 0.4 ppm (Komhyr, personal communication), the results of both flights show reasonably good agreement. Under such conditions the continuous measurements from MLO are representative of the middle troposphere.

4.6 CO₂ Measurements at Barrow, Alaska

The GMCC CO₂ measurement record from Barrow, Alaska, was analyzed in some detail from the beginning of the record (1973) through 1979. A selected data set was prepared, with periods of local influence removed, along with a description of year-to-year and within-year CO₂ variability. The full report of this study is given in Peterson et al. (1982). A synopsis is given in this Summary Report.

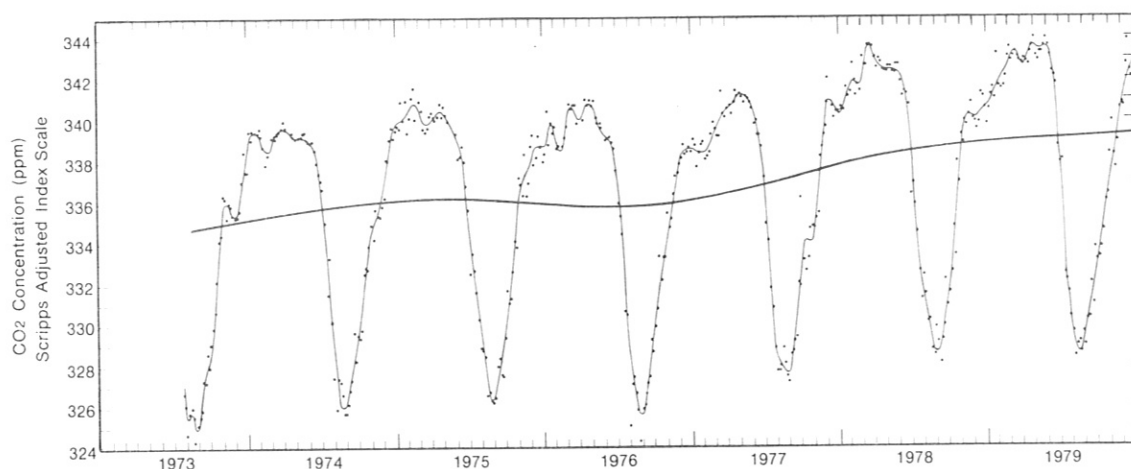


Figure 37.--Five-day average CO₂ concentrations (dots) at Barrow, 1973-79, using selected data only. The continuous curved lines are cubic spline functions showing short-term (thin line) and long-term (thick line) CO₂ variations.

Herein, we will report dry-air atmospheric CO₂ concentrations in relative and absolute scales. The relative scale is the 1959 SIO adjusted index scale, whereas the absolute scale is the WMO 1974 CO₂ calibration scale with our tentative pressure-broadening correction applied to give mole fractions. Following the nomenclature of Keeling et al. (1976), we refer to our data in these two scales as CO₂ adjusted index (J) and mole fraction (X) values with units of parts per million by volume (ppm).

To obtain a data set representative of larger space-scale conditions, we used an objective statistical selection scheme that probably deletes most locally contaminated values. The underlying philosophy of the method is that a homogeneous airmass, free of local contamination, has small within-hour and hour-to-hour CO₂ concentration changes. Specifically, when the hour-to-hour change exceeded 0.25 ppm, values for both hours were deleted from the data set. A much smaller group of values was also deleted on the basis of within-hour variability. Finally, after these criteria were applied, a few remaining outlying values (representing far less than 1% of the data) were subjectively deleted.

The impact of data selection on the Barrow record strongly depends on season. For example, CO₂ variability during May is at a minimum, and few values are selected out of the record. In contrast, the midsummer period exhibits the greatest variability, and our selection scheme removed about 60% of the hourly data. August monthly averages for selected and complete data sets differ by more than 1.5 ppm.

To focus on the longer-time-scale Barrow CO₂ variability, the data were smoothed by averaging the selected hourly values by 5-day periods (dots in fig. 37). In addition, cubic spline functions (Wold, 1974) with knots every 20 days were fitted to the 5-day average points over the full measurement record (thin continuous line in fig. 37). The thick continuous line in fig. 37 is a cubic spline function designed to show interannual and long-term CO₂ secular change.

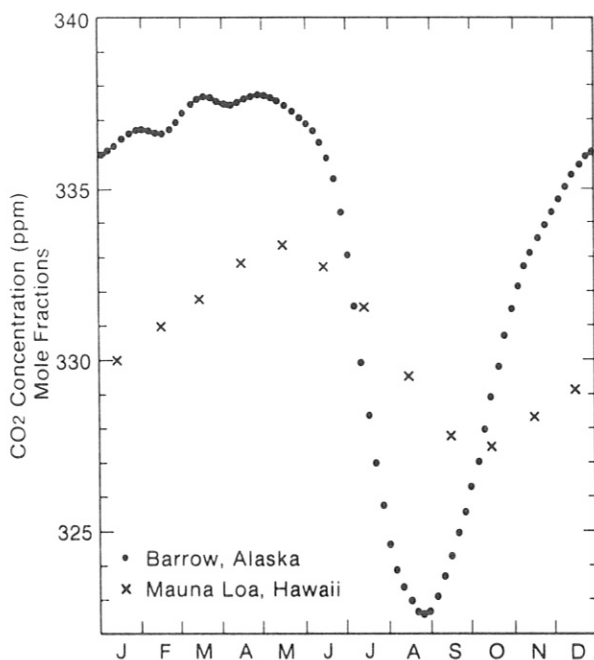


Figure 38.--Composite average annual CO₂ concentration at Barrow. Each dot represents a 5-day average. Monthly average concentrations at Mauna Loa (crosses) are from Keeling (personal communication, 1980). Data are referenced to January 1, 1974, and are expressed in absolute mole fraction units with pressure-broadening corrections applied.

A main feature of fig. 37 is the leveling-off and decreasing trend of the long-term curve during the middle of the Barrow record. The slope of that curve is negative from May 1975 to July 1976. Recent analysis of the Ocean Station P (50°N, 145°W) CO₂ measurements (Hanson et al., 1981) showed a 1975-76 trend similar to that described for Barrow. The Station P CO₂ dip was ascribed to an anomalously cold region of sea surface temperatures in the North Pacific (and consequent anomalous ocean uptake of CO₂).

A composite annual cycle of CO₂ concentrations at Barrow was computed from the data of fig. 37. The data were detrended for adjustment to a reference of January 1, 1974, and then averaged through the calendar year by each 5-day interval. The resulting mean 5-day concentrations (referenced to January 1, 1974), converted from adjusted index scale to mole fractions, are presented in fig. 38. For comparison, we include in fig. 38 Scripps monthly averages from Mauna Loa (also in mole fractions), detrended and referenced to January 1, 1974.

The Barrow CO₂ annual cycle has an amplitude of 15.2 ppm (absolute mole fraction units) and is very asymmetric. The amplitude compares well with that from other high-latitude measurements: 15.0 ppm for 1- to 3-km altitude over Scandinavia and about 14 to 15 ppm from Ocean Station P. The asymmetry is evidenced by the average date for the maximum on April 28 with the minimum just 4 months later on August 26.

Comparison of the Barrow and Mauna Loa average annual cycles in fig. 38 shows distinct differences in both amplitude and phase. The low-latitude, high-altitude Hawaiian measurements have smaller amplitude (less than 6 ppm), a more symmetric annual cycle, and a phase lag of about 1/2 month at the spring maximum and nearly 2 months at the autumn minimum, in comparison with the Barrow record. The fig. 38 data also show the annual variation of the north-south CO₂ interstation gradients. The absolute value of these gradients and associated concentrations should not be taken too literally, and we do not

imply that the gradients are linear over the 50° of latitude between the sites. The Barrow values have their greatest margin over Mauna Loa (more than 6 ppm) during December and January. In summer the gradient reverses, with its largest value exceeding 6 ppm in August.

Averaging the fig. 38 data over the year gives a Barrow annual mean that is about 2.5 ppm greater than that at Hawaii. This contrasts with a Barrow-Mauna Loa difference of about 1.2 ppm reported by Bolin and Keeling (1963). Why does the mean CO₂ concentration at Barrow exceed that at Mauna Loa? Among possible reasons are anthropogenic CO₂ release centered in Northern Hemisphere mid-latitudes north of Hawaii or natural (i.e., oceanic and/or biospheric) mean CO₂ sources north of Mauna Loa or natural sinks to the south. Cautious acceptance of the approximate doubling of the mean Barrow-Mauna Loa concentration difference over some 15 years suggests that the first or anthropogenic reason for sustaining the difference may be important. During this period worldwide emissions of CO₂ increased 80% (Rotty, 1978).

4.7 Some Optical Properties of Arctic Haze at Barrow, Alaska

4.7.1 Introduction

Observations of Arctic haze date back to the early 1950's. The cause and physical nature of the haze at that time were uncertain, but its coverage extended to hundreds of kilometers across and to heights of 3.0 km. Recent investigations of Arctic haze at the GMCC Observatory in Barrow, Alaska, show that it is a winter and early spring phenomenon (Larssen and Hanssen, 1980; Peterson et al., 1980; Kerr, 1979; Rahn et al., 1977). Furthermore, enriched amounts of anthropogenic pollutants have been detected in the haze, suggesting that part of the material in it comes from heavily industrialized regions quite distant from the Arctic (Rahn and McCaffrey, 1980).

4.7.2 Procedure

Radiation measurements at the surface using sun photometers, pyrheliometers, and pyranometers were made on clear days with cloudless skies when the transmission was high (control days) and on cloudless days with Arctic haze episodes. The instruments and bandwidths used are shown in table 28.

A perturbation technique (DeLuise et al., 1977) was used to determine the increase in optical depth ($\Delta\tau_h$) due to the haze at constant solar elevations on cloudless days.

Attenuation of the direct solar beam irradiance was investigated using very low wavelength resolution. It was observed that during hazy days, as opposed to control days, an increase in attenuation toward the shorter wavelengths occurred (table 28). A more uniform attenuation across the spectrum was observed in the hemispherical total irradiance measurements (table 28).

To separate the attenuation of the Arctic haze and water vapor, a correction was applied for water vapor extinction between the control days and hazy days. The resulting attenuation values are given in table 28 in the column labeled "H₂O corrected." Corrections for water vapor extinction were necessary because precipitable water vapor amounts calculated from NWS rawinsonde

Table 28.--Aerosol optical depth change and percent decrease in total irradiance due to aerosols and water vapor*

Measurement	Measurement bands	Percent decrease (airmass 2.5)		Change in optical depth (airmass 2.5) $\Delta\tau_h$
		Haze and H ₂ O	H ₂ O corrected	
Turbidity	Narrow band			
	.38	100	--	.107
	.50	100	--	.145
Direct-beam normal inci- dent irradi- ance	Broad band			
	.28-3.0	20	16	.09
	.53-3.0	19	14	.08
	.695-3.0	17	11	.075
	Differential bands			
	.28-.53	29	--	.137
	.28-.695	26	--	.121
	.53-.695	24	--	.110
	Horizontal hemispherical total irradi- ance	Broad band		
.28-3.0		4.3	1.0	.017
.53-3.0		4.4	0.5	.017
.695-3.0		4.0	0.5	.016
Differential bands				
.28-.53		4.0	--	.016
.28-.695		4.7	--	.019
.53-.695		5.4	--	.022

*These data were calculated as a difference between hazy days and control days.

data (taken nearby) on the days of the measurements showed a 30% increase in total precipitable water vapor on hazy days. Furthermore, relative humidities increased from ~50% on control days to >90% at 1.0 km on days when Arctic haze was observed.

After the water vapor extinction corrections were applied, most of the extinction due to the haze alone in the global hemispherical radiation flux was seen to occur at wavelengths less than 0.7 μm .

4.7.3 Results

The change in optical depth of the haze ($\Delta\tau_h$) was calculated using direct-beam pyrhelometer measurements, Volz turbidity measurements, and the perturbation technique developed by DeLuisi et al. (1977). A straight-line best-fit curve was computed for the change of optical depth between control days and hazy days as a function of wavelength (fig. 39), as

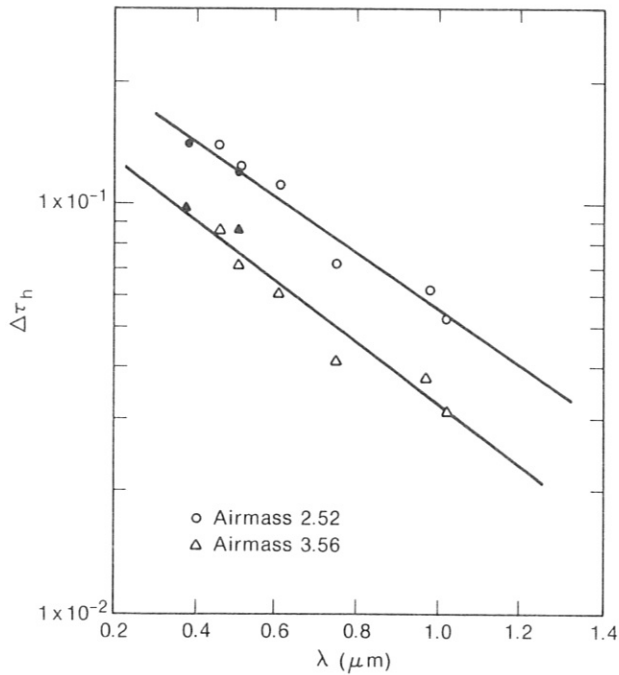


Figure 39.--Change in optical depth ($\Delta\tau_h$) between control and hazy days at Barrow, Alaska.

$$\Delta\tau_h = a\lambda^n ,$$

where

a = constant (for airmass 2.52, $a = 15.6$; for airmass 3.56, $a = 18.9$),
 λ = wavelength, ranging from 0.385 to 1.0 μm , and
 n = slope of the curve.

Measurements were made at airmass 2.52 and 3.56, and corrections for water vapor were made.

Values obtained for n were -1.05 for measurements made at airmass 2.52 and -1.16 for measurements made at airmass 3.56. The power law size distribution relationship for aged continental aerosols with diameters between 0.1 and 1.0 μm was used to relate the value of n to the size distribution characteristics of the Barrow Arctic haze. Thus,

$$\frac{dN}{d \log r} = b r^{-\beta} , \quad \text{and } \beta = n + 2 ,$$

where N is the particle number concentration (cm^{-3}) of aerosols, b is a constant, and r is the aerosol radius in μm . The values of β computed for the Arctic aerosol at Barrow were 3.1 for measurements made at airmass 2.52 and 3.2 for measurements made at airmass 3.56. These values were well within the values of β that describe an aged continental aerosol size distribution.

Finally, an attempt was made to compute the albedo of single scattering w using the direct beam and total hemispherical fluxes:

$$\omega = \frac{\tau_{\text{scat}}}{\tau_{\text{scat}} + \tau_{\text{abs}}}$$

When $\omega \approx 1.0$, all solar irradiance intercepted by Arctic haze is scattered; when $\omega \approx 0.0$, all solar irradiance intercepted by Arctic haze is absorbed. The values obtained for ω are listed in table 29. The lower values of ω are obtained at wavelengths $< 0.7 \mu\text{m}$, indicating that more of the absorption of incident irradiance by the Arctic haze occurs toward the shorter wavelengths.

Table 29.--Values of albedo of single scatter for airmasses 2.5 and 3.6

Airmass (average)	Albedo of single scatter (ω)		
	$.28 < \lambda (\mu\text{m}) < 3.0$	$\lambda < .7 \mu\text{m}$	$\lambda < .7 \mu\text{m}$
2.5	.77	.89	.68
3.6	.76	.97	.60

4.7.4 Conclusions

The following conclusions were made concerning some optical properties of Arctic haze at Barrow.

- (1) The Arctic haze attenuated up to 29% of the direct beam incident irradiance in the visible spectrum. The relationship between wavelength and extinction is similar to the relationship observed in aged continental aerosols from $0.2 < \lambda (\mu\text{m}) < 1.2$.
- (2) The total global hemispheric irradiance shows a more uniform extinction than the direct irradiance (about 4% loss to the surface) across the spectrum measured. For wavelengths $> 0.7 \mu\text{m}$ the extinction was primarily due to an increase in water vapor that accompanied the Arctic haze events in this study. For wavelengths $< 0.7 \mu\text{m}$ the extinction was primarily due to the Arctic haze aerosols.
- (3) From the single-scatter albedo calculation, greater radiation absorption occurs at wavelengths $< 0.7 \mu\text{m}$ than at wavelengths $> 0.7 \mu\text{m}$.
- (4) The relationship between moisture and Arctic haze needs further investigation.

4.8 Mauna Loa Atmospheric Transmission: An Update

Atmospheric transmission calculations using normal incidence pyreheliometer measurements made at the Mauna Loa Observatory over the last 22 years have shown secular decreases attributed to explosive volcanic activity and the



Figure 40.--Mauna Loa average apparent transmission data. Shown are 12-mo running averages for 1958-1981. $\bar{T} = [I_5/I_4 + I_4/I_3 + I_3/I_2]/3$, where \bar{T} = average apparent transmission, I = normal incident flux (mW cm^{-2}) in the mornings, and integers = secants of zenith angles.

spread of volcanic ash clouds into the stratosphere (Mendonca et al., 1978). Once there, volcanic ash clouds persist for several years with recovery times dependent on the location and magnitude of the eruption, and the amount of debris that reaches the stratosphere. Figure 40 is an updated MLO transmission record. Twelve-month running means are plotted so that only long-term (>1-yr) changes are seen. The earlier decreases following the eruptions of Agung (1963), Awu (1966), and DeFuego (1974) are seen. A period of high transmission is evident during 1977 and 1978. No major eruptions occurred during this interval, and lidar measurements at MLO show extremely low aerosol concentrations (perhaps background) in the stratosphere (Fegley et al., 1978). This period of high transmission might be associated with Northern Hemisphere general circulation changes that were responsible for the cold northeastern U.S. winters of 1976-77 and 1977-78. Airflow over Mauna Loa at this time was probably altered to some extent.

The most recent period of a secular downward trend in atmospheric transmission is evident after 1978 at Mauna Loa. The three volcanic eruptions that occurred during this period and injected volcanic debris into the stratosphere were LaSoufrière, April 1979; Sierra Negra, November 1971; and Mt. St. Helens, May 1980. None were as severe as Agung. The corresponding decrease in atmospheric transmission at MLO is the smallest in magnitude attributable to volcanic eruptions, for the entire record, except for Awu.

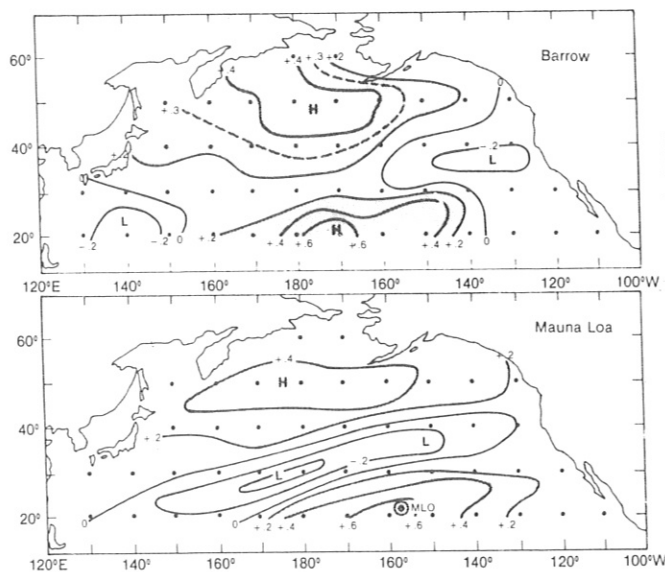


Figure 41.--Correlations of Barrow and Mauna Loa CO₂ departures from normal vs. North Pacific Ocean SST departures from normal for the period 1974-78. The highest correlations observed in 0- to 3-mo lag periods are plotted.

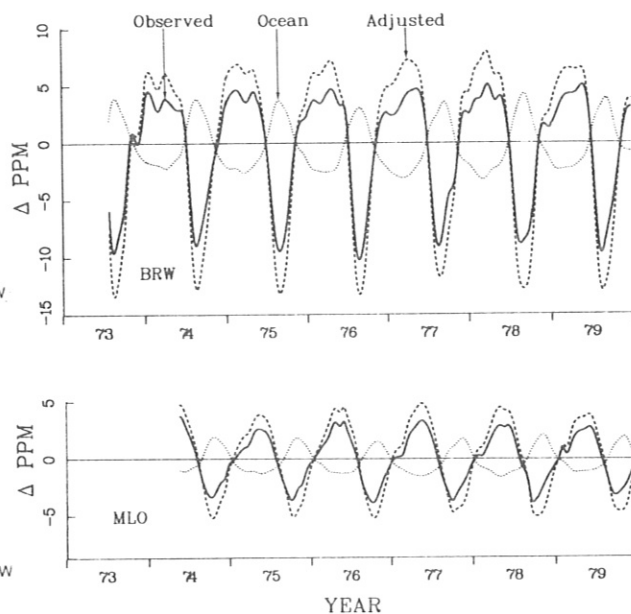


Figure 42.--Detrended annual CO₂ cycles observed at Barrow and Mauna Loa showing the possible effects on CO₂ from the annual temperature cycle in the North Pacific Ocean.

With the exception of the high transmission period during 1977 and 1978, a linear projection of atmospheric transmission from 1958 to 1981 at Mauna Loa suggests a decreasing trend. The validity of this downward trend, and whether it is associated with volcanic dust or other atmospheric attenuators such as tropospheric H₂O or dust, are still under investigation.

4.9 A Relationship Between Pacific Ocean Temperatures and Atmospheric CO₂ Concentrations at Barrow and Mauna Loa

Previous research has shown that the 1976 decrease in the slope of the long-term CO₂ record from Ocean Weather Station P (PAPA) is significantly correlated with coincident below-normal sea surface temperatures over a broad area of the North Pacific Ocean (Hanson et al., 1981). Our research finds a similar relationship for North Pacific Ocean temperatures and the Barrow and Mauna Loa CO₂ records, with the maximum CO₂ deviations lagging the sea surface temperature deviations by 0 to 3 months as shown in fig. 41. By regression analyses, exchange factors of 0.73 ± 0.08 (R = 0.74) ppm CO₂ measured at Barrow, and 0.36 ± 0.05 (R = 0.68) ppm CO₂ measured at Mauna Loa, per °C change in Pacific Ocean temperature, have been calculated from the CO₂ and sea surface temperature (SST) departures from normal.

The annual sea surface temperatures in the North Pacific Ocean are warmest in August and coldest in March with a well-defined latitudinal gradation. When these annual temperature cycles are superimposed on the CO₂ cycles from Barrow, PAPA, and Mauna Loa, they are in opposing phase. Thus,

the relatively warmer oceans would be releasing (or taking up less) atmospheric CO₂ in northern summer and absorbing (or releasing less) CO₂ in northern winter, essentially opposite to the biospheric CO₂ cycle. An annual cycle of atmospheric CO₂, driven by (or related to) the annual temperature cycle in the ocean, may be constructed by multiplying the average monthly temperature departure from the annual mean by the CO₂ exchange factors obtained from the regression analysis (given above) to produce an "ocean-induced" CO₂ cycle. By combining the ocean-induced cycle with an "observed" CO₂, larger "adjusted" CO₂ cycles are obtained as shown in fig. 42.

Thus, if an annual sea-temperature-driven CO₂ cycle operates in the manner described above and the empirically derived exchange factors are valid for annual sea temperature change, the actual amount of CO₂ passing through the global CO₂ budget could be greater than it is now considered when observed annual CO₂ cycles are used to determine biospheric CO₂ budgets.

Computer simulations are being conducted to determine the theoretical framework for the magnitude and phase of the ocean-induced cycle in the North Pacific. Preliminary results suggest that the ocean-induced CO₂ cycle lags the observed cycle by 2 to 3 months and the magnitude is less than shown in fig. 42.

4.10 A Possible Drought-Induced Signal in the Global Atmospheric CO₂ Record

Global net primary plant productivity data (in 10° latitude bands) have been divided by growing season and ocean-to-land ratios to produce CO₂ draw-down rates. These rates and the amplitudes of observed annual CO₂ cycles are essentially in agreement as shown in fig. 43. It may also be seen from this figure that the largest global CO₂ fixation rate occurs in the range of 55° to 65° north latitude, mainly in response to a large Eurasian vegetation zone.

To study possible biospheric effects on the global CO₂ cycle, long-term trends were removed from the Barrow, Ocean Station PAPA, and Mauna Loa (GMCC) CO₂ records, and spline functions were fitted to the detrended data. Subsequently, the dates on which the falling and rising portions of the annual cycle crossed the detrended means were determined and compared. It was observed that in all three records, two coincident features occurred in 1975 in the form of slightly earlier-than-normal falling dates, and significantly earlier rising dates, as shown in fig. 44.

A study of global weather, sea temperature, and plant growth data showed that an early spring followed by a drought in the U.S.S.R. in 1975 constituted probably the largest single perturbations in the global weather pattern that might influence global net primary productivity. These weather events are described in superlatives such as "earliest spring on record," "most severe drought in U.S.S.R. history," "hottest and driest summer on record," etc. Other data from the U.S.S.R.--such as grain production records, total tree ring growth rate, and the ratio of spring-to-summer tree ring growth--show that vigorous spring plant growth was followed by a drastic reduction in summer growth, as shown in fig. 45.

On the basis of the above, it is hypothesized that an earlier-than-normal spring across the western and central U.S.S.R. resulted in an earlier-than-normal drawdown in the annual CO₂ cycle. This was followed by a widespread

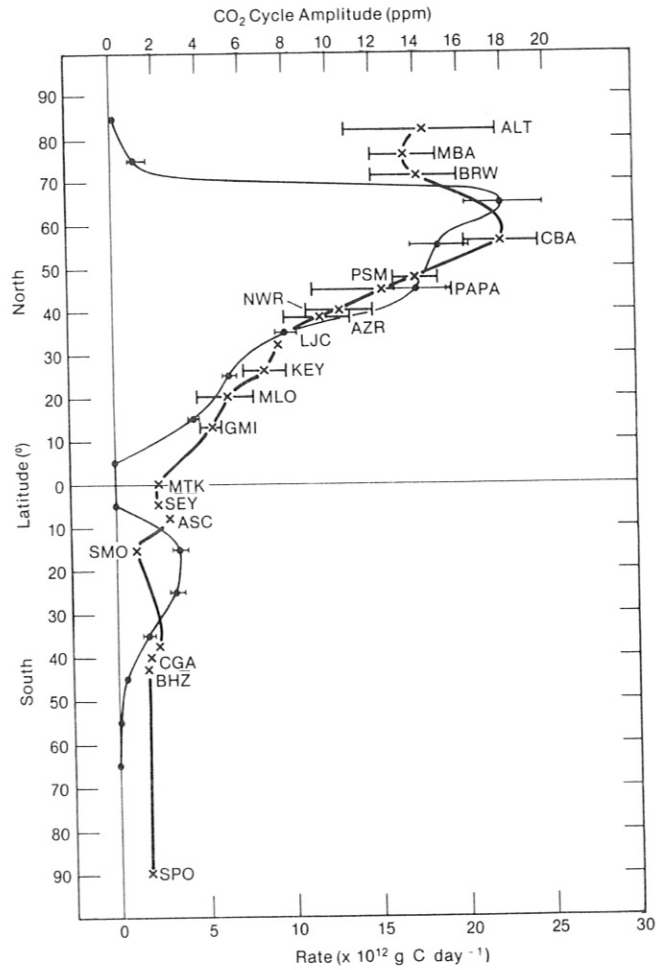


Figure 43.--Terrestrial net primary productivity drawdown rate (in grams of carbon per day) related to the amplitudes of observed CO₂ cycles. (Error bars are for maximum ranges of net primary productivity and CO₂ cycle amplitude.)

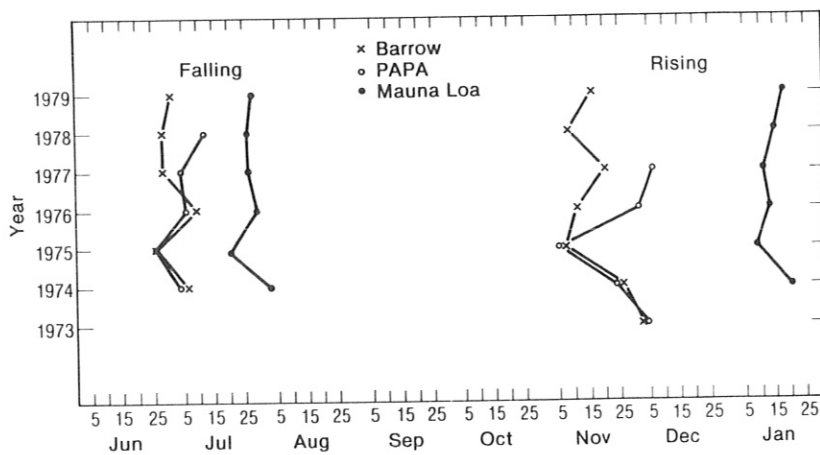


Figure 44.--A plot of the crossing dates of the Barrow, Ocean Station PAPA, and Mauna Loa annual CO₂ cycles exhibiting anomalous advances in the cycle in 1975.

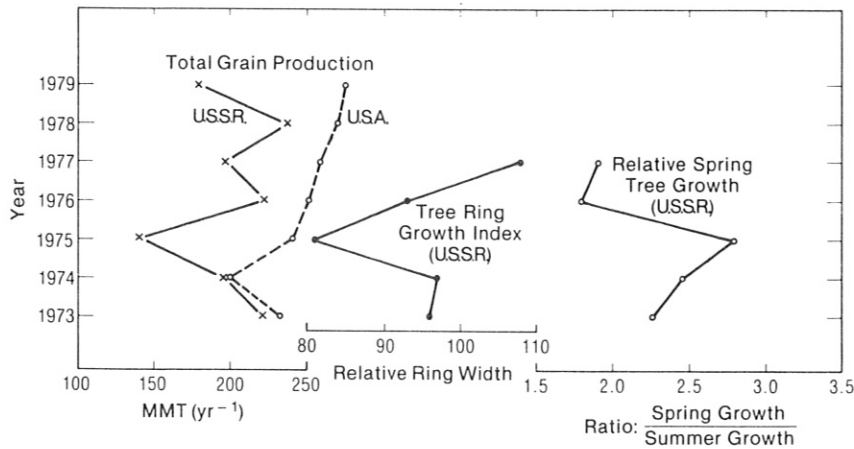


Figure 45.--Total grain production (in million metric tons, MMT) in the U.S.S.R. and the U.S., 1973-79, and tree growth indices for a stand of fifteen 167-yr-old trees in the Caucasus region of the U.S.S.R.

and severe drought that reduced summertime CO₂ fixation, resulting in an earlier-than-normal rising in the annual CO₂ cycle. These changes in the normal pattern of the CO₂ cycle were then detected at the three monitoring locations, which are all east (downwind, for the most part) of the Eurasia land mass.

4.11 Studies of Variability in CO₂ Concentration at Barrow Related to Synoptic Meteorology

The atmospheric CO₂ record at Barrow is being studied to gain an understanding of the causes of the short-term (within-day and day-to-day) variability. The work has led to an understanding of sources and sinks of CO₂ in the Alaskan region and provides a basis for selecting baseline values--a major goal of the GMCC carbon dioxide program. Data from the summer of 1978 and winters of 1977, 1978, and 1979 have been studied so far.

The long-term record shows that CO₂ concentration during the year falls roughly into three classes of short-term variability. The summer months exhibit departures from the mean of up to 10 ppm, whereas winter variability is about 3 ppm at most. The CO₂ concentration during April and May is nearly steady.

The summer variability reflects exchange with land and ocean surfaces on the local and regional scale. The lowest CO₂ concentrations occurred with airflow from areas of open water in the Bering, Chukchi, and Beaufort Seas, where significant undersaturations of CO₂ with respect to air have been measured (Kelley and Gosink, 1979; Park et al., 1974).

Large variations in CO₂ concentration characterized periods of airflow from over land. CO₂ was generally highest with this flow pattern, reflecting an overall tundra source of CO₂ to the atmosphere throughout most of the summer. A pronounced diurnal cycle of CO₂ concentration with airflow from over land was evident during the growing season, which begins in June and

lasts until senescence of vegetation in late August or early September. The highest CO₂ concentrations occurred overnight, when the rate of photosynthetic CO₂ uptake falls below the rate of respiration CO₂ release in tundra vegetation, despite the midnight sun (Coyne and Kelley, 1975). These high concentrations were related to the accumulation, in a shallow nocturnal surface inversion layer, of CO₂ respired by vegetation and soil microbes. Better mixing in the lower atmosphere and CO₂ uptake by vegetation resulted in lower daytime concentrations. The areas of pack ice in the Arctic Ocean appear to be neither pronounced sources nor sinks of CO₂. The steady CO₂ concentrations of intermediate magnitude that were observed with airflow from the central pack ice are probably the closest to Arctic background CO₂ concentrations to be observed at Barrow during summer.

Because the local and regional influences that are active in summer are greatly diminished in midwinter, the effects of larger scale CO₂ gradients can be observed in the Barrow CO₂ record in winter. An earlier study (Peterson et al., 1980) showed that winter CO₂ concentrations were higher with 5-day air trajectories from the north than with trajectories from the south. The cause of the higher concentrations in air from the north was unclear, partly because the 5-day trajectories could not distinguish between relatively warm air, which had come to Barrow across the Arctic from midlatitude anthropogenic source areas on the opposite side of the globe, and cold air having a long history in the Arctic. The present study used temperature patterns and trajectories of up to 15 days duration to obtain more information on airmass history. Fifteen of the largest deviations of CO₂ concentration from "average" values were taken from January or February of 1977, 1978, and 1979 for examination. Nearly all the cases of elevated CO₂ concentration were associated with cold air that had spent 12 to 15 days in the Arctic. There was no direct transport from middle latitudes in any of these cases. In contrast, nearly all the cases of below-average CO₂ concentration were associated with warm air that had traveled to Barrow from middle latitudes in 8 days or less. Air arriving from off the U.S. northeast coast was associated with lowered CO₂ concentrations. These results suggest that the cause of periods of elevated CO₂ concentration is other than transport into the Arctic of anthropogenic CO₂ from middle latitudes.

4.12 A Report on the Short Umkehr Method

4.12.1 Introduction

The short Umkehr method for observing the vertical ozone distribution requires zenith sky measurements on the A-, C-, and D-wavelength pairs of the Dobson ozone spectrophotometer while the solar zenith angle is between 80° and 89°. It has been shown by DeLuise (1979) in a theoretical-numerical study that such measurements should contain at least as much information about the ozone profile as do the conventional Umkehr observations taken on the C-wavelength pair while the solar zenith angle is between 60° and 90°. The short Umkehr requires about one-third of the observing time needed for the conventional Umkehr.

This shorter observing time gives the short Umkehr at least three distinct advantages over the conventional Umkehr. First, there is less chance that significant changes in the ozone profile will occur during the course of the observation; second, there is a better chance that the zenith sky will

remain clear; and, third, it costs less per Umkehr observation in terms of observer time.

We give here a brief report (done in collaboration with C. L. Mateer of the Atmospheric Environment Service, Toronto) on the development of the short or multiwavelength Umkehr method for estimating the vertical ozone profile. For further details see Mateer and DeLuisi (1980).

4.12.2 Details of the Short Umkehr Method

Following our earlier work (DeLuisi and Mateer, 1971) on the conventional Umkehr, we are using the optimum or maximum likelihood inversion procedure (Rodgers, 1976; Westwater and Strand, 1968) with a partial derivative formulation of the inversion problem (Dütsch, 1959). The development of the short Umkehr method has involved the following tasks.

(1) A study of balloon ozonesonde and rocketsonde data on the ozone profile and the relationship of these to concurrent observations of total ozone. The object of this study was to formulate "standard" ozone profiles as a function of total ozone and latitude band and to obtain the covariance matrix of the profiles. In short, given this prior statistical information, each inversion starts with the most likely ozone profile and its error covariance matrix, using a concurrent total ozone measurement as a predictor.

(2) The development and testing of an inversion algorithm, including the calculation of any basic mathematical tables that can be precomputed once and for all.

(3) A study of specific related problems that impact on the random error and bias of the retrieved ozone profiles. These problems have included the temperature dependence of the ozone absorption coefficients, scattering by both tropospheric and stratospheric aerosols, and lower surface pressure at high-altitude stations.

(4) An assessment of the potential of the short Umkehr method, in particular, as a tool for monitoring long-term changes in the ozone profile between 30 and 50 km.

We have completed tasks (2), (3), and (4). The results of task (1) have been reported separately (Mateer et al., 1980).

The standard ozone profiles used in the short Umkehr method are shown in fig. 46, where the mean ozone partial pressure for each layer is plotted at the midpoint of the layer. These profiles correspond to total ozone amounts of .230 and .300 atm-cm for low latitudes; .250, .350, .450, and, .550 atm-cm for middle latitudes; and .250, .350, .450, .550 and .650 atm-cm for high latitudes.

Following Dütsch (1959), the inversion problem is formulated as

$$\frac{\delta N_o(\theta, \lambda)}{\delta f_i} \Delta f_i = N(\theta, \lambda) - N_o(\theta, \lambda),$$

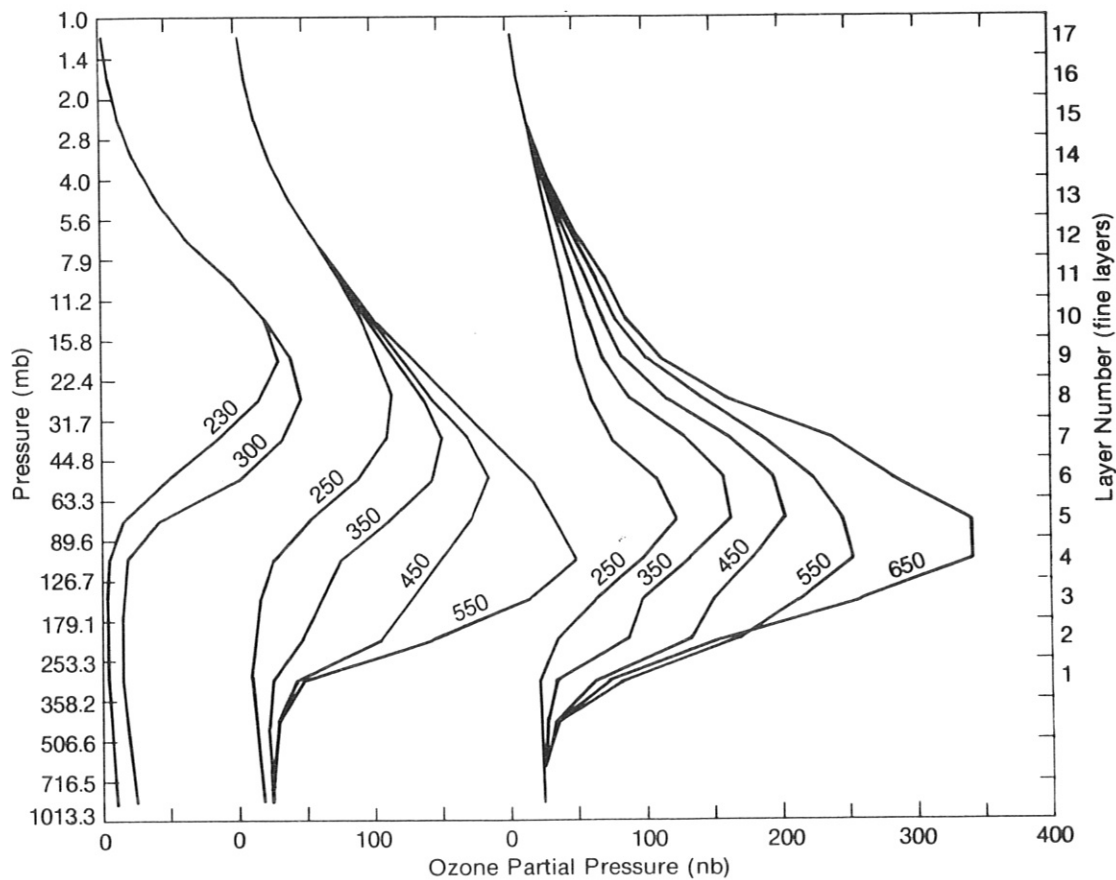


Figure 46.--Standard ozone profiles for low latitudes (left), middle latitudes (center), and high latitudes (right). The ticks on the ordinate axes indicate the upper and lower bounds of the layers. Layer-mean ozone partial pressure (nanobars) is plotted at the midpoint of each layer.

where

$N(\theta, \lambda)$ is the observed log-intensity ratio for wavelength pair λ at solar zenith angle θ ,

$N_o(\theta, \lambda)$ is the log-intensity ratio calculated for the standard or first-guess profile, and

Δf_i is the unknown, the fractional change of the solution from the standard profile in layer i .

In the system of equations to be inverted, there is one equation for each zenith angle and wavelength pair. The measurements are taken with all three wavelength pairs for solar zenith angles of 80° , 83° , 85° , 86.5° , 88° , and 89° . In order to eliminate an undetermined instrument constant, the equation for $\theta = 80^\circ$ is subtracted from each of the other equations (using the same procedure for each wavelength pair). Since this subtraction also removes the information about total ozone from the measurements, an additional equation, providing moderate forcing to conserve total ozone, is added to the system. In summary, this provides a system of 16 equations in 13 unknowns. The system of equations is nonlinear, and it is necessary to perform iterations.

Table 30.--Profile covariance matrix

Layer	12	11	10	9	8	7	6	5	4	3	2	1
12	.040	.032	.024	0.000	0.000	0.000	0.000	0.000	0.000	0.000	0.000	0.000
11	.032	.040	.032	.024	0.000	0.000	0.000	0.000	0.000	0.000	0.000	0.000
10	.024	.032	.040	.032	.024	0.000	0.000	0.000	0.000	0.000	0.000	0.000
9	0.000	.024	.032	.040	.032	.013	0.000	0.000	0.000	0.000	0.000	0.000
8	0.000	0.000	.024	.032	.040	.020	.005	0.000	0.000	0.000	0.000	0.000
7	0.000	0.000	0.000	.013	.020	.025	.020	0.000	0.000	0.000	0.000	0.000
6	0.000	0.000	0.000	0.000	.005	.020	.028	.011	0.000	0.000	0.000	0.000
5	0.000	0.000	0.000	0.000	0.000	0.000	.011	.020	.004	-.023	0.000	0.000
4	0.000	0.000	0.000	0.000	0.000	0.000	0.000	.004	.026	.040	.040	0.000
3	0.000	0.000	0.000	0.000	0.000	0.000	0.000	-.023	.040	.186	.201	.021
2	0.000	0.000	0.000	0.000	0.000	0.000	0.000	0.000	.040	.201	.413	.078
1	0.000	0.000	0.000	0.000	0.000	0.000	0.000	0.000	0.000	.021	.078	.139
Ω	0.000	0.000	0.000	0.000	0.000	0.000	0.000	0.000	0.000	0.000	.055	.110

An estimate of the error covariance matrix of the standard or first-guess profile is part of the prior statistical information required for the optimum inversion procedure. The covariance matrix we used is given in table 30. The diagonal elements and the lower level off-diagonal elements are estimated from the balloon and rocket observations. This matrix has been adjusted to be consistent with the fact that we have prior information about total ozone (see Westwater and Strand, 1968). The off-diagonal elements at upper levels are moderately large, implying a high probability that adjacent-layer deviations from the first-guess profile are well correlated. Off-diagonal elements more than two rows or columns from the diagonal are set to zero. We have tested a number of different covariance matrices in an attempt to optimize the inversion system. This testing is incomplete, and it will suffice for present purposes to say that the matrix in table 30 produced the best overall results by a relatively small margin.

An estimate of the error covariance matrix of the observations is also required. In reality, this matrix should include some allowance for errors in the mathematical modeling of the atmosphere. For the present, we have used a matrix with nonzero elements only on the diagonal and have assumed a measurement error of 1 N-unit (equivalent to 2.3%) in the log-intensity ratios, applicable to all zenith angles and wavelength pairs. A standard error of .003 atm-cm is assumed for the concurrent measurement of total ozone.

Altogether, 46 short Umkehr's with "ground truth" in the form of concurrent balloon ozonesondes were available for testing purposes. These Umkehr's were for Arosa, Switzerland (46.8°N, 2 cases); Boulder, Colorado (40.0°N, 9 cases); Edmonton, Alberta (53.5°N, 19 cases); Goose, Labrador (53.3°N, 9 cases); and Resolute, Canada (74.7°N, 7 cases). In the case of the Arosa Umkehr's, the concurrent balloon ozone soundings were taken at Payerne, Switzerland. Again, for details on the performance of the short Umkehr see Mateer and DeLuisi (1980).

We summarize our findings as follows. Although it is uncertain that the Umkehr provides useful results below 25 mb, it does appear to have the potential for monitoring ozone changes between 10 and 1 mb (30 and 50 km) and

especially near 40 km (middle of layer 8) where depletion by the chlorofluorocarbons is predicted to be at a maximum. One cautionary note is in order. It is clear (Dave et al., 1980) that Umkehr results for these upper layers are significantly affected by stratospheric aerosol scattering, and it is quite clear that corrections for these scattering effects will have to be applied if high-altitude ozone is to be monitored by means of Umkehr observations.

4.13 Remote-Sensing Observations of the Mt. St. Helens Cloud

4.13.1 Introduction

On 3 June 1980, the dust cloud from the May 18 eruption of Mt. St. Helens was located, by remote-sensing techniques, over the western United States at an altitude between 10 and 15 km. The cloud had completed a single circuit of the globe and had entered the United States from a southwesterly direction. The lateral dimensions of the cloud were considerably enlarged because of natural dispersion processes. On June 4 the main portion of the cloud had passed by Boulder so that the total optical depth (tropospheric and stratospheric) was nearly back to normal. (Lidar measurements also verified the presence of the cloud.) On both days the sky was cloudfree until afternoon. These conditions permitted us to make observations of the integral and spectral, diffusely and directly transmitted, solar radiation, which we subsequently analyzed for spectral extinction, absorption refractive index, and backscattering properties.

4.13.2 Spectral Extinction

To eliminate the background tropospheric aerosol characteristics from our measurements, we used a perturbation technique developed by DeLuisi and Herman (1977). For identical solar zenith angles on the days that observations were taken, spectral extinction optical depth was obtained simply by an adaption of Beer's law, viz.,

$$-\tau_d(\lambda) = \frac{1}{\sec \theta_o} \ln \frac{I(\lambda)_{3rd}}{I(\lambda)_{4th}},$$

where $\tau_d(\lambda)$ is the optical depth at wavelength λ , and $I(\lambda)$ is the intensity of the directly transmitted radiation at the same wavelength. Measurements of $I(\lambda)$ were made with a filter photometer at eight wavelengths in the solar band.

Figure 47 shows points for observed optical depth vs. wavelength. An excellent analytical fit can be made to the points with the expression

$$\Delta\tau_d(\lambda) = 0.160 \lambda^{-0.473} \quad (\lambda \text{ in } \mu\text{m}),$$

where the exponent -0.473 is customarily referred to as Angstrom's exponent. The point at 945 nm is a water vapor wavelength. This indicates some change in water vapor between the two days. We believe this to be an exceptionally good representation of the volcanic cloud's spectral extinction because it constitutes an average of several hours of measurements that did not show considerable variation.

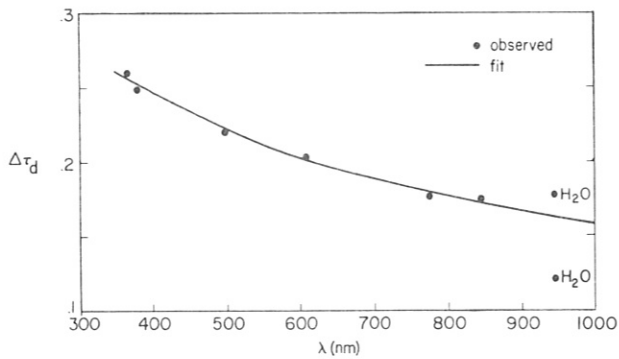


Figure 47.--Least square fit of the spectral extinction optical depths (dots) determined from the difference between June 3 and 4.

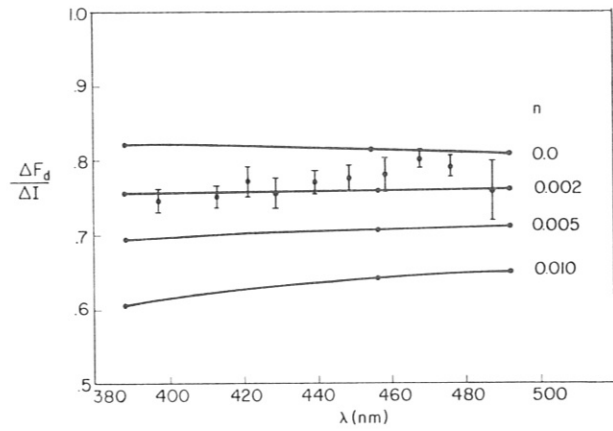


Figure 48.--Solution for absorption refractive index. Each dot represents an average and standard deviation of five nearby values of observed $\Delta F_d/\Delta I$. The smooth curves are theoretically calculated values of $\Delta F_d/\Delta I$ for conditions observed on June 3 and 4, and for different values of absorption refractive index n .

4.13.3 Refractive Index: Diffuse-Direct Method

To make observations of the diffusely and directly transmitted radiation we used a double monochromator set to scan continuously from 380 to 500 nm. The light collector was a flat, horizontally oriented diffuser plate. The wavelength resolution of this instrument was 0.78 nm. After alternately exposing the diffuser to the total hemispheric sky and diffuse sky flux, we obtained the direct flux by taking the difference between the measurements. We did this on June 3 and 4. We were able to define 50 values of $\Delta F_d/\Delta I$ (change in diffuse to change in direct measurements) in the 380- to 500-nm band. These measurements were then analyzed for the imaginary term of the complex refractive index of the stratospheric cloud by finding a best match with theoretical calculations of $\Delta F_d/\Delta I$. These advantages are gained by the technique:

- (1) Elimination of an instrumental calibration,
- (2) Elimination of a need for precise surface reflectivity for the theoretical calculations,
- (3) Virtual elimination of the tropospheric aerosol effect, assuming it remains reasonably invariant during the two days.

Figure 48 shows the results of an analysis of the spectral diffuse-direct measurements $\Delta F_d/\Delta I$. The observed points represent averages of five nearby wavelengths. The standard deviations of these groupings are shown as bars. The smooth lines represent theoretical calculations for an aerosol size distribution consistent with the spectral extinction measurements, a surface

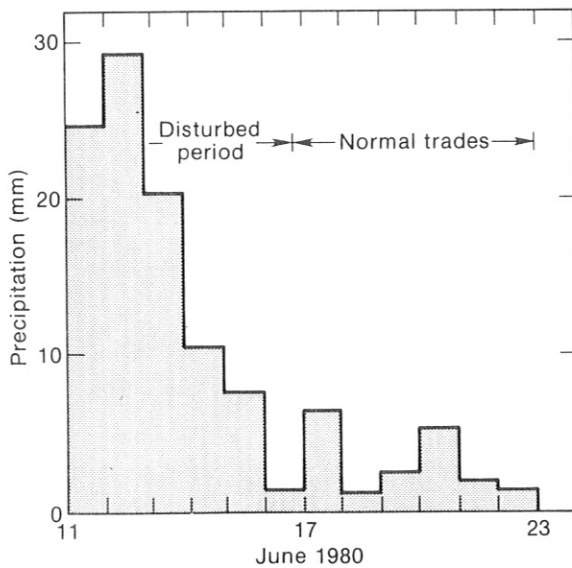


Figure 49.--Daily precipitation amounts in millimeters, at Hilo, Hawaii, during HAMEC project.

reflectivity of 0.15, and a real part of the complex refractive index of 1.5. The differential $\Delta F_d/\Delta I$ was calculated for changes in optical depth consistent with the spectral extinction measurements. We note that there is in fig. 48 some variation in the inferred refractive index. At this time we cannot say whether this is real or due to measurement error.

The data shown in fig. 48 are easily converted to an albedo of single scatter of the dust cloud. The value is about 0.95.

4.13.4 Backscatter Fraction of Solar Flux

Integral solar-band radiation measurements were also obtained on both days. These were made with pyranometers and pyrhemometers having a bandpass of 300 to 3,000 nm. With these measurements we were able to deduce a $\Delta T/\Delta I_v$, where T stands for total hemispheric flux, and v stands for the vertically incident direct flux. If the albedo of single scatter of the cloud is reasonably defined we can deduce the backscattering by the cloud using a simple two-stream formulation based on conservation of radiant energy (DeLuisi et al., 1977). The expression for backscatter to total scatter is given by

$$b = 1 - \frac{1}{(1 - R)} \left[\left(1 - \frac{\Delta T}{\Delta I_v} \right) \frac{1}{\omega_o} - R \right],$$

where R is the surface reflectivity, and ω_o is the albedo of single scattering.

Using this expression and letting $\omega_o = 0.95$, and $\Delta T/\Delta I_v = 0.23$, the backscatter fraction b is 0.22. This means that about 21% of the radiation intercepted by the cloud is scattered back to space; 74% is scattered downward toward the earth, and 5% is absorbed. Absorption to backscatter ratio is 0.23. It is worthwhile to note that the ratios $\Delta T/\Delta I$ for the Agung volcanic aerosol were 0.2, 0.25, and 0.3, respectively, for the years 1963-65 (DeLuisi and Herman, 1977) during the austral summer season.

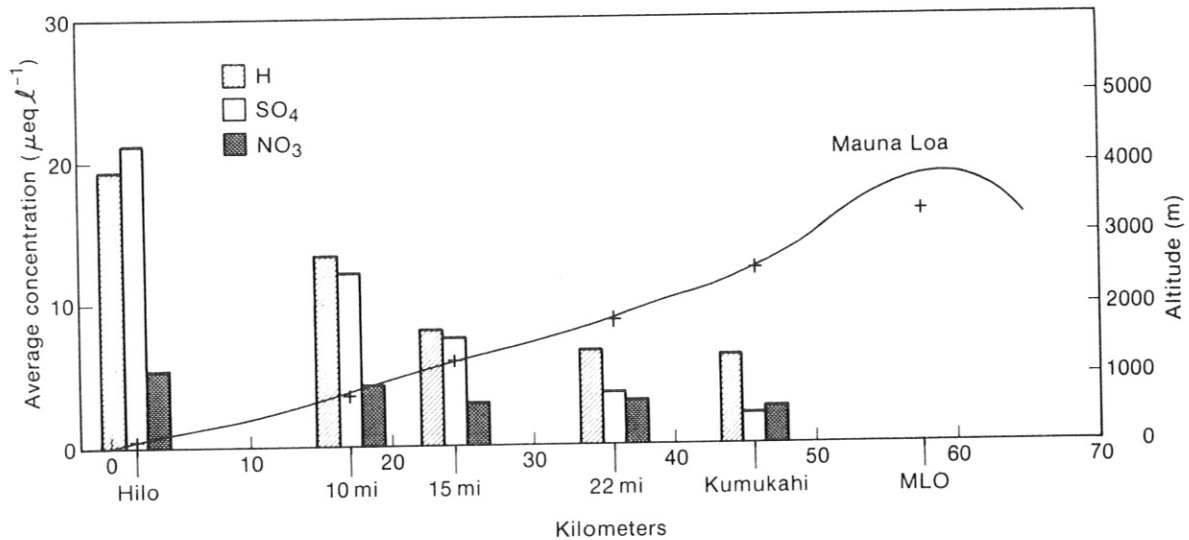


Figure 50.--Average concentration of hydrogen, sulfate (excess), and nitrate ions during the HAMEC project, June 11-23, 1980.

4.14 Interpretation of Precipitation Chemistry Event Sampling at Elevations From Sea Level to 3400 Meters on the Island of Hawaii

The Hawaii Mesoscale Energy and Climate Project (HAMEC) was conducted on the island of Hawaii from June 12 to 24, 1980. The main objective of this project was to describe the mesoscale meteorological structure and atmospheric chemistry around the island. As a part of the project, event precipitation chemistry samples were collected at nine sites at elevations from sea level to 3400 m. The 2-wk period was dominated by two distinct meteorological patterns. The first week was a period of disturbances in the trade flow that produced heavy rains throughout. The second week, in contrast, was one of undisturbed trade flow, typical of that time of year. This dichotomy is reflected in precipitation amounts shown in fig. 49.

Data and results from the study will be presented in a forthcoming publication. Chemical results are summarized in fig. 50. The atypical character of the period is shown by the decrease in acidity with elevations, in contrast to the 5-yr average of increase in acidity with altitude (Miller and Yoshinaga, 1981).

4.15 Stratospheric Lidar Investigations of the Mt. St. Helens Volcanic Cloud Over Boulder, Colorado

4.15.1 Introduction

On May 18, 1980, Mt. St. Helens, a previously inactive volcano located in the Cascade Range in southwestern Washington State, violently erupted. This provided the continental United States with its first locally derived volcanic aerosol cloud since the 19th century.

During late spring and early summer of 1980, the GMCC stratospheric lidar program in Boulder was performing final tests and training new observatory

personnel on the lidar system that was to be installed at Pt. Barrow, Alaska. (GMCC Summary Report No. 6, sec. 3.5 [Peterson, 1978]) gives the characteristics of the Boulder-BRW lidar system electronics.) First, a series of extensive equipment-adjusting observations was taken. Then, immediately after the May 18 eruption, observations began at regular intervals. Between May 18 and July 29, 1980, 17 observations show volcanically induced aerosol enhancement at various levels over Boulder, Colorado.

4.15.2 Data Reduction

The total (aerosol and molecular) backscattered-lidar return, divided by the expected purely molecular atmospheric return (Rayleigh backscatter), is the accepted lidar data presentation. It is referred to as the backscatter ratio.

Log molecular (Rayleigh) backscattering coefficient profiles were computed using Denver NWS rawinsonde data provided by NCAR. The rawinsonde observations corresponded in time as closely as possible to the lidar observations.

The lidar data and the corresponding calculated (Rayleigh) backscattering coefficient profiles previously described were plotted. The difference between the two superimposed curves reveals the aerosol layers. The plots in fig. 51 are for eight lidar observations that are indicative of special features warranting more detailed discussion. The complete data set will be published in a NOAA Technical Memorandum during early 1982.

4.15.3 Discussion

Sequential examination of the profiles in fig. 51 reveals the layering, vertical extent and migration, intensity, and temporal variability of the volcanic aerosol cloud. Fernald and Frush (1975) and Russell and Hake (1977) give primary descriptive features of volcanic aerosol clouds: (1) the largest effects are at altitudes below 20 km; (2) the structure is multilayered at early stages; and (3) the structure changes to one broad, less intense, backscattering peak. The observation series presented here exhibits all three features.

Large backscatter ratios, where the particulate backscattering contribution is sometimes greater than 20 times the molecular (Rayleigh) contribution, can be detected from lidar observations (Fegley and Ellis, 1975). Such ratios, which were obtained during study of the 1974 Volcán de Fuego aerosol cloud overpass above Mauna Loa, indicate extreme particulate layer overloading. The Boulder observation series, taken on the Mt. St. Helens volcanic cloud overpass, gave a peak backscatter ratio of 30 at 17.5 km A.S.L. (fig. 51c). Twenty-four hours later, at the same altitude, the ratio was 7.1 (fig. 51d). Assuming no molecular (Rayleigh) backscattering component change, the ratio drop represents a 79% volcanic aerosol backscattering component decrease, and is an example of the transient nature and temporal variability of volcanic clouds in early stages of formation. The peak backscatter ratio differences between figs. 51c and 51d can be explained by a 0.5-km upward vertical migration of the primary aerosol layer.

Danielsen (1981) gives a global transit time of ~15 days for the upper tropospheric portion (200 to 150 mb) of the volcanic aerosol cloud. Two

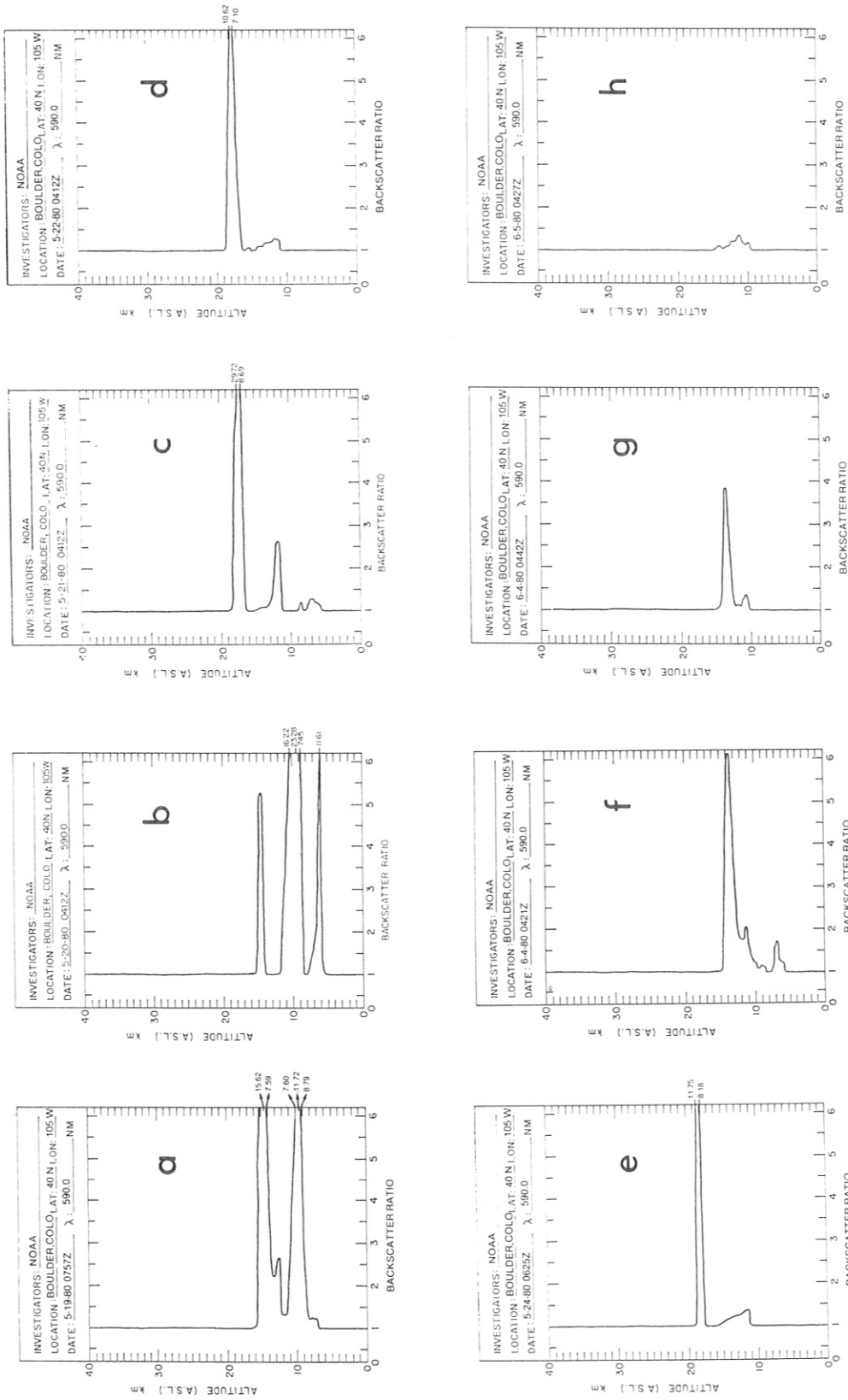


Figure 51. --Backscatter ratio vs. altitude (A.S.L.), from the Mt. St. Helens volcanic cloud, over Boulder, Colorado.

supplemental lidar observations were taken on May 28 and 29, between the observation times of figs. 51e and 51f, which show no volcanic aerosol backscatter. Figure 51f, however, shows more intense backscattering at 13.7 km A.S.L. (170 mb) than that seen at the same altitude in fig. 51e. This is just under 16 days after the cloud was first seen over Boulder (fig. 51a). The primary layer in fig. 51f is the remains of the somewhat diminished, but still existent, volcanic cloud after its first global transit.

5. COOPERATIVE PROGRAMS

5.1 Size-Elemental Profiles of Fine Particulate Matter at Mauna Loa and Hilo, Hawaii

Thomas A. Cahill, Lowell L. Ashbaugh, and Bruce Kusko
Air Quality Group, Crocker Nuclear Laboratory and Department of Physics
University of California, Davis, CA 95616

In January 1980, the Air Quality Group initiated a program of continuous particulate monitoring over weekly intervals during downslope nighttime winds at the Mauna Loa Observatory. The primary purposes of this program were to distinguish between local and transported particles through size discrimination and to provide sensitive and statistically sound measurements of clean air at this site.

The instrument used for the study is a three-stage Lundgren-type impactor, which samples downslope winds each night on a fixed clock schedule. The cut points of the impactor deliver size fractions of 10 to 3.5 μm , 3.5 to 0.6 μm , and less than 0.6 μm . The two impaction surfaces are Mylar types, coated with 5 $\mu\text{g cm}^{-2}$ Apiezon-L grease. For the first year, the third-stage filters were Nuclepore with 0.3- μm pore diameter. Now Ghia stretched-Teflon filters are used. Samples are analyzed at Davis by proton induced X-ray emission (PIXE) for elements with the atomic weight of sodium and heavier.

During the first year of operation, sensitivities (minimum detectable limits) on the impaction stages were approximately 0.4 ng m^{-3} for elements like sulfur, and approximately 0.07 ng m^{-3} for transition metals. The filter stage sensitivities were much poorer, however: approximately 100 ng m^{-3} for sulfur and 2 ng m^{-3} for iron. For this reason, the decision was made to switch to Ghia stretched-Teflon filters with a smaller exposed area. This change should provide sensitivities of about 1 ng m^{-3} for sulfur and 0.2 ng m^{-3} for iron.

Although analysis has just been completed for 1980, several interesting features are seen. Sampler discrimination by size is excellent, with mass ratios often higher than 1,000 between fine and coarse stages for some elements. No fine-particle chlorine appears to be present, even when there are large amounts on coarse stages. Na/Cl ratios in such episodes are close to seawater, but occasional Na-rich deviations have been observed in polluted air (often traced by lead contamination). Forty times more sulfur is observed in the 0.6- to 3- μm (stage 2) size range than in the range with coarsest (stage 1) particles, and about 10 times more sulfur is observed below 0.6 μm than above this cut. Dramatic changes occur in the elemental composition of soil-like elements above and below the 3- μm cut, with the typical basaltic ratios above that cut, but with soil profiles not at all like those of Hawaii in the two fine stages. These changes are being examined relative to synoptic weather patterns. A study was also made of aerosols in Hilo, Hawaii, at two sites in June 1980. These data have also been recently analyzed, showing correlation of fine particulate sulfur (but not coarse particulate sulfur of marine origin) with sulfur content of rain.

5.2 Ultraviolet Erythema Global Measuring Network

Daniel Berger
Temple University
Philadelphia, PA 19140

A global network of meters continues to record the half-hourly dose of the shortest ultraviolet radiation on the Earth's surface. The spectral response of these meters approximates the skin's sunburn (erythema) action spectrum. The response is, therefore, sharply skewed toward the shortest ultraviolet wavelengths.

Meter response correlates with DNA damage and Vitamin D synthesis. Correlation has also been made between the meter output and such biologic effects as nonmelanoma skin cancer, UV-induced plant stresses, and sewage water purification. The variability of annual erythema dose correlates with annual ozone variability.

The number of regularly reporting network stations has risen from 11 in 1973 to 29 by the end of 1980. Their locations are given in the GMCC Summary Report 1979 (Herbert, 1980), with the exception of La Jolla, California, which was not included in that list. Instruments at stations are calibrated annually.

A report for 14 stations having at least 4 years of continuous data is now in press and will be published in 1982 (Berger, 1982). Average daily doses are given there. The half-hourly values of dose and the total daily dose are obtainable from NOAA, 8060 13th Street, Silver Spring, MD 20910.

5.3 Radiation Balance Measurements at Barrow

G. Wendler and F. Eaton
Geophysical Institute, University of Alaska
Fairbanks, AK 99701

When analyzing climatological measurements at Barrow, we found that clear days in April, May, and the first part of June were colder than cloudy ones. This held true for maximum as well as for mean diurnal temperatures. In spring of 1979 we carried out some radiation spot measurements that showed the surface radiation balance to be actually more positive in the presence of clouds than in bright sunshine, as long as there is a high surface albedo. This effect was first observed by Hanson (1961), Holmgren (1971) and later by Ambach (1974) in Greenland, who coined the word "radiation paradoxan" for such an occurrence. Even at solar noon, the increased solar radiation in the absence of clouds is overcompensated by a loss in the infrared radiation, thus resulting in a less positive radiation balance and a lower air temperature. This effect can be observed only in the presence of a high surface albedo, which influences the radiation balance in two ways:

- (1) The increased solar radiation is mostly reflected and, hence, has a relatively smaller effect on the energy budget.
- (2) Because of multiple reflection (Wendler et al., 1981), the decrease in global radiation for cloudy conditions is not as important as for the time when the snowcover has disappeared.

As a part of our plans to study these interesting relationships more systematically, we have added a PD-4 Davos radiometer to the GMCC equipment at Barrow. This instrument, built to high accuracy by the World Radiation Center at Davos, Switzerland, has four sensors. Two measure the incoming and reflected global radiation, and the other two sensors measure the all-wave radiation with Lupolen-covered domes.

5.4 Characteristics of Aerosol Concentrations at the Threshold of Detectability

A. W. Hogan, S. C. Barnard, and W. Winter
Atmospheric Sciences Research Center
State University of New York at Albany, Albany, NY 12222

5.4.1 Introduction

The extremely low total-number concentration of atmospheric particles, as measured with a variety of Nolan-Pollak derived photoelectric nucleus counters, is often indistinguishable from the concentration measured after the air has been filtered. These episodes of near-zero aerosol concentration persist for periods of a few minutes to tens of hours at many places, and are not detected by filter and impactor sampling because long sampling times are required to collect the mass needed for analysis.

Near-zero concentrations are frequently measured over calm seas following dissipation of fog, but aerosol generation by bubble mechanisms causes recovery of the aerosol concentration in a few minutes. The most interesting cases of near-zero surface aerosol concentration are found over the Arctic in summer. The concept of "zero" particle concentration is a relative one, dependent on the amount of air the investigator is willing to examine in order to find a particle (Pollak, 1957; Hogan et al., 1981). The photoelectric nucleus counters used in this study examine 100 to 200 ml of air per measurement and can repeatably detect total number concentrations of $<10 \text{ cm}^{-3}$ at 1-min intervals.

5.4.2 Results

Chronologies of events, where Aitken nucleus concentrations near zero (i.e., indistinguishable from filtered air when measured with an instrument capable of resolving $<10 \text{ cm}^{-3}$) were measured for periods of hours, are shown in fig. 52. The first event was observed on the Greenland ice cap, at DYE II, in August 1973 (Flyger et al., 1976); the second at the NOAA/GMCC observatory near Barrow, Alaska, in July 1977; and the third at Igloolik, Fox Basin, N.W.T., Canada, in August 1981. We briefly describe here the results of the Barrow measurements. A complete analysis for all three sites will be published in the formal literature in the near future.

The surface wind was onshore (from the east) throughout the period, but winds aloft were from ESE 0.5 to 2 km above the surface during the latter half of the observation period. The total Aitken concentration was of the order of hundreds cm^{-3} in sunny conditions at the start of the experiment. About 40 cm^{-3} of this population were transmitted through 30 cm of a collimated-holes diffusion battery (Sinclair, 1972). Fog formed during twilight of 25-26 July and began to precipitate at about 1700 local time 26 July.

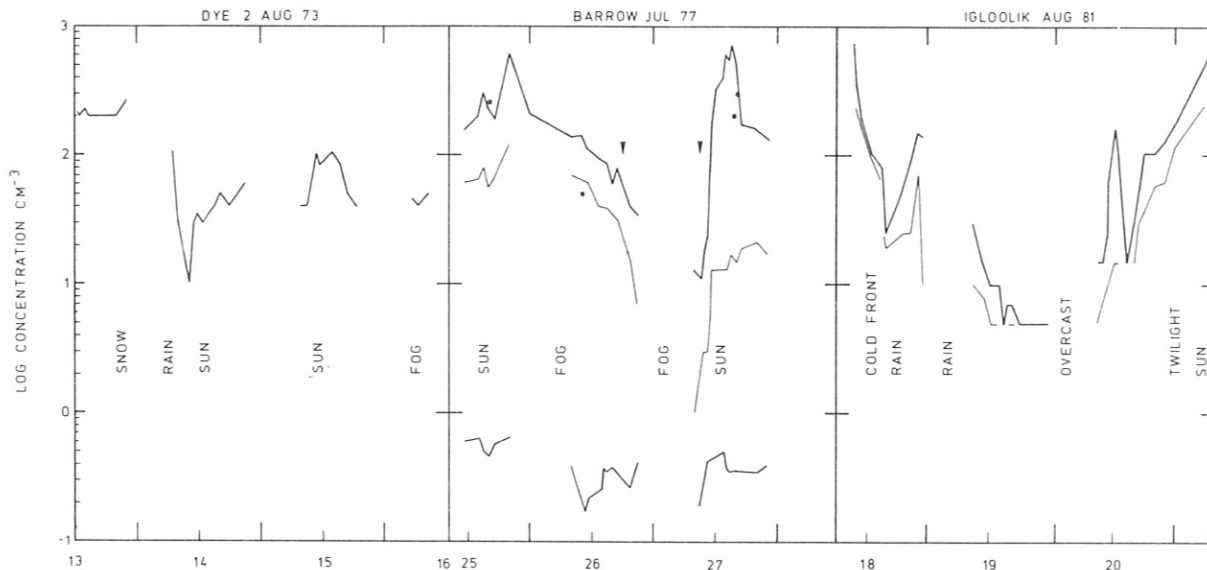


Figure 52.--Chronologies of Aitken nucleus concentrations and other aerosol and meteorological variables measured on the Greenland ice cap, on the tundra 2 km inland from the Arctic Ocean at Barrow, Alaska, and on Igloolik Island, in Fox Basin, N.W.T., Canada. The time scales are equal although the events are separated by 3-yr intervals. In each case, the surface aerosol concentration approaches that of filtered air following liquid precipitation. An aerosol of low concentration reformed very slowly over the ice cap, even in bright sun; an aerosol of very high concentration of very small ($r < 0.01 \mu\text{m}$) particles formed in a few hours over the Alaska tundra; an aerosol of similar concentration to filtered air remained for 18 hours under overcast at Igloolik, then reformed to 500 cm^{-3} , half of which were less than $r = 0.01 \mu\text{m}$, in a few hours of sunlight. Temperature and wind measurements do not indicate that the rise in aerosol concentration accompanied a new airmass; advection of warmer air to the station did not result in increased aerosol concentration at the ice cap site, and preceded aerosol increase by several hours at the island site.

The total Aitken nucleus concentration and the number of nuclei penetrating the diffusion battery (i.e., those of $r > 0.05 \mu\text{m}$) decreased during the period of fog and precipitating fog, to less than 30 cm^{-3} total at 2200 hours. None penetrated the entire diffusion battery. At 0800 local time on 27 July the stratus overcast was beginning to break, with a visibility of 8 km in a light fog. The total Aitken concentration was measured at 10 cm^{-3} with a Pollak counter, and no particles penetrated the total diffusion battery, which indicated that the particle size was below $0.05 \mu\text{m}$. Measurement with a light-scattering device showed a total of 0.2 cm^{-3} of diameter greater than $0.5 \mu\text{m}$. Cloud base lifted through the morning, and solar radiation was significantly strong to generate a surface mirage by 1030 when the aerosol concentration reached 25 cm^{-3} , of which 3 cm^{-3} passed the diffusion battery and 0.4 cm^{-3} were larger than $d = 0.5 \mu\text{m}$, as indicated by the light-scattering device. A rapid increase in aerosol concentration occurred between 1100 and 1200, under very thin stratus. The total Aitken particle concentration reached 600 cm^{-3} by 1400 hours, but only 13 cm^{-3} penetrated the diffusion battery, and only 0.3 cm^{-3} were sufficiently large to be detected by light scattering. A maximum

concentration of 700 cm^{-3} occurred at 1500 hours, followed by a slow decrease in concentration through the evening hours as high-level cirrostratus cloudiness increased. On the morning of 28 July, winds shifted to south at the surface, carrying air from the settlement to the station and ending the experiment.

It was hypothesized, earlier in the experiment period, that organic vapors from tundra plants may have been converted to Aitken nuclei in the presence of sunshine or strong oxidants, by the mechanisms suggested by Coulier (1875), Aitken (1911), Went (1964), and Rasmussen and Went (1965). Parallel measurements of total Aitken nucleus concentrations were made at the seashore, upwind of the tundra plants at several times during the experiment as shown by the large dots in fig. 52. Although agreement is not precise, it would appear that approximately the same number of particles passed over the shoreline as arrived at the GMCC station 2 km inland. Iodine vapor was added to ambient air at 1700 on 26 July and 0900 on 27 July (shown by arrows in fig. 52) but did not produce additional particles. Adding organic vapors (from an orange rind) to the air caused the nucleus counter to read full scale a few moments later. This verifies that the proper conditions existed to cause generation of particles from organic vapors if a sufficient quantity were present; also the absence of reactions with iodine vapor indicates that a strong oxidant was not necessary to complete a natural reaction. Ozone concentration was about 0.030 ppm throughout the experiment, and apparently had little influence.

5.5 Aerosol Characteristics at Mauna Loa Observatory, Hawaii, After East Asian Dust Storm Episodes*

Michael Darzi and John W. Winchester
Department of Oceanography
Florida State University, Tallahassee, FL 32306

5.5.1 Introduction

Concentrations of elements, including S, Al, Si, K, Ca, Ti, and Fe, in aerosols sampled sequentially with 3.7-h time resolution over a 2-wk period in April and May 1979 at the Mauna Loa Observatory, Hawaii, indicate that long-range transported "background" crustal dust aerosol can reach concentrations in excess of $20 \mu\text{g m}^{-3}$ with more than $8 \mu\text{g m}^{-3}$ of additional sulfate. Favorable regional meteorology after known dust storm episodes, as well as similarities in crustal element ratios, point to dry areas of northern China as the major source for this crustal aerosol. Time series analyses for crustal elements show a dominant 21-h period but no 24-h period, a result that can be accounted for by a diurnally varying source process with subsequent modification of periodicity, e.g., by windspeed convergence during transport. Time-dependent associations between S and the crustal elements, especially high coherency at long periodicities, also imply a long-range transport for much of the S, possibly from populated areas in eastern Asia, including China and Japan. This source may contribute much of the sulfuric acid believed to cause the relatively high acidity of rainwater observed at higher altitudes in Hawaii. MLO, at a 3,400-m altitude, is apparently an excellent location for detecting Asian dust and pollutant transport during spring, with little interference from Hawaii-derived aerosol.

*Most material in this section is from Darzi, M., and J. W. Winchester, *J. Geophys. Res.* (in press), copyrighted by American Geophysical Union.

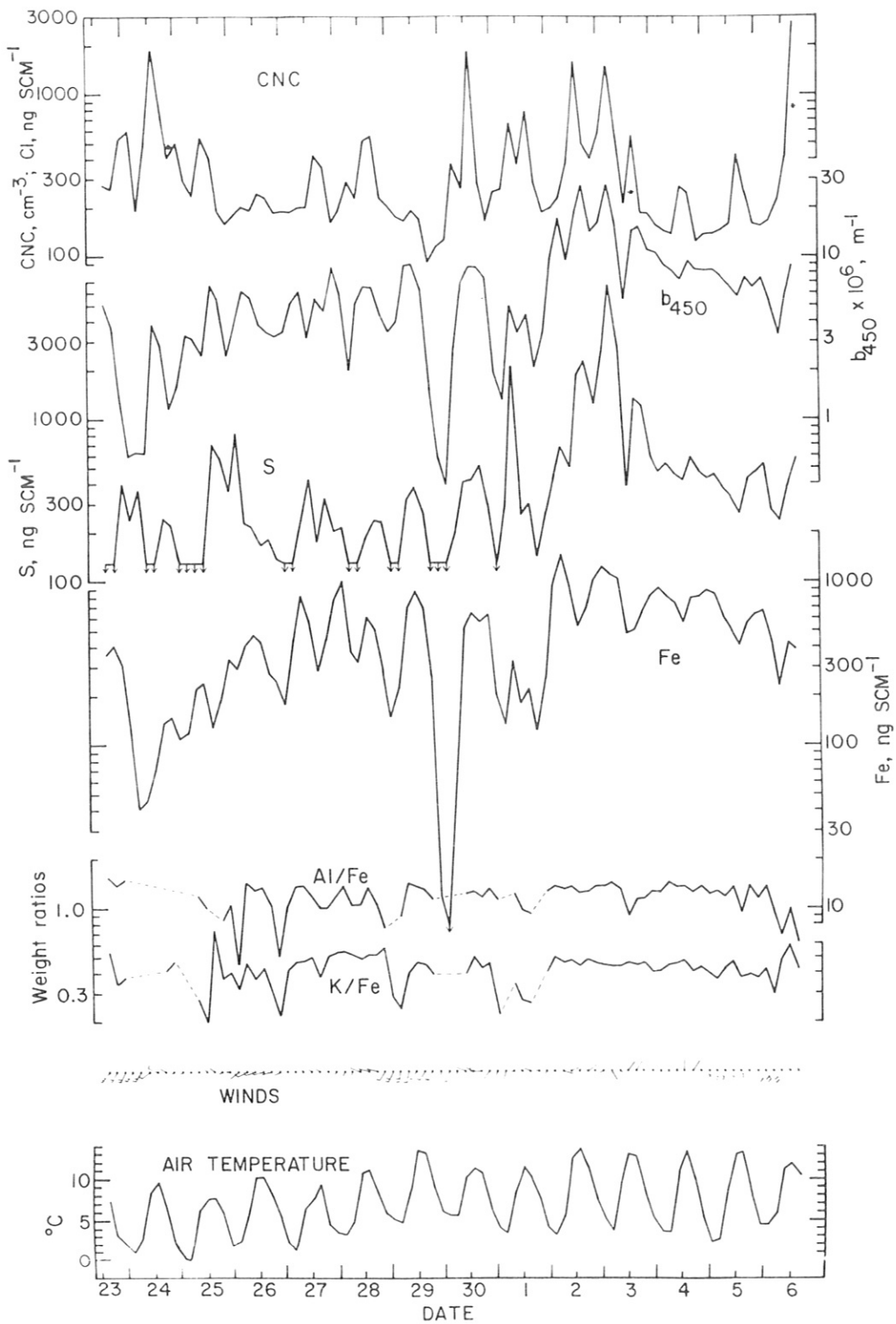


Figure 53.--Aerosol and meteorological data for MLO, 23 April to 6 May 1979, in 3.68-h intervals. (Shafts of wind arrows have lengths proportional to speeds from 2.5 to 5 m s^{-1} ; barbs represent increments of 3 m s^{-1} above 5 m s^{-1} .)

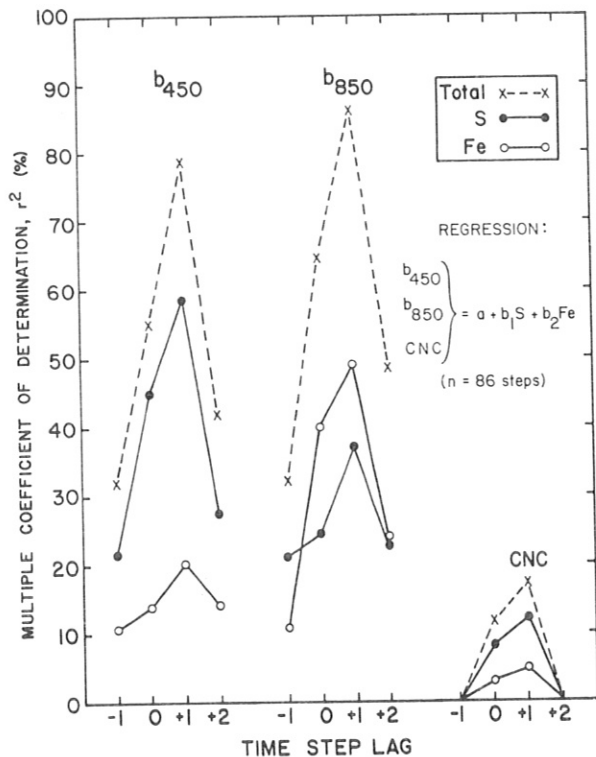


Figure 54.--Results of linear regression analysis of b_{450} , b_{850} , and CNC as the dependent variable vs. both S and Fe aerosol concentrations as independent variables for MLO data of fig. 53 (23 April-6 May 1979). Element concentrations $<DL$ were set at $\frac{1}{2}DL$.

5.5.2 Results

Brief descriptions of the salient points in this investigation (Darzi and Winchester, 1981) are given below.

(1) Figure 53 presents aerosol and meteorological data for MLO, from 23 April to 6 May 1979, in 3.68-h intervals. Element data are obtained from a streaker sample analyzed by PIXE (particle induced X-ray emission); element ratios with numerator or denominator $<DL$ (detection limit) are not plotted. CNC (condensation nucleus count), b_{450} (volume scattering coefficient of particles at a wavelength of 450 nm), and meteorological data are from NOAA/GMCC and are 3.68-h averages of hourly means. Windspeeds and wind directions are shown for winds $>2.5 \text{ m s}^{-1}$. The measurements followed a documented dust storm in eastern Asian deserts during mid-April 1979. Satellite photographs verify transport of the dust over the western North Pacific toward Hawaii.

(2) Results of linear regression analysis of b_{450} , b_{850} , and CNC as the dependent variable vs. both S and Fe aerosol concentrations as independent variables for the MLO data of fig. 53 are shown in fig. 54. Maxima in correlations at a lag of +1 time step (3.68 hours) mean that S and Fe concentrations are best correlated with later b_{450} , b_{850} , or CNC data by a difference within the precision of the time intercalibration for the measurements. Element concentrations $<DL$ were set at $\frac{1}{2}DL$. Most of the variability in light scattering is accounted for by variability in element concentrations, with typically fine aerosol sulfur being more important at the shorter wavelength and typically coarse aerosol iron being more important at the longer wavelength, 450 and 850 nm, respectively. Variability in CNC is only weakly related to element concentrations.

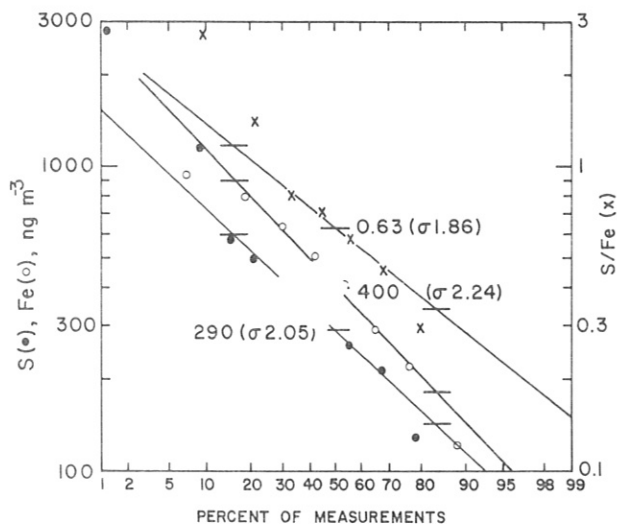


Figure 55.--Log-probability distributions of aerosol Fe, S, and S/Fe measurements for MLO Fe and S data of fig. 53. Linear trend lines represent a log-normal approximation of the middle 50% range of each distribution.

(3) Log-probability distributions of aerosol Fe, S, and S/Fe measurements for the MLO Fe and S data of fig. 53 are given in fig. 55.

(4) Median and 25th percentiles of element weight ratios for streaker samples collected at the Hawaii Volcano Observatory (HVO) and MLO are presented in fig. 56. For each, the number of 3.68-h time step ratios considered is indicated. Average values for the Earth's crust and Hawaiian basalt are indicated as EC and HB, respectively. (HB values are averages of Mauna Loa and Kilauea lavas, which differ significantly only for Ti/Fe and K/Fe. The percent values for Mauna Loa and Kilauea of Ti/Fe, K/Fe, and Fe are 0.17, 0.037, 8.68, and 0.19, 0.051, 8.89, respectively.) Element ratios at MLO differ from those simultaneously measured at HVO (1200-m altitude). During spring, continental dust predominates at MLO, but at HVO a mixture of continental dust and dust of Hawaii basalt origin is found. At HVO a higher element ratio variability in spring and decreasing K/Fe ratio by June indicate a much smaller continental dust concentration during summer. However, the measured springtime aerosol compositions at MLO and HVO indicate that the sources and atmospheric transport pathways of continental dust found at the two altitudes are not necessarily the same; two distinct continental dust components were apparently present.

(5) Variance-preserving spectra of Fe and S aerosol concentrations, wind-speed, and air temperature are shown in fig. 57 for MLO, from 23 April to 6 May 1979. Each spectrum is for 86 data points (3.68 hours apart) that were linearly detrended by least squares and tapered, 10% at each end of the series, by a split cosine bell window. Except for air temperature, which is not smoothed, the spectra represent periodograms smoothed over three bands using a rectangular filter and multiplied by frequency. Element concentrations <DL were set at $\frac{1}{2}$ DL. The frequency distributions of variance density for Fe and S differ from those of windspeed and temperature, indicating little effect of local meteorology on aerosol concentration variability and implying long-range aerosol transport to MLO. The prominence of a 21-h period for Fe and absence of a 24-h period may be accounted for by dust generation through an initially diurnal continental source process in Asia and modification of the periodicity during transport across the Pacific.

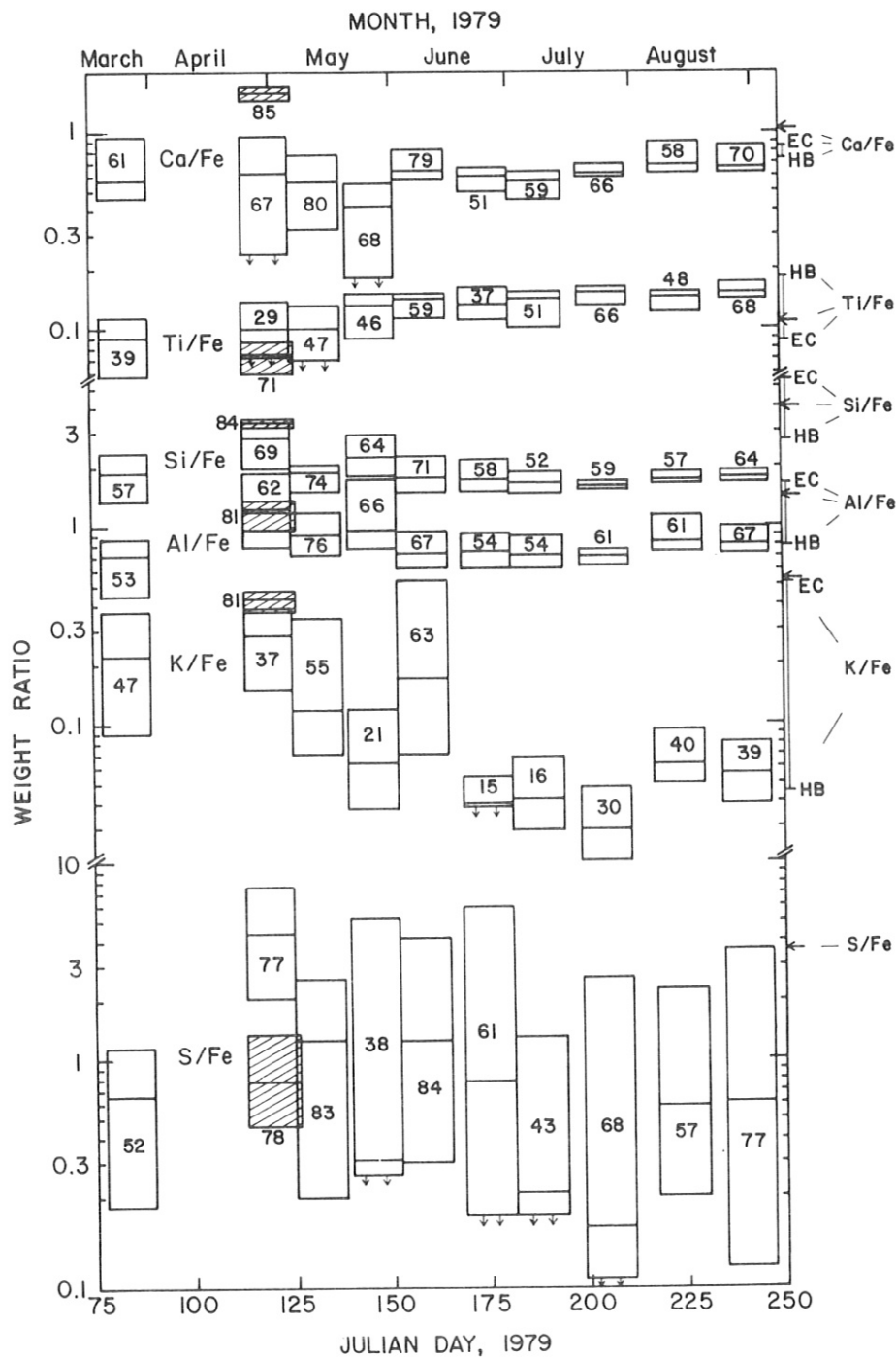


Figure 56.--Median and 25th percentiles of element weight ratios for streaker samples collected at HVO and MLO (shaded). For each, the number of 3.68-hour time step ratios considered is indicated. Average values for the Earth's crust (Mason, 1966) and Hawaiian basalt (Macdonald and Katsura, 1964) are indicated as EC and HB, respectively, on the right. Arrows at the right are the median values for a streaker sample collected during a kosa episode, 19 to 25 April 1980, in Niigata, Japan (Hashimoto et al., 1981, unpublished data).

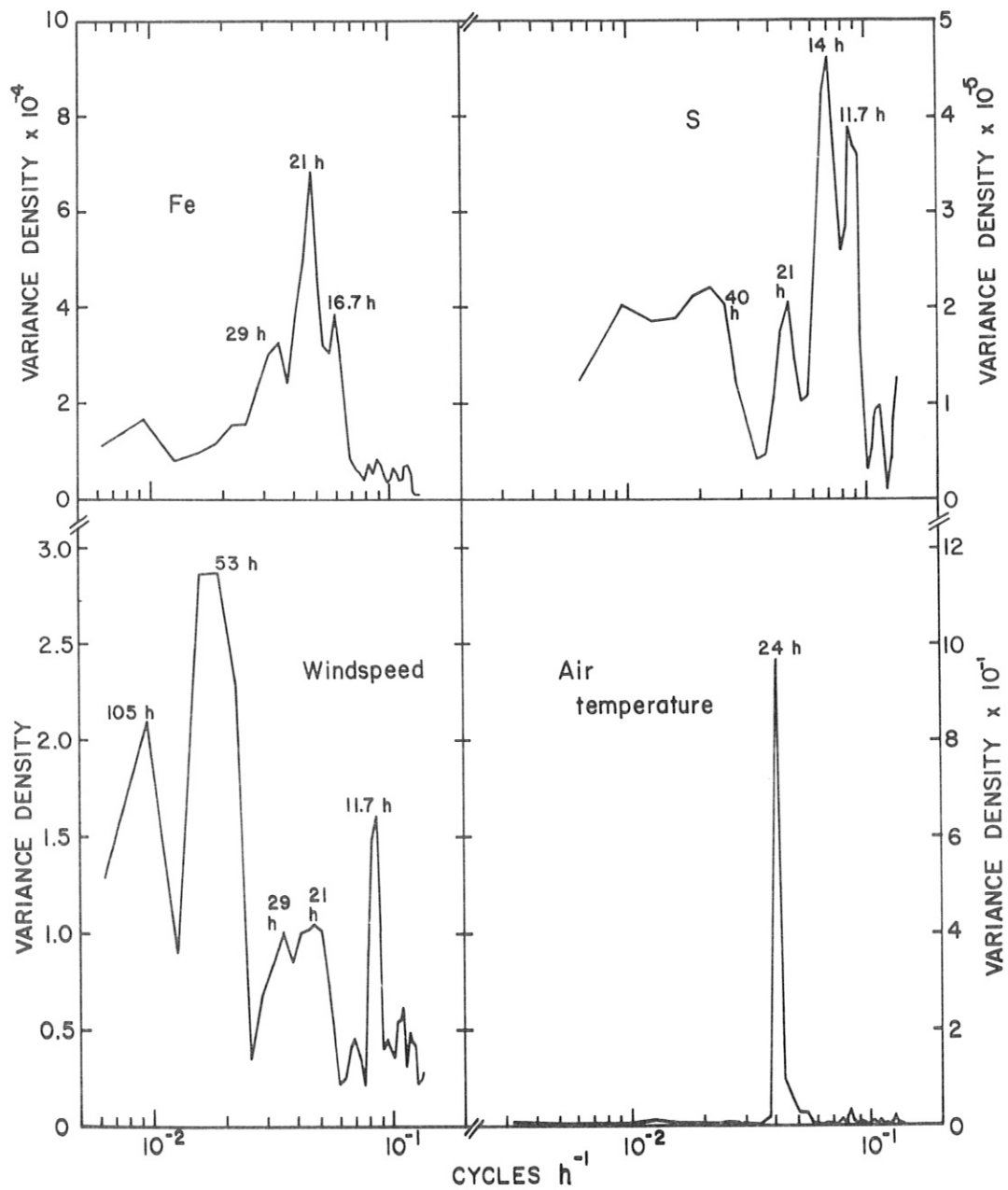


Figure 57.--Variance-preserving spectra of Fe and S aerosol concentrations (ng SCM^{-1}), windspeed (m s^{-1}), and air temperature ($^{\circ}\text{C}$) for MLO from 23 April to 6 May 1979. Each spectrum is for 86 data points, 3.68 hours apart.

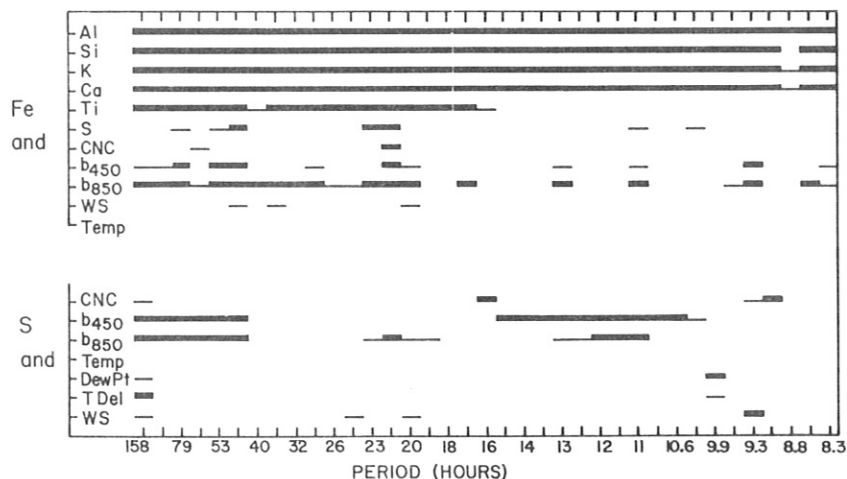


Figure 58.--Spectral periods with squared coherency of >95% (thick line) and >90% (thin line) significance for given pairs of time series, each with 86 data points, 3.68 hours apart, for MLO, 23 April to 6 May 1979. WS is windspeed; TDel is Temp minus DewPt.

(6) Figure 58 delineates spectral periods with squared coherency of >95% and >90% significance for given pairs of time series, each with 86 data points, 3.68 hours apart, for MLO from 23 April to 6 May 1979. Data and autopereidograms were treated as for fig. 57. (For these computations, the Temp [air temperature] periodogram was also smoothed over three bands.) The strong coherency of Fe with other crustal elements over all periods indicates a common source composition. If significant admixture of local basaltic aerosol with continental dust had occurred, this would have resulted in weaker coherency because of the compositional differences of the two aerosol components. The absence of coherency between Fe or S and meteorological parameters is consistent with long-range aerosol transport to MLO.

(7) Results of a cross-spectral analysis of Fe and S aerosol concentrations for MLO, given in fig. 53, are shown in fig. 59. The positive phase indicates S leading Fe. Generally high coherency of Fe and S for periods greater than about 20 hours indicates mixing of the elements on a regional scale and implies sources of Fe and S remote from MLO. A desert source of soil dust containing Fe and an east Asian urban pollution source for S are consistent with these relationships.

5.6 Arctic Haze Studies at Barrow

Kenneth A. Rahn

Center for Atmospheric Chemistry Studies, Graduate School of Oceanography
University of Rhode Island, Kingston, RI 02881

During 1980 we sampled aerosol continuously at the Barrow GMCC Observatory. Through May, one of our high-volume samplers took daily samples, concluding a program begun in December 1979. This pump was shut down for the summer and resumed daily sampling in November. The other high-volume sampler took regular 4-day samples throughout the year.

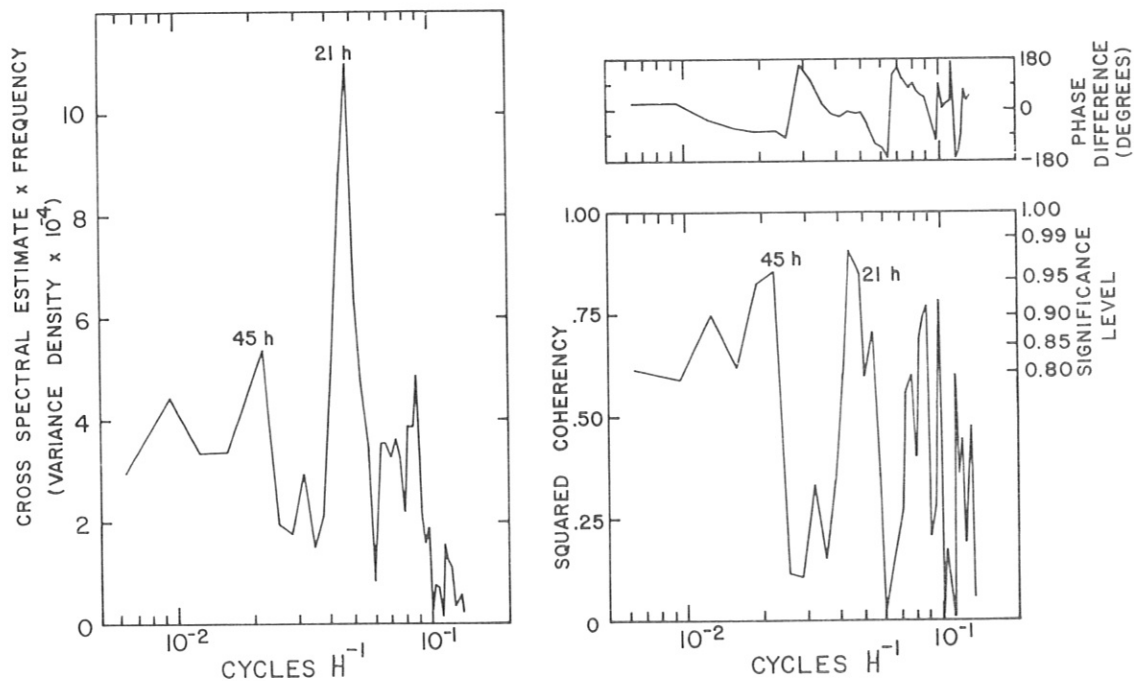


Figure 59.--Cross spectral analysis of Fe and S aerosol concentrations for MLO given in fig. 53. Treatment of data and autoperiodograms is the same as for fig. 57.

At URI, we spent much of 1980 developing the new finding that the pollution fraction of the aerosol at Barrow has a demonstrably different composition from that sampled in the Norwegian Arctic; hence it is probably from a different source. This is a significant step forward in our understanding of atmospheric chemistry in the Arctic. Since 1976 we have known that the Arctic atmosphere is filled with pollution aerosol during winter, of surprisingly similar composition from place to place. Now, as data multiply, we can see that there are at least two characteristic kinds of pollution aerosol in the Arctic.

Figure 60, from Rahn (1981), shows the original formulation of this idea. A scatter diagram of noncrustal Mn vs. noncrustal V in the aerosol shows that Mould Bay (N.W.T.) and Barrow have a different Mn/V ratio than Bear Island and Spitsbergen in the Norwegian Arctic. Because the Mn/V ratio decreases by factors of 2 to 4 during long-range transport, aerosol in the Norwegian Arctic is compatible with a European precursor, whereas that of the North American Arctic must have come from a source with a higher Mn/V ratio than Europe. A variety of independent evidence suggests strongly that this previously unrecognized source is the central U.S.S.R.

Figure 60 represents mean conditions during winter at Barrow. Figure 61 shows frequency distributions of Mn/V ratio for our daily samples during winter 1977-78. (Filters were supplied to URI by B. Ottar of the Norwegian Institute for Air Research.) This plot confirms the mean values in fig. 60

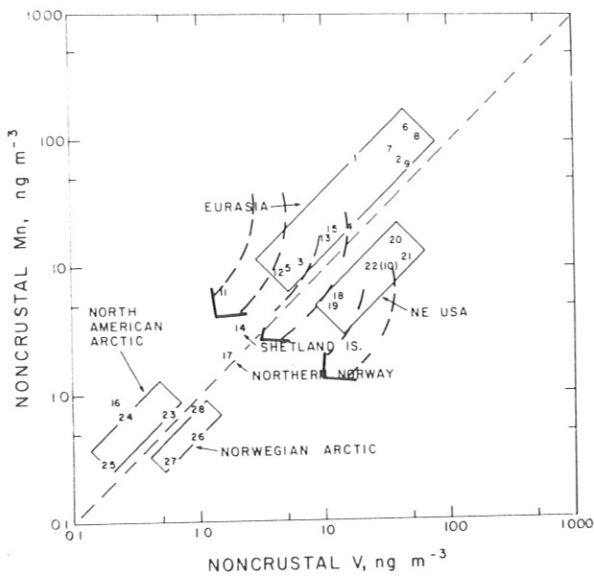


Figure 60.--Scatter diagram of atmospheric concentrations of noncrustal Mn and V in the northeast United States, Europe, and the Arctic. Point 23 is mean winter at Barrow, point 24 is mean November-December at Barrow, and point 25 is mean November-December at Mould Bay, N.W.T. (After Rahn, 1981.)

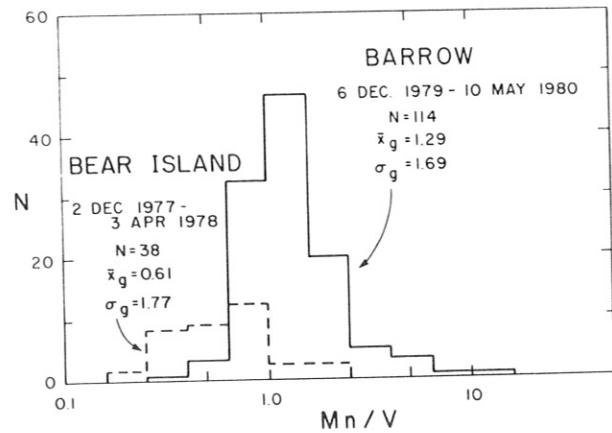


Figure 61.--Frequency distributions of Mn/V ratios at Barrow and Bear Island during winter. Barrow data by N. Lewis, URI.

and shows a shift to lower values of the entire frequency distribution for Bear Island.

Figure 62 shows the sequence of Mn, V, and Mn/V for the daily samples at Barrow during 1979-80. After an initial period of high Mn/V ratio during early December, the ratio remained between 1 and 2 through February, except for very brief excursions and a somewhat longer period of low values during early February. In March, however, the ratios dropped to well below 1 and did not return to the earlier values until late April.

We believe that these variations in Mn/V ratio are highly significant and interpretable. They show seasonal shifts in pollution sources affecting Barrow and changes in transport paths that pure meteorological analysis has not been able to resolve. During December 1979 through February 1980, Barrow was evidently receiving aerosol mainly from the central Soviet Union. This is consistent with broad patterns of near-surface airflow for winter, which are from the Asian side across the pole to the North American side. In early March 1980, aerosol reaching Barrow changed abruptly to a European character as the Mn/V ration dropped to values very similar to those of Bear Island. This is consistent with the springtime establishment of a high-pressure cell between the pole and Alaska, an annual feature of Arctic circulation. During this period, Europe was also affected by a westward extension of the Asiatic high, which promoted flow of its aerosol directly north into the European

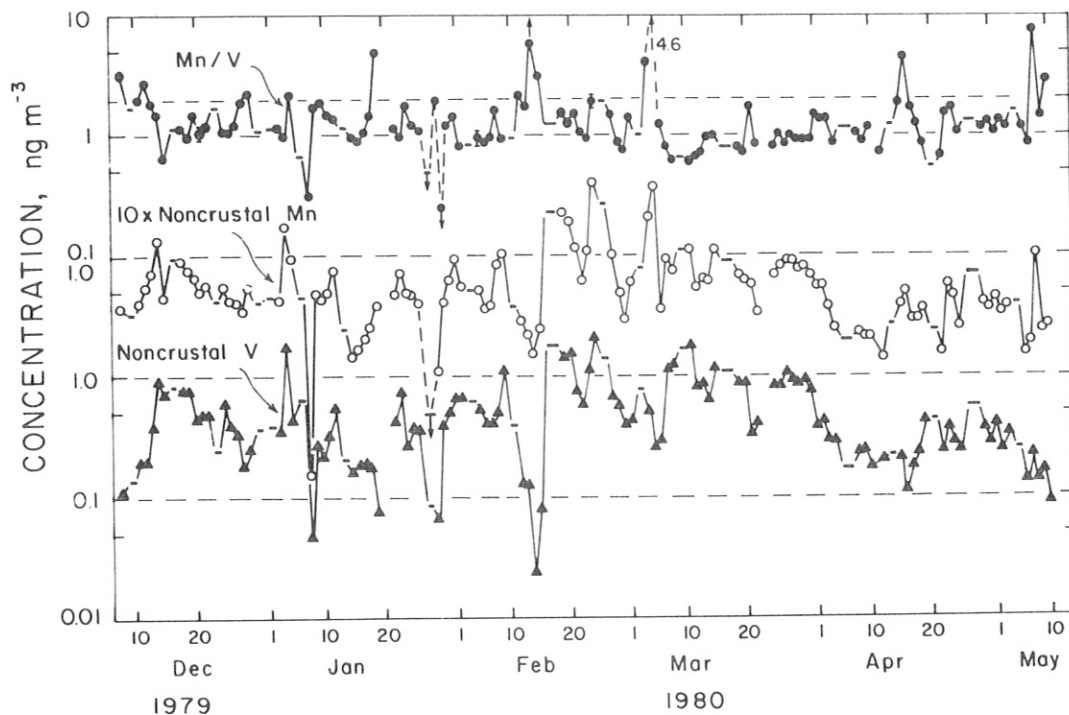


Figure 62.--Mn, V, and Mn/V in daily aerosol samples at Barrow. Analyses by N. Lewis, URI.

Arctic. Thus, chemistry and meteorology concur that the Barrow aerosol of March 1980 was an aged version of that at Bear Island.

During the coming years we will pursue the use of pollution aerosols as tracers in and around the Arctic. At least in the short term, chemical tracers present an attractive way, and perhaps the most efficient way, to understand large-scale circulation in this area where distances are great and meteorological data are very few.

5.7 The SEAREX Program--An Overview

Robert A. Duce and Roger J. Cayer, Jr.
 Center for Atmospheric Chemistry Studies, Graduate School of Oceanography
 University of Rhode Island, Kingston, RI 02881

Increasing interest in atmospheric transport of both anthropogenic and natural trace substances to marine areas was highlighted by a workshop on "Tropospheric Transport of Pollutants to the Ocean," held in Miami in December 1975. Discussions at the workshop quickly uncovered an almost total ignorance of the fluxes of trace metals and virtually all organic substances between the atmosphere and the ocean, the mechanisms of exchange of these substances across the sea-air interface, and the great difficulty in distinguishing between natural and pollution sources for many of the trace substances found in marine air. There was a consensus that a major coordinated research program investigating these sea-air exchange problems should be undertaken. The Sea-Air Exchange (SEAREX) program represents an initial step in that direction. Its general objectives, agreed upon at an organizational meeting held

at Scripps Institution of Oceanography in early January 1977, prior to proposal submittal to the National Science Foundation, are as follows:

- (1) The quantitative measurement of atmospheric fluxes to the ocean surface of selected heavy metals (e.g., Pb, Cd, Zn, Se, Sb, As, Cu, Hg, Ag); ^{210}Pb and its daughter ^{210}Po ; and organic compounds such as the anthropogenic-source PCB, DDT, polynuclear aromatic and aliphatic hydrocarbons, phthalate plasticizers, and the naturally occurring steroidal and terpenoid hydrocarbons, fatty acids and alcohols, and compounds with low molecular weights (e.g., ketones, aldehydes, and carboxylic acids).
- (2) The identification of the sources for these substances in the marine atmosphere.
- (3) The investigation of mechanisms of exchange of these substances across the sea-air interface.

Since more than 90% of the atmospheric pollutants are injected into the Northern Hemisphere and since the tropospheric residence times of atmospheric particles are relatively short (days to 1-2 weeks) compared with relatively long (6 months to 2 years) tropospheric mixing times between the Northern and Southern Hemispheres (Junge, 1963; Duce et al., 1974; Newell et al., 1974), significant differences may be observed for anthropogenic source substances present in atmospheric particles at remote areas in the two hemispheres. Therefore, major differences in atmospheric concentration or deposition observed at these sites may be related to anthropogenic sources. Islands chosen as atmospheric sampling bases, therefore, must necessarily be thousands of miles from continents and in strong trade wind and westerly wind regimes, thereby exhibiting nearly ideal marine atmospheric conditions. Areas chosen by the SEAREX program that most closely resemble these conditions are Bokandretok Island, Eniwetok Atoll, Marshall Islands (Northern Hemisphere trades); Tutuila Island, American Samoa (Southern Hemisphere trades); the area north of Te Pahi Stream, North Island, New Zealand (Southern Hemisphere westerlies); and a cruise track north of the Hawaiian Islands in an area described roughly by 40° - 50° N latitude (Northern Hemisphere westerlies). Additionally, seawater investigations have been made as part of the SEAREX program, both in the Sargasso Sea region and in the coastal-upwelling region off the coast of Peru, as part of the BIMS (Bubble Interfacial Microlayer Sampler) experiments.

The atmospheric sampling program that began in Eniwetok in March 1979 will continue through the end of the North Pacific cruise in July 1984. The Samoan atmospheric sampling phase of the SEAREX program has just recently been completed and will be the subject of next year's report to NOAA/GMCC.

5.8 Site Evaluation and Facility Construction for SEAREX Experiments in American Samoa

Robert A. Duce, Roger J. Cayer, Jr., and John T. Merrill
Center for Atmospheric Chemistry Studies, Graduate School of Oceanography
University of Rhode Island, Kingston, RI 02881

and

Danny D. Reible and Frederick H. Shair
Department of Chemical Engineering
California Institute of Technology, Pasadena, CA 91125

The NOAA/GMCC station located at Cape Matatula in American Samoa was chosen by the Sea-Air Exchange (SEAREX) program as an atmospheric sampling site because of its location in the Southern Hemisphere trade wind regime. The tall bluff immediately to the west of the proposed location of the two atmospheric sampling towers posed a potential problem. The ledge surrounding the towers on three sides, which dropped vertically 30 m to the water below, posed another potential problem. Each of these problems had to be considered as a contamination threat to atmospheric samples scheduled to be collected there in 1981.

To investigate the possibility of contamination to SEAREX atmospheric samples due to eddying around the local topography, series of tests were designed to help reveal the local flow patterns so that optimum sampling-tower locations and heights could be determined. The first series (Reible et al., 1981), which took place in April 1980, consisted of 18 atmospheric tracer studies using smoke bombs and sulfur hexafluoride (SF_6). These tracer studies were designed to investigate the effect of local and far-field ground level sources on sampling locations at the top of the two proposed sampling towers. Emphasis was placed on the determination of minimum tower height and site location. The maximum width of the sampling window, in terms of uncontaminated wind directions, was also investigated.

The possible sources of contamination to marine air samplers located on these two towers were grouped into two broad categories: (1) the near-field sources, and (2) the far-field sources. The near-field sources include vegetation (e.g., organic contaminants) and exposed rock (e.g., crustal contaminants) on and around Cape Matatula. The far-field sources include planes and ships passing near the cape and both natural and anthropogenic sources on the islands of Aunu'u and Tutuila.

The near-field sources of contamination were investigated during all but two of the field tests. Releases of various tracers were made from a number of different locations and under a number of different wind conditions. SF_6 was used to quantify the impact of these sources on the proposed sampling towers. The meteorological regimes studied can be divided into three different wind directions: (1) southeasterly flow, (2) easterly or east-northeasterly flow, and (3) northerly or north-northeasterly flow. A southeasterly flow over the cape separates from the surface of the water at a distance upwind of the cape approximately equal to the height of the cliff forming the southern boundary of Cape Matatula (in this instance, the upwind side). The region within the separation streamline is characterized by poorly organized, recirculating flow that is only weakly coupled with the freestream flow. This combination causes relatively good mixing of pollutants within the separated zone but poor ventilation of the region by the freestream flow. A similar

separated zone encompasses the entire cape because of the inability of the flow to conform instantaneously to variations in terrain. Separation in this second zone is enhanced by a knoll at the top of the cliff. This zone is called a wake and is similar to wake flow structures behind buildings and other bluff bodies. These two large, separated zones control the vertical transport of pollutants from sources on the cape during a southeasterly wind.

SF₆ tracer tests investigated the contamination of the proposed towers by pollutant sources on the cape under conditions of a southeasterly flow. The tests showed that SF₆ released in the upwind separated zone strongly impacted the tower at elevations between the surface and 7 to 10 m. Above this altitude, SF₆ concentrations dropped rapidly. The tower top (20 m) concentrations detected during these tests were between 0.01 and 0.19 ppb (g-mol)⁻¹ h⁻¹, and between 0.2% and 3% of the peak tower concentration. Because of the possibility of sample contamination, the tower top concentrations represent maximum values (i.e., an upper bound to the impact of a ground level source under the conditions of the experiment). During an easterly or east-northeasterly flow, because of the relative smoothness of the easterly approach to the proposed sampling towers, the effects of flow separation are expected to be minimized.

Tests were made to investigate the effect of a ground level source of contamination on the proposed sampling-tower locations under the easterly flow regime. SF₆ from this release impacted the proposed auxiliary tower (or rain tower) more directly than the main (or air-sampling) tower. Essentially no SF₆ was detected at the air-sampling tower. At the 15-m elevation on the rain tower the detected SF₆ levels ranged from 0.02 to 0.4 ppb (g-mol)⁻¹ h⁻¹, or 4% to 13% of the tower peak concentration. This is significantly higher than the tower top concentrations detected during other meteorological regimes.

The "bluffness" of the northern edge of Cape Matatula is similar to that of the southern edge of the cape. It is made up of several levels of small cliffs. The gross characteristics of a northerly flow should thus be similar to a southerly flow. An upwind separated zone and a downwind wake would be expected to control the vertical transport of pollutants released at the surface of the cape.

Tests were designed to investigate the effect of surface sources on the proposed tower locations during a northerly flow. During one test, SF₆ was released at the base of the air-sampling tower. SF₆ levels decreased rapidly above the 7-m elevation. The tower top concentrations ranged from 0.001 to 0.01 ppb (g-mol)⁻¹ h⁻¹, which are less than 0.1% of the peak tower concentrations. During another test, in which SF₆ was released from a location about 70 m upwind of the towers, levels of 0.005 to 0.22 ppb (g-mol)⁻¹ h⁻¹ were detected at the air-sampling tower top (20 m), and a maximum level of 0.026 ppb (g-mol)⁻¹ h⁻¹ was detected at the rain tower top (15 m). The air-sampling tower top concentrations were between 0.02% and 0.3% of the peak tower concentrations. SF₆ levels dropped off rapidly above an elevation of 10 m.

The effects of far-field sources were investigated during two tests. Since the proposed marine air-sampling window covers only northerly, easterly, or southerly winds, Tutuila sources were not considered important. Smoke tests showed no evidence of transport from the region of the downwind GMCC tower and observatory toward the proposed sampling sites. The two far-field

tests were instead designed to determine the effect of Aunu'u Island (south of Cape Matatula) on the proposed sampling locations. These tests were used to determine the southern extent of the sampling window. An SF₆ release from upwind (southeast) of Aunu'u Island was designed to investigate the effect of the island on the crosswind dispersion of pollutants. Wake and other lee effects of bluff bodies can greatly enhance crosswind dispersion of airborne pollutants. It was found, however, that Aunu'u Island seemed to have very little effect on the dispersion of the tracer (and thus airborne pollutants). Automobile traverses on the shore of Tutuila showed that the crosswind standard deviation in concentration corresponded roughly to Pasquill-Gifford stability class D of the Gaussian plume model (Turner, 1970). The maximum concentration detected at Cape Matatula during this test was 0.092 ppb. Again, there was insufficient redundancy to rule out the possibility that this level was due to sample contamination. In any event, the level detected at Cape Matatula was extremely low (0.0006 ppb (g-mol)⁻¹ h⁻¹). An SF₆ release from the channel between Aunu'u and Tutuila was designed to investigate the crosswind dispersion of pollutants in the absence of bluff body effects. Again the tracer dispersed according to stability class D of the Gaussian plume model. Essentially no SF₆ was detected at the GMCC observatory during this test.

It was possible to estimate the wind direction at which contamination from Aunu'u could be detected at Cape Matatula by using the experimentally determined stability classification. Cape Matatula lies about 5 km from the eastern edge of Aunu'u Island. Turner suggests a crosswind standard deviation in concentration of about 325 m under neutrally stable conditions (D stability). A concentration of 1% of the peak concentration occurs at three times the standard deviation in the Gaussian plume model. Thus the southern extent of the marine air-sampling window should not include winds whose trajectory from Aunu'u falls within 1,000 m of Cape Matatula. Using this criterion, the southern extent of the marine air-sampling window should be about 145° true north. A similar procedure can be used to estimate the impact of passing ships on the sampling location.

A separate study (Merrill, 1981) was undertaken in July 1980 to assess the possible effects of eddying caused by the steep ridge beneath the 20-m atmospheric sampling tower and the tall bluff crosswind behind the site. This study was made using micrometeorological techniques and is complementary to the SF₆ studies. Fast-response anemometers and temperature sensors were located approximately 13, 15, and 19 m above tower base. A vertical anemometer was also located at a height of 19 m during part of the study, which lasted 12 days. The windspeed varied from 5 to 15 m s⁻¹ (about 10 to 30 kn) and the direction was southwest through south, east, and north to northwest, covering the entire (proposed) sampling sector.

Analysis of the data indicated that no sampling problems would occur. In all sectors except the east and east-northeast, even a casual observation of the instruments in operation showed no evidence of eddying at tower levels above 15 m. From the east and east-northeast, eddying does extend higher, perhaps as far as 16 m. From some sectors there is a shift in wind direction with height, caused by the airflow over the ridge; also, there is a noticeable jet of increased windspeeds from the surface of the ridge up to about 10 or 12 m (with winds in that layer up to 15 m s⁻¹ vs. 12 m s⁻¹ at tower top). Furthermore, there is substantially increased gustiness at the 13-m level and even at 15 m under some conditions. All of this indicates that turbulent eddies generated by the topography are confined below the 20-m sampling

height. Thus these measurements corroborated the SF₆ study as to the depth of the disturbed layer.

From the above discussion, the following conclusions can be drawn concerning adequate criteria for the Samoa sampling site:

- (1) The sampling towers should be as close as possible to the upwind edge of the cape.
- (2) The towers should be a minimum of 10 m in height. At the existing main tower site, the maximum impact of local sources on a 20-m tower in a southeasterly or northeasterly wind would be $<0.2 \text{ ppb (g-mol)}^{-1} \text{ h}^{-1}$.
- (3) The tower support structures should not be enclosed. An enclosed structure will develop a wake that can efficiently transport pollutants vertically.
- (4) Because of possible contamination of the marine air samples by Aunu'u Island, the southern extent of the marine air-sampling window should be a wind direction of 145° true north.
- (5) Because of possible contamination from inland sources on Tutuila, the marine air-sampling window should exclude wind directions less than 360° true north (145° through 360°).

Since the criteria outlined in the conclusions above were followed by the SEAREX program at the GMCC site, the site should now be considered excellent for the collection of locally uncontaminated samples representative of the ambient marine atmosphere in that region.

On the strength of the positive results of these two studies, the SEAREX facility, consisting of six buildings and two walk-up towers, was constructed in July and August of 1980 (SEAREX Newsletter, 1980).

The first tower, 20 m in height, was used as a platform for the collection of particulate and trace gas samples by both the organic and the trace metal groups in SEAREX. The second tower, 14 m in height, was used exclusively for the collection of rain and dry-deposition samples. Both towers are aluminum and are identical in configuration to towers used in the past by all of the SEAREX groups.

Three 10' × 16' and two 8' × 12' buildings were erected. One of the larger buildings was used as an organic chemistry laboratory, one as a conference and storage facility, and the third as an electrical power equipment center. One of the two smaller buildings housed the trace metal laboratory, and the second 8' × 12' building contained analytical instrumentation including a gas chromatograph, an ion chromatograph, and a water-purifying system. An 8' × 8' building constructed at the site by URI several years ago housed all the electronics, recorders, minicomputer, etc. The analytical instrumentation building was located on the top of the cliff, near the NOAA observatory, some 40 m above the towers and other buildings. The towers and other support buildings were on an exposed cliff about 30 m above the ocean surface.

5.9 Carbon Particles in the Arctic Aerosol

H. Rosen and T. Novakov
Lawrence Berkeley Laboratory
University of California, Berkeley, CA 94720

and

B. A. Bodhaine
Geophysical Monitoring for Climatic Change, NOAA/ERL
Boulder, CO 80303

5.9.1 Introduction

Recent studies in the Arctic (e.g., Kerr, 1981) show the presence of unexpectedly high aerosol concentrations, which appear to have a large anthropogenic component. In order to investigate the chemical composition, origins, and climatic impact of the aerosol, a collaborative sampling program was started by Lawrence Berkeley Laboratory (LBL) and NOAA in October 1979. This program has emphasized the analyses of the carbonaceous aerosol and its optical properties, but also has the capability to determine the other major aerosol components. Preliminary results from this study show that large concentrations of combustion-generated particles are present in the Arctic and that they may have a significant impact on the heat balance over this region.

An aerosol sampler was designed and constructed at LBL to collect parallel filter samples on 47-mm quartz fiber and millipore substrates at a flow rate of approximately $1.5 \text{ ft}^3 \text{ min}^{-1}$. The sampler was put into operation on 18 October 1979 and coupled to a wind controller on 7 January 1980, to minimize local contamination by collecting samples only when the wind was blowing from the clean-air sector. Approximately 100 filter pairs were collected at sampling time intervals ranging from 2 days to 1 week. All filters were analyzed to determine the total carbon content of the aerosol, the absorption coefficient of the aerosol, and, by the X-ray fluorescence technique, concentrations of elements with $Z > 11$. The absorption coefficients reported here were at 0.5μ and were corrected in a preliminary way for filter penetration effects. Only selected filters were analyzed by Raman spectroscopy and optic-thermal analysis.

5.9.2 Chemical Composition of the Arctic Aerosol

If one excludes the obvious natural aerosol components (e.g., sea salt and soil), the predominant components of the Barrow aerosol are carbon- and sulfur-containing particles. The carbonaceous aerosol has a large graphitic component, which has been identified by Raman spectroscopy. There is considerable indirect evidence that a major part of the Arctic aerosol is produced from combustion processes. However, the strongest and most direct substantiation of this fact is provided by the Raman spectra shown in fig. 63. These spectra demonstrate the presence of substantial quantities of graphitic species that have a similar structure to carbon black and can be produced only by combustion processes. Associated with these species are large optical absorption coefficients ($\approx 10 \text{ m}^2 \text{ g}^{-1}$), which are shown in fig. 64. If one ignores the possible contribution of natural burning processes (e.g., forest fires), which is expected to be small during the indicated times of the year in the Northern Hemisphere, this component can be attributed directly to anthropogenic combustion processes.

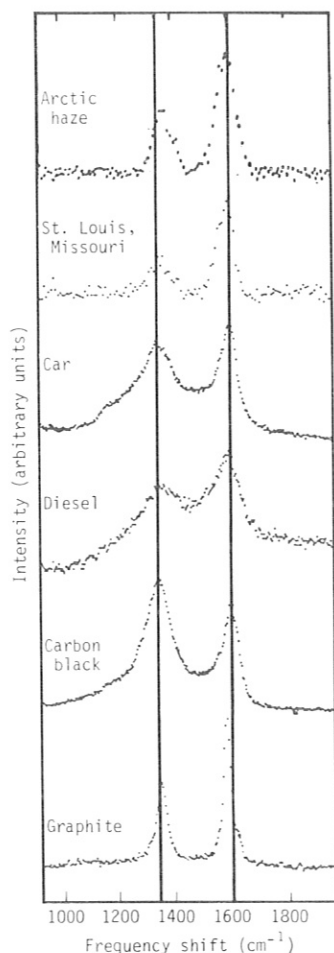


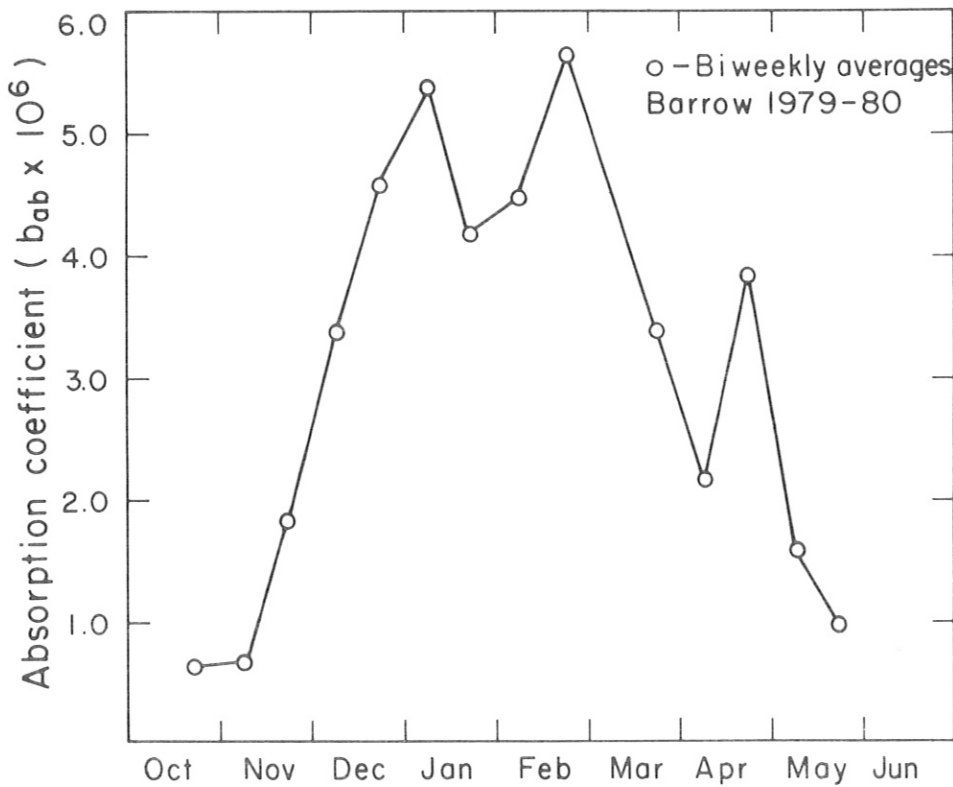
Figure 63.--Raman spectrum of an Arctic sample compared with spectra of urban particulates, various source emissions, carbon black, and polycrystalline graphite.

Total carbon concentrations were measured by combusting the aerosol samples in oxygen at 800°C and measuring the evolved CO₂. Total sulfur content was determined by X-ray fluorescence analysis. In figs. 65 and 66 the concentrations of these two components, determined for various times of year, are compared with those found in urban environments. It is clear from these figures that the concentrations of these aerosol components are large during the period of early winter to spring. These levels, of course, are less than those found in urban areas, but, surprisingly, not by large factors.

5.9.3 Model Calculation of the Effect of Absorbing Aerosols on the Heat Balance Over the Arctic

A simple model calculation of the possible effects of the Arctic aerosol on the heat balance can be made, using the absorption coefficients presented in fig. 64. For the calculation we assume a uniform aerosol distribution from ground level to a height h (see fig. 67) and use the two-stream approximation of Chylek and Coakley (1974). With these assumptions the effective albedo of the Earth-atmosphere system can be written as

$$I_r/I_o = A - 2\tau_a A + \tau_b (A - 1)^2 ,$$



Typical Absorption Coefficients in Urban Areas	
Argonne, Illinois	$2.8 \times 10^{-5} \text{ m}^{-1}$
Gaithersburg, Maryland	$2.1 \times 10^{-5} \text{ m}^{-1}$
Denver, Colorado	$2.4 \times 10^{-5} \text{ m}^{-1}$
Anaheim, California	$4.9 \times 10^{-5} \text{ m}^{-1}$
Fremont, California	$3.4 \times 10^{-5} \text{ m}^{-1}$
Berkeley, California	$2.1 \times 10^{-5} \text{ m}^{-1}$
New York, New York	$6.4 \times 10^{-5} \text{ m}^{-1}$

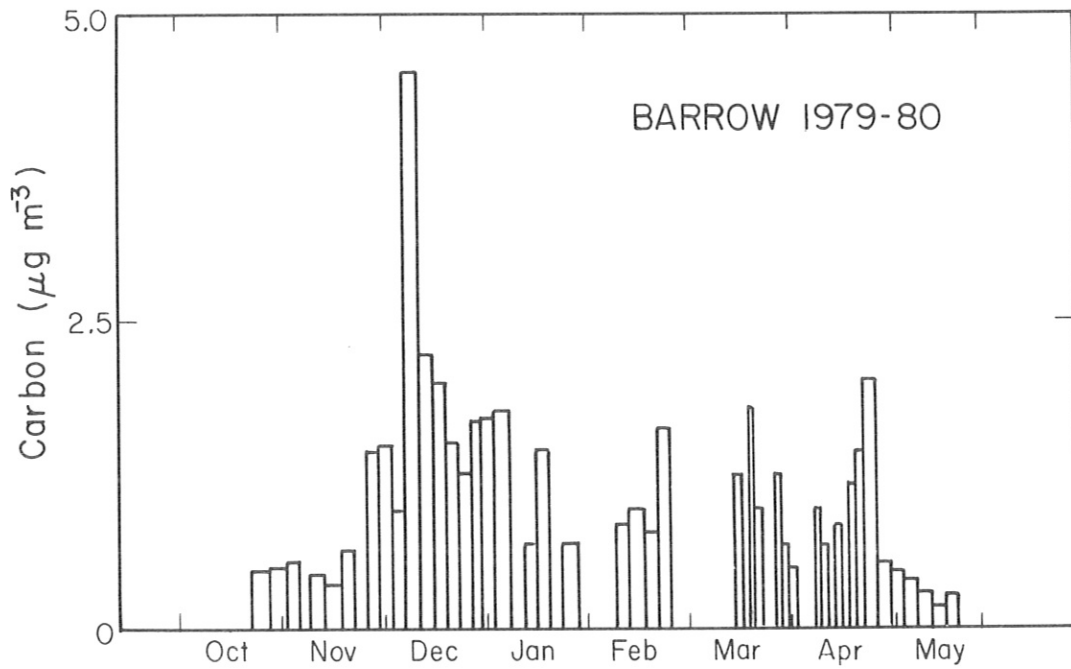
Figure 64.--Comparison of optical absorption coefficients at Barrow with those found in various urban locations.

where

- A = albedo of surface,
- τ_a = optical depth due to absorption,
- τ_b = optical depth due to backscattering,
- I_o = incident radiation, and
- I_r = reflected radiation.

Over snow-covered regions, $A \approx 0.8$ so that the scattering or cooling term is negligible compared with the absorption or heating term for all reasonable τ_a and τ_b . The equation above then becomes

$$I_r = I_o A - 2\tau_a A I_o ,$$



Typical total carbon concentrations in urban areas	
Gaithersburg, Maryland	6.1 µg m ⁻³
Argonne, Illinois	8.1 µg m ⁻³
Denver, Colorado	9.8 µg m ⁻³
Anaheim, California	16.6 µg m ⁻³
Fremont, California	12.0 µg m ⁻³
Berkeley, California	6.7 µg m ⁻³
New York, New York	15.2 µg m ⁻³

Figure 65.--Comparison of the total carbon concentrations at Barrow with those found in various urban locations.

so that the change in light reflected due to aerosols is

$$I_r - I_r^a = 2\tau_a A I_o$$

This change in irradiance is calculated for a plane perpendicular to the incoming radiation. If we calculate the change in irradiance parallel to the Earth's surface, we get

$$\Delta = (I_r - I_r^a) \cos \theta = 2\tau_a A I_o \cos \theta$$

But τ_a can be written as $b_a h / \cos \theta$ so that

$$\Delta = 2b_a h A I_o$$

where b_a is the absorption coefficient. I_o is the average incident radiation from the sun, and we will approximate it by

$$I_o = I_o^s f_1 f_2, \quad I_o^s = 1350 \text{ W m}^{-2} = \text{solar constant}$$

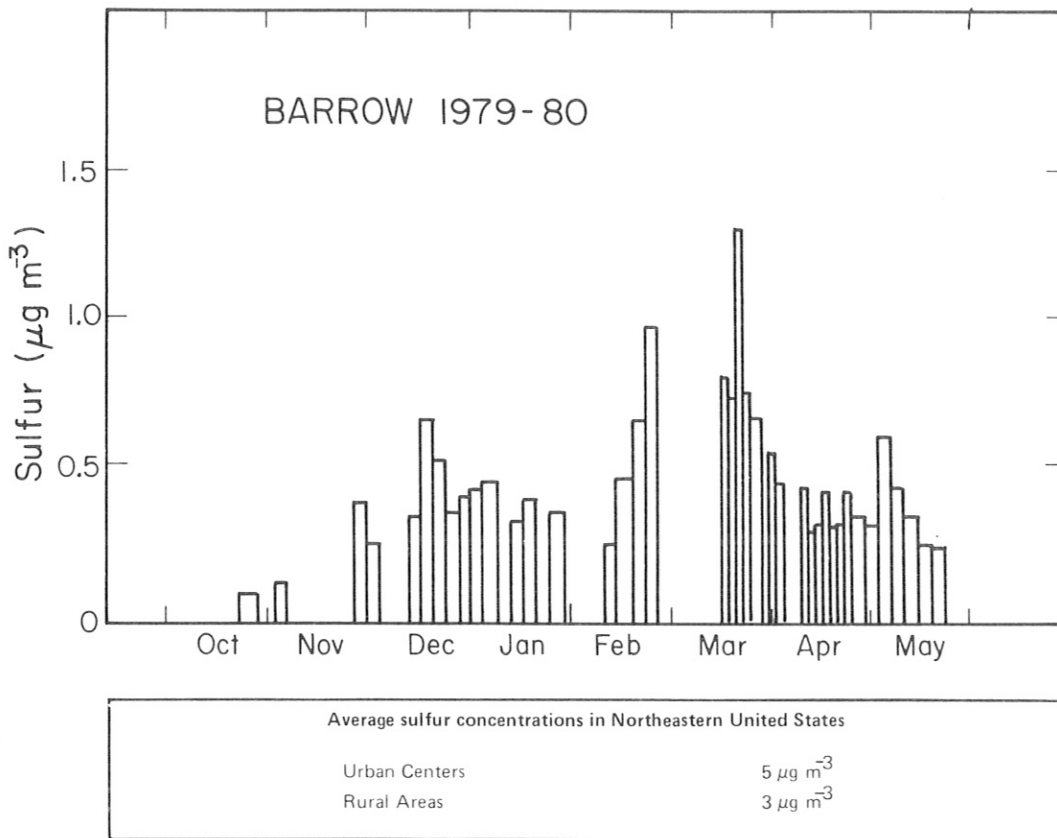


Figure 66.--Comparison of particulate sulfur concentrations at Barrow with those found in urban areas.

where f_1 is the fractional cloud cover, and f_2 is the fractional length of day. Then,

$$\Delta = 2(1350 b_a h A f_1 f_2) W m^{-2} = 2700 b_a h A f_1 f_2 W m^{-2} .$$

For this calculation let $A = 0.8$, $f_1 = 0.5$, and $h = 5 \times 10^3$ m; then,

$$\Delta = 5.4 \times 10^6 b_a f_1 f_2 .$$

Note that values for f_1 and h are rough approximations that can be refined when more data become available.

We now use our measurements of the absorption coefficient at Barrow and values of f_2 obtained from the Smithsonian Meteorological Tables (List, 1949) to calculate the results shown in fig. 68. Since one-half the sun's irradiance is above and below 0.75μ , the absorption coefficients reported in fig. 66 have been corrected to this wavelength, assuming a $1/\lambda$ dependence characteristic of graphitic carbon. The results, shown in fig. 68, indicate rather substantial change in the heat balance during the months of February, March, April, May, and possibly June. During these months approximately $6 W m^{-2}$ more energy is absorbed by the Earth-atmosphere system because of the presence of the haze. This energy change is about equivalent to the change in the radiation balance at midlatitudes expected from a 4% increase in the solar

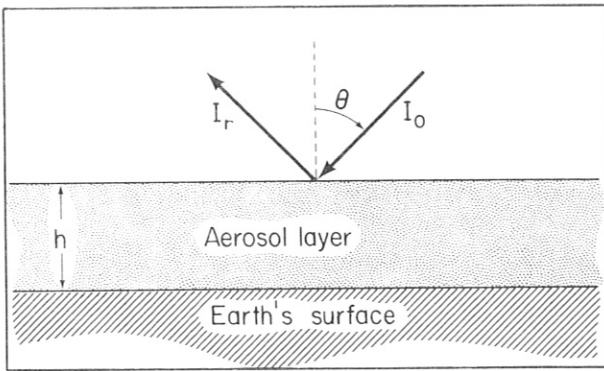


Figure 67.--Schematic representation of model calculation, where h is the height of the aerosol layer, I_r is the reflected radiation, and I_0 is the incident radiation.

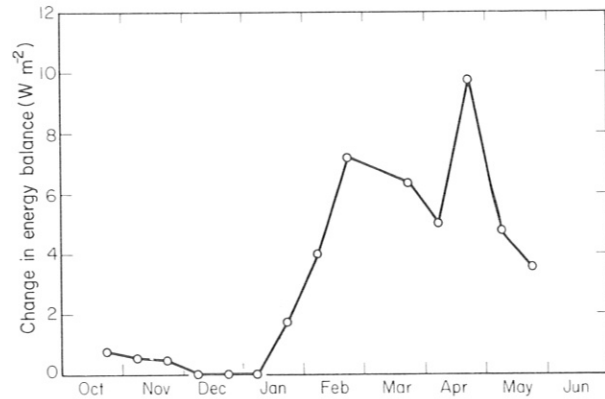


Figure 68.--Change in heat balance calculated from simple model of Arctic aerosol. This calculation is obviously oversimplified and should be viewed only as being indicative of a possible large climatic effect of the Arctic haze.

constant and is comparable with the change in the terrestrial radiation balance due to a doubling of CO_2 . It is difficult to translate this into a ground-level temperature change; however, there have been many models predicting that a 1% increase in the solar constant would lead to an increase of ~ 1 K in the surface temperature of the Earth. This calculation is obviously oversimplified and should be viewed only as being indicative of the possible large climatic effect of the Arctic aerosol. A more sophisticated treatment of this problem is under way at Lawrence Livermore Laboratory.

Acknowledgment

This work was supported by the National Oceanic and Atmospheric Administration through the U.S. Department of Energy under contract W-7405-ENG-48.

5.10 Solar Spectral Irradiance and the Transmissivity of the Atmosphere at Mauna Loa During 1980

Glenn E. Shaw
Geophysical Institute, University of Alaska
Fairbanks, AK 99701

5.10.1 Introduction

A multiwavelength solar radiometer was operated at Mauna Loa from February 1980 to February 1981 to establish the absolute value and variability of the sun's spectral irradiance at the time of maximum solar activity. A secondary objective of the study was to determine the wavelength dependency and seasonal variation of the optical extinction of light arising from absorption and scattering by natural aerosols suspended in the atmosphere above the mixing layer in the central Pacific Ocean.

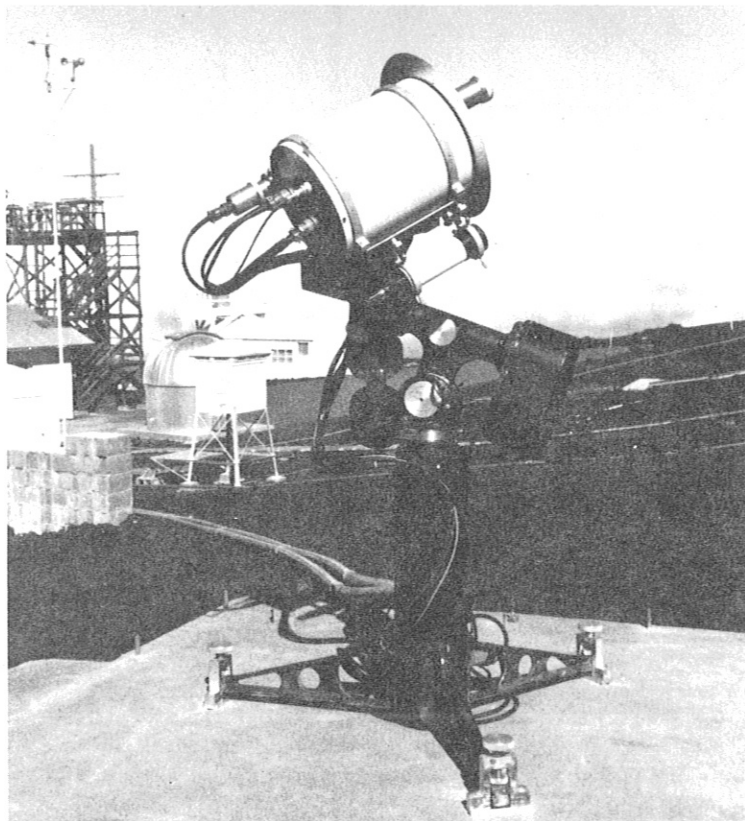


Figure 69.--The multiwavelength solar radiometer at Mauna Loa.

A photograph of the radiometer is shown in fig. 69; the optics are in the insulated, sealed cylindrical container maintained at uniform temperature and at low humidity. An automatic quadrant-diode tracker kept the instrument pointed at the sun to ± 1 -ft accuracy; light from the full disk of the sun was viewed.

Data were taken primarily during the morning hours when aerosols from the ocean and from the Hawaiian Islands were trapped beneath the Observatory by the marine boundary layer, as evidenced by low Aitken count ($< 500 \text{ cm}^{-3}$). In the 1-yr period of data acquisition, measurements for 136 days were suitable for analysis.

5.10.2 Solar Spectral Irradiance Time Series

Deviations from the mean of day-averaged values of solar irradiance at 10 wavelengths are shown in fig. 70, and the corresponding frequency distributions for these deviations are shown in fig. 71. The constancy of the extrapolated extraterrestrial values of solar spectral irradiance increases with increasing wavelength. It is to be noted, however, that uncertainties in extrapolating through the atmosphere with the Langley method decrease with increasing wavelength, so caution must be used in interpreting the deviations in figs. 70 or 71 as being true variations in extraterrestrial spectral irradiance.

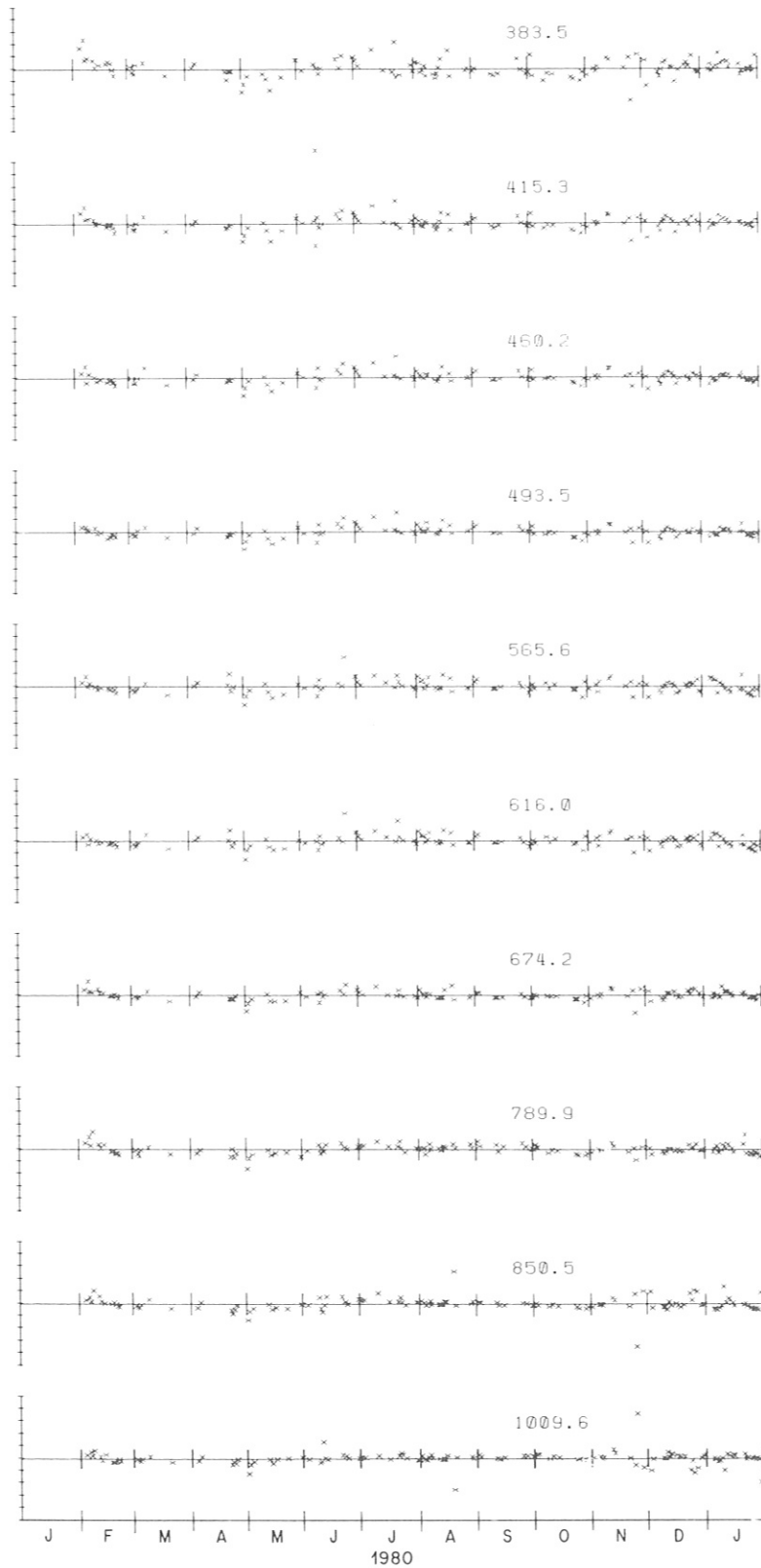


Figure 70.--Deviation of daily extrapolated values of spectral solar irradiance about the mean at 10 wavelengths. Tick marks are 1% intervals.

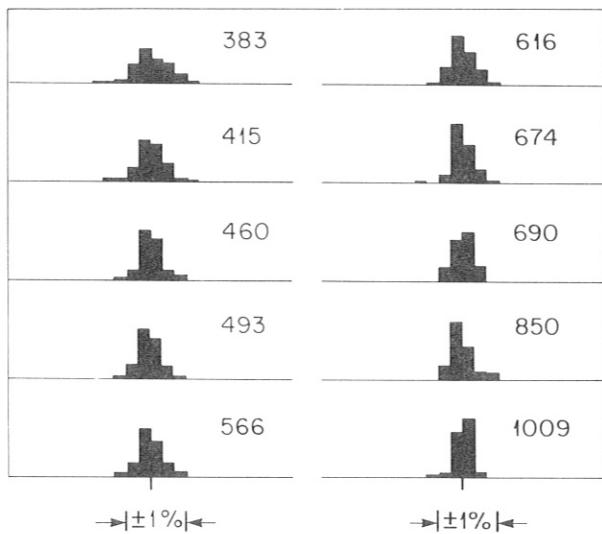


Figure 71.--Frequency distributions of extrapolated values of solar spectral irradiance for the period January 1980-January 1981.

The dominant error source in the determination of the solar spectral irradiance was nonconstancy of the optical atmospheric transmissivity throughout the morning period of data collection. To obtain a quantitative index of this particular error source, data were split into two sets: one for data acquired in the early morning hours when the relative airmass was >3 , the other in the later morning hours when the relative airmass was <3 . If the atmospheric transmissivity and solar brightness remain constant during the ~ 5 hours of data acquisition, the extrapolated solar irradiance values would be identical for both data sets. In this way it was determined that the accuracy with which one can extrapolate through the atmosphere from Mauna Loa is $\sim 0.5\%$ at $\lambda = 383$ nm, and 0.1% at $\lambda = 1009$ nm. It was concluded that the sun's irradiance was constant during 1980 to at least 1% at $\lambda = 383$ nm, and $<0.5\%$ at 800 nm, taking all the known sources of error into account. In the near ultraviolet band ($\lambda = 383$ nm) the solar luminosity may have been slightly low in May 1980 and December 1980 (by $\sim 1\%$) and slightly high during July 1980 (by $\sim 0.7\%$).

5.10.3 Absolute Values of Solar Spectral Irradiance

The Mauna Loa radiometer was placed on the SI thermodynamic scale of units by calibrating it with a National Bureau of Standards 1000-W type FEL quartz iodine lamp (lamp F-56). The calibration was cross-checked at three wavelengths by experimentally deducing the quantum efficiency and reflectivity of the photodetector (Geist et al., 1980). The mean values of solar spectral irradiance are listed in column 5 of table 31, and the ratio of these values to those tabulated by Labs and Neckel (1968) is shown in column 6. The agreement with determinations of Labs and Neckel is to 1% or 2% except at the three shortest wavelengths where the Mauna Loa radiometer provided consistently higher irradiances.

5.10.4 Aerosol Optical Extinction Spectrum

Calculations show that the particle column-integrated size distribution, for particles in the size range $0.2 < \theta$ (μm) < 0.8 at Mauna Loa, follows an

Table 31.--Absolute solar spectral irradiance values

Wavelength (nm)	Bandwidth (nm)	E(ATMOS)* (%)	E(CAL)† (%)	Spectral irradiance ($\mu\text{m cm}^{-2} \text{ nm}^{-1}$)	F ₀ /F ₀ (LN)**
383.5	7.6	0.5	1.6	97.3	1.12
415.3	6.8	0.4	1.5	177.3	1.04
460.2	6.7	0.3	1.4	212.6	1.07
493.5	6.9	0.3	1.2	197.4	1.01
565.6	7.8	0.2	1.2	182.4	1.00
616.0	7.6	0.2	1.2	165.4	0.99
674.2	6.4	0.2	1.2	147.8	0.98
789.9	6.4	0.2	1.2	113.2	0.97
850.5	6.6	0.1	1.2	93.2	0.91
1009.6	7.8	0.1	1.2	73.6	0.99

*rms uncertainty in atmospheric extrapolation.

†rms uncertainty in absolute calibration.

**Ratio of Mauna Loa irradiance to the values of spectral irradiance of Labs and Neckel (1968).

r^{-v} dependency with a power law exponent $3 < v < 4$. This power law form of the aerosol size spectrum falls off more slowly with increasing radius ($r > 0.2 \mu\text{m}$) than the aerosol size spectrum tabulated by Bigg (1980), suggesting that direct particle-sampling experiments tend to underestimate large particles or that large particles are somewhat more common in aerosol layers above the Observatory than they are at the Observatory itself.

5.10.5 Seasonal Variations in the Aerosol Extinction Spectrum

The time series of aerosol extinction is shown in fig. 72. A seasonal trend occurred with maximum aerosol extinction occurring in the spring months, approximately from March through May. During the remainder of the year the aerosol extinction was constant to $\sim \pm 10\%$; this behavior suggests that a background aerosol pervades the atmosphere above the marine boundary layer over the oceans.

In addition to the variations in aerosol extinction magnitude throughout the year, the wavelength dependency (fig. 73) of optical extinction also underwent systematic trends, being flatter (less variation with wavelength) during spring and steeper during the remainder of the year. This behavior indicates that there are more larger particles present in spring months than at other times. This is consistent with an interpretation of dust reaching the Hawaiian Island chain from the great deserts in Mongolia (Bodhaine et al, 1981; Dittenhoefer, 1981; Duce et al., 1980). That the material affecting the turbidity of the central Pacific Ocean was crustal was evidenced by X-ray

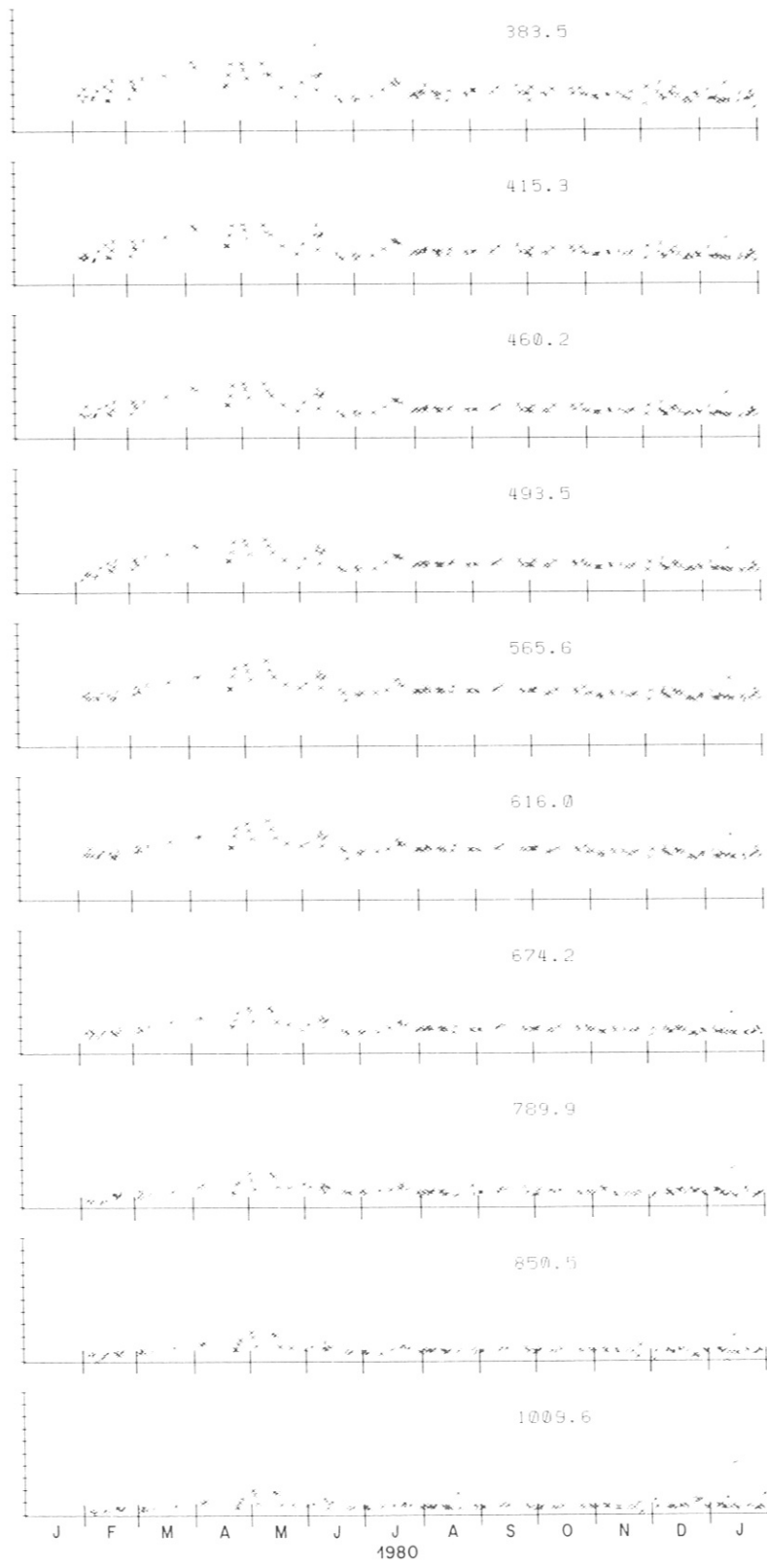


Figure 72.--Time series of aerosol optical depth at different wavelengths above Mauna Loa. Asian desert dust was detected at the Observatory in March-April 1980. Distance between tick marks is $\Delta\tau = 0.005$.

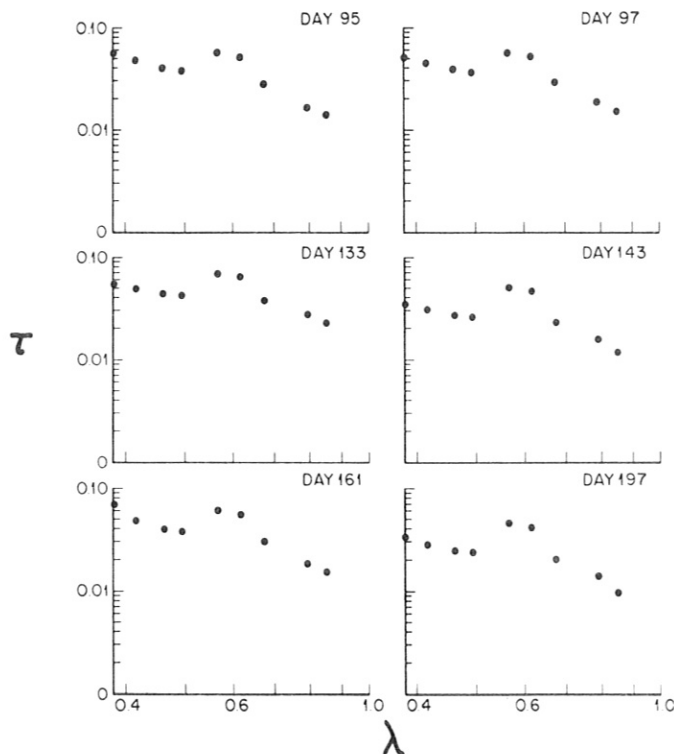


Figure 73.--Example of wavelength dependence of aerosol-plus-ozone optical depth above Mauna Loa.

spectrometry, conducted by the Geophysical Institute's electron microscope laboratory, on particles collected at Mauna Loa during spring 1980 by A. Dittenhoefer. The X-ray spectra showed major peaks in aluminum and silicon.

5.10.6 Conclusions

(1) Solar spectral irradiance at 10 wavelength bands ($\Delta\lambda \approx 5$ nm) in the region $380 < \lambda$ (nm) < 1000 varied by no more than 1% at $\lambda = 380$ nm, and 0.5% at $\lambda = 800$ nm, during the period February 1980 to February 1981. This was at the time of maximum solar activity.

(2) The absolute values (on the electrical scale of SI units) of solar spectral irradiance agreed to $\pm 1\%$ with the tables of Labs and Neckel at $\lambda > 493$ nm, but were higher by 7% and 4% at $\lambda = 460$ nm and at 415 nm, respectively. The experiment gave a value of spectral irradiance 12% higher than that of Labs and Neckel at $\lambda = 383$ nm. The estimated uncertainty in the present values of spectral irradiance ranged from 2.1% at $\lambda = 383$ nm to 1.3% at $\lambda = 1,000$ nm.

(3) The atmospheric optical depth arising from absorption and scattering above the Mauna Loa Observatory (elevation 3.38 km, pressure 670 mb) is $\tau_0 = 0.017 \pm 0.005$ at $\lambda = 500$ nm. This number should be compared closely with other similar observations in the coming decades to assess whether pollution is increasing on global scales. The wavelength dependence of the baseline aerosol optical depth above MLO is of the form

$$\tau(\lambda) = \text{Const } \lambda^{-\alpha}$$

where $1.5 < \alpha < 2.0$.

(4) A spring month enhancement in the aerosol optical thickness above Mauna Loa may be attributable to Asian desert soil particles transported across the Pacific Ocean. The optical depth increase at Mauna Loa in 1980 due to this long-range transport of dust was $\Delta\tau(500\text{-nm wavelength}) = 0.020$, and the dust caused detectable effects in the middle Pacific turbidity from March to June 1980. The dust and sulfate aerosol stratospheric plume resulting from the explosive eruption of Mt. St. Helens was $\tau(500\text{-nm wavelength}) < 0.005$ over Mauna Loa from the time of the eruption (May 1980) to February 1981.

5.11 Increases in Atmospheric Concentrations of Halocarbons and N₂O

M. A. K. Khalil and R. A. Rasmussen
Oregon Graduate Center
Beaverton, OR 97006

Increasing human population and industrialization are altering the composition of the Earth's atmosphere and setting into motion processes that will change the global environment and ecology in the future. Foremost among the processes that are expected to endanger human health or the global environment are the depletion of the stratospheric ozone layer and the warming of the Earth. To evaluate quantitatively both the threats and the protective feedbacks in the global environment, it is necessary to obtain direct observational information on the composition of the atmosphere, its natural variability, the sources and sinks of its constituents, and the changes that can be directly attributed to human activities. Our research program is directed toward this end and is based on the experimental and theoretical analyses of four distinct, though not mutually exclusive, groups of atmospheric trace gases.

The first group of trace gases consists of purely anthropogenic compounds, principally chlorine-containing halocarbons, which threaten the ozone layer. This group includes CCl₃F (F-11), CCl₂F₂ (F-12), CHClF₂ (F-22), CCl₄, and CH₃CCl₃. The second group consists of primarily natural compounds that are being increased by human activities. This group includes CH₄, N₂O, and CO₂. Increases of these gases in the atmosphere can lead to global warming by enhancing the natural greenhouse effect, but may also protect the stratospheric ozone layer from depletion by anthropogenic fluorocarbons (Rasmussen and Khalil, 1981b; Groves and Tuck, 1979). The third group consists of compounds that are believed to be responsible for maintaining the observed natural physical features of the current atmospheric environment. These studies determine the critical strengths, weaknesses, and feedbacks created by natural atmospheric chemistry and the vulnerability of the environment to changes brought about by human activities. CO, OCS, CS₂, CH₃I, CH₃Cl, CHCl₃, and selected hydrocarbons belong to this group. Finally, the fourth group consists of gases that, because of their low concentrations, do not pose a direct threat to the environment but are tracers of anthropogenic air pollution on scales ranging from pollution from small cities to long-distance transport responsible for Arctic haze to global-scale atmospheric dispersion. In this group are of a large number of exotic trace gases, including C₂HCl₃, C₂Cl₄, C₂F₃Cl₃ (F-113), C₂F₄Cl₂ (F-114), CHCl₂F, CF₄, C₂F₆, CF₃Cl, CF₃Br, C₂F₅Cl, CH₃Br, and SF₆.

Our global flask sampling network consists of six sites: Pt. Barrow, Alaska (70°N); Cape Meares, Oregon (45°N); Cape Kumukahi, Hawaii (22°N); Samoa

Table 32.--Average concentrations of CH₄, CO, CH₃Cl, CH₃I, C₂Cl₄, and CHCl₃ in Alaska and Samoa

	Alaska (70°N)				Samoa (14°S)				Gradient (G ± δG)
	\bar{C}	est σ	n	Δ	\bar{C}	est σ	n	Δ	
CH ₄ (ppbv)	1647	16	122	1608-1695	1528	22	66	1496-1583	7.7 ± 0.4
CO (ppbv)	137	43	122	59-243	49	14	66	30-95	180 ± 21
CH ₃ Cl (pptv)	585	45	80	460-660	635	33	40	588-713	-9 ± 2
CH ₃ I (pptv)	1.3	0.6	27	0.3-4.0	2.6	1.7	18	1.0-5.0	-100 ± 15
C ₂ Cl ₄ (pptv)	86	26	33	60-144	--	--	--	--	--
CHCl ₃ (pptv)	41	8	8	35-55	--	--	--	--	--

Note: \bar{C} = average concentration; est σ is the standard deviation; n = number of independent samples or the number of weeks of data; Δ = range of observed concentrations on individual days (range of monthly average concentrations is generally much smaller than Δ); G = 100% {[\bar{C} (Alaska)/ \bar{C} (Samoa)] - 1}; ±δG values are estimated 90% confidence limits.

(14°S); Cape Grim, Tasmania (42°S); and the South Pole (90°S). At three of these sites, namely, Barrow, Samoa, and the South Pole, the air samples are obtained every week in triplicate by NOAA/GMCC personnel as a part of their cooperative program. Samples are collected with equipment supplied by the Oregon Graduate Center and are then sent to us by air. Soon after they arrive at the OGC trace gas laboratory, they are analyzed for the various trace gases. To determine concentrations, EC/GC, FID/GC, temperature-programed GC, and GC/MS techniques are employed. Most of the flask sampling and analytical techniques as well as experimental studies of the stability of trace gases in the container are described in detail in the paper of Rasmussen and Khalil (1980).

Here we summarize results that are based in part on the data obtained from the samples collected under the NOAA/GMCC cooperative program, between August 1979 and September 1981. (This was an ongoing project, and for the sake of continuity it was decided to include 1981 data in this report.) These studies include atmospheric abundances of CH₄, CO, CH₃Cl, CH₃I, C₂Cl₄, and CHCl₃; long-term increases in the concentrations of CCl₃F, CCl₂F₂, CHClF₂, CCl₄, and CH₃CCl₃; the rate of increase of N₂O in the atmosphere; and the use of fluorocarbons, CH₃CCl₃, CO, and C₂Cl₄ as possible tracers of pollution leading to Arctic haze.

5.11.1 Concentrations of Trace Gases at Barrow and Samoa

Concentrations of trace gases observed over the past 2 years are summarized in figs. 74 and 75 and table 32, with additional discussion as follows.

CO-CH₄

The concentrations of both CO and CH₄ show seasonal patterns over time scales of a year and less, but the natural variability of the concentrations is too large for long-term increases or decreases to be evident in such a short sequence of measurements. In other studies, using continuous measurements, we have established that CH₄ is increasing in the atmosphere at

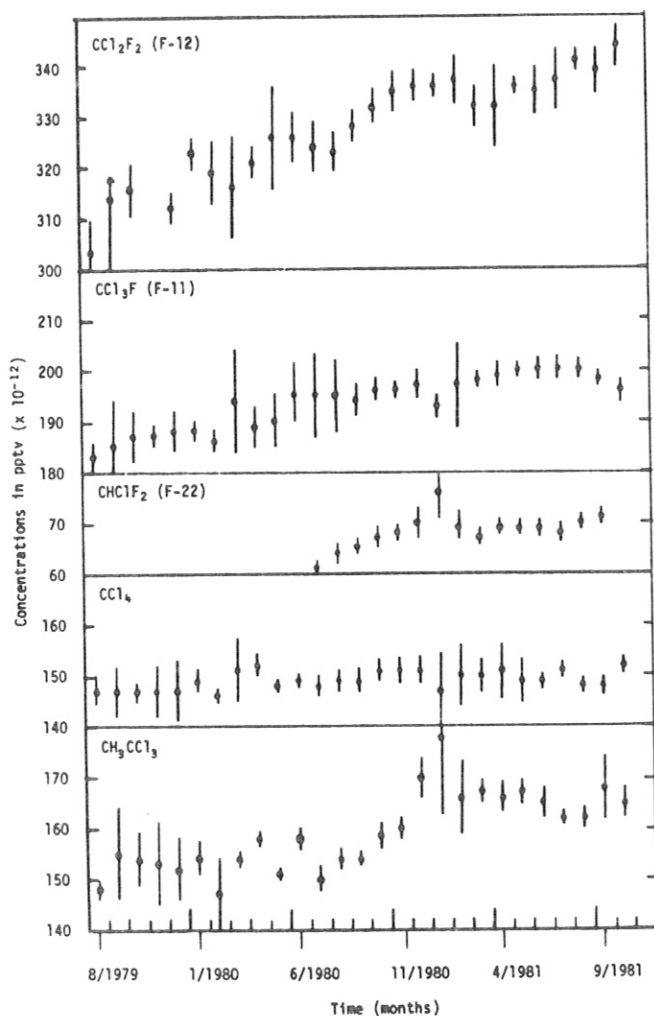


Figure 74.--Monthly average concentrations (pptv) of halocarbons at Pt. Barrow and Poker Flats in Alaska ($\sim 70^{\circ}\text{N}$). Error bars represent 90% confidence limits of the average concentrations based on the t-statistic.

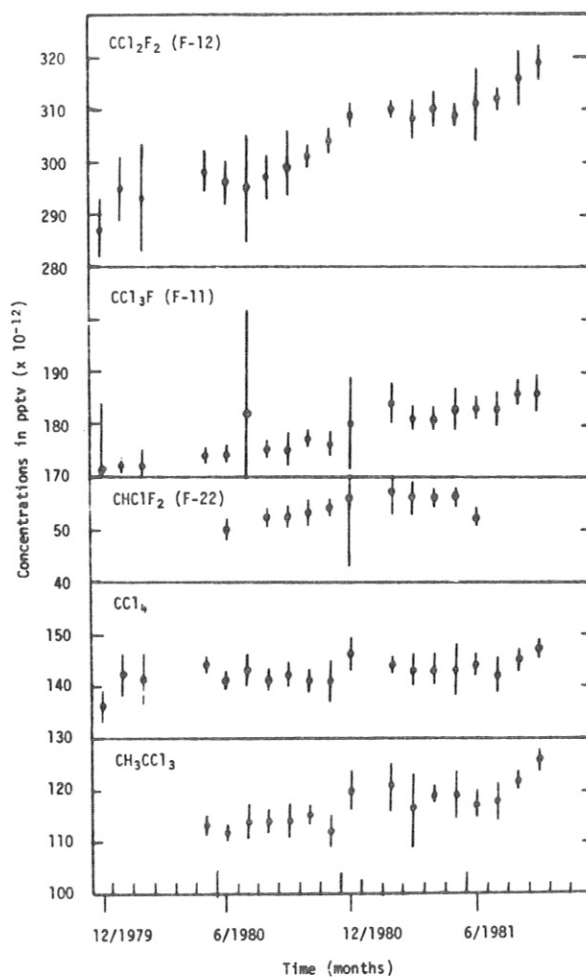


Figure 75.--Monthly average concentrations (pptv) of halocarbons at American Samoa (14°S). Error bars represent 90% confidence limits of the average concentrations based on the t-statistic.

$1.9\% \pm 0.4\% \text{ yr}^{-1}$, most likely because of human activities (Rasmussen and Khalil, 1981b).

CH₃I

Concentrations of CH₃I were generally much lower than indicated by the few data from the past. Concentrations of 1 to 3 pptv were found in the boundary layer, dropping to half this value above the boundary layer. CH₃I was more abundant in tropical regions (see table 32) than at high latitudes. Near oceanic regions characterized by high biomass productivity, concentrations of 10 to 20 pptv were observed, which along with our measurements of CH₃I in seawater led us to suggest that these high-productivity regions of the ocean may provide most of the yearly global flux of CH₃I to the atmosphere (Rasmussen et al., 1981b).

Table 33.--Increase in concentrations of anthropogenic trace gases

Trace gas	Poker Flats and Barrow Alaska (~70°N)			Samoa (~14°S)		
	$b \pm \delta b$ (% yr ⁻¹)	a_0 (pptv)	n (mo)	$b \pm \delta b$ (% yr ⁻¹)	a_0 (pptv)	n (mo)
CCl ₃ F (F-11)	4.2 ± 0.6	185	26	4.9 ± 0.9	168	19
CCl ₂ F ₂ (F-12)	4.3 ± 0.7	313	25	5.3 ± 0.6	284	19
CHClF ₂ (F-22)	8 ± 5	65	15	9 ± 6	48	11
CCl ₄	0.9 ± 0.6	148	26	2 ± 1	139	19
CH ₃ CCl ₃	6.1 ± 1.8	149	26	6.9 ± 2.3	106	16

Note: b = average rate of increase; $\pm\delta b$ are the 90% confidence limits of the increase based on the t-statistic; a_0 = average concentration during 8/1979; n = number of months during which data were obtained (see also figs. 74 and 75). Data represent analyses of approximately 450 samples.

CH₃Cl

Observations of CH₃Cl at Barrow and Samoa, combined with results from the rest of our global sampling network, show that there is about 6% ($\pm 3\%$) more CH₃Cl in the tropical atmosphere than at high latitudes--a pattern also observed for CH₃I--suggesting the possibility of related production mechanisms (Zafirou, 1975).

On the average the concentrations of CH₃Cl were the same in the two hemispheres, from which we concluded that the average concentration of OH radicals must also be the same in the two hemispheres $[\text{OH}]_{\text{S.H.}} \leq 1.3[\text{OH}]_{\text{N.H.}}$ (Khalil and Rasmussen, 1981a).

5.11.2 Increase in Concentrations of Halocarbons

Increases in atmospheric concentrations of CCl₃F (F-11), CCl₂F₂ (F-12), CHClF₂ (F-22), CCl₄, and CH₃CCl₃ are summarized in table 33. Similar analyses based on 6 years of observations at the South Pole are reported in the paper of Rasmussen et al. (1981a). The rates of increase of CCl₃F, CCl₂F₂, CCl₄, and CH₃CCl₃ at Barrow and Samoa all appear to be much slower over the last 2 years compared with older data from comparable locations in the two hemispheres. This slowing down of the accumulation rates has been established by Khalil and Rasmussen (1981b) from the 6 years of observations at the South Pole and is explained by the abrupt halting of the increase in the global emissions of CCl₃F, CCl₂F₂, and CCl₄, and a marked slowdown in the increasing rate of global emissions of CH₃CCl₃ (see also Rasmussen and Khalil, 1981a).

5.11.3 Increase in Atmospheric Concentration of N₂O

Observations of increasing nitrous oxide (N₂O) were reported by Rasmussen et al. (1981b) and more recently by Weiss (1981). Our continuous measurements made at Cape Mearns (45°N) and Tasmania (42°S) show that N₂O is increasing at between 0.2% and 0.3% yr⁻¹ (Khalil and Rasmussen, 1981d). Unlike CH₄, N₂O has a very long atmospheric lifetime; thus its atmospheric concentration is not subject to large variations. Indeed, this is why the increase of N₂O is also evident in the flask samples from Barrow and Poker Flats in Alaska, from Samoa, and from the additional South Pole data. As shown in table 34, the rate of increase is found to be 0.3% ± 0.2% yr⁻¹ and is significantly greater than zero ($\alpha = 0.05$, t-test). These increases in N₂O are explained by combustion sources, as shown by the models of Weiss (1981) and Khalil and Rasmussen (1981d).

5.11.4 Gaseous Tracers of Arctic Haze

Over the past 4 years it has been established that the occurrence of Arctic haze during winter and early spring results from long-range transport of anthropogenic pollutants. As industrialization and population grow, Arctic haze is likely to become more pronounced.

Table 34.--Increase of N₂O in the atmosphere

	C ₀ (ppbv)	b ± δb (% yr ⁻¹)	r	n (mo)	Sampling period
Alaska (~70°N)	307.7	0.3 ± 0.2	0.48	24	9/1977-9/1981
Samoa (~14°S)	306.2	0.3 ± 0.27	0.48	16	5/1980-9/1981
South Pole (90°S)	306.0	0.4 ± 0.16	0.97	5	1/1977-1/1981

Note: C₀ = average calculated concentration during January 1979; b = rate of increase; ±δb are the 90% confidence limits of the increase based on the t-statistic; r = correlation coefficient; n = number of months during which data are available; sampling period = length of time over which data are available.

Our work, based on air samples collected over two winters through the NOAA/GMCC cooperative program at Barrow, Alaska, has now established, by statistical analyses and by filtering out trends, that the anthropogenic gases, CHClF₂ (F-22), perchloroethylene (CCl₂=CCl₂), CCl₂F₂ (F-12), CH₃CCl₃, and CO, are more abundant in the Arctic during winter than at any other time of the year ($\alpha = 0.01$). Gases that did not show any significant difference of concentration during winter include CCl₃F (F-11) and C₂Cl₃F₃ (F-113). For identifying the locations of sources of Arctic haze, the absence of excessive

F-11 and F-113 is perhaps as useful an indicator as the presence of excessive amounts of other anthropogenic gases. Most of these gases are practically inert over the time periods required for transport to the Arctic. This is especially true during winter when there is not much OH present at high latitudes to remove F-22, CH₃CCl₃, CO, or C₂Cl₄. Sample results for C₂Cl₄ are shown in table 35. Although data are few, the result is dramatic and not hidden by long-term trends as for CH₃CCl₃, F-12, and F-22. Currently we are also considering other rarer and more exotic gaseous tracers of Arctic haze, some of which are listed in the fourth group at the beginning of this report. These results, discussed in more detail by Khalil and Rasmussen (1981c), are still preliminary but hold promise for future research on Arctic haze.

Table 35.--Concentrations of C₂Cl₄ over the Arctic during the four seasons (1980-81)

	\bar{C} (pptv)	est σ	N (weeks)
Winter	154	13	2
Spring	96	17	16
Summer	70	10	12
Fall	57	4	2

Note: \bar{C} = average concentration; est σ is the standard deviation; N = number of weeks of data.

5.12 Precipitation Chemistry at Samoa and Mauna Loa

Donald C. Bogen, Stuart J. Nagourney, and Camille C. Torquato
 Environmental Measurements Laboratory
 U.S. Department of Energy, New York, NY 10014

Monthly samples of wet, dry, and total deposition are collected at SMO and MLO. The samples are sent to the Environmental Measurements Laboratory (EML) for physical and chemical measurements. Sample-handling techniques and analytical methods are described in the EML Procedures Manual (U.S. DOE, 1981).

The average monthly deposition values and range of results at SMO and MLO for April 1979 through December 1980 are presented in tables 36 and 37. Results from measurements for past years can be found in earlier GMCC reports.

Table 36.--Physical and chemical analyses of total, wet, and dry deposition at SMO, April 1979 through December 1980

	Bulk collector		Wet collector		Dry collector	
	Mean	Range	Mean	Range	Mean	Range
Volume (ℓ)	6.56	1.74-12.9	8.30	4.90-13.0	--	--
pH	6.13	5.48-6.61	5.77	5.45-6.14	--	--
Conductivity ($\mu\text{S cm}^{-1}$)	86.8	25.4-223	31.7	15.1-72.6	--	--
Cl ⁻ (mg mo ⁻¹)	108	62-171	60	26-135	48	10-76
SO ₄ ⁻² (mg mo ⁻¹)	19	13-29	10	4.1-21	9	1.5-12
NO ₃ ⁻ (mg mo ⁻¹)	ND*	--	ND*	--	ND*	--
Na ⁺ (mg mo ⁻¹)	64	43-98	34	18-76	30	13-49
Mg ⁺² (mg mo ⁻¹)	8.2	5.1-16	4.5	2.0-12	3.7	1.7-5.9
Ca ⁺² (mg mo ⁻¹)	3.3	2.2-6.5	1.7	0.8-2.7	1.5	0.9-2.6
K ⁺ (mg mo ⁻¹)	3.2	1.8-6.0	1.6	0.7-4.5	1.5	0.8-2.3

*ND = not detectable

Table 37.--Physical and chemical analyses of total, wet, and dry deposition at SMO, April 1979 through December 1980

	Bulk collector		Wet collector		Dry collector	
	Mean	Range	Mean	Range	Mean	Range
Volume (ℓ)	1.62	0-13.5	3.23	0.12-12.6	--	--
pH	5.03	4.41-6.36	5.71	4.92-6.48	--	--
Conductivity ($\mu\text{S cm}^{-1}$)	11.2	1.7-23.9	5.52	1.6-16.9	--	--
Cl ⁻ (mg mo ⁻¹)	0.15	0.01-0.49	0.34	0.02-1.64	0.06	0.01-0.08
SO ₄ ⁻² (mg mo ⁻¹)	1.29	0.11-3.58	0.94	0.07-4.12	0.37	0.10-1.67
NO ₃ ⁻ (mg mo ⁻¹)	0.20	ND*-0.65	0.48	0.07-1.29	0.07	ND*-0.24
Na ⁺ (mg mo ⁻¹)	0.19	0.07-0.69	0.19	0.04-0.60	0.08	0.02-0.15
Mg ⁺² (mg mo ⁻¹)	0.04	0.01-0.09	0.03	ND*-0.09	0.01	ND*-0.02
Ca ⁺² (mg mo ⁻¹)	0.08	0.05-0.13	0.06	0.02-0.09	0.06	0.02-0.12
K ⁺ (mg mo ⁻¹)	0.05	0.01-0.14	0.02	ND*-0.06	0.02	0.01-0.04

*ND = not detectable

5.13 Atmospheric Particulate Chemistry at the South Pole and Mauna Loa

W. H. Zoller, J. R. Parrington, and N. K. Aras
Department of Chemistry, University of Maryland
College Park, MD 20742

5.13.1 Instrumentation at SPO and MLO

Atmospheric monitoring of aerosols continued at the South Pole through 1980. This study is part of a long-term monitoring project that the University of Maryland has been conducting since 1975. A sector controller was installed in November 1980, similar to the unit that was installed at Mauna Loa in April 1980 and is discussed later. The design of the SPO controller is simplified in that only three parameters, rather than the five at MLO, are necessary, and a second sector is not included. The parameters are the following.

Wind direction ($\pm 1^\circ$)	$330^\circ \rightarrow 0^\circ \rightarrow 120^\circ$
Windspeed ($\pm 1 \text{ mi h}^{-1}$)	$2 \rightarrow 30 \text{ mi h}^{-1}$
Condensation nuclei ($\pm 0.01 \log \text{ CN cm}^{-3}$)	$< 300 \text{ nuclei cm}^{-3}$

The primary function of the controller is to prevent contamination of samples by switching pumps on only when winds are blowing from the clean-air sector. Winds normally come from this clean-air sector about 90% of the time, but, if they shift, sampling must be stopped to prevent contamination from the main station. The condensation nucleus parameter functions as a safeguard should contamination from vehicles or aircraft occur downwind of the samplers. Four types of filters collect aerosols at SPO. Three high-volume filters, a 110-mm Fluoropore, a 25-cm Whatman, and an 8- by 12-in Gelman glass fiber filter collect samples every 10 days that are used for the chemical analyses.

The wind-directional control system for MLO that we designed, constructed, and installed became fully operational on April 29, 1980, and replaced the previous time-of-day system used in 1979 and early 1980. The system is constructed in two parts: one that makes the logic decision to turn on the samplers, and another (near the sampling equipment) that contains the relays and clocks needed to run the pumps.

The decision to sample can be based on each or any subset of the following parameters.

	<u>Downslope</u>	<u>Upslope</u>
Time of day ($\pm 10 \text{ min}$)	1900 \rightarrow 0600	0700 \rightarrow 1800
Wind direction ($\pm 1^\circ$)	$100^\circ \rightarrow 250^\circ$	$290^\circ \rightarrow 0^\circ \rightarrow 80^\circ$
Windspeed ($\pm 1 \text{ mi h}^{-1}$)	$2 \rightarrow 20 \text{ mi h}^{-1}$	$4 \rightarrow 30 \text{ mi h}^{-1}$
Condensation nuclei ($\pm 0.01 \log \text{ CN cm}^{-3}$)	$< 600 \text{ nuclei cm}^{-3}$	$< 1000 \text{ nuclei cm}^{-3}$
Light scattering (<u>b</u> scat)	(not used in 1980)	

If all the desired parameters are within settable limits, an "on" signal is generated. Any or all of the parameters can be used in making the decision to initiate sampling. Because of the predicted usage, parameter controls are duplicated for two independent sampling sectors. Labels of "Sector I" and

"Sector II" are used. Sector I is set up to sample downslope winds, and Sector II is for upslope conditions, as listed above. A third case exists when neither Sector I nor II is sampling. In this case an "interim pump circuit" is activated to allow collection of samples that could contain information on aerosols collected under wind conditions carrying source contaminants to the station. Pumps are prevented from toggling under marginal fluctuating conditions by an integration circuit in the sector controller that requires all parameters to be in an "on" state for 100 seconds before the pump controller is switched on. A similar off-integration time is also required. Conditions might arise, such as combustion engine exhaust, when a rapid shutoff is provided by an instant-off circuit that bypasses the off integrator. This circuit is coupled with NOAA's G.E. condensation nucleus counter that senses such contamination in a few seconds. The wind direction and speed are sensed by a low-threshold vane and anemometer mounted on a tower near the site.

The pump controller and sampling pumps are located under the radiation tower. The pump controller contains circuitry to switch up to 12 high-current sampling loads. Five timers on the controller front panel record elapsed sampling times for each circuit. Four pumps are currently used to collect samples. For downslope conditions, two high-volume pumps are activated: one on a 110-mm diameter, 0.4- μ m Nuclepore filter; the other on quartz-fiber filters, which are currently being analyzed for carbon by J. Moyers at the University of Arizona. The upslope pump is also a high-volume Nuclepore filter sampler. The interim setup is a lower volume pump pulling through an identical Nuclepore filter for comparison. All filters are located about 10 m above the pumps on the top of the radiation tower in a Lucite shelter. These filters are changed weekly in a clean hood and are mailed back by the staff at MLO to the University of Maryland for instrumental neutron activation analysis. Although the system is set up to collect atmospheric particles for chemical analyses, other investigators requiring equipment controls could use their pumps with our controller.

5.13.2 Results of 1980 Measurements at MLO

Samples of atmospheric particulate materials were collected continuously during 1980 at MLO. The samples show strong seasonal variations as observed in the past (Zoller et al., 1979). During this year, a strong influx of crustal material began in March and lasted through June. Figure 76 shows this trend as a plot of the mass of Al in the atmosphere vs. months of the year. The concentrations of various crustal elements (Al, Sc, Mn, Fe) reached peaks in late April to early May, the same period at which the peaks occurred in 1979. For 1980 downslope conditions, this increase is about 25 times the concentration observed during the time period of low atmospheric dust loading, i.e., from July through early January. Upslope crustal material shows a very similar trend, but during normally clean conditions a somewhat higher crustal concentration is seen, apparently from the entrainment of finely divided local basalt into the upslope winds. Concentrations of elements primarily of marine origin--Na, Cl, K, and Mg--do not have significant peaks during this same period as shown by the time variation of the marine sodium concentration given in fig. 77. The lack of an increase in marine aerosol during the spring suggests there is no significant increase in atmospheric mixing across the boundary layer to account for the increase in crustal material found at MLO. Thus, the crustal material is probably not of local origin and comes from the Asian mainland, as shown by air mass trajectories for other years with the same

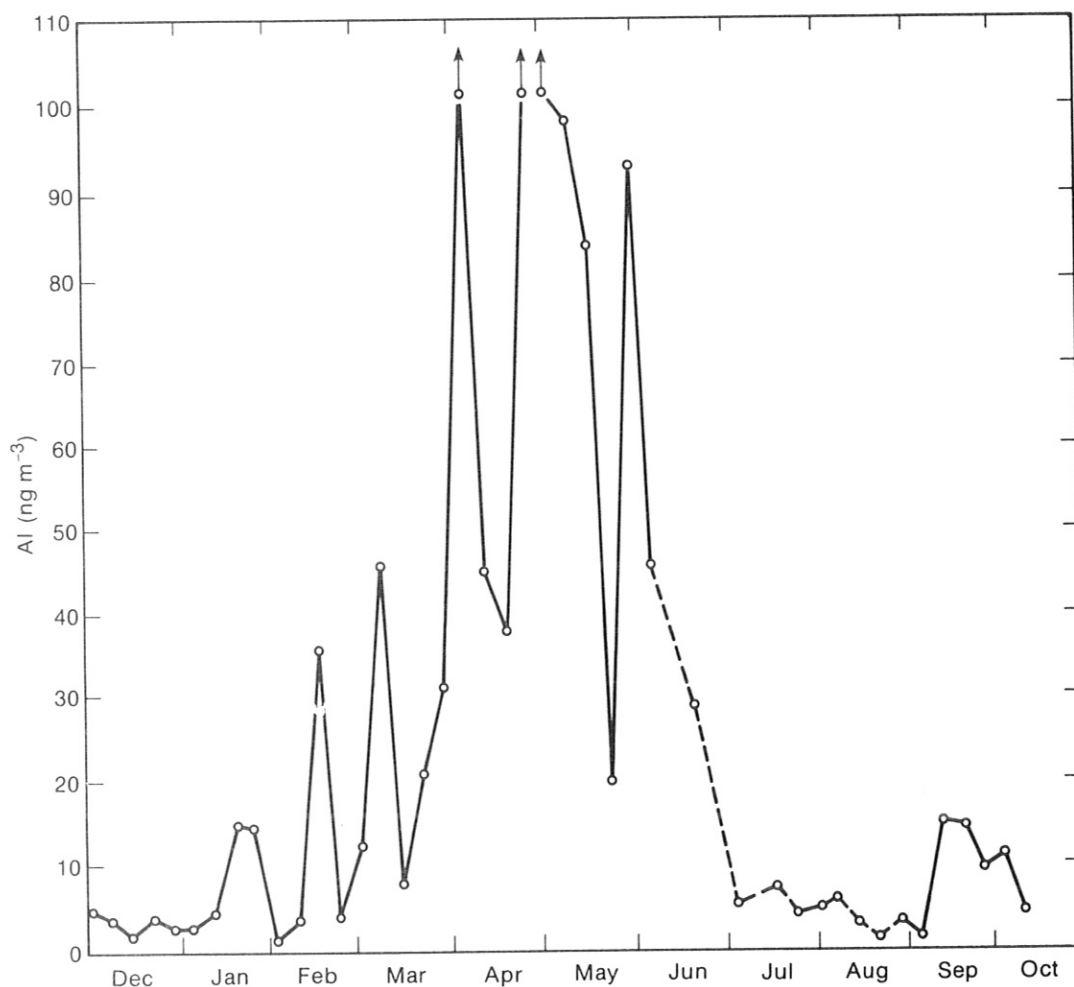


Figure 76.--Plot of the weekly Al concentration in downslope samples for MLO, 1980.

meteorological conditions and as suggested by several authors (Duce et al., 1980; Shaw, 1980).

A plot of the marine sodium concentration vs. time is shown in fig. 77. As can be seen from these results, the concentration of sea salt, shown by marine sodium, is much lower in the downslope samples than in upslope samples collected during the same months of the year. This difference is shown by a histogram of the occurrence of different concentrations of total sodium (fig. 78), where most of the downslope samples have Na concentrations less than 25 ng m^{-3} , whereas the upslope samples usually contain at least 60 ng m^{-3} of Na, and some even greater than 120 ng m^{-3} . A similar histogram for Al is given in fig. 79. There is very little difference between the patterns for upslope and downslope conditions except that there are fewer samples with concentrations less than 5 ng m^{-3} in the upslope group, and there are a few more samples with higher concentrations scattered throughout the entire region with concentrations greater than 50 ng m^{-3} .

Average concentrations of several elements are shown in table 38 for the high crustal dust period vs. the cleaner months of the year. Calculations of

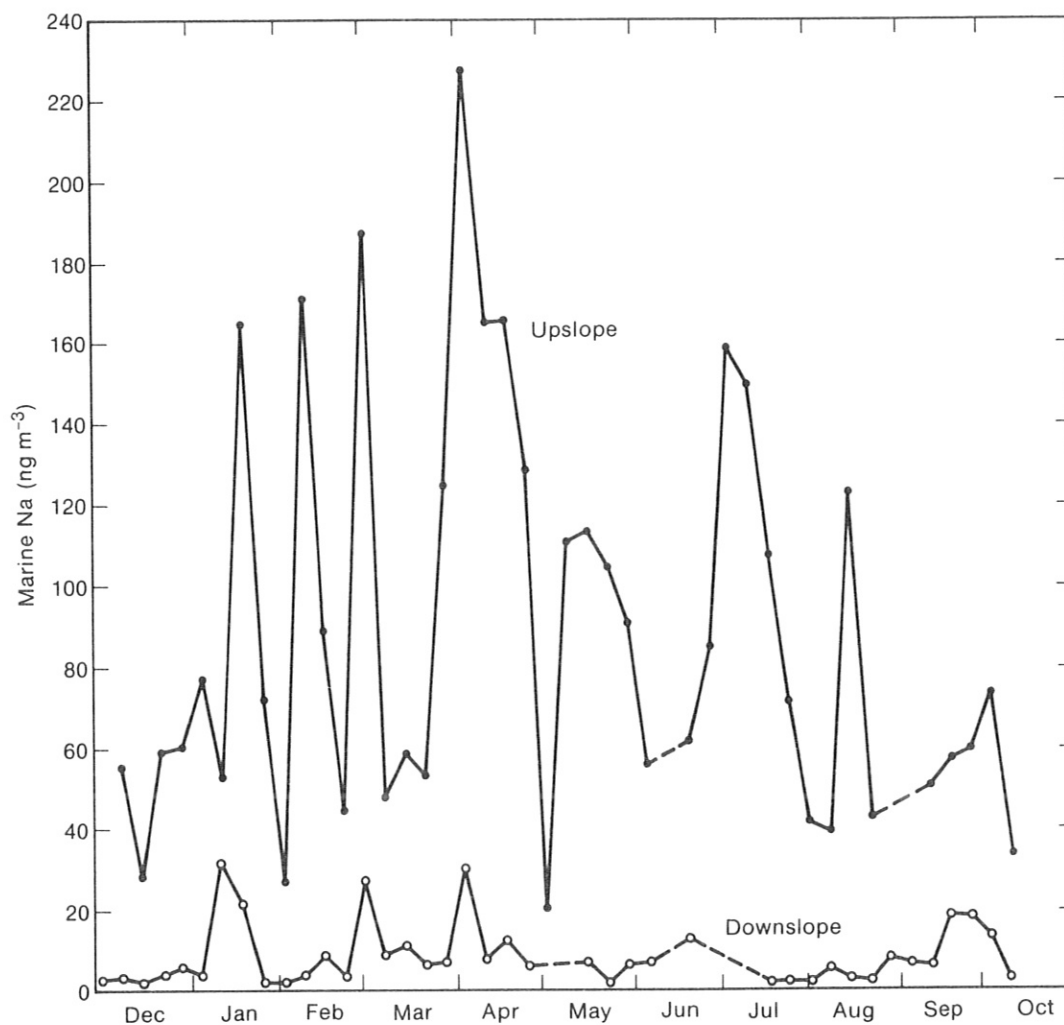


Figure 77.--Marine Na concentration for upslope and downslope conditions at MLO, 1980.

enrichment factors (EF) using Taylor crustal abundances (Taylor, 1964), Hawaiian basalt and Asian sand compositions, as well as rare earth ratios from these samples, show that there is a definite change in chemical composition of the crustal aerosol during the spring season, and it occurs in both the upslope and downslope wind conditions.

The chemical composition of the dust found in Hawaii is probably different from that observed closer to the Asian mainland; only the smaller sized particles will eventually be transported to the islands. As can be seen in table 38, the crustal elements are clearly in much higher concentrations during dust conditions. Crustal enrichment factors have been calculated for these average concentrations to compare the distribution patterns with those of Hawaiian basalt, which should be a primary component of island-generated aerosols (table 39). As can be seen in table 39, the elements usually associated with the marine aerosols (Na and Cl) have very high enrichments during upslope and downslope conditions, except in downslope conditions during high dust episodes.

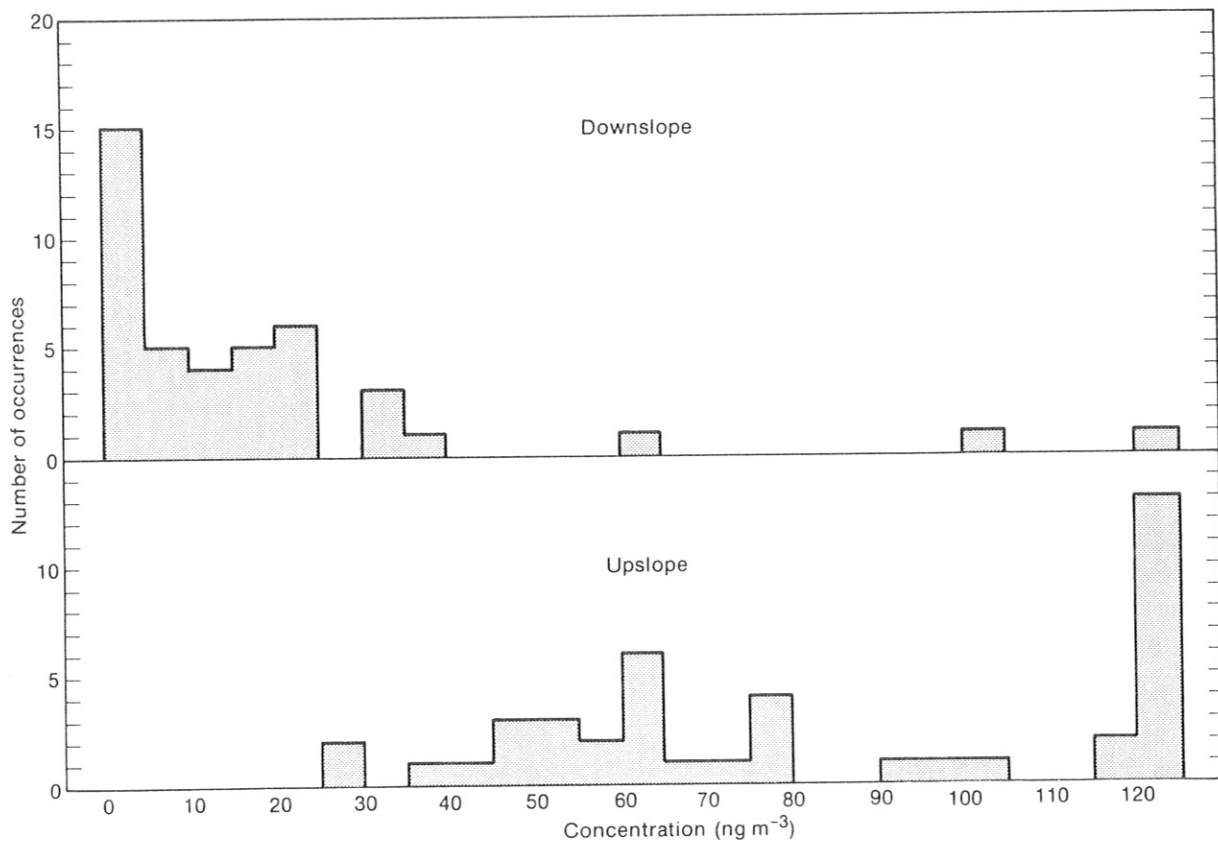


Figure 78.--Histogram of Na concentration in MLO samples, 1980.

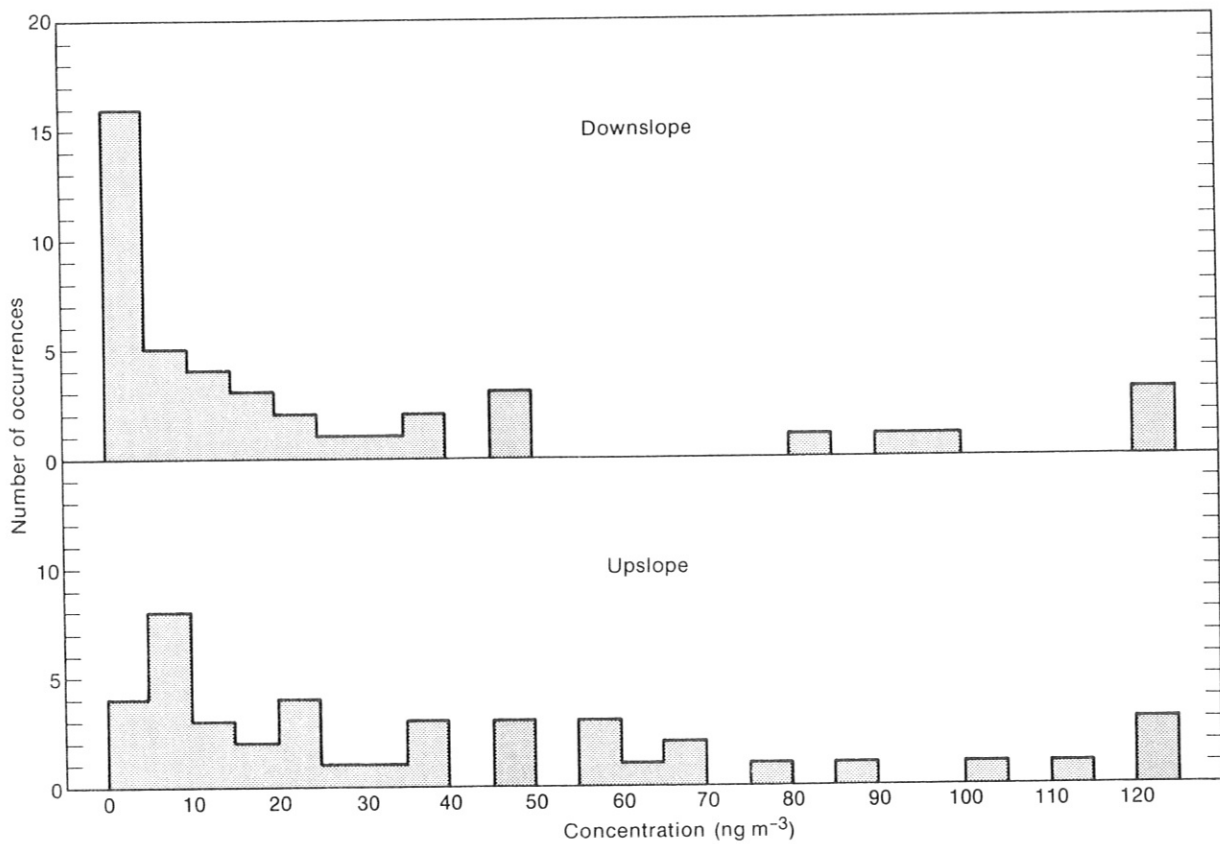


Figure 79.--Histogram of Al concentration in MLO samples, 1980.

Table 38.--Mean chemical concentrations of MLO aerosols for 1980

Element	Downslope		Upslope	
	Clean	Dust	Clean	Dust
Na (ng m ⁻³)	5.9 ± 2.8	28 ± 16	91 ± 46	168 ± 69
Mg (ng m ⁻³)	4.6 ± 4.6	39 ± 17	12 ± 7	103 ± 77
Al (ng m ⁻³)	5.5 ± 4.5	115 ± 68	24 ± 12	168 ± 160
Cl (ng m ⁻³)	2.2 ± 1.4	4.6 ± 3.1	13 ± 12	71 ± 55
Sc (pg m ⁻³)	2.6 ± 1.9	30 ± 19	9.5 ± 5.7	41 ± 46
Mn (pg m ⁻³)	76 ± 44	1300 ± 750	412 ± 240	2110 ± 1800
Fe (pg m ⁻³)	8.4 ± 6.4	90 ± 54	32 ± 17	150 ± 140

The average mass of the major components of the MLO aerosol during clean conditions can easily be calculated on the basis of the atmospheric concentrations of elements associated with each source. The results of these calculations are shown for the downslope samples in table 38, and the average concentrations of crustal dust are given for only the clean periods in table 40. The sea salt sodium values are shown in fig. 77, and table 40 gives the average concentrations during clean conditions.

In most remote areas sulfate dominates the aerosol mass, and at MLO this is also true since sulfate accounts for approximately 70% of the aerosol mass identified by our chemical analyses. Calculations show that the crustal input of sulfate is negligible, being less than 0.1% during all conditions. The

Table 39.--Crustal enrichment factors for MLO aerosols*

Element	Downslope		Upslope		Hawaiian basalt
	Clean	Dust	Clean	Dust	HBVO†
Na	3.7	0.85	13	3.5	0.77
Mg	3.0	1.20	1.77	2.2	2.1
Cl	250	25	340	270	0.78
Sc	1.77	0.98	1.48	0.91	1.58
Mn	1.20	0.98	1.49	1.09	1.60
Fe	2.2	1.14	1.95	1.31	1.64

*Taylor's crustal abundance was used for comparison (Taylor, 1964).

†HBVO is a USGS standard basalt.

Table 40.--Major components of MLO aerosols for 1980 under clean conditions

	Upslope	Downslope
Mass of crust	97 ng m ⁻³	45 ng m ⁻³
% of total due to crust	13%	24%
Mass of sea salt	170 ng m ⁻³	10.3 ng m ⁻³
% of total due to sea salt	23%	5%
Mass of SO ₄ ⁼	480 ng m ⁻³	135 ng m ⁻³
% of total due to SO ₄ ⁼	64%	71%
% of SO ₄ ⁼ from crust	<0.1%	<0.1%
% of SO ₄ ⁼ from sea salt	2.7%	0.34%
% of SO ₄ ⁼ from stratosphere	3.8%	13%

ocean accounts for about 3% during upslope conditions and only 0.3% during clean downslope conditions. The rest of the sulfate, we must assume, comes from the stratosphere or is formed by gas-to-particle conversion processes.

The stratospheric input can be estimated by assuming that all of the ⁷Be measured at MLO comes from the stratosphere, and some sulfate aerosol comes down as the transport aerosol. By using data from the ratio of SO₄⁼ to ⁷Be measured in the lower stratosphere (0.092 ng SO₄⁼/fCi ⁷Be), we estimate that only 3.8% and 13% (as upper limits) of the sulfate during upslope and downslope conditions, respectively, could be associated with a stratospheric source. Also, the concentration of ⁷Be is the same during upslope and downslope conditions, showing that it is relatively well mixed in the lower troposphere, whereas the sulfate is much higher during upslope conditions.

Since the sulfate is much higher during upslope conditions, and not directly associated with sea salt, it appears that a large portion of the sulfate is formed by gas-to-particle conversion in the lower layers of the troposphere. Therefore, the sulfur gaseous precursor is probably of biogenic origin from the ocean, having been released as H₂S, (CH₃)₂S, SO₂, or in some other form.

6. INTERNATIONAL ACTIVITIES

In June 1980, J. Peterson attended a WMO-sponsored ad hoc meeting at Raleigh, North Carolina, on publications of BAPMoN (Background Air Pollution Monitoring program) data. The discussions included chemistry of precipitation, atmospheric turbidity, and carbon dioxide data with emphasis on the latter subject. The WMO Secretariat is encouraging timely publication of BAPMoN data, and many suggestions were made on the mechanics of such publications that could meet WMO needs and provide a scientifically useful product.

J. DeLuisi and W. Komhyr participated in a WMO-sponsored workshop in June of 1980 concerned with the reliability of various ozone measurement systems. DeLuisi gave a presentation on the accuracy and precision of the Umkehr method and the nature of errors arising from tropospheric-stratospheric haze effects, and the temperature dependence of ozone absorption. Komhyr gave presentations on the accuracy of the Dobson instrument for measuring total ozone, and the accuracy and precision of the wet chemical ozonesonde instrument for measuring the vertical distribution of ozone. A report of the findings of the workshop will be published by WMO.

B. Bodhaine attended the "First International Workshop on Light Absorption by Aerosol Particles," 28 July-8 August 1980, at Colorado State University, Fort Collins, Colorado. This workshop, organized under the auspices of the Radiation Commission of the International Association for Meteorology and Atmospheric Physics (IAMAP) and cosponsored by the Optical Society of America and the American Meteorological Society, was designed to provide investigators the opportunity to intercompare, under controlled conditions, their techniques for measuring the light absorption properties of aerosols. The GMCC four-wavelength nephelometer was installed at the workshop to monitor continuously the aerosol present in the sampling manifold. This instrument was accepted as the standard for comparison during the workshop.

D. Gillette gave four lectures on desert dust at the "Autumn Course on Physics of Flow in the Oceans, Atmosphere and Desert," 30 September-28 November 1980, at the International Center for Theoretical Physics, Trieste, Italy. The lectures were on (1) meteorological conditions for dust production, (2) the relation of visibility to dust concentration, (3) production of dust, and (4) threshold velocities for dust production.

B. Mendonca participated in the "Fourth WMO Course on Background Air Pollution Monitoring" at Budapest, Hungary. The course was held at the Institute for Atmospheric Physics from October 27 to November 15, 1980, and was conducted by E. Mészáros and his staff under the auspices of WMO. It was designed to introduce and train representatives from interested countries for participation in the WMO's BAPMoN program. The purpose of Mendonca's attendance at the course was to become familiar with the program and with the instrumentation and methods being used by the program to monitor background air pollution and its effect on climate. Participating in the class were representatives from China, Egypt, Jordan, Libya, Switzerland, Syria, Yugoslavia, and Zambia.

In October 1980, a meeting of the U.S.-U.S.S.R. Committee on Environment was held at Miami, Florida. Attending this meeting from GMCC were K. Hanson, project leader on Effects of Pollution of the Atmosphere on Climate, Working Group VIII, and J. DeLuisi, coordinator for the U.S. part of the U.S.-U.S.S.R.

monograph on the assessment of aerosol research and climatic effects. Hanson conducted a session concerned with reporting the progress of U.S.-U.S.S.R. efforts already under way and recommendations for future directions. DeLuisi gave a presentation on the scientific effort that was made in the United States to study atmospheric effects of the May 29 eruption of Mt. St. Helens, including some findings, and a status report on the plans for the U.S. part of the aerosol and climate research assessment monograph.

GMCC was designated in 1980 by WMO as the World Dobson Spectrophotometer Calibration Center. Activities of the Center during 1980 were the following. A program that began in 1977 under the auspices of the WMO Global Ozone Research and Monitoring Project to upgrade Dobson spectrophotometers in use throughout the world was continued. At the request of WMO, Komhyr prepared Operations Handbook--Ozone Observations with a Dobson Spectrophotometer (Komhyr, 1980) to standardize Dobson instrument operating and calibrating procedures throughout the world. World Primary Standard Dobson Instrument no. 83 was recalibrated at Mauna Loa Observatory, Hawaii. Additionally, R. Grass traveled to South America to modernize and calibrate nos. 97 and 99 in Buenos Aires, Argentina, and no. 113 in Cachoiern Paulista, Brazil.

While in Argentina, Grass made a brief trip to Port Stanley in the Falkland Islands to brief United Kingdom weather station personnel on the scope of the GMCC CO₂ project and to instruct personnel in how to collect CO₂ samples.

The GMCC CO₂ flask sampling program was expanded in 1980 to include three new stations, viz., Stanley, Falkland Islands; Mould Bay, N.W.T.; and Seychelles, Mahé Island, Indian Ocean. This brought the number of operating stations to 19. Negotiations were begun to include three final stations in the sampling network: Ocean Station "M", North Pacific; San Cristobal, Galapagos; and Easter Island, South Pacific.

7. 1980 PUBLICATIONS AND PRESENTATIONS BY GMCC STAFF

- Bodhaine, B. A., and M. E. Murphy. Calibration of an automatic condensation nuclei counter at the South Pole. J. Aerosol Sci. 11(3):305-312.
- Bodhaine, B. A., J. M. Harris, and G. A. Herbert. Aerosol light scattering and condensation nuclei measurements at Barrow, Alaska. Presented at Second Symposium on Arctic Air Chemistry, Kingston, R.I., May 6-8, 1980.
- Bodhaine, B. A., J. M. Harris, G. A. Herbert, and W. D. Komhyr. Identification of volcanic episodes in aerosol data at Mauna Loa Observatory. J. Geophys. Res. 85(C3):1600-1604.
- Bortniak, J. C., and B. G. Mendonca. Geophysical Monitoring for Climatic Change at the South Pole, 1979. Antarct. J. U. S. 15(5):186-188.
- Coulson, K. L. Characteristics of skylight at the zenith during twilight as indicators of atmospheric turbidity: Part 1, Degree of polarization. Appl. Opt. 19:3469-3480.
- Coulson, K. L. Intensity and color ratios of the zenith sky during twilight. Proceedings of the International Radiation Symposium, Fort Collins, Colo., August 11-16, 1980, Colorado State University, Fort Collins, 477-479.
- Coulson, K. L., and Y. Howell. Solar radiation instruments. Sunworld 4:87-94.
- DeLuise, J. J. Disparities in the determination of atmospheric ozone from solar ultraviolet transmission measurements 298.1-319.5 nm. Geophys. Res. Lett. 7:1102-1104.
- DeLuise, J. J., B. G. Mendonca, and K. J. Hanson. Measurements of stratospheric aerosol over Mauna Loa, Hawaii, and Boulder, Colorado. Presented at Mount St. Helens' Eruption: Its Atmospheric Effects and Potential Climatic Impact Symposium, Washington, D.C., November 18-19, sponsored by NASA, Office of Space and Terrestrial Applications.
- Demerjian, K. L., K. L. Schere, and J. T. Peterson. Theoretical estimates of actinic (spherically integrated) flux and photolytic rate constants of atmospheric species in the lower troposphere. Adv. Environ. Sci. Tech. 10:369-459.
- Fegley, R. W., H. T. Ellis, and J. L. Heffter. Volcanic contributions to the stratospheric sulfate layer. J. Appl. Meteorol. 19(6):683-690.
- Gillette, D. Major contributions of natural primary continental aerosols: source mechanisms. Ann. N.Y. Acad. Sci. 338:348-358.
- Gillette, D. A., J. Adams, A. Endo, D. Smith, and R. Kihl. Threshold velocities for input of soil particles into the air by desert soils. J. Geophys. Res. 85(C10):5621-5630.

- Gushcin, G. P., J. T. Peterson, V. A. Kovaley, and T. A. Pavlyuchenkova. Cooperative measurements of atmospheric spectral transparency with Soviet and American instruments. Trans. Main Geophys. Obs., Leningrad, U.S.S.R. 445. (In Russian.)
- Hanson, K. J. Carbon dioxide. Weatherwise 33(6):253-258.
- Hanson, K. J. Determining spatial and secular variations of solar radiation for energy applications. Proceedings of the 1980 Annual Meeting, American Section of the International Solar Energy Society, Inc., Newark, Del., June 1980, ISES, Inc., University of Delaware, Newark, 1376-1380.
- Hanson, K. J., and J. J. DeLuisi. Forecasting solar energy on synoptic and longer time scales with mean values and persistence methods. In Satellite and Forecasting of Solar Radiation, Proceedings of the First Workshop on Terrestrial Solar Resource Forecasting and on Use of Satellites for Terrestrial Solar Resource Assessment, Newark, Del., June 1980, International Solar Energy Society, Inc., University of Delaware, Newark, 17-21.
- Harris, J. M., and G. A. Herbert. Carbon dioxide, condensation nuclei, and wind climatology of the Barrow GMCC Observatory. NOAA Data Rep. ERL ARL-2, NOAA Environmental Research Laboratories, Boulder, Colo., 112 pp.
- Herbert, G. A. Geophysical Monitoring for Climatic Change--No. 8: Summary Report 1979. NOAA Environmental Research Laboratories, Boulder, Colo., 120 pp.
- Komhyr, W. D. Dobson spectrophotometer systematic total ozone measurement error. Geophys. Res. Lett. 7(2):161-163.
- Komhyr, W. D. Operations Handbook--Ozone Observations With a Dobson Spectrophotometer. WMO Global Ozone Research and Monitoring Project Rep. No. 6, World Meteorological Organization, Geneva, Switzerland, 125 pp.
- Komhyr, W. D., and R. D. Evans. Dobson spectrophotometer total ozone measurement errors caused by interfering absorbing species such as SO₂, NO₂, and photochemically produced O₃ in polluted air. Geophys. Res. Lett. 7(2):157-160.
- Mateer, C. L., J. J. DeLuisi, and C. C. Porco. The short Umkehr method: Part I, Standard ozone profiles for use in the estimation of ozone profiles by the inversion of short Umkehr observations. NOAA Tech. Memo. ERL ARL-86, NOAA Environmental Research Laboratories, Boulder, Colo., 36 pp.
- Mendonca, B. G., J. J. DeLuisi, and K. J. Hanson, 1980. Secular trends in atmospheric transmission and turbidity: factors in climate change? Proceedings of the International Radiation Symposium, Fort Collins, Colo., August 11-16, 1980, Colorado State University, Fort Collins, sec. 3.10.
- Murphy, M. E., and B. A. Bodhaine. The Barrow, Alaska, automatic condensation nuclei counter and four wavelength nephelometer: instrument details and four years of observations. NOAA Tech. Memo. ERL ARL-90, NOAA Environmental Research Laboratories, Boulder, Colo., 101 pp.

- Murphy, M. E., and B. A. Bodhaine. The South Pole automatic condensation nuclei counter: instrument details and five years of observations. NOAA Tech. Memo. ERL ARL-82, NOAA Environmental Research Laboratories, Boulder, Colo., 91 pp.
- Nimira, J. K. Comparison of estimated and observed values for solar radiation at the surface of the African Continent. NOAA Tech. Memo. ERL ARL-83, 48 pp.
- Peterson, J. T. Within-year and year-to-year atmospheric turbidity variation in central North Carolina, U.S.A. Proceedings of the International Radiation Symposium, Fort Collins, Colo., August 11-16, 1980, Colorado State University, Fort Collins, 173-174.
- Peterson, J. T., K. J. Hanson, B. A. Bodhaine, and S. J. Oltmans. Dependence of CO₂, aerosol, and ozone concentrations on wind direction at Barrow, Alaska, during winter. Geophys. Res. Lett. 7(5):349-352.
- Schnell, R. C. (ed). The Mount Kenya Baseline Station Feasibility Study. WMO Executive Committee Panel of Experts on Environmental Pollution, 3rd Session, Geneva, Switzerland, April 8-12, 1980, Final Rep., World Meteorological Organization, Geneva, 171 pp.
- Schnell, R. C., B. Wrobel, and S. W. Miller. Seasonal changes and terrestrial sources of atmospheric ice nuclei at Boulder, Colorado. Preprints, Eighth International Conference on Cloud Physics, vol. 1, Clermont-Ferrand, France, July 15-19, 1980, International Association of Meteorology and Atmospheric Physics, Boulder, Colo., 53-56.
- Schnell, R. C., R. F. Pueschel, H. K. Weickmann, and D. L. Wellman. Ice nucleus and aerosol measurements in the plume of the Johnstown, PA, steel mill. Geophys. Res. Lett. 7(5):397-400.

8. REFERENCES

- Aitken, J., 1911. On some nuclei of cloudy condensation. Proc. R. Soc. Edinb. 31:478-498.
- Ambach, W., 1974. The influence of cloudiness on the net radiation balance of a snow surface with high albedo. J. Glaciol. 13(67):73-84.
- Berger, D., and F. Urbach, 1982. A climatology of sunburning ultraviolet radiation. Photochem. Photobiol. (In press.)
- Bigg, E. K., 1980. Comparison of aerosol at four baseline atmospheric monitoring stations. J. Appl. Meteorol. 19:521-533.
- Bodhaine, B. A., J. M. Harris, G. A. Herbert, and W. D. Komhyr, 1980. Identification of volcanic episodes in aerosol data at Mauna Loa Observatory. J. Geophys. Res. 85(C3):1600-1604.
- Bodhaine, B. A., B. G. Mendonca, J. M. Harris, and J. M. Miller, 1981. Seasonal variations in aerosols and atmospheric transmission at Mauna Loa Observatory. J. Geophys. Res. 86(C8):7395-7398.
- Bolin, B., and Keeling, C. D., 1963. Large-scale atmospheric mixing as deduced from the seasonal and meridional variations of carbon dioxide. J. Geophys. Res. 68(13):3899-3920.
- Bortniak, J. C., 1981. The wind climatology of American Samoa. NOAA Tech. Memo. ERL ARL-98, NOAA Environmental Research Laboratories, Boulder, Colo., 67 pp.
- Chylek, P., and J. A. Coakley, Jr., 1974. Aerosols and climate. Science 183:75-77.
- Connell, P. S., R. A. Perry, and C. J. Howard, 1980. Tunable diode laser measurement of nitrous oxide in air. Geophys. Res. Lett. 8:1093-1096.
- Coulier, M., 1875. Note sur une nouvelle propriété de l'air. J. Pharm. Chim. 22:165-173; 254-255.
- Coyne, P. I., and J. J. Kelley, 1975. Carbon dioxide exchange over the Alaskan Arctic tundra: meteorological assessment by an aerodynamic method. J. Appl. Ecol. 12:587-611.
- Danielsen, E. F., 1981. Trajectories of the Mt. St. Helens eruption plume. Science 211:819-821.
- Darzi, M., and J. W. Winchester, 1981. Aerosol characteristics at Mauna Loa Observatory, Hawaii, after East Asian dust storm episodes. J. Geophys. Res. (In press.)
- Dave, J. V., C. L. Mateer, and J. J. DeLuisi, 1980. An examination of the effect of haze on the short Umkehr method for deducing the vertical distribution of ozone. Proceedings of the Quadrennial International Ozone Symposium, Boulder, Colorado, 4-9 August 1980, vol. 1, J. London (ed.), IAMAP/International Ozone Commission (available National Center for Atmospheric Research, Boulder, Colo.), 222-229.

- DeLuisi, J. J., 1979. Shortened version of the Umkehr method for observing the vertical distribution of ozone. Appl. Opt. 18:3190-3196.
- DeLuisi, J. J., and B. M. Herman, 1977. Estimation of solar radiation absorption by volcanic stratospheric aerosols from Agung using surface-based observations. J. Geophys. Res. 82(C24):3477-3480.
- DeLuisi, J. J., and C. L. Mateer, 1971. On the application of the optimum statistical inversion technique to the evaluation of Umkehr observations. J. Appl. Meteorol. 10:328-334.
- DeLuisi, J. J., J. E. Bonelli, and C. E. Sheldon, 1977. Spectral absorption of solar radiation by the Denver brown (pollution) cloud. Atmos. Environ. 11:829-836.
- Dias, M., I. Nolt, E. Nickerson, and D. Welsh, 1981. Hawaii Mesoscale Energy and Climate Project (HAMEC): II, P-3 aircraft data set. NOAA Environmental Research Laboratories, Boulder, Colo., 323 pp.
- Dittenhoefer, A. C., 1981. An investigation of the effects of sulfate and nonsulfate particles on light scattering at the Mauna Loa Observatory. Water Air Soil Pollut. (Submitted.)
- Duce, R. A., J. G. Quinn, and T. L. Wade, 1974. Residence time of nonmethane hydrocarbons in the atmosphere. Mar. Pollut. Bull. 5:59-61.
- Duce, P. A., C. K. Unni, B. J. Ray, J. M. Prospero, and J. T. Merrill, 1980. Long-range atmospheric transport of soil dust from Asia to the tropical north Pacific: temporal variability. Science 209:1522-1524.
- Dütsch, H. U., 1959. Vertical ozone distributions from Umkehr observations. Arch. Meteorol. Geophys. Bioklimatol. A11:240-251.
- Fegley, R. W., and H. T. Ellis, 1975. Lidar observations of a stratospheric dust cloud layer in the tropics. Geophys. Res. Lett. 2:139-141.
- Fegley, R. W., E. W. Barrett, and H. T. Ellis, 1978. Lidar measurements at Mauna Loa. Mauna Loa Observatory: a 20th anniversary report, J. M. Miller (ed.), NOAA Spec. Rep., NOAA Environmental Research Laboratories, Boulder, Colo., 59-65.
- Fernald, F. G., and C. L. Frush, 1975. Lidar observations of the enhanced stratospheric dust layer associated with the eruption of Volcán de Fuego. Trans. Am. Geophys. Union 56:366.
- Fishman, J., and P. J. Crutzen, 1978. The origin of ozone in the troposphere. Nature 274:855-858.
- Flyger, H., N. Z. Heidam, K. Hansen, W. J. Megaw, E. G. Walther, and A. W. Hogan, 1976. The background level of the summer tropospheric aerosol, sulphur dioxide, and ozone of Greenland and the North Atlantic Ocean. J. Aerosol Sci. 7:103-140.
- Geist, J., E. F. Zalewski, and A. R. Schaefer, 1980. Spectral response self-calibration and interpolation of silicon photodiodes. Appl. Opt. 19(22):3795-3799.

- Gillette, D. A., 1981. Decomposition of annual variation of CO₂ concentration at GMCC flask sampling stations into three patterns. Atmos. Environ. (Provisionally accepted.)
- Gillette, D. A., and K. J. Hanson, 1981. Sampling strategy to obtain data used in models of global annual CO₂ increase and global carbon cycle. J. Geophys. Res. (Submitted.)
- Gillette, D. A., and A. T. Steele, 1981. Short-term variations of atmospheric CO₂ concentrations at three stations of the Geophysical Monitoring for Climatic Change program: relation to selection of CO₂ concentration data obtained by whole air sampling. (In review.)
- Goldan, P. D., W. C. Kuster, A. L. Schmeltekopf, F. C. Fehsenfeld, and D. L. Albritton, 1981. Correction of atmospheric N₂O mixing-ratio data. J. Geophys. Res. 86(C6):5385-5386.
- Groves, K. S., and A. F. Tuck, 1979. Simultaneous effects of CO₂ and chlorofluoromethanes on stratospheric ozone. Nature 280:127-129.
- Hanson, K. J., 1961. Some aspects of the thermal energy exchange on the South Polar snow field and Arctic ice pack. Mon. Weather Rev. 89: 173-177.
- Hanson, K. J. (ed.), 1977. Geophysical Monitoring for Climatic Change, No. 5: Summary Report 1976. NOAA Environmental Research Laboratories, Boulder, Colo., 110 pp.
- Hanson, K. J., J. T. Peterson, J. Namais, R. Born, and C. S. Wong, 1981. On the influence of Pacific Ocean temperatures on atmospheric carbon dioxide concentration at Ocean Weather Station P. J. Phys. Oceanogr. 11:905-912.
- Harris, J. M., and G. A. Herbert, 1980. Carbon dioxide, condensation nuclei, and wind climatology of the Barrow GMCC Observatory (1973-1979). NOAA Data Rep. ERL ARL-2, NOAA Environmental Research Laboratories, Boulder, Colo., 112 pp.
- Herbert, G. A. (ed), 1980. Geophysical Monitoring for Climatic Change, No. 8: Summary Report 1979. NOAA Environmental Research Laboratories, Boulder, Colo., 120 pp.
- Hogan, A. W., S. Barnard, and W. Winters, 1981. Photoelectric nucleus counters for aerosol climatology. J. Aerosol Sci. (Accepted.)
- Holmgren, B., 1971. Climate and energy exchange on a sub-polar ice cap in summer. Arctic Institute of North America Devon Island Expedition 1961-1963: Part E, Radiation climate. Meddelanden fran Uppsala Universitets Meteorologiska Institution, Nr. 111, Sweden, 111 pp.
- Junge, C. E., 1963. Air Chemistry and Radioactivity. International Geophysics Series, vol. 4, Academic Press, New York, 382 pp.
- Keeling, C. D., R. B. Bacastow, A. E. Bainbridge, C. A. Ekdahl, Jr., P. R. Guenther, L. S. Waterman, and J. F. S. Chin, 1976. Atmospheric carbon dioxide variations at Mauna Loa Observatory, Hawaii. Tellus 28:538-551.

- Kelley, J. J., and T. A. Gosink, 1979. Gases in sea ice: 1975-1979. Final Rep. to Office of Naval Research Contract No. N000 14-76C-0331, Institute of Marine Science, University of Alaska, Fairbanks, 104 pp.
- Kerr, R. A., 1979. Global pollution: is the Arctic haze actually industrial smog? Science 205:290-293.
- Kerr, R. A., 1981. Pollution of the Arctic atmosphere confirmed. Science 212:1013-1014.
- Khalil, M. A. K., and R. A. Rasmussen, 1981a. Atmospheric methyl chloride (CH_3Cl). Chemosphere 10:1019-1023.
- Khalil, M. A. K., and R. A. Rasmussen, 1981b. Decline in the atmospheric accumulation rates of CCl_3F (F-11), CCl_2F_2 (F-12), and CH_3CCl_3 . J. Air Pollut. Control Assoc. (Accepted.)
- Khalil, M. A. K., and R. A. Rasmussen, 1981c. Gaseous tracers of Arctic haze. Oregon Graduate Center report. (Submitted.)
- Khalil, M. A. K., and R. A. Rasmussen, 1981d. Increase in the global concentration of nitrous oxide. Oregon Graduate Center preprint. (Submitted.)
- Komhyr, W. D., 1980. Operations Handbook Ozone--Observations with a Dobson Spectrophotometer. Rep. No. 6, WMO Global Ozone Research and Monitoring Project, World Meteorological Organization, Geneva, Switzerland, 125 pp.
- Komhyr, W. D., W. R. Taylor, and T. B. Harris, 1980. A semi-automatic flask sample CO_2 analyzer. Proceedings of the WMO Technical Conference on Regional and Global Observations of Atmospheric Pollution Relative to the Climate, Boulder, Colo., August 20-24, 1979, WMO No. 549, Spec. Environ. Rep. No. 14, World Meteorological Organization, Geneva, Switzerland, 65-71.
- Komhyr, W. D., R. D. Grass, E. G. Dutton, and R. K. Leonard, 1981a. Trend determinations from provisional and corrected 1963-1979 Bismarck total ozone data. Proceedings of the Quadrennial International Ozone Symposium, Boulder, Colorado, 4-9 August 1980, vol. 1, J. London (ed.), IAMAP/International Ozone Commission (available National Center for Atmospheric Research, Boulder, Colo.), 371-377.
- Komhyr, W. D., R. D. Grass, R. D. Evans, and R. K. Leonard, 1981b. Dobson spectrophotometer calibrations, possible errors in ozone absorption coefficients, and errors due to interfering pollutant gases. Proceedings of the Quadrennial International Ozone Symposium, Boulder, Colorado, 4-9 August 1980, vol. 1, J. London (ed.), IAMAP/International Ozone Commission (available National Center for Atmospheric Research, Boulder, Colo.), 230-235.
- Komhyr, W. D., R. D. Grass, and R. K. Leonard, 1981c. WMO 1977 international comparison of Dobson ozone spectrophotometers. Proceedings of the Quadrennial International Ozone Symposium, Boulder, Colorado, 4-9 August 1980, vol. 1, J. London (ed.), IAMAP/International Ozone Commission (available National Center for Atmospheric Research, Boulder, Colo.), 27-32.

- Komhyr, W. D., T. Harris, L. Waterman, W. Taylor, K. Hanson, and D. Gillette, 1981d. CO₂ annual cycle amplitudes, meridional gradients, and global abundances derived from discrete sampling during 1979 at 15 stations. (In review.)
- Komhyr, W. D., T. M. Thompson, and E. G. Dutton, 1981e. Chlorofluorocarbon-11, -12, and nitrous oxide measurements at the U.S. GMCC baseline stations (16 September 1973 to 31 December 1979). NOAA Tech. Rep. ERL/ARL. (Accepted.)
- Komhyr, W. D., E. G. Dutton, and T. M. Thompson, 1982. Use of known concentration CO₂ trace gas admixtures in calibrating N₂O, CCl₃F, CCl₂F₂, and other trace reference gases. (In preparation.)
- Kozo, T. L., 1979. Evidence for sea breezes on the Alaskan Beaufort Sea coast. Geophys. Res. Lett. 6(11):849-852.
- Kozo, T. L., 1980. Mountain barrier baroclinity effects on surface winds along the Alaskan Arctic coast. Geophys. Res. Lett. 7(5):377-380.
- Labs, D., and H. Neckel, 1968. The radiation of the solar photosphere from 2000 Å to 100 μ. Z. Astrophys. 69:1-73. (In English.)
- Larssen, S., and J. E. Hanssen, 1980. Annual variation and origin of aerosol components in the Norwegian Arctic-Subarctic region. Proceedings of the WMO Technical Conference on Regional and Global Observations of Atmospheric Pollution Relative to Climate, Boulder, Colo., August 20-24, 1979, WMO No. 549, Spec. Environ. Rep. No. 14, World Meteorological Organization, Geneva, Switzerland, 251-258.
- List, R. J., 1949. Smithsonian Meteorological Tables. 6th rev. ed., Smithsonian Institution, Washington, D.C., 527 pp.
- Liu, S. C., D. Kley, M. McFarland, J. O. Mahlman, and H. Levy, II, 1980. On the origin of tropospheric ozone. J. Geophys. Res. 85(C7):7546-7555.
- MacDonald, G. A., and T. Katsura, 1964. Chemical composition of Hawaiian lavas. J. Petrol. 5:82-133.
- Mason, B. H., 1966. Principles of Geochemistry. 3rd ed., Wiley and Sons, New York, 329 pp.
- Mateer, C. L., and J. J. DeLuisi, 1980. The estimation of the vertical distribution of ozone by the short Umkehr method. Proceedings of the Quadrennial International Ozone Symposium, Boulder, Colorado, 4-9 August 1980, vol. 1, J. London (ed.), IAMAP/International Ozone Commission (available National Center for Atmospheric Research, Boulder, Colo.), 64-73.
- Mateer, C. L., J. J. DeLuisi, and C. C. Porco, 1980: The short Umkehr method: Part I, Standard ozone profiles for use in the estimation of ozone profiles by inversion of short Umkehr observations. NOAA Tech. Memo. ERL ARL-86, NOAA Environmental Research Laboratories, Boulder, Colo., 36 pp.
- Maykut, G. A., and P. E. Church, 1973. Radiation climate of Barrow, Alaska, 1962-1966. J. Appl. Meteorol. 12:620-628.

- Mendonca, B., 1969. Local wind circulations on the slope of Mauna Loa. J. Appl. Meteorol. 8:533-541.
- Mendonca, B. G. (ed.), 1979. Geophysical Monitoring for Climatic Change, No. 7: Summary Report 1978. NOAA Environmental Research Laboratories, Boulder, Colo., 133 pp.
- Mendonca, B. G., K. J. Hanson, and J. J. DeLuisi, 1978. Volcanically related secular trends in atmospheric transmission at Mauna Loa Observatory, Hawaii. Science 202:513-515.
- Merrill, J. T., 1981. Micro-meteorological evaluation of the SEAREX atmospheric sampling site at the NOAA/GMCC station in American Samoa. Boundary-Layer Meteorol. (Submitted.)
- Miller, J. M., 1978. The complexity of the wind patterns at Mauna Loa Observatory. Mauna Loa Observatory: a 20th anniversary report, J. M. Miller (ed.), NOAA Spec. Rep., NOAA Environmental Research Laboratories, Boulder, Colo., 122-127.
- Miller, J. M., 1979. National Atmospheric Deposition Program: analysis of data from the first year. In Atmospheric Sulfur Deposition, Environmental Impact and Health Effects, Ann Arbor Publishers, Ann Arbor, Mich., 469-476.
- Miller, J. M., 1981. A five-year climatology of back trajectories from the Mauna Loa Observatory, Hawaii. Atmos. Environ. 15:1553-1558.
- Miller, J. M., and J. F. S. Chin, 1978. Short-term distributions in the carbon dioxide record at Mauna Loa Observatory. Geophys. Res. Lett. 5(8):669-671.
- Miller, J. M., and A. M. Yoshinaga, 1981. The pH of Hawaiian precipitation: a preliminary report. Geophys. Res. Lett. 8(7):779-782.
- Newell, R. E., G. J. Boer, and J. W. Kidson, 1974. An estimate of the inter-hemispheric transfer of carbon monoxide from tropical general circulation data. Tellus 26:103-107.
- Nickerson, E., and E. Magaziner, 1976. A three-dimensional simulation of winds and non-precipitating orographic clouds over Hawaii. NOAA Tech. Rep. ERL 377-APCL 39, NOAA Environmental Research Laboratories, Boulder, Colo., 41 pp.
- Nolt, I. G., E. C. Nickerson, W. R. Caldwell, M. Dias, D. C. Welsh, D. Bartels, F. J. Holitza, E. S. Salazar, F. N. Gould, J. A. Zysko, H. W. Davis, C. S. Ramage, and T. A. Schroeder, 1980. Hawaii Mesoscale Energy and Climate Project (HAMEC): I, Data user's guide, NOAA Environmental Research Laboratories, Boulder, Colo., 71 pp.
- Oltmans, S. J., 1981. Surface ozone measurements in clean air. J. Geophys. Res. 86(C2):1174-1180.

- Oltmans, S. J., and J. London, 1981. The quasi-biennial oscillation (QBO) in atmospheric ozone. Proceedings of the Quadrennial International Ozone Symposium, Boulder, Colorado, 4-9 August 1980, vol. 1, J. London (ed.), IAMAP/International Ozone Commission (available National Center for Atmospheric Research, Boulder, Colo.), 397-409.
- Pales, J. C., and C. D. Keeling, 1965. The concentration of atmospheric carbon dioxide in Hawaii. J. Geophys. Res. 70:6053-6076.
- Park, P. K., L. I. Gordon, and S. Alvarez-Borrego, 1974. The carbon dioxide system of the Bering Sea. In Oceanography of the Bering Sea, D. W. Hood and E. J. Kelley (eds.), Institute of Marine Science, University of Alaska, Fairbanks, 107-147.
- Parungo, F., C. Nagamoto, R. Schnell, I. Nolt, E. Nickerson, and W. Caldwell, 1981. Hawaii Mesoscale Energy and Climate Project (HAMEC): III, Atmospheric aerosol and cloud microphysics measurements, NOAA Environmental Research Laboratories, Boulder, Colo., 75 pp.
- Peterson, J. T. (ed.), 1978. Geophysical Monitoring for Climatic Change, No. 6: Summary Report 1977. NOAA Environmental Research Laboratories, Boulder, Colo., 145 pp.
- Peterson, J. T., K. J. Hanson, B. A. Bodhaine, and S. J. Oltmans, 1980. Dependence of CO₂, aerosol, and ozone concentrations on wind direction at Barrow, Alaska, during winter. Geophys. Res. Lett. 7(5):349-352.
- Peterson, J. T., W. D. Komhyr, T. B. Harris, and L. S. Waterman, 1982. Atmospheric carbon dioxide measurements at Barrow, Alaska, 1973-1979. Tellus. (Accepted.)
- Pollak, L. W. (1957). Methods of measuring condensation nuclei. Geofis. Pura Appl. 36:21-26.
- Rahn, K. A., 1981. The Mn/V ratio as a tracer of large-scale sources of pollution aerosol for the Arctic. Atmos. Environ. 15:1457-1464.
- Rahn, K. A., and R. J. McCaffrey, 1980. On the origin and transport of the winter Arctic aerosol. Ann. New York Acad. Sci. 338:486-503.
- Rahn, K. A., R. D. Borys, and G. E. Shaw, 1977. The Asian source of Arctic haze bands. Nature 268:713-715.
- Ramanathan, V., 1981. Ozone effects on climate: a review. Proceedings of the Quadrennial International Ozone Symposium, Boulder, Colorado, 4-9 August 1980, vol. 1, J. London (ed.), IAMAP/International Ozone Commission (available National Center for Atmospheric Research, Boulder, Colo.), 1053-1059.
- Rasmussen, R. A., and M. A. K. Khalil, 1980. Atmospheric halocarbons: measurements and analyses of selected trace gases. Proceedings of the NATO Advanced Study Institute on Atmospheric Ozone: Its Variation and Human Influences, A. C. Aikin (ed.), Algarve, Portugal, October 1-13, 1979, U.S. Federal Aviation Administration, Washington, D.C., 209-231.

- Rasmussen, R. A., and M. A. K. Khalil, 1981a. Global atmospheric distribution and trend of CH_3CCl_3 . Geophys. Res. Lett. 8(9):1005-1007.
- Rasmussen, R. A., and M. A. K. Khalil, 1981b. Increase in the concentration of atmospheric methane. Atmos. Environ. 15:883-886.
- Rasmussen, R. A., and F. W. Went, 1965. Volatile organic matter of plant origin in the atmosphere. Proc. Natl. Acad. Sci. 53:215-220.
- Rasmussen, R. A., M. A. K. Khalil, and R. W. Dalluge, 1981a. Atmospheric trace gases in Antarctica. Science 211:285-287.
- Rasmussen, R. A., M. A. K. Khalil, R. Gunawardena, and S. D. Hoyt, 1981b. Atmospheric methyl iodide (CH_3I). J. Geophys. Res. (Submitted.)
- Reible, D. D., F. H. Shair, R. J. Cayer, and D. W. Nelson, 1981. Atmospheric tracer studies associated with the evaluation of the SEAREX atmospheric sampling site at the NOAA/GMCC station in American Samoa. Boundary-Layer Meteorol. (Submitted.)
- Rodgers, C. D., 1976. Retrieval of atmospheric temperature and composition from remote measurements of thermal radiation. Rev. Geophys. Space Phys. 14:609-624.
- Rotty, R., 1978. The atmospheric CO_2 consequences of heavy dependence of coal. In Carbon Dioxide and Society, J. Williams (ed.), Pergamon Press, New York, 263-273.
- Russell, P. B., and R. D. Hake, Jr., 1977. The post-Fuego stratospheric aerosol: lidar measurements, with radiative and thermal implications. J. Atmos. Sci. 34:163-177.
- SEAREX Newsletter, 1980. Samoa sampling site construction. 3(3):1-2.
- Shaw, G. E., 1980. Transport of Asian desert aerosol to the Hawaiian Islands. J. Appl. Meteorol. 19:1254-1259.
- Sinclair, D., 1972. A portable diffusion battery. J. Amer. Hyg. Assoc. 33:729-735.
- Stidd, C. K., 1966. The use of eigenvectors for climatic estimates. Preprint Series no. 36, Desert Research Institute, Reno, Nev., 20 pp.
- Taylor, S. R. 1964. Abundances of chemical elements in the continental crust: a new table. Geochem. Cosmochim. Acta 28:1273-1281.
- Thompson, T. M., 1981. Pyrheliometer observations as an indicator of the climatological persistence of clouds. NOAA Tech. Memo. ERL ARL-97, NOAA Environmental Research Laboratories, Boulder, Colo., 78 pp.
- Turner, D. B., 1970. Workbook of atmospheric dispersion estimates. EPA Rep. AP-26, Environmental Protection Agency, Office of Air Programs, Research Triangle Park, N.C., 84 pp.
- U.S. DOE (U.S. Department of Energy), 1981. EML procedures manual. Rep. HASL-300, Washington, D.C. (Updated annually.)

- Weiss, R. F. 1981. The temporal and spatial distribution of tropospheric nitrous oxide. J. Geophys. Res. 86(C3):7185-7195.
- Wendler, G., F. D. Eaton, and T. Ohtake, 1981. Multiple reflection effects on irradiance in the presence of Arctic stratus clouds. J. Geophys. Res. 86(C3):2049-2057.
- Went, F. W., 1964. The nature of Aitken condensation nuclei in the atmosphere. Proc. Natl. Acad. Sci. 51:1259-1267.
- Westwater, E. R., and O. N. Strand, 1968. Statistical information content of radiation measurements used in indirect sensing. J. Atmos. Sci. 25: 750-758.
- Wold, S., 1974. Spline functions in data analysis. Technometrics 16:1-11.
- Wylie, C. R., Jr., 1966. Advanced Engineering Mathematics. McGraw-Hill, New York, 813 pp.
- Zafiriou, O. C., 1975. Reaction of methyl halides with seawater and marine aerosols. J. Mar. Res. 33:75-81.
- Zoller, W. H., W. C. Cunningham, and N. K. Aras, 1979. Chemical composition of atmospheric aerosols. Geophysical Monitoring for Climatic Change, No. 8: Summary Report 1979, G. A. Herbert (ed.), NOAA Environmental Research Laboratories, Boulder, Colo., 88-93.

9. 1980 GMCC STAFF

Director's Office

Kirby J. Hanson, Director
Bernard G. Mendonca, Deputy Director
Gail M. Phillips, Secretary
Dale A. Gillette, CIRES
Edward Green, Electronic Engineer
Cynthia McFee, NOAA Corps
Jerome K. Nimira, CIRES
John Osborn, Lt. NOAA Corps
Judy Schroeder, Computer Programmer
Constance Shilvock, Jr. Fellow

Acquisition and Data Management Group

Gary A. Herbert, Chief
Patricia Angel, Secretary
Joyce M. Harris, Computer Programmer
Lee Johnson, Computer Programmer
Milton S. Johnson, Electronic Technician
James Jordan, Electronic Engineer
Steven Waas, Jr. Fellow

Monitoring Trace Gases Group

Walter D. Komhyr, Chief
Patricia Angel, Secretary
Ruth Alvirez, COOP
Eduardo Blanco, COOP
Ellsworth Dutton, CIRES
Robert Evans, CIRES
Robert D. Grass, Physicist
Thomas B. Harris, Meteorological Technician
Kent Leonard, CIRES
Samuel Oltmans, Physicist
Frank Polacek, III, Meteorological Technician
William Taylor, CIRES
Lee Waterman, Chemist

Aerosols and Radiation Monitoring Group

John J. DeLuisi, Chief
Bonnie M. Hill, Secretary
Barry A. Bodhaine, Meteorologist
Richard Cram, Meteorologist
Ronald W. Fegley, Physicist

Analysis and Interpretation Group

James T. Peterson, Chief
Bonnie M. Hill, Secretary
John Bortniak, Lt. (jg.) NOAA Corps
Carol J. Fee, COOP
Bradley C. Halter, CIRES
Cheryl Reynolds, Jr. Fellow
Russell C. Schnell, CIRES
Thayne Thompson, Physicist

Mauna Loa Observatory

Kinsell L. Coulson, Director
Judith B. Pereira, Secretary
John F. S. Chin, Physicist
Thomas DeFoor, Electrical Engineer
Howard Ellis, Physicist
Mamoru Shibata, Electronic Technician
Alan M. Yoshinaga, Analytical Chemist

Barrow Observatory

David Smith, Physical Scientist, Station Chief
Kenneth Bauer, Electronic Technician
Robert Drury, Electronic Technician
Robert Hanby, Electronic Technician

Samoa Observatory

Donald W. Nelson, Station Chief
Roger A. C. Williams, Electronic Technician

South Pole Observatory

William Hiscox, Lt. (jg.) NOAA Corps, Station Chief
Gregory M. Siedelberg, Electronic Technician

